TU Graz
Graz University of Technology

IBK Fachbereich Ingenieurbaukunst

Unreinforced and reinforced openings in GLT beams- A comparison based on experimental investigations

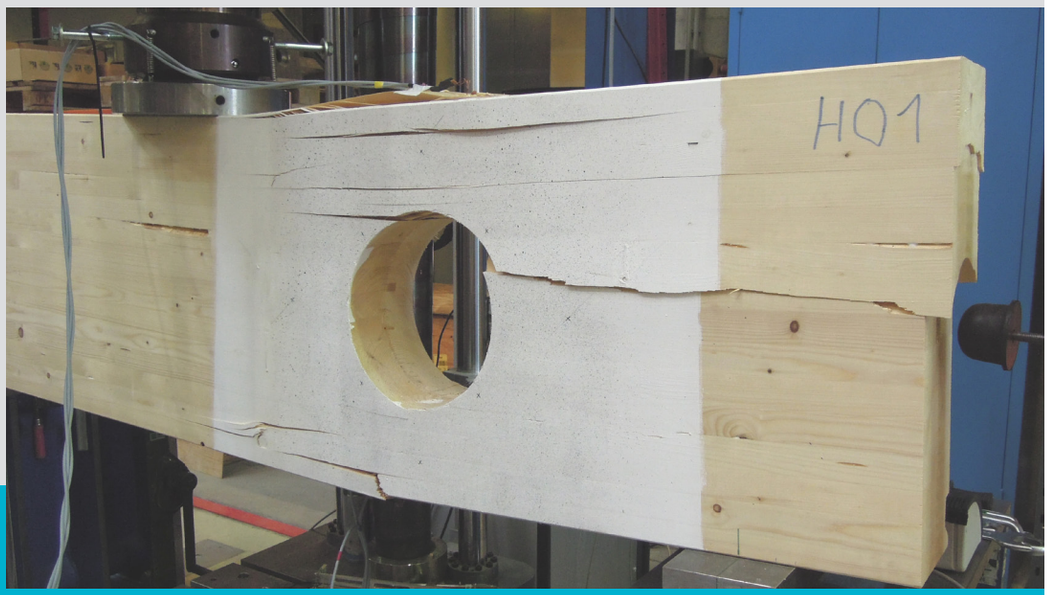

M-4-6/2017

Lada ILIĆ
Institute of Timber Engineering and Wood Technology
Graz University of Technology

Forschungsberichte | **Masterarbeiten** | Skripten | Vorträge/Tagungen

Lada Ilić, BSc

UNREINFORCED AND REINFORCED OPENINGS IN GLT BEAMS - A COMPARISON BASED ON EXPERIMENTAL INVESTIGATIONS

MASTER THESIS

for obtaining the academic degree
graduate engineer
Civil Engineering Sciences - Structural Engineering

Submitted at

Graz University of Technology

supervising tutor
Univ.-Prof. Dipl.-Ing. Dr.techn. Gerhard Schickhofer
Institute of Timber Engineering and Wood Technology
DI Julia Dröscher
DI Severin Zimmer
Institute of Timber Engineering and Wood Technology

Graz, May 2017

STATUTORY DECLARATION
AFFIDAVIT

I declare that I have authored this thesis independently, that I have not used other than the declared sources/resources, and that I have explicitly indicated all material which has been quoted either literally or by content from the sources used. The text document uploaded to TUGRAZonline is identical to the present master‘s thesis.

Ich erkläre an Eides statt, dass ich die vorliegende Arbeit selbstständig verfasst, andere als die angegebenen Quellen/Hilfsmittel nicht benutzt, und die den benutzten Quellen wörtlich und inhaltlich entnommenen Stellen als solche kenntlich gemacht habe. Das in TUGRAZonline hochgeladene Textdokument ist mit der vorliegenden Masterarbeit identisch.

Date / Datum	Signature / Unterschrift

Thank-you note

In the following lines, I would like to thank all the people who have accompanied, encouraged and motivated me during my studies and during the development of this master thesis.

First of all, I would like to thank both the employees of the Institute of Timber Engineering and Wood Technology and the Laboratory for Structural Engineering. They supported me in the practical work in the workshop and also advised and motivated me in a variety of conversations.

Furthermore, my thanks go to:

Mr. Univ.-Prof. Dipl.-Ing. Dr.techn. Gerhard Schickhofer, who was able to inspire me even more for timber constructions with his interesting lectures.

Ms. Dipl.-Ing. Julia Dröscher, who showed me that all people are the same.

Mr. Dipl.-Ing Severin Zimmer, who helped me with his corrections and suggestions to finish my master thesis.

My friends and colleagues, Čedomir Oparnica, Uroš Todorović, Milica Janković, Meldijana Ćehić, Deni Obid, Darko Pejić, Thomas Laggner, Rita Wolf, Eva Virgolini, with whom I could enjoy a fun and very educational time. Without them, I could not have graduated in this short time and with this success.

Finally, I would like to thank my whole family. They are a reliable support in my life and have always supported me in my decisions. Without them I would not be the human being I am. I would especially like to call:

My parents, Kosta Ilić and Branka Carić, who gave me a sheltered home and study. Special thanks goes to my Aunt Ljiljana Carić and my grandparents Vojislav and Justina Ilić, who believed in me, when no one else did.

Abstract

Openings in main and secondary ceiling beams took common place in current timber engineering. Constructional and architectural requirements must be fulfilled, which might be challenging, particularly with large-scale ventilation ducts near supports. Those concerns are not only for wide-span hall carriers, but also offices, municipal and residential buildings. The openings in supporting construction lead to a reduction of the carrying capacity and higher deformation of these elements and require separate proofs, which are partly regulated in standards. The related normative regulations were restrictive to each new standard output, and this meant that today unreinforced openings are almost not allowed. In this thesis, the standard rules are critically examined, different internal strengthening methods are discussed and set out in comparison. Lab tests should provide the carrying and deformation capacity for 6 test series (29 test specimens) which will be evaluated regarding their mode of operation and overall efficiency. Based on these investigations, comments and proposals for the actual standard are a result as well as a better understanding of the behavior of different internal reinforcements.

Kurzfassung

Die Anordnung von Durchbrüchen in Haupt- und Nebenträgern von Deckenkonstruktionen ist im aktuellen Ingenieurholzbau von großer Bedeutung. Die konstruktiven und architektonischen Anforderungen müssen berücksichtigt werden, wobei gerade in der Nähe von Auflagern Durchbrüche mit großflächigen Lüftungskanälen eine Herausforderung darstellen. Dies zu berücksichtigen ist nicht nur für weitgespannte Träger in Hallen, sondern auch Büros, Kommunal- und Wohngebäude sehr wichtig. Die Durchbrüche in Konstruktionen führen zu einer Verringerung des Trag- und Verformungsvermögen dieser Elemente und erfordern separate Überprüfungen, die normativ teilweise reguliert wurden. Die entsprechenden normativen Regelungen wurden mit jeden Überarbeitung der Normenwerk restriktiver. In dieser Masterarbeit werden die Standardregeln kritisch geprüft und unterschiedliche Verstärkungsmaßnahmen diskutiert und verglichen. Die Laborprüfungen zeigen das Trag- und Verformungsvermögen anhand von sechs verschiedenen Prüfserien (29 Prüfkörper) mit unterschiedlichen internen Verstärkungsmaßnahmen inklusiv zwei Referenzserien. Ergebnis der Untersuchungen sind neben Kommentaren und Anregungen für die Norm auch ein besseres Verständnis für die Wirkungsweise und Effizienz von innenliegenden Verstärkungsmaßnahmen.

Content

CHAPTER 1: INTRODUCTION

Wood is an organic and natural material and it is characterized as anatomically inhomogeneous material, in a mechanical sense, and it shows a very strong anisotropy, which represents different behaviour of material in different directions and different strains behaviour depending on the stress state. Since it is naturally occurring processes, wood in its structure and anatomy may have disadvantages which are usually reflected in knots, resin channels, cracks, grained irregularities etc. Spruce, pine and larch, as well as the hard wood species such as oak and beech are usually used in constructional engineering. Laminating, and cutting the trunk lengthwise into thin lamella (strips) thickness up to 30 mm, is a very effective way to eliminate all these shortcomings and errors in trees because of all deficiencies observed and eliminated from the bracket, in contrast to monolithic wood i.e. classical timber, where it is very difficult to note irregularities in the internal structure of the wood. This wood based material found great use in construction due to the extremely favourable characteristics such as small volume weight, high strength parallel to the grain, small sensitivity to temperature changes and differences as well as the chemically aggressive environment and so on [1], [2], [3].

The concept of glue laminated structures consists of beams or elements that are formed by special technological processes under strictly controlled conditions, factoring plants, gluing slats (boards) with certain thickness under enormous pressure with the use of special waterproof synthetic adhesives based on formaldehyde, which is now due to the toxicity mainly replaced with adhesives based on polyurethane. Such technological processes enable building a material with uniform properties, therefore there are possible increased stress brackets. The GLT beams have found great use in the construction work, with roofs of small and large ranges, for making prefabricated permanent or temporary buildings, pedestrian or road bridges and so on. Very simple and easy mounting by using light mechanization, limitlessness regarding the length of the elements, forming arbitrary beams and cross-section are just some of the advantages of these types of elements [1], [2], [3].

The design and construction of structures often have requirements imposed by the need of drilling supports or leaving openings in elements from different aesthetic, architectural and structural reasons. The openings in the roof beams and the columns are designed for the passage of various installations (pipes, cables ...), as well as facilitated the assembly of the element itself etc.

Depending on the geometry, size and their position on the beam, openings in GLT and CLT beams, can represent a very critical zone in places near the opening edge, where redistribution of tensile stress perpendicular to the grain occurs. Therefore, this issue had previously been studied enough so that some regulations for the timber engineering provide basic recommendations that are primarily related to the opening size and favourable location within the beams depending on the tension condition [1], [2], [3].

Basic information related to this issue was established in the 1970`s and 1980`s, and the modern tests are performed by Höfflin, Aicher, Tapia, and many others [4], [5], [6], [7], [8], [9], [10], [11], [12], [13], [14], [15]. In all standards and regulations, it is emphasized that it is necessary to analyse and check the stress distribution around the opening in beams and the influence of the opening on the beam bearing capacity.

To counteract the stress concentrations, an effective reinforcement of weakened support areas is required. The aim is to restore or prevent a brittle failure of the opening region to the full capacity of a non-weakened carrier.

Openings in beams loaded on shear and bending are the subject of many European tests and projects with the aim of obtaining results and guidance during the design and analysis of stress and strain. Some of the most important standards and codes that specifically treat the mentioned issues are: Eurocode 5 [16] national annexes, DIN 1052 [17], SIA 265 [18] and others which are connected to the aforementioned standards. Based on a detailed analysis of the given regulations for the timber constructions, it can be

concluded that the rules and recommendations vary slightly, given the fact that some are based on empirical relations, while others are derived from numerical and experimental results.

As already mentioned, openings in beams are provided for different reasons such as engineering, installation, or architectural requirements. Those openings disrupt the flow of the stress perpendicular and parallel to grain in beams which may cause severe problems in transferring the load. All of this is going to be explained in the chapter two with the review of the previous important tests as well as the norms and standards.

Further in this master thesis, lab tests were conducted on 6 series, where 1 series had 8 test specimens, 2 series had 3 test specimens and 2 series had 5 test specimens each. The six series contained two reference series with and without opening beside four series with beams with an internally reinforced opening

The main purpose of these tests is to evaluate previous tests and to review the standards and norms as well as to introduce some new innovative possibilities that should be considered as an alternative to the existing ways of reinforcing the round openings.

CHAPTER 2: STATE OF THE ART

2-1 OPENINGS IN GLT AND CLT BEAMS

2-1.1 CLASSIFICATION AND DEFINITON OF OPENINGS IN ENGINEERING STANDARDS

There are five different standards and design books that are dealing with beams with openings that are going to be mentioned in this thesis:

• new standard ON B 1995-1-1:2015 [19]) (old: ON B 1995-1-1:2014 [20]; previous standard: ON B 1995-1-1:2010 [21]),

• DIN EN 1995-1-1/NA:2010 [22] (the same as DIN 1052:2008 [23])

• SIA 265:2012 [18]

• enBR:2007 [24]

• Limträhandbok (Glulam Handbook) [25]

Earlier, it was assumed that beams with openings show similar behaviour such as supports with rectangular or oblique notches (see figure 2.1). These assumptions were represented in drafts of the Eurocode 5 (prEN 1995-1-1:2002 [26]). Over the years, many experiments were made, which led to the conclusion that this method of assessment is on the unsafe side, which is why it was ultimately not included in the Eurocode 5 [19], [20].

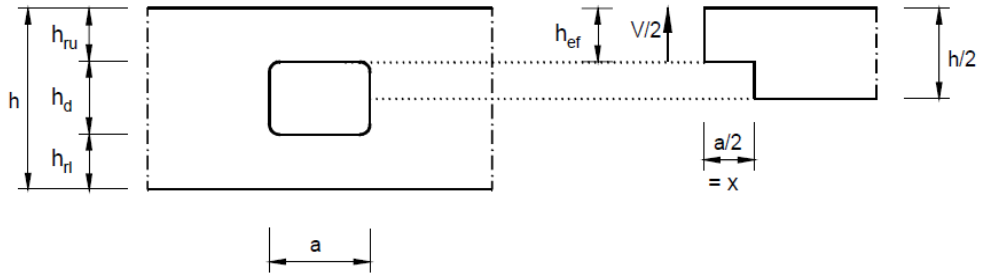

a)

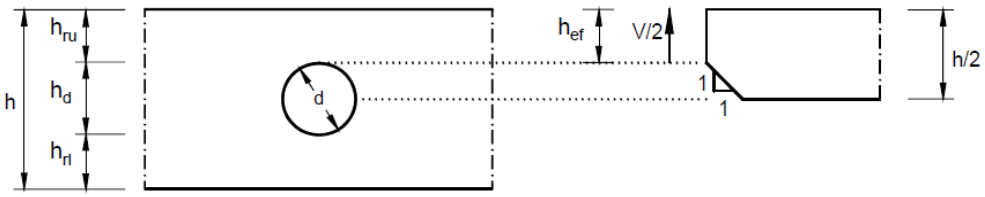

b)

Figure 2.1: Dimensions of openings in beams and respective approximation of the end notched beam design, left side: actual geometry; right side: end notched beam approximations (according to Eurocode 5 [19]) [27]

a) rectangular openings b) round openings

Determining and defining the opening properties, according to the different standards, are listed on this page of this master thesis, as well as an overview in table 2.1 [28]:

- *small openings:*
  1. if $d \leq 50\ mm$ (according to DIN EN 1995-1-1/NA:2010 [22])
  2. if $d < 0.1 \cdot h$ (according to enBR:2007 [24])
  3. if $d < \{0.1 \cdot h; 80\ mm\}$ (according to ON B 1995-1-1:2014 [20])

  Following steps are required in calculation process:

  - comply geometric limitations as shown in figure 2.2 and table 2.1.

  - no additional verification of stress analyses are necessary

  - perform stress analyses with the net cross-section

- *large openings:*
  1. if $d \geq 50\ mm$ (according to DIN EN 1995-1-1/NA:2010 [22])
  2. if $d > 0.1 \cdot h$ (according to enBR:2007 [24])
  3. if $d > \{0.1 \cdot h; 80\ mm\}$ (according to ON B 1995-1-1:2014 [20])

  Following steps are required in calculation process depending on whether the openings are unreinforced or reinforced:

  - **unreinforced openings**

    - permitted only for service classes 1 and 2

    - not allowed at ordinary tensile stress perpendicular to the grain

    - geometric limitations as shown in figure 2.2 and table 2.1

    - additional verifications (tension, shear, bending) are necessary

  - **reinforced openings**

    - allowed for service classes 1, 2 and 3

    - comply with geometric limitations as shown in figure 2.2 and table 2.1

    - additional proofs (lateral tension, shear, bending) are necessary

Table 2.1: Geometric boundaries for openings by [18], [22], [24], [19] taken from [28] (adapted)

	ON B 1995-1-1:2015 [19]		**enBR:2007 [24]**	**DIN EN 1995-1-1/NA:2010 [22]**		**SIA 265:2012 [18]**
	unreinforced	**reinforced**		**unreinforced**	**reinforced**	**reinforced**
l_A	$\geq 0.5 \cdot h$	$\geq 0.5 \cdot h$	$\geq 0.5 \cdot h$	$\geq 0.5 \cdot h$	$\geq 0.5 \cdot h$	$\geq 0.5 \cdot h$
l_v	$\geq h$	$\geq h$	$\geq h$	$\geq h$	$\geq h$	-
l_z	$\geq$ max {$1.5 \cdot h$; 300 mm} [1)]	$\geq$ max {h; 300 mm}	$\geq$ max {h; 300 mm}	$\geq$ max {$1.5 \cdot h$; 300 mm} [4)]	$\geq$ max {h; 300 mm}	$\geq$ max {h; 300 mm}
h_d	$\leq 0.15 \cdot h$ [2)]	$\leq 0.4 \cdot h$ … for external reinforcements [3)] $\leq 0.3 \cdot h$ … for internal reinforcements [3)]	$\leq 0.4 \cdot h$	$\leq 0.15 \cdot h$ [5)]	$\leq 0.4 \cdot h$ … for external reinforcements $\leq 0.3 \cdot h$ … for internal reinforcements	$\leq 0.4 \cdot h$ … for external reinforcements $\leq 0.3 \cdot h$ … for internal reinforcements
a	$\leq 2.5 \cdot h_d$	$\leq 2.5 \cdot h_d$	$\leq h$	$\leq 0.4 \cdot h$ [6)]	$\leq h$ $\leq 2.5 \cdot h_d$ [8)]	$\leq h$ $\leq 2.5 \cdot h_d$ [8)]
h_r	$\geq 0.35 \cdot h$	$\geq 0.25 \cdot h$	$\geq 0.25 \cdot h$	$\geq 0.35 \cdot h$ [7)]	$\geq 0.25 \cdot h$	$\geq 0.25 \cdot h$

[1)] $l_z \geq$ max {$1.25 \cdot h$; 300 mm}, according to [21]
[2)] $h_d \leq 0.2 \cdot h$, according to [21]
[3)] $h_d \leq 0.4 \cdot h$, according to [21]
[4)] $l_z \geq$ max {h; 300 mm}, according to [17]
[5)] $h_d \leq 0.4 \cdot h$, according to [17]
[6)] $a \leq h$, according to [17]
[7)] $h_r \leq 0.25 \cdot h$, according to [17]
[8)] Condition does not apply to [17]

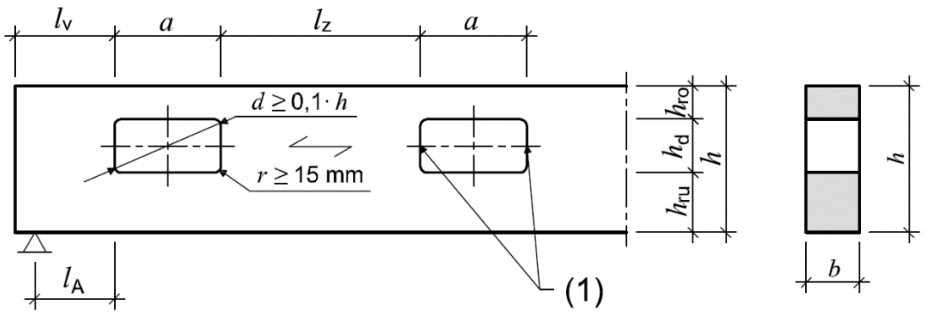

a)

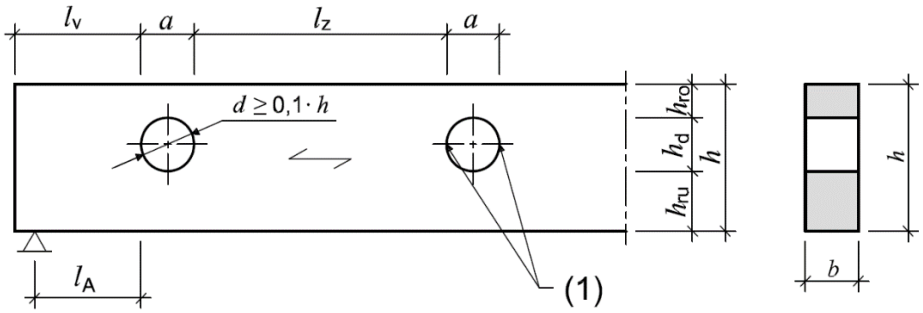

b)

Figure 2.2: Geometry definition of beams with openings [19]

a) rectangular openings ***b) round openings***

Additional remarks to standards:

According to ON B 1995-1-1:2015 [19] as well as DIN EN 1995-1-1/NA:2010 [22] the corners of rectangular openings should be rounded with a radius $r \geq 15$ mm, because non-rounded ones are more brittle to the load.

2-1.2 STRESS DISTRIBUTION AND FAILURE BEHAVIOR OF BEAMS WITH OPENINGS

The stress distribution in the vicinity of the opening has to be acknowledged as a 3D problem which can be observed in two separate dimensional problems: in length and depth axis. The opening causes disturbance in the stress flow and additional compression and tensile stresses perpendicular to the grain. A beam with an opening that is loaded with combined shear force and moment is represented in figure 2.3. The two diagonal opposite areas, *af* and *an*, are the areas with tensile stress, and the remaining ones are the areas with compression stresses. Varying the ratio between the moment *M* and the shear force *V* leads to a significant change in the stress distribution [6].

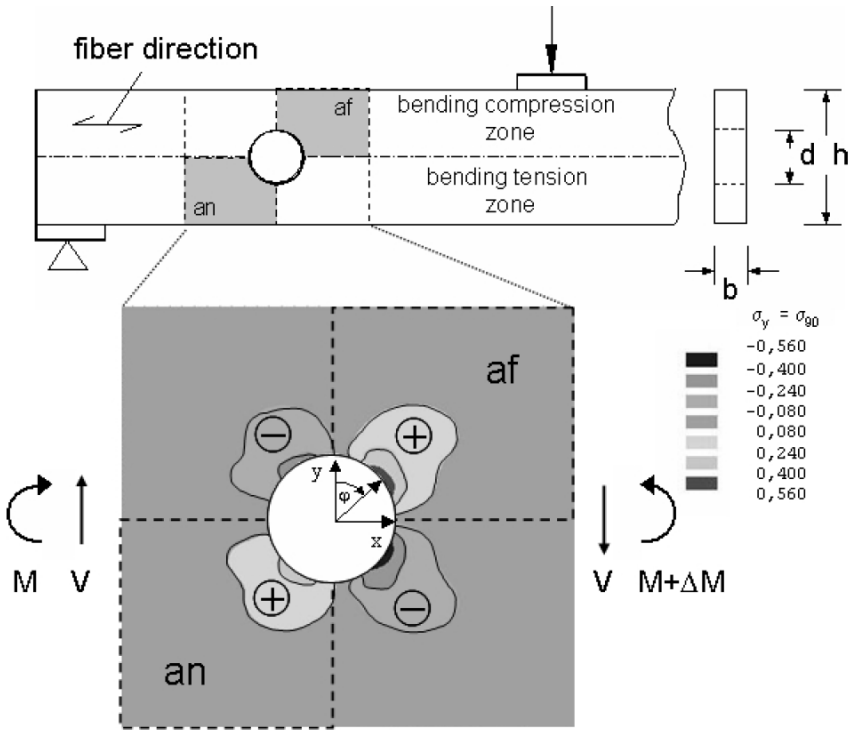

Figure 2.3: Isolines of stress distribution perpendicular to grain direction [5]

Aicher and Höfflin [6] did tests on 68 glulam beams with a single round opening placed in the middle of the beam height and loaded with a combination of bending moment *M* and shear force *V*.

In the investigations of [6] the behavior of the fracture was divided into four different steps, which is shown in figure 2.4. The first step was occurrence of the first crack on the upper tense corner of the beam. The second step was crack propagation toward the edges of beam width. In the third step, the crack spread along the whole width, while the fourth and the last step was defined as crack propagation along the beam length until the ultimate failure of the beam V_u (V_f) (figure 2.4).

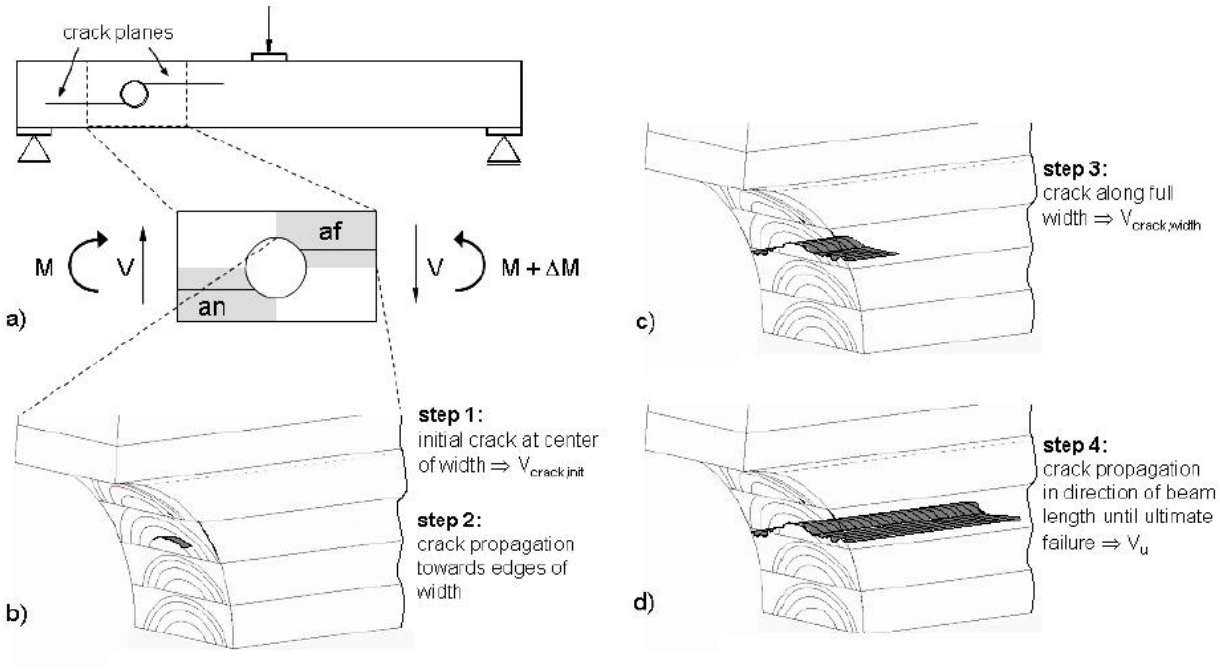

Figure 2.4: Illustration of the crack spreading [5]

The following subheadings are focused on the opening stresses in the vicinity of the opening and their calculation.

2-1.2.1 Bending stresses

The bending stress, as presented in the equation 2.1, is defined as the sum of the global bending moment M_d, and the secondary bending moments, which are caused by the shear force V_d which reaches its peak in the corners (see sections 1 and 2 in figure 2.5) [28].

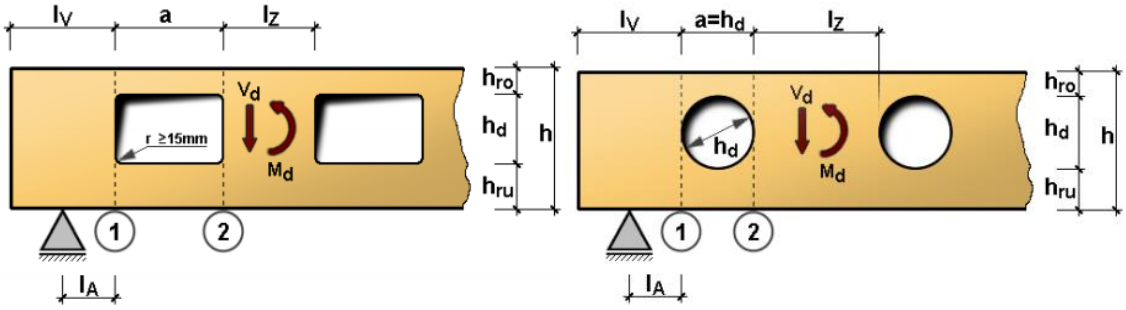

Figure 2.5: Bending moment and shear force on rectangular and round openings [29]

$$\sigma_{m,d} = \frac{M_d}{W_n} + \frac{M_{down/up,d}}{W_{down/up}} \leq f_{m,d} \quad 2.1$$

$$M_{down/up,d} = V_{up/down,d} \cdot \frac{a}{2} = \frac{A_{down/up}}{A_{down} + A_{up}} \cdot V_d \cdot \frac{a}{2} \quad 2.2$$

$\sigma_{m,d}$	...	design bending stress
M_d	...	design global bending moment on the left or right opening edge
W_n	...	effective section modulus on the net cross section; $W_n = I_n \cdot z_{max}$
$M_{down/up,d}$	...	design secondary bending moment on the opening edge
$W_{down/up}$	...	section modulus on the upper or lower girder; $W_{down/up} = b \cdot h_{down/up}^2 / 6$
$f_{m,d}$	...	design bending strength
I_n	...	moment of inertia of the net cross-section; $I_n = I_{up}' + A_{up} \cdot z_{s,up}^2 + I_{down}' + A_{down} \quad z_{s,down}^2$
$I_{up/down}'$	...	moment of inertia of the upper or lower girder
z_{max}	...	maximum distance from the section edge to the y-axis
$z_{s,down/up}$	...	distance of the center of gravity of $A_{up/down}$ to the y-axis
$A_{up/down}$	...	surface of the upper or lower girder; $A_{up/down} = b \cdot h_{up/down}$ (in the figure $h_{ro/ru}$)
$V_{up/down,d}$	...	design shear force in the upper or lower girder
$a / 2$	...	lever arm
V_d	...	design shear force on the opening edge (left or right)

According to ON B 1995-1-1:2015 [19], the secondary bending moment can be calculated with the help of the equation 2.2, whereby the shear force will be considered as if it was appearing to the right side of each edge of the opening. The shear force V_d is divided into two parts, which are equivalent to the upper and lower cross section area ($V_{up,d}$, $V_{down,d}$). As the neutral axis of the secondary bending moment is assumed to be in the center of the opening, the lever arm in the case of rectangular openings is set to $a / 2$ for each corner. Multiplying the values of the lever arm for each corner of the rectangular opening with the corresponding lateral force, the secondary bending moments can be determined. All of the four secondary bending moments in the corners of the rectangular opening are of the same value, if the opening is placed symmetrically along the beam height [28].

The standard ON B 1995-1-1:2015 [19] further states, that the secondary moment can be neglected for beams with round openings, whereby only the verification of the bending moment, considering the remaining net cross section, must be performed. According to enBR:2007 [24] as well as DIN EN 1995-1-1/NA:2010 [22], the secondary moment can be neglected in general.

2-1.2.2 Shear stresses

The calculation defined in the ON 1995 1-1: 2015 [19] is modified to fit for the beams with openings (see equation 2.3). The coefficient k_τ, defined in the equation 2.4, takes into consideration the shear stress concentrations in the corners of the opening. Although it applies for both, rectangular and round openings, the coefficient k_τ imply a conservative results for round openings [28].

$$\tau_d = k_\tau \cdot \frac{1.5 \cdot V_d}{b_{ef} \cdot (h - h_d)} \leq f_{v,d} \quad 2.3$$

$$k_\tau = 1{,}85 \cdot \left(1 + \frac{a}{h}\right) \cdot \left(\frac{h_d}{h}\right)^{0.2} \quad 2.4$$

τ_d	...	design shear stress
k_τ	...	coefficient for calculation of the maximum shear stress
V_d	...	maximum design shear force
$f_{v,d}$	...	design shear strength

The equations 2.3 and 2.4 can also be used for beams with reinforcements in forms of steel rods, which are screwed or glued-in under the angle of 90° to the grain, because the bending and shear stiffness of the beam remain largely unaffected by the reinforcement. For those reinforced with screws which are inclined under 45° to the grain, the shear stress concentrations with the $k\tau$-coefficient is very conservative due to increased stiffness values caused by the reinforcements [28].

Due to the fact that beams with round openings have a favourable opening shape which causes substantially lower stress concentrations than in beams with rectangular openings, it can be assumed that the result of this action is not in accordance to the equations 2.3 and 2.4 [28].

The enBR:2007 [24] states that, in addition to the verification of tensile stress perpendicular to the grain further stresses have to be verified on the net cross section. These results are a proof of the shear stress without considering the stress concentrations around the edge of round or rectangular openings (see equation 2.5).

$$\tau_{d} = \frac{1.5 \cdot V_{d}}{A_{net}} = \frac{1.5 \cdot V_{d}}{b \cdot \left(h - h_{d}\right)} \leq f_{v,d} \qquad 2.5$$

2-1.2.3 Tensile stress perpendicular to the grain

An opening in a glulam beam, under application of a bending load, disturbs the distribution of bending and shear stresses. Large tension stresses perpendicular to the grain appear at explicit areas at the opening edges (figures 2.6 a, b). The peak of tension stress perpendicular to grain is around the edges of the opening (figures 2.7 a, b). On the upper right and down left side of the opening, the cracks appear under the angle of 60° and 180 + 45° respectively, due to the influence of the applied load combination of the bending moment and shear force (see figure 2.7 a). In the case of applying a pure bending moment, this places are set to the opening periphery by the angles of 60° and 360° - 60° (see figure 2.7 b). The differences between applied loads are causing the appearance of the crack on different places on the periphery of the opening. The value of the tensile stress area decreases exponentially with increasing distance from the opening. Loading conditions of the beam are influencing the location and the magnitude of the maximum tensile stress perpendicular to grain and can be related to the proportion of bending moment *M* to shear force *V*. Also the ratio of the opening diameter *d* to beam height *h* has a strong influence on tension stress perpendicular to grain. Based on these findings, the tension stress perpendicular to the grain can be expressed as a function of opening diameter *d*, beam height *h*, and bending moment *M* to shear force *V* ratio (equation 2.6) [7]:

$$\sigma_{y}(x, y) = f\left(M / V; d / h\right) \qquad 2.6$$

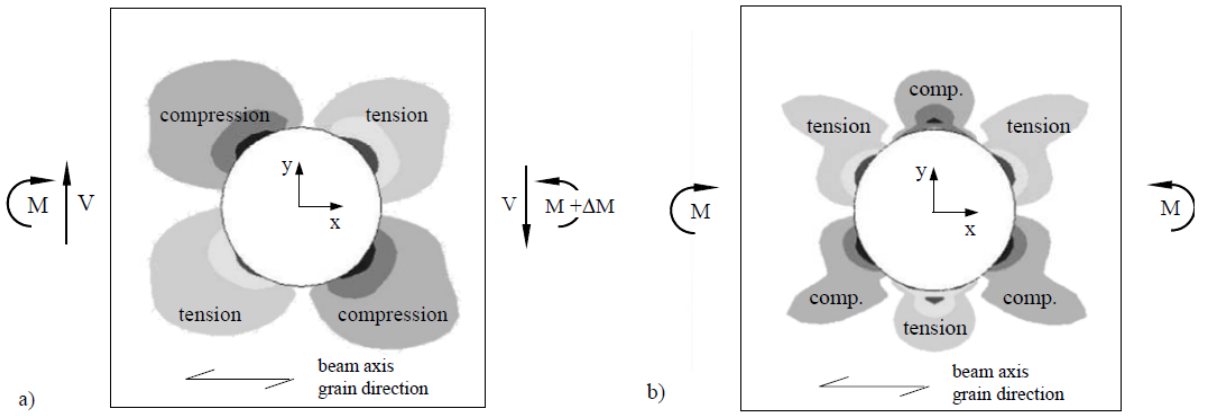

Figure 2.6: Tension and compression stress fields perpendicular to grain at the opening periphery depending on the M / V-ration and opening height to opening diameter ratio d / h = 0.4; a) M / V = 1.5 · h; b) M / V = ∞ (pure moment) [7]

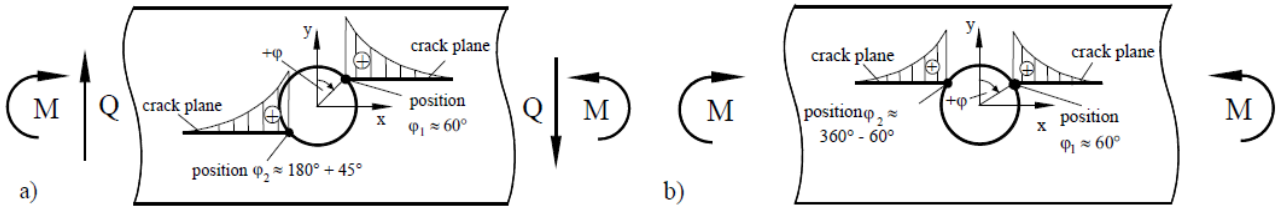

Figure 2.7: Schematic representation of distribution of tension stress perpendicular to grain along highest stressed sections at the opening periphery for two very different moment / shear force ratios [7]

a) M / V small ***b) M / V = ∞ (pure moment)***

Determination of the tensile stresses perpendicular to the grain

The calculation of the transverse tensile stress perpendicular to the grain $\sigma_{t,90,d}$ could be found e.g. in standards ON B 1995-1-1:2015 [19], ON B 1995-1-1:2014 [20], DIN EN 1995-1-1/NA:2010 [22], SIA 265:2012 [18], enBR:2007 [24].

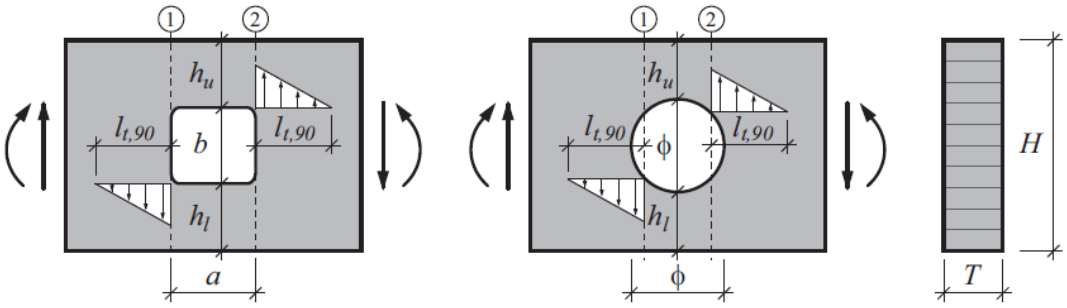

Figure 2.8: Tensile stresses perpendicular to the grain in the corners of rectangular (left) and at the edges of the round (right) openings based on ON B 1995-1-1:2015 [19] and DIN EN 1995-1-1 / NA:2010 [22], [30]

The tensile stresses perpendicular to the grain are determined according to ON B 1995-1-1:2015 [19] using the equation 2.7 and shall not exceed the design value of the tensile strength perpendicular to the grain $f_{t,90,d}$.

The design tensile force perpendicular to the grain $F_{t,90,d}$ is composed of a shear force part and bending moment part acting on the edge of the opening and is determined according to the Eq. 2.8.

$$\sigma_{t,90,d} = \frac{F_{t,90,d}}{0.5 \cdot l_{t,90} \cdot b_{ef} \cdot k_{t,90}} \leq f_{t,90,d} \qquad 2.7$$

$$F_{t,90,d} = F_{t,V,d} + F_{t,M,d} = \left[\frac{V_d \cdot h_d}{4 \cdot h} \cdot \left(3 - \frac{h_d^2}{h^2}\right)\right] + \left[0.008 \cdot \frac{M_d}{h_r}\right] \qquad 2.8$$

$\sigma_{t,90,d}$	...	design value of tensile stress perpendicular to the grain
$F_{t,90,d}$	...	design value of tensile force perpendicular to the grain, determine for both opening edges $F_{t,90,d} = \max \{F_{t,90,d,left}; F_{t,90,d,right}\}$
$l_{t,90}$	...	load distribution length; $l_{t,90} = 0.5 \cdot (h_d + h)$ for rectangular openings; $l_{t,90} = 0.35 \cdot h_d + 0.5 \cdot h$ for round openings (by [19]: factor 0.353 instead of 0.35) (additional condition $l_{t,90} \leq 1.5 \cdot h_d$)
b_{ef}	...	effective width of the beam; $b_{ef} = k_{cr} \cdot b$
$k_{t,90}$	...	factor which takes into account the beam height; $k_{t,90} = \min \{1; (450 / h)^{0.5}\}$, h in mm
$f_{t,90,d}$	...	design tensile strength perpendicular to the grain
$F_{t,V,d}$	...	design tensile force perpendicular to the grain part of the shear force V_d
$F_{t,M,d}$	...	design tensile force perpendicular to the grain part of the bending moment M_d
V_d	...	design value of shear force on the left or right edge of the opening
h_d	...	opening height; for round openings $h_d = 0.7 \cdot d$ may be used
h	...	beam height
M_d	...	design value of the moment at the left or right edge of the opening
h_r	...	opening dimension; $h_r = \min \{h_{r,down}; h_{r,up}\}$ for rectangular openings; $h_r = \min \{h_{r,down} + 0.15 \cdot h_d \quad h_{r,up} + 0.15 \cdot h_d\}$ for round openings ($h_l = h_{down}$; $h_u = h_{up}$ in figure)

For the calculation of the effective beam width b_{ef} the crack factor k_{cr}, has to be defined in accordance to the standard ON EN 1995-1-1:2015 [19]: $k_{cr} = 0.67$ for solid timber and glue-laminated timber; $k_{cr} = 1.0$ for other wood-based products. In national annex F of [19] the crack factor is defined as $k_{cr} = 1.0$ for solid timber, glue-laminated and other wood-based products. In the DIN EN 1995-1-1/NA:2010 [22], the beam width b is used instead b_{ef}.

In the enBR:2007 [24], the verification of the tensile stresses perpendicular to the grain is performed without the consideration of k_{cr} and $k_{t,90}$.

According to the standard [19] a triangular distribution of the design tensile stress perpendicular to the grain $\sigma_{t,90,d}$ can be assumed over the load distribution length $l_{t,90}$ (see figure 2.9). The maximum value of $\sigma_{t,90,d}$ is at φ = 45°, measured from the vertical axis of the beam (Fig. 2.9).
The tensile force $F_{t,V,d}$ represents the half part of the shear stress τ_{xy} of an undisturbed beam, which cannot be transferred regularly over the remaining cross section [28].
The moment part of the tensile force perpendicular to the grain of the eq. 2.8, $F_{t,M,d}$, was determined semi-empiric [31].

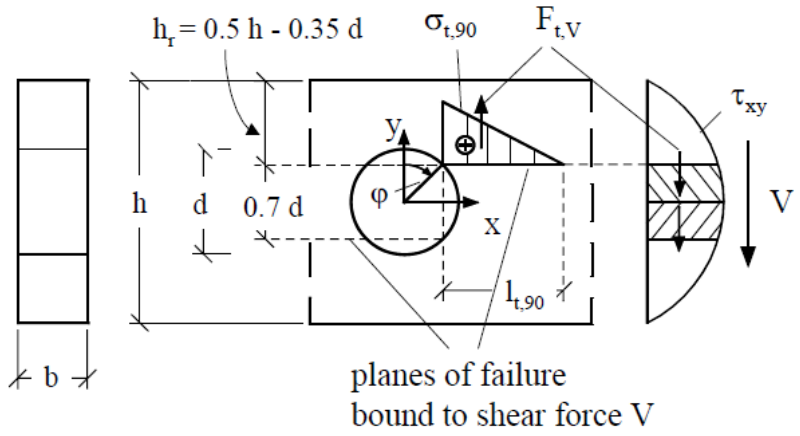

Figure 2.9: Triangular distribution of the tensile stress perpendicular to the grain and the shear forces redistribution [4]

2-1.2.4 Combination of shear and perpendicular to the grain stresses

The worst case scenario in loading timber beams is a combination of tensile and shear stresses. Series of case studies were conducted by Spengler [32] in 1982. Spengler investigated the behavior of the shear strength of spruce under a combined load of shear and tensile or compression stresses perpendicular to the grain. In figure 2.10 the shear test specimen [32] is shown. The load introduction onto the board's laminations was carried over by adhered plates. To avoid stress peaks at the level of action, rounded cavities were planned in the end regions of the specimens. Tests with tube specimens were introduced by [Hemmer 1984] [32], where he investigated different stress combinations of tubular specimens of silver fir, see figure 2.11. Transverse stresses were applied by internal pressure in the tube or by external compression of the tube. The shear stress occurred due to torsion moment.

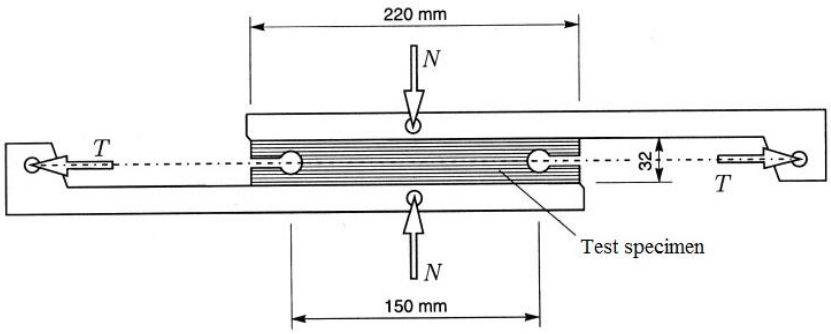

Figure 2.10: Test set of [Spengler 1982], from [32]

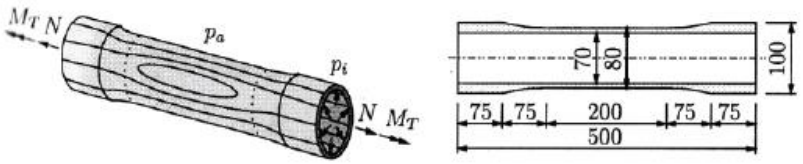

Figure 2.11: Test set of [Hemmer 1984], from [32]

The test results of these two previous mentioned tests are to see in figure 2.12.

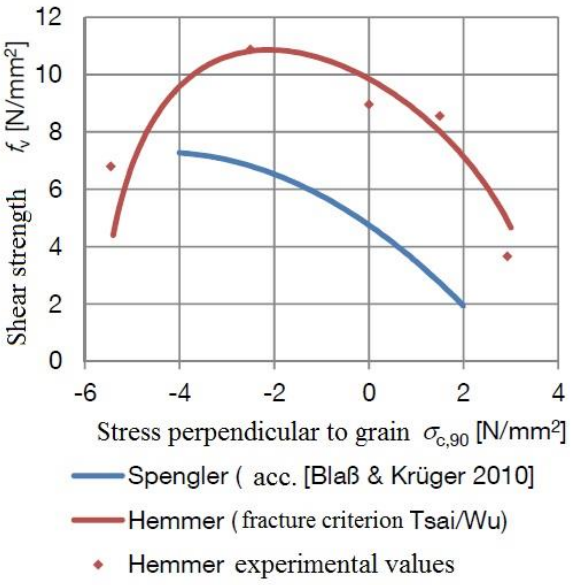

Figure 2.12: Comparison of the regression curves of the experimental results of [Spengler 1982] and [Hemmer 1984], from [32]

For the corresponding representation of the results determined by [Spengler 1982] [32], there were 740 tests and the interaction behavior was the following:

$$\tau = 4.75\ N/mm^2 - 1.15 \cdot \sigma_{\perp} - 0.13 \cdot \sigma_{\perp}^2 \qquad 2.9$$

The increase in the shear strength under combined compressive stress perpendicular to the grain can clearly be seen in figure 2.12.

The interactional behavior should be taken into account when it comes to design codes. The Swiss design standard for timber structures SIA 265:2012 [18] states the following verification for the combined stress of shear parallel and the normal force perpendicular to the grain:

$$\left(\frac{f_{c,90,d} + \sigma_{90,d}}{f_{c,90,d} + f_{t,90,d}}\right)^2 + \left(\frac{\tau_d}{f_{v,d}}\right)^2 \left[1 - \left(\frac{f_{c,90,d}}{f_{c,90,d} + f_{t,90,d}}\right)^2\right] \leq 1 \qquad 2.10$$

$\sigma_{90,d} = \sigma_{t,90,d}$ ... for the tensile stress perpendicular to the grain
$\sigma_{90,d} = -\sigma_{c,90,d}$ ... for the compression stress perpendicular to the grain

The principles enclosed in the SIA 265:2012 [18] are not based on test values. The interaction behavior of the curve from an interpolation between the two known reference points of the pure transverse tensile and shear stress as well as results of extrapolation of the lateral-pressure area are shown in figure 2.13.

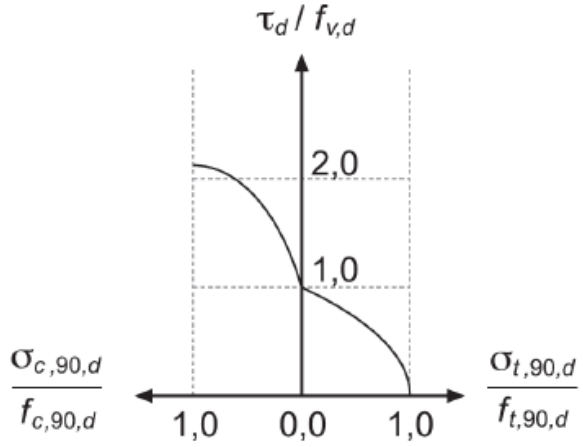

Figure 2.13: Interaction of transverse compression and shear [32]

It is noticeable that, the maximum compression strength occurs simultaneously with the maximum shear strength, which is approximately double the value of the shear strength compression perpendicular to the grain. In terms of mechanics, one might expect that if the maximum compression stress perpendicular to the grain occurs, it will lead to a failure and therefore no additional loads can be taken.

2-1.3 UNREINFORCED OPENINGS

2-1.3.1 Austrian standards

In Austria, Eurocode 5 [19] with national annexes F is used as the leading standard for timber constructions.

In ON B 1995-1-1:2010 [21], annex C2, ON B 1995-1-1:2014 [20], annex F2, ON B 1995-1-1:2015 [19], annex F the beams with opening are defined, but only for glue laminated timber (GLT) and laminated veneer lumber (LVL).

According to ON B 1995-1-1:2015 [19], annex F, in order to define an opening, the opening diameter d has to be wider than 80 mm or $d \geq h / 10$ where h is the beam height.

Remaining geometric boundaries for unreinforced openings in ON B 1995-1-1:2015 [19] are calculated according to table 2.1 and figure 2.2 (2-1.1).

Verifications of stress loads like tensile stress perpendicular to grain, shear force and bending moment, are addressed and stated in couple of previous sections.

Tensile stress perpendicular to grain presents special challenge for unreinforced openings in GLT beams. Therefore, special attention should be dedicated to verifying the tensile stress perpendicular to the grain.

In ON B 1995-1-1:2015 [19] without national annexes, no allegation for openings are found.

2-1.3.2 Other standards

In Eurocode 5, **pr EN 1995-1-1:2002 [26], part 6.6**, some general principles for verification of the beams with openings are given, but were left out in the following draft prEN 1995-1-1:2003 [33] due to progressive results.

In **enBR:2007 [24], part 6.7.4,** beams with openings made of various types of timber like GLT and LVL are defined.

Principles of calculation and verification of tensile stress perpendicular to the grain, shear force and bending moment are very similar to ON B 1995-1-1:2015 [19], annex F, with the exception of b_{ef} (effective width of the beam), which is sized with b (beam width).

Remaining geometric boundaries for unreinforced openings by enBR:2007 [24] are calculated according to table 2.1 and figure 2.2 (2-1.1).

In German standard **DIN EN 1995-1-1/NA:2010 [22], part NCI NA.6.7 and DIN 1052:2008 [23], part 11.3,** there are definitions and calculating methods for openings in timber constructions. Differences to ON B 1995-1-1:2015 [19] are that openings are defined with a diameter of $d \geq 50$ mm as well as the enBR:2007 [24] consider cracks in the beam which would reduce the width b. The remaining geometric boundaries for unreinforced openings of [22] are calculated according to table 2.1 and figure 2.2 (2-1.1).

The Swiss Norm **SIA 265:2012 [18], part 5.24.** only proposes general guidelines like determining the openings shear force and bending moment in the same way like for the end notched beam, which was also proposed in the draft of the Eurocode 5, but further abandoned as it is inexact.

Swedish regulations are based on **pr EN 1995-1-1:2002 [26]**. For the purpose of this thesis, **Limträhandbok: Glulam Handbook** [25] was used. The calculation process is very similar to already mentioned ones in German and Austrian standards.

2-1.3.3 Experimental tests

As early as 1977 Kolb and Frech [34] have performed tests on unreinforced glulam beams. The specimens were divided into three groups with different forms and geometry parameters of openings:

- Group I: A (8400 mm x 550 mm x 80 mm; without openings), F and K, where F and K had two reinforced openings.
- Group II: Type D, G, E and H had two openings outlying 50 cm and 100 cm from each support were equipped with quadratic (25 cm x 25 cm) and rectangular (15 mm x 25 mm) shaped openings.
- Group III: C, B and J. C and B (type B, C: 16000 mm x 1000mm x 140 mm) were beams with quadratic openings 30 cm x 30 cm and round ones with diameter of 30 cm respectively. Type J were beams with nine openings over the whole beam length each one with a diameter of 30 cm (see figure 2.14). Some of the beams were also reinforced.

There was also the reference beam without the opening in it (type A). The beams were 8 m long and tested in a 4-point-bending configuration. The deflection was measured in five different places, while tensile stress was calculated with the help of the mechanical extensometer, which measured elongations, in the corners of the rectangular openings, and on the tangent regions of the opening, for round ones, where the maximum tensile stress was expected. The strain was measured around the opening with the help of 15 measuring places.

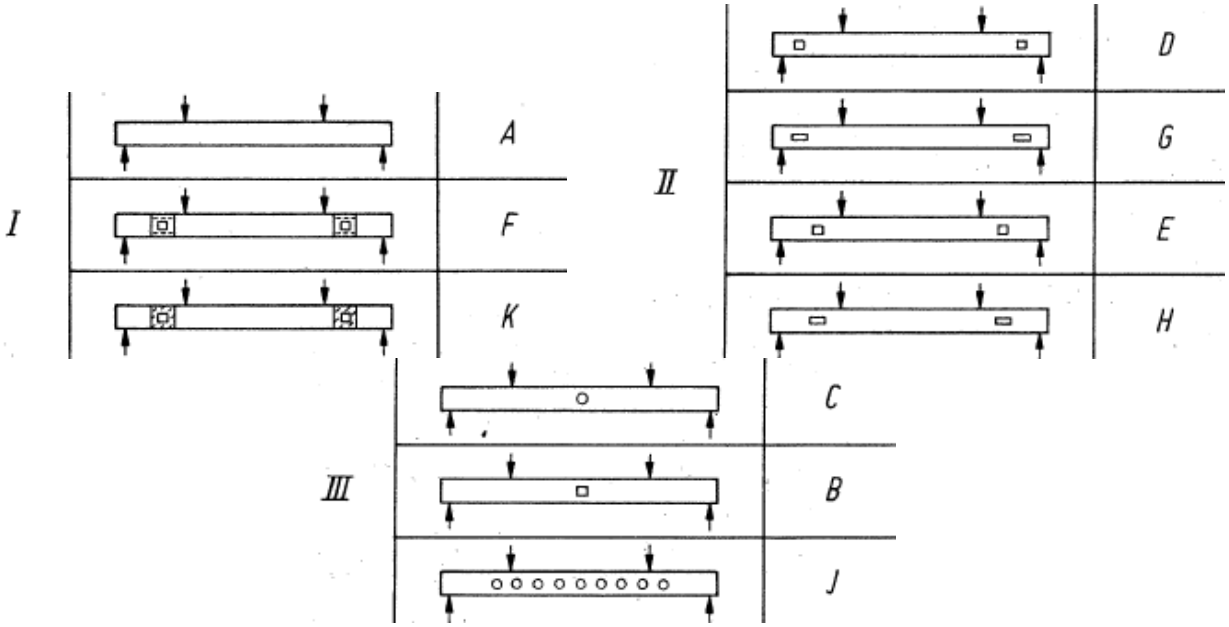

Figure 2.14: Schematic presentation of the tested beams [34]

Those experimental tests have shown that beams without openings (14 specimens total), as well as those with openings in the middle of the beam and the reinforced ones with external plywood reinforcement, could bear almost the same load. It is also apparent from the research, that rectangular openings are more brittle then round ones because of the stress concentration in the edges. In this research, the rectangular openings had no rounded edges, because the high brittle effect of the angular corners of the rectangular openings was not acknowledged at that moment. With the increase of the size of the opening, the load-bearing capacity decreased. First cracks occurred, as expected, at the upper left and lower right edges of the rectangular openings and at the upper left and lower right tangent of the round ones, respectively (figure 2.15). Every beam failed due to a tensile stress perpendicular to the grain or a combination of tensile stress perpendicular to the grain and bending moment.

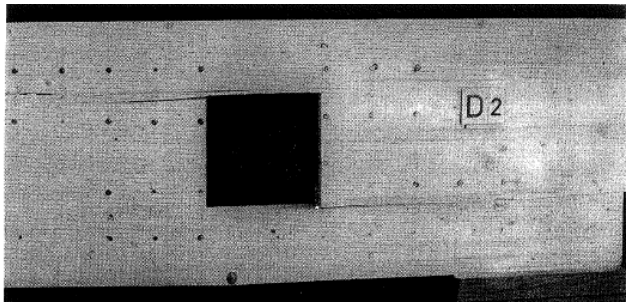

Figure 2.15: Cracks in tensile stress area on the D2 beam [34]

In 1985, Kolb and Epple [31] also did an extra research on glulam beams with openings. This time the beams were classified and divided into different groups, taking into consideration whether the beams were reinforced or not, the type of reinforcement, the test configuration, how the beam was loaded and also the geometry of the opening.

It was assumed that the stress distribution is the same for rectangular and round openings (see figure 2.16).

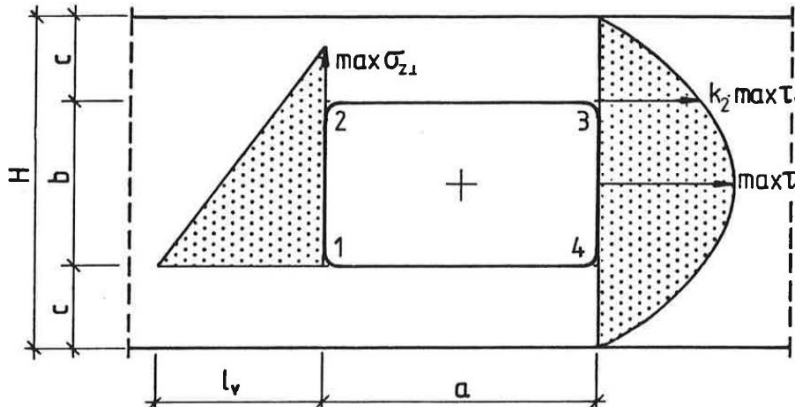

a)

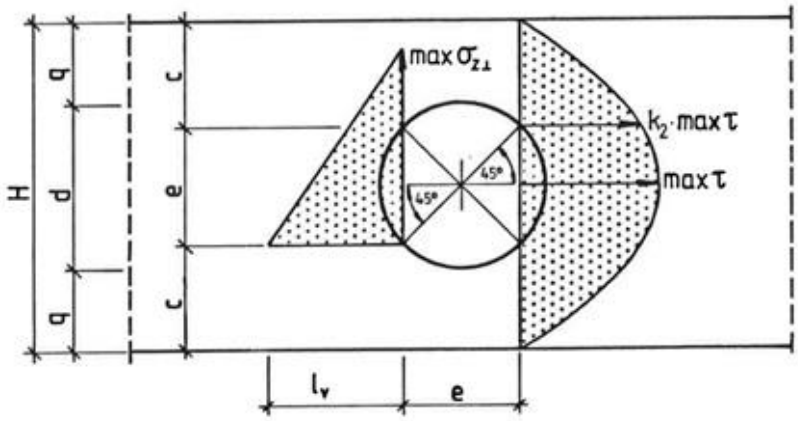

b)

Figure 2.16: Stress distribution on the rectangular a) and round b) openings [31]

As the stress distribution was known to be different for the beams with and without opening, the *k* factors were introduced for conversion of the shear stress through the beam on the places of openings in beams.

The beams were made of GLT. At that time DIN 1052 [31] (unknown year of the standard, taken out of the Kolb and Epple report) had a proposal for beams reinforced with plywood only. These tests were conducted to get some new findings for regulations and limits for calculations of beams with openings. Finite element calculations were performed to determine the stress distribution for beams with openings. Gained from this theoretical knowledge of the stress distribution, first calculation proposals for the verification of beams with unreinforced openings were established.

The research by Kolb and Epple [31] showed similar results as the one from [34]. Almost every beam failed due to tensile stress perpendicular to grain, followed by a shear stress failure along the beam length. As in the last tests by Kolb and Frech [34], beams with a round opening in the middle of the beam failed only due to the bending moment except those with the same geometry but with rectangular openings, which failed by tensile stress perpendicular to grain too. Beams with a single opening near the support collapsed only due to tensile stress perpendicular to grain. The reinforced beams could bear the greatest loads, followed by those with only one opening and those with two or more openings, which corresponded to the calculations of the design.

In 2001, Aicher and Höfflin [11], made a contribution to the analysis of beams with openings with FE model for the DIN 1052:2000 [35]. General stress distributions perpendicular to the grain around the opening are given in figures 2.17 and 2.18. Tension stress areas appear on the opposite sides of the opening for the pure shear force (see figure 2.18). Tension stress areas caused by the pure bending moment are to be seen on down opening side (see figure 2.17) and compression stresses on the upper opening edge.

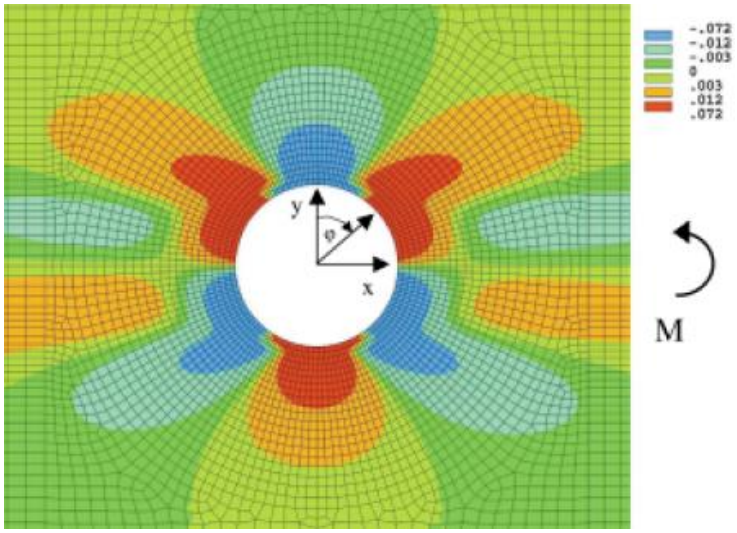

Figure 2.17: Stress distribution on the round opening edge due to constant moment action [11]

Aicher and Höfflin [11] were able to improve the knowledge for the design of the openings with their contribution. Previous assumptions like those of the DIN 1052:2000 [35] and other theoretical ones according to [11] were mostly wrong. In the FE model of [11] it was shown that the assumptions in DIN 1052:2000 [35] concerning the maximum stress perpendicular to the grain at the edge vicinity was set too low because the assumed distribution length was set as too long while the tensile force perpendicular to the grain was too low (see equation 2.3), so there was a need for a new calculation proposals.

In literature, it was wrongly assumed that the bending moment cannot cause tension stress perpendicular to the grain in the periphery of the opening, which was here proved to be very wrong.

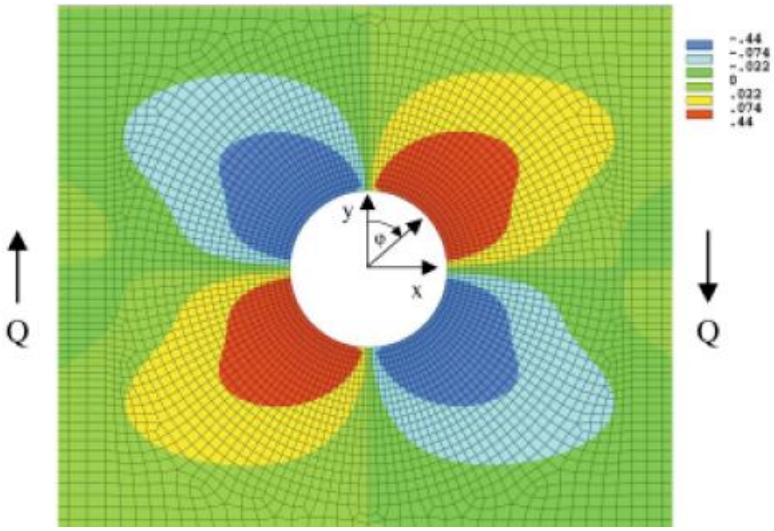

Figure 2.18: Stress distribution on the round opening edge due to pure shear force action [11]

The conclusion of this experimental analysis based on FEM was that shear force and bending moment stay in correlation and that the distribution of tensile stress is strongly dependent on the M / V ratio.

Aicher and Höfflin [12] did experimental tests on beams with round openings. The beam height varied from h = 450 mm to h = 900 mm and the beam height to opening diameter ratio d / h also varied from 0.2, 0.3 to 0.4. Moment to shear force ratios were M / V = 1.5 and M / V = 5.0. The schematic view of the tested

beams is represented in figure 2.19. The timber strength class used for all tested beams was GL32h. During these tests, all beams were observed on three failure stages:

- the crack initiation in the opening periphery in the tension stress region
- spreading of the crack through the whole width of the beam; tension stress failure
- the crack propagation occurs throughout the length of the beam, starting from the opening and heading to the support which is closer to the opening; shear stress failure

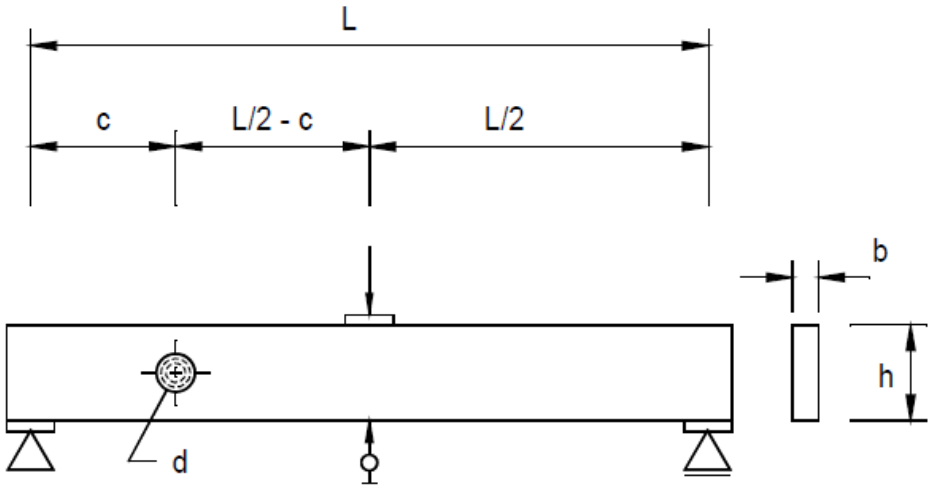

Figure 2.19: Schema of the test configuration beams [12]

In 2007, Aicher and Höfflin [6] were discussing two different approaches dealing with the problem of glulam beams with round openings: fracture mechanics design according to the Eurocode 5 [6] (the exact year is unknown and taken out of [6]), based on similarity between end notched beams and also strength of material design out of the DIN 1052 [6] (the exact year is unknown and taken out of [6]), which is based on bending moment and shear force calculation. Also the Weibull design model was introduced. The Weibull model is based on mechanical problem of glulam beams with round openings and deals with the theory of probability which describes failures in beams made of brittle materials. The design model for glulam beams with round openings presented in Weibull [12] overcomes the deficiencies of the code design approaches. Both, size effect and moment influence the load capacity in a transparent manner.
Through different corrected formulas (similar to those in DIN 1052 [6] (the exact year is unknown and taken out of [6])) and stress distribution factors, a new calculation method was established which was validated by experimental tests. The beams used were all produced in European strength class GL32h. The opening was always centered in height at least $1.5 \cdot h$ away from supports and loads (figure 2.20). The d / h –ratio was 0.2, 0.3 and 0.4, which was the same like in [12]. The beam heights were 450 mm and 900 mm and width was 120 mm. The M / V ratio was 1.5. The cracks appeared on the upper side closer to load application and lower side closer to support.

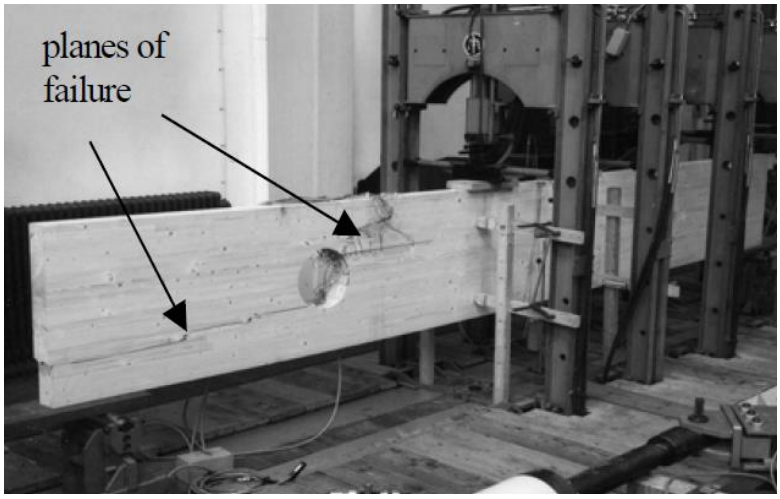

Figure 2.20: Test set up with specimen at failure [7]

The tests lead them to the conclusion that the Weibull based model produces good predictions for the beams with large scale of relative opening sizes and absolute beam size.
In 2008, Aicher and Höfflin [5] made further investigations about stress distribution on glulam beams. They tested a total of 68 beams made of strength class GL32h with dimensions of 450 mm and 900 mm in height, *b* 120 mm in width, lengths of 6750 mm, 9450 mm and 9950 mm, *M / V* ratios of 1.5 and 5, relative opening sizes of *d / h*-ratio 0.2, 0.3 and 0.4. Furthermore, some beams were slightly curved, with a h / r_m-ratio of 0.03, where r_m was the radius curvature at the middle of the beam (see figure 2.21).

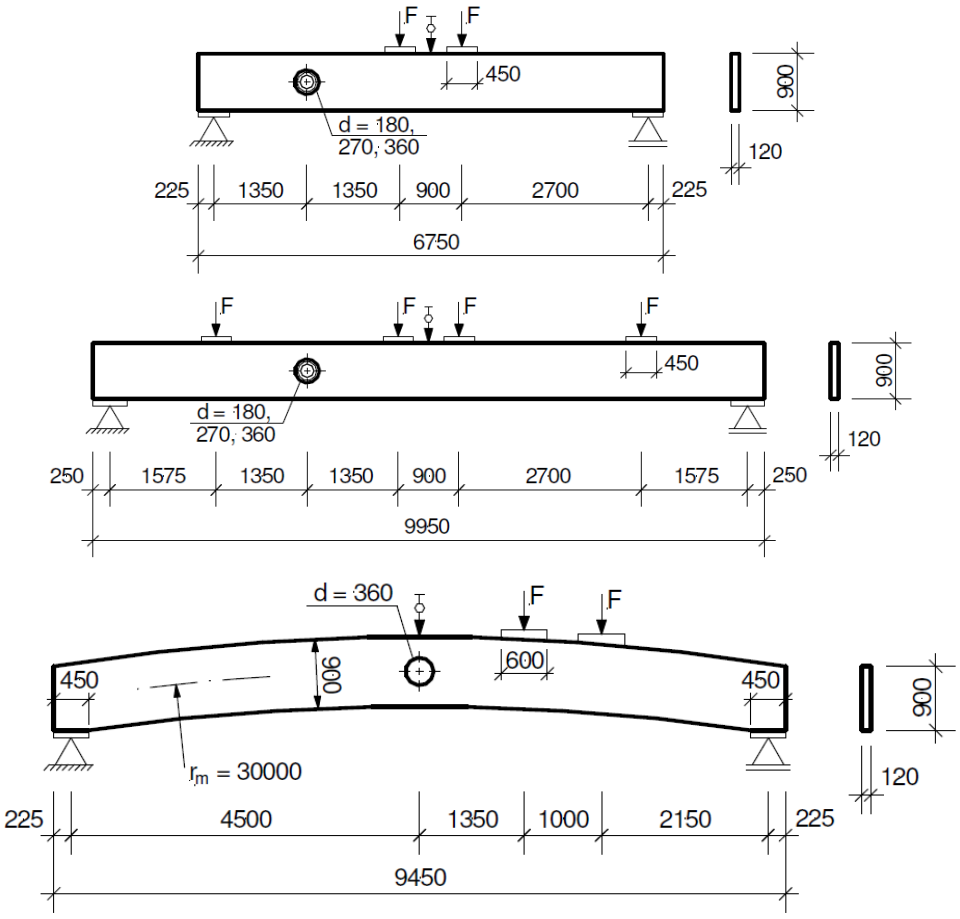

Figure 2.21: Geometry set up of the test beams [6]

The four stages of beam failure were investigated and the main shear forces were established (see 2-1.2).
The Weibull model was used to estimate the ultimate load (load over full beam width) and the shear force capacities [12].
Danielsson and Gustafsson [36] did a research on glulam beams with quadratic openings. Nine beam series, with four beams for each series, two different test setups, different heights, opening sizes, curves and strength classes (see table 2.2 and figure 2.22). All the beams were made of spruce. The material strength class for homogeneous material corresponds to GL32h. For the AMc series the strength class was a combination of lamination strength class LS22 and LS15.

Table 2.2: Geometric boundaries test beams [37]

Test series	Number of test series	Test setup	Opening placement	Strength class type	Beam size TxH [mm]	Hole size axb [mm]	Curvature r* [mm]
AMh	4	1	Middle	homogeneous	115x630	210x210	25
AMc	4	1	Middle	combined	115x630	210x210	25
AUh	4	1	Upper	homogeneous	115x630	210x210	25
ALh	4	1	Lower	homogeneous	115x630	210x210	25
BMh	4	2	Middle	homogeneous	115x630	210x210	25
CMh	4	1	Middle	homogeneous	115x180	60x60	7
CUh	4	1	Upper	homogeneous	115x180	60x60	7
CLh	4	1	Lower	homogeneous	115x180	60x60	7
DMh	4	2	Middle	homogeneous	115x180	60x60	7

*curvature of the rectangular opening corners

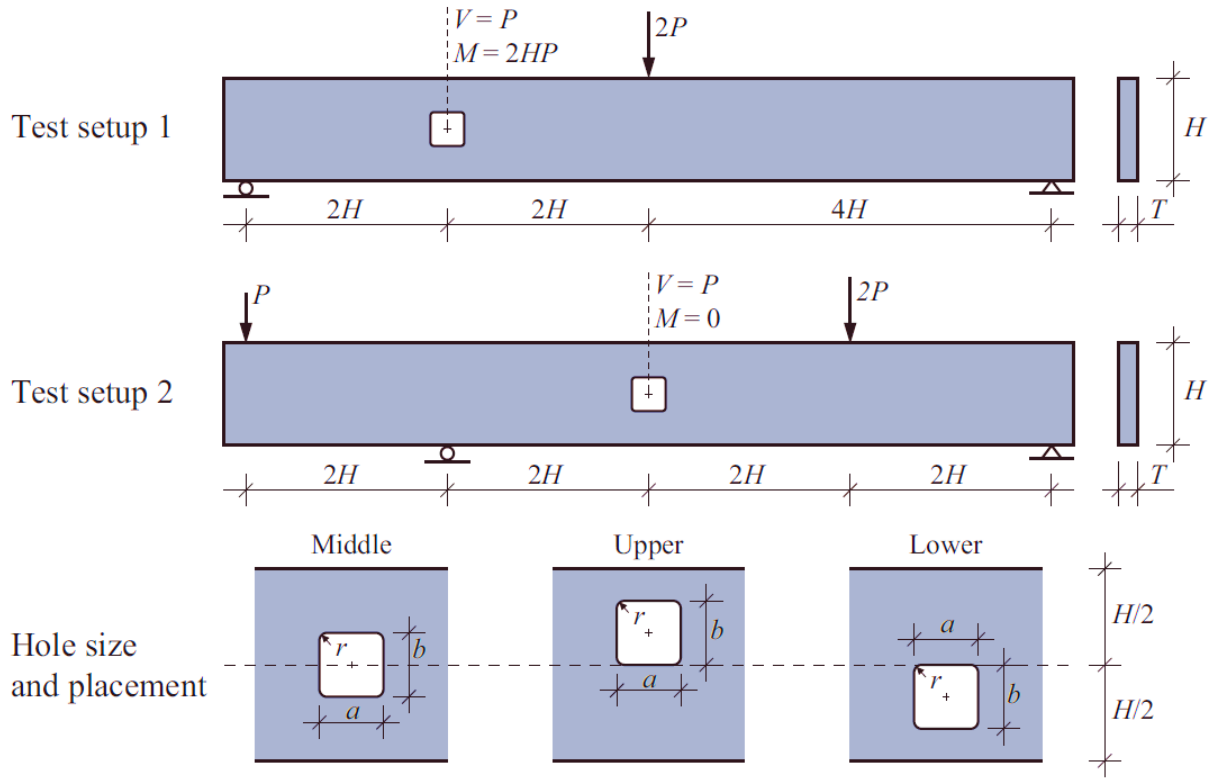

Figure 2.22: Geometry set up of the beams [36]

Three different load levels or rather shear forces were determined in order to compare the results. The crack initiation shear force V_{c0} is the load level at which the first crack appears in one of the corners. The V_c is the crack shear force by which the crack spread over the opening width. Maximum shear force V_f is the force which causes the shear failure of the beam (figure 2.23).

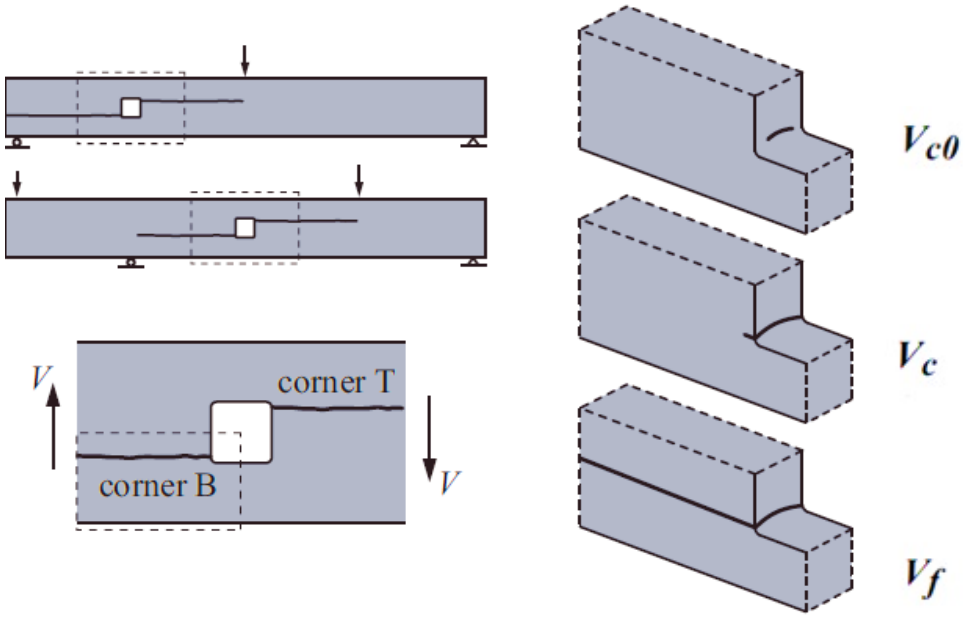

Figure 2.23: Definition and illustration of load levels [36]

2-1.4 REINFORCED OPENINGS

The basic idea of the reinforcement design is based upon the assumption that the shear stresses cannot be transferred through the opening. Therefore, a part of the resulting shear force is relocated to an equivalent tension and compression force perpendicular to the grain of the remaining cross-sections above and below the opening. The resulting tension force perpendicular to the grain $F_{t,90}$ forms the basis of the design of beams with unreinforced and reinforced openings.

As shown in table 2.1, different standards deal with the problem of reinforcing beams with openings. An overview of regulations in standards will be introduced in next couple of sections of this master thesis.

Reinforcement measures can be divided into two big groups:

- external reinforcement (glued-on LVL panels)
- internal reinforcement (screws, threaded rods and glued-in rods).

2-1.4.1 External reinforcement

2-1.4.2.1 Austrian standards

In ON B 1995-1-1:2015 [19] annex F.3 (ON B 1995-1-1:2010 [21], annex C3 and ON B 1995-1-1:2014 [20], annex F3,) only the openings in glue laminated timber and laminated veneer lumber beams are defined.

According to ON B 1995-1-1:2015 [19] allowed external reinforcements are timber products or boards that are externally glued onto the beam. Reinforcement is applied to take the tensile stresses perpendicular to

grain in the beam. The application of the reinforcing panels according to ON B 1995-1-1:2015 [19] is limited to beam widths up to 240 mm. With larger widths the sufficient load distribution cannot be ensured within the beam. Dimension limitations which may not be disregarded (see figure 2.24 a) and b)) are set to: $0.25 \cdot a \leq a_r \leq 0.3 \cdot (h_d + h)$ and $0.25 \cdot a \leq h_1 \leq h_r$.

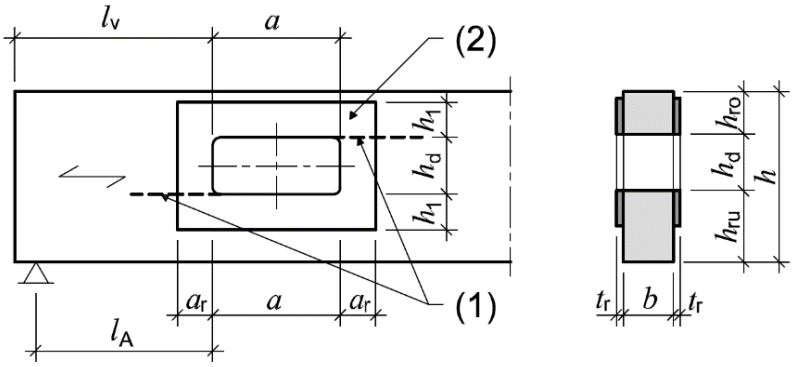

a)

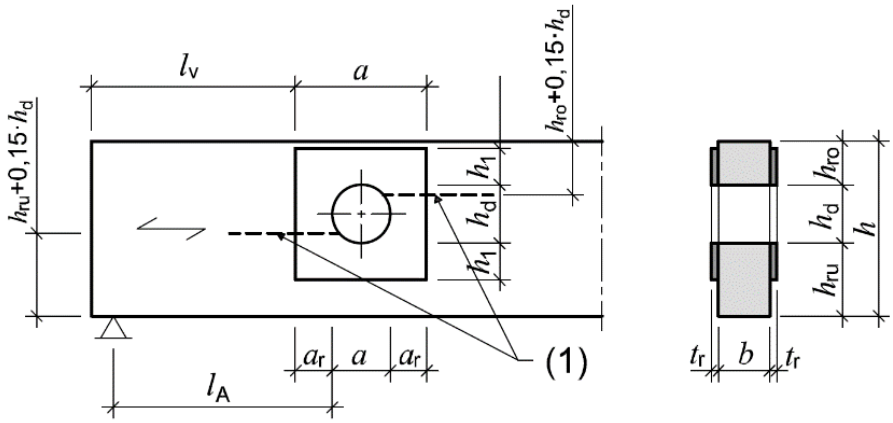

b)

Figure 2.24: Reinforcement with lateral glued on wood-based panels [19]

a) rectangular openings b) round openings;

(1) line of crack propagation

According to the ON B 1995-1-1:2015 [19] a failure of the beam may happen if either the strength of the bond line or the rolling shear strength is exceeded. The glueline shear stress reacts between the reinforcing panels and the outer side of the beam and should be calculated as in equation 2.11.

$$\tau_{ef,d} = \frac{F_{t,90,d}}{2 \cdot a_r \cdot h_{ad}} \leq f_{k,d} \qquad 2.11$$

$\tau_{ef,d}$	...	design value of glueline shear stress
$F_{t,90,d}$	...	design value of tensile force perpendicular to the grain (equation (2.8))
a_r	...	effective length of the reinforcing panels
h_{ad}	...	effective height of the reinforcing panels; $h_{ad} = h_1$ for rectangular openings; $h_{ad} = h_1 + 0.15 \cdot h_d$ for round openings
$f_{k,d}$	...	characteristic glueline shear strength $f_{k2,d}$ (from ON B 1995-1-1:2015 [19]) between the support surface and reinforcing panel and rolling shear strength $f_{r,d}$, respectively

The tensile stress within the reinforcement panels should also be verified according to ON B 1995-1-1:2015 [19] (see equation 2.12).

$$k_k \cdot \sigma_{t,d} = k_k \cdot \frac{F_{t,90,d}}{2 \cdot a_r \cdot t_r} \leq f_{t,d} \qquad 2.12$$

k_k	...	coefficient for consideration of an uneven distribution of stress within the reinforcement panels; absence of detailed verification may be set with k_k = 2.0
$\sigma_{t,d}$	...	design tensile stress within the reinforcement panels
t_r	...	thickness of the reinforcing panels
$f_{t,d}$	...	design tensile strength of the panel material in the direction of $F_{t,90,d}$

The verification of shear force and bending moment should be performed in the same way as for the unreinforced beams. The reinforcement panels may not be considered for shear proofing any further.

2-1.4.1.2 Other standards

In the **DIN EN 1995-1-1 / NA:2010 [22], part 6.8.4**, glued-on plywood panels, LVL panels as well as glued boards and pressed in nail plates are defined as possible reinforcements for beams with openings.

The geometry limitations are to be seen in table 2.1.

In the **enBR:2007 [24]**, as well as in ON B 1995-1-1:2015 [19], the characteristic bond line shear strength between the beam surface and reinforcing panel is specified with the value of $f_{k2,k}$ = 0.75 N/mm². In the combination of different materials for the determination of $f_{k2,d}$, the use of partial safety factor γ_M is mandatory and, preferably, the biggest value for γ_M is taken.

The Swiss norm, **SIA 265:2012 [18], part D.4,** defines externally reinforced beams with openings. The geometry boundaries are to take out from table 2.1. The peculiarity in this standard is that there is no separation between calculations for externally and internally reinforced beams with openings.

Swedish regulations are based on Eurocode 5 **pr EN 1995-1-1:2002 [26]**. For the purpose of this thesis **Limträhandbok: Glulam Handbook** [25] is used. The calculation process is the same to already mentioned ones in German and Austrian standards. According to Limträhandbok [25], the panel thickness is determined by using a utilization factor μ, which depends on the shear load and gross cross section, see Eq. 2.13:

$$\mu = \frac{1.5 \cdot V}{b \cdot h \cdot f_v} \qquad 2.13$$

where:

V	...	shear force in the middle of the opening
b	...	width of the gross cross section
h	...	height of the gross cross section
f_v	...	shear strength

With increasing factor μ, the thickness t_r of the panels has to be increased. This could be represented as an alternative for the design of the glulam beams with the reinforcement panels.

The standards **ON EN 13986 [38]** and **ON EN 636 [39][38]** can be applied for the external reinforcements glued-on plywood panels. Standards **ON EN 14374 [40]** and **ON EN 13986 [38]**can be applied for the latter LVL and pressed-in nail panels, respectively. According to the standard, the latter reinforcement has to be done in the same way as for the glued-on panels.

2-1.4.1.1.3 Experimental tests

As the subject matter of this thesis are GLT beams reinforced internally with screws or threaded rods, the experimental test will not be discussed into much detail here.

2-1.4.2 Internal reinforcement

Steel bars are used as internal reinforcement for glulam beams with openings that were either glued (glued-in rods) or screwed (self-tapping screws or screw rods) into the timber. According to the regulations, the reinforcing medium is allowed to be at 90° angle to the beam longitudinal axis only.
When calculating the internal reinforcement, the influence of the stiffness of the reinforcement is not considered.

2-1.4.1.1.1 Austrian standards

In **ON B 1995-1-1:2015 [19], annex F**, it is determined that inner reinforcements may only be used when the conditions from Eq. 2.3 are fulfilled. Otherwise, the external reinforcement measures need to be used. The determination of this requirement is not quite clear, as in the point F.3.1 – General part, it is defined that verifying shear stresses on the periphery of the openings using the Eq. 2.3 has to be fulfilled. Furthermore, the internal reinforcement strength has to be disregarded in the shear verification.

According to the ON B 1995-1-1:2015 [19], annex F.3.3 and F.4 there are two possibilities for internal reinforcement for glulam beams with openings:

-screws $\varnothing \leq 20$ mm

-glued-in rods $\varnothing \leq 20$ mm

When reinforcing with internal steel rods (shown in figure 2.25), the verification of the glueline shear stress has to be proven:

$$\frac{\tau_{ef,d}}{f_{k1,d}} \leq 1 \qquad 2.14$$

$$\tau_{ef,d} = \frac{F_{t,90,d}}{n \cdot d_r \cdot \pi \cdot l_{ad}} \leq 1 \qquad 2.15$$

$\tau_{ef,d}$	...	design value of glueline shear stress
$f_{k,1,d}$	...	design value of glueline shear strength [N / mm^2]
$F_{t,90,d}$	...	design value of tensile force perpendicular to the grain
n	...	number of steel rods at the opening edge; where only one row of steel rods could be used in calculation
d_r	...	outside diameter of the steel rod (for example, threaded rod) [mm]
l_{ad}	...	effective height of the reinforcing screw or threaded rod; $l_{ad} = h_{,down}$ or $l_{ad} = h_{r,up}$ for rectangular openings; $l_{ad} = h_{rup} + 0.15 \cdot h_d$. or $l_{ad} = h_{rdown} + 0.1 \cdot h_d$ for round openings ($h_{r,down}$, $h_{r,up}$, h_d according to figure 2.25 whereby the $h_{r,down} = h_{r,u}$ and $h_{r,up} = h_{r,o}$)

The minimum length of each steel rod is $2 \cdot l_{ad}$ and the diameter d_r should not be bigger than 20 mm.

The tension stress of the steel rods has to be verified.

The spacing of fasteners within one row parallel to grain, which is only allowed according to the [19] is $a_1 \geq 7 \cdot d$.

There are defined distances between axial loaded, glued-in threaded rods and edges of the beam [22]:

- spacing of fasteners within one row parallel to grain $a_1 \geq 4 \cdot d$
- spacing of rows of fasteners perpendicular to grain $a_2 \geq 4 \cdot d$
- distance between fastener and end grain $a_{1,c} \geq 2.5 \cdot d$
- distance between fastener and edge $a_{2,c} \geq 2.5 \cdot d$

The geometry boundaries are shown in table 2.1 and in figure 2.25.

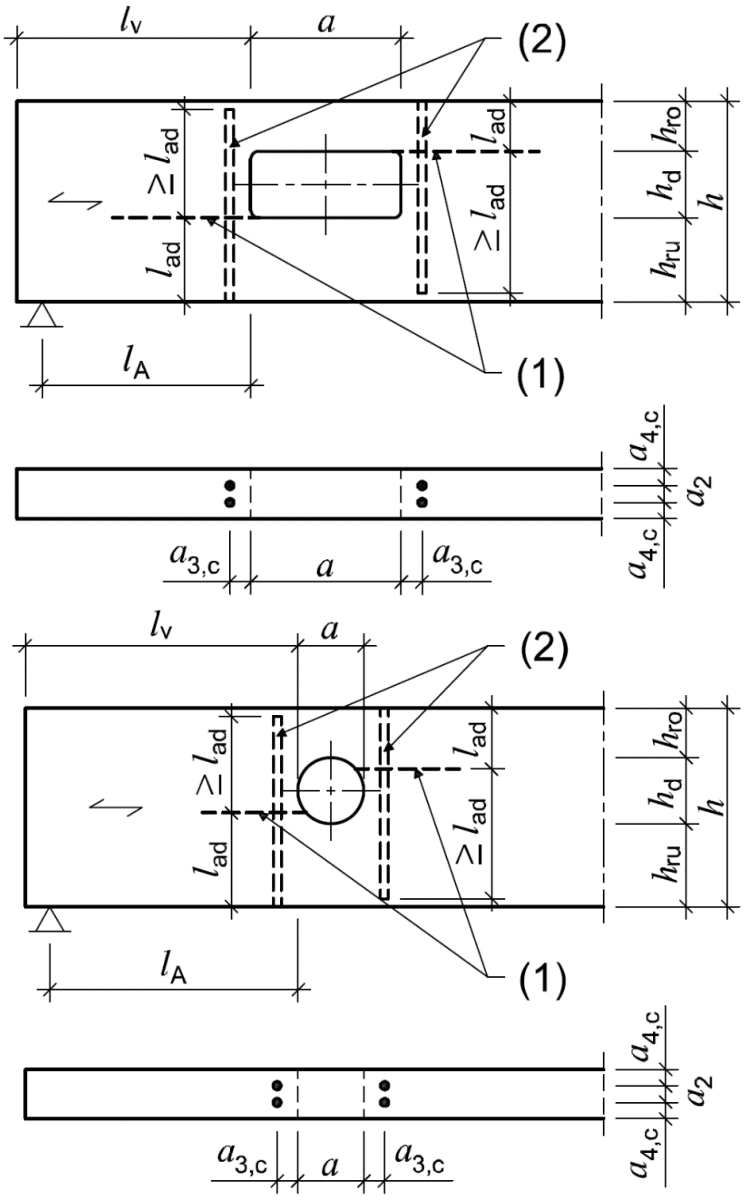

Figure 2.25: Reinforcement of openings with internal glued-in steel bars [19]

(1) risk of cracking due to lateral stress (2) steel bar (e.g. threaded rod)

Instructions for the screwed steel rods can be found in ON B 1995-1-1:2015 [19], (e.g. self-drilling full-thread screws or screw rods). The calculation is the same as for the glued-in steel rods. Similarly to steel rods, screws should be used with a thread over the entire shaft length.

2-1.4.2.2 Other standards

For calculation of the glued-in steel bars the **DIN EN 1995-1-1:2008 [23]** along with the D**IN EN 1995-1-1/NA:2010 [22]** have regulations that should be taken into consideration, unless it is specified differently.

The dimensions of the reinforced openings with glued-in threaded rods are shown in Fig. 2.25. The minimum spacing between the steel rods and steel rods to the beam edges, perpendicular and parallel to the grain in DIN EN 1995-1-1/NA:2010 [22] is set as for the ON B 1995-1-1:2015 [19].
For service class 2, as well as for effective glued-in length of $l_{ad} \leq 500$ mm, the values are applied in DIN EN 1995-1-1/NA 2010 [22]. The relation between the design value of glueline shear strength $f_{k1,k}$ and the effective glued length l_{ad} is shown in table 2.3.

Table 2.3: Relation between characteristic adhesive joints strength $f_{k1,k}$ and effective length l_{ad}, taken from [28]

Effective glued length l_{ad} in [mm]	**characteristic value of glueline shear strength $f_{k1,k}$ in [N/mm²]**
	acc. DIN EN 1995-1-1:2010 [22]
$l_{ad} \leq 250$ mm	4.0
250 mm < $l_{ad} \leq 500$ mm	$5.25 - 0.005 \cdot l_{ad}$
500 mm < $l_{ad} \leq 1000$ mm	$3.5 - 0.0015 \cdot l_{ad}$

When checking the viability of threaded rods according to DIN EN 1995-1-1/NA:2010 [22] the following failure mechanisms have to be considered:

- failure of the steel rod
- failure of the bond line or the timber along the borehole
- failure of the timber part.

The resistance of a threaded rods according to DIN EN 1995-1-1/NA:2010 [22] is determined similar to the ON B 1995-1-1:2015 [19] and equations 2.14 and 2.15.

The resistance of the glueline is determined with the nominal diameter *d*. According to Steiger [41] the failure mechanism "Timber failure near the glueline" is shear failure in timber. Therefore, the failure is not determined by the diameter of the threaded rod, but rather from the borehole diameter.

According to the DIN EN 1995-1 -1/NA:2010 [22] screwed-in rods should be treated in the same way as glued-in rods, where no detailed design rules are provided.

The **enBR:2007 [24], part 6.7.4.2** gives minimum distances between screws or steel rods and their distances from the beam edges perpendicular and parallel to the grain. Precise verification steps for the calculation process, as well as the verification of the reinforcing components.

The Swiss norm **SIA 265:2012 [18], part D.4.2,** defines internally reinforced beams with openings. The geometry boundaries are given in the table 2.1. The peculiarity, which was already stated in this work is that there is no separation from the calculation for externally and internally reinforced beams with openings.

Swedish regulations are based on Eurocode 5 **pr EN 1995-1-1:2002 [26]**. For the purpose of this thesis **Limträhandbok: Glulam Handbook** [25] was used, which only recommended timber service class 1. The design screw force should be smaller than the carrying capacity of the screws (see equation 2.16):

$$F_s = 0.5 \cdot V \cdot \left[3 \cdot \left(\frac{h - h_0}{h} \right)^2 - 2 \cdot \left(\frac{h - h_0}{h} \right)^3 \right] \leq F_R \qquad 2.16$$

where:

V	...	critical shear force at the centre of the opening
h	...	beam height
h_0	...	opening height
F_S	...	design screw force
F_R	...	carrying capacity of the screws

2-1.4.2.3 Experimental tests

In a case study, Aicher and Höfflin [13] were carried out the tests on glulam beams with a span of 3500 mm and cross-sectional dimensions of b / h = 120 / 450 mm. The beams were made of boards of class C35 and the end product resulted in beams of a strength class of GL32h. Each beam had an opening diameter h_d of 180 mm at the same position (see figure 2.26). There were three different test series, two with reinforced opening, which had six test specimens (test series V1 to V5), and one with an unreinforced opening, with seven test specimens (test series U). First reinforced series (V1) had self-tapping screws with screw diameter d of 12 mm, second (V2) had glued-in steel rods with metric thread and diameter d of 12 mm.

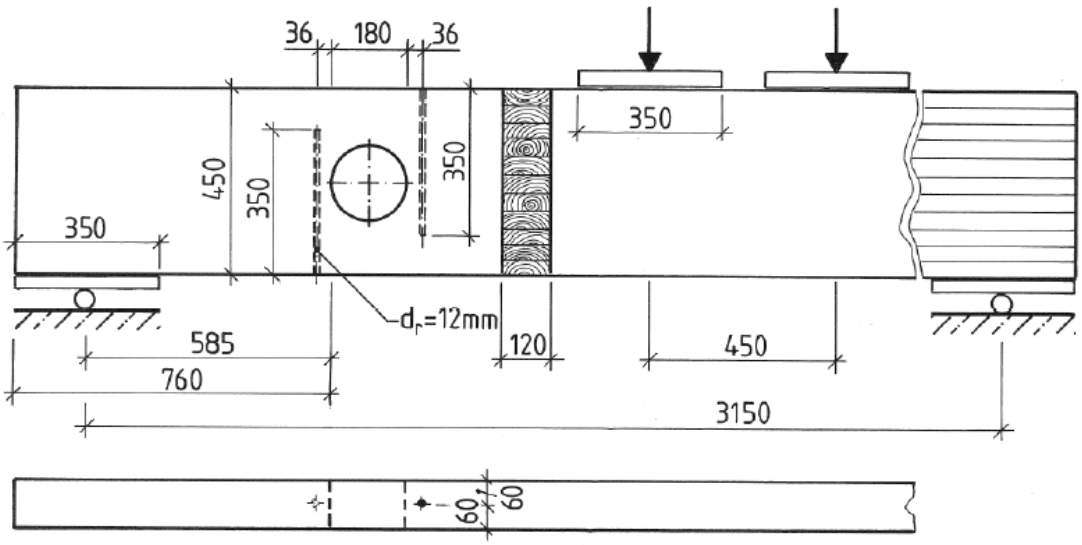

Figure 2.26: Test set up of the beams with reinforced openings [13]

According to Aicher and Höfflin [13] the stress distribution is a function of the corresponding parameters of the reinforcing medium: cross-sectional area, stiffness and the geometry of the distance to the opening. By increasing the rod diameter, the increased stiffness of the rod causes a decrease in the maximum of tension stress perpendicular to grain. At the same time, the position of the steel rods influences the force in them. The tension stress perpendicular to the grain reaches its limit within a certain distance (usually 10-40 mm) away from the opening of the beam.

The investigations on the reinforced beams have shown that the shear capacity increases in comparison to the beams without reinforcement. The largest increase was visible in the ultimate shear force V_u (V_f) where mean values increased 55 % and 64 % in cases of test configurations V1 and V5. The smallest, still appreciable, increase in the load level was observed by initial crack level V_{int} (V_{c0}) with values of 27 % and 41 % in cases of V1 and V5. For the load level V_c the capacities increased 38 % and 49 %, for V1 by V5. Glued-in rods provided higher shear force capacities compared to series with self-tapping screws [13].

Internal reinforcements for glulam beams with openings (screws or threaded rods), make a significant increase in shear strength compared to corresponding unreinforced beams.

Aicher and Tapia [14] did computational analysis on minimum distances of the internal reinforcement of GLT beams with round openings to the beam opening. The investigations were conducted on the GLT beams with one and two openings in them, therefore, case of pure bending moment was considered, as well as the case of combination of shear force and bending moment.

This case study was done on regulations according to DIN EN 1995-1-1:2013 [42] and with the help of calculations of FE models, they came to the following conclusions:

The presented FE calculations of the stress distributions and the determined design shear forces showed that smaller distances between two unreinforced round openings compared to the minimum distance in [42] are computationally possible. With relative opening sizes of h_d / h ≤ 0.15 today's minimum distance of $l_z = 1.5 \cdot h$ could be reduced to $l_z = 1.0 \cdot h$ without verification. For opening sizes h_d / h in the range from $0.1 \cdot h$ to $0.15 \cdot h$, the distance could also be reduced to $l_z = 1.0 \cdot h$, whereby the tensile force perpendicular to the grain $F_{t,90,d}$ should be increased by 10 % at the opening edge further away from the support. Generally speaking, these proposals are in the context of a correct determination of the tensile forces perpendicular to the grain. In this regard, it should be noted that the tensile force perpendicular to the grain is dependent on the moment to shear force ratio whereat the part of the bending moment, is too inaccurate, which then leads to conservative results [14].

2-1.4.2.4 New developments

1. <u>ALP GSA® method of n'H neue Holzbau AG</u>

The n'H new Holzbau AG, in cooperation with professor Gehri, developed a new, alternative method ALP GSA®, a so called ``alternative load path`` method. This method consists of [28]:

- glulam beams,
- threaded rod,
- rod anchor ("GSA®") and
- GSA® resin

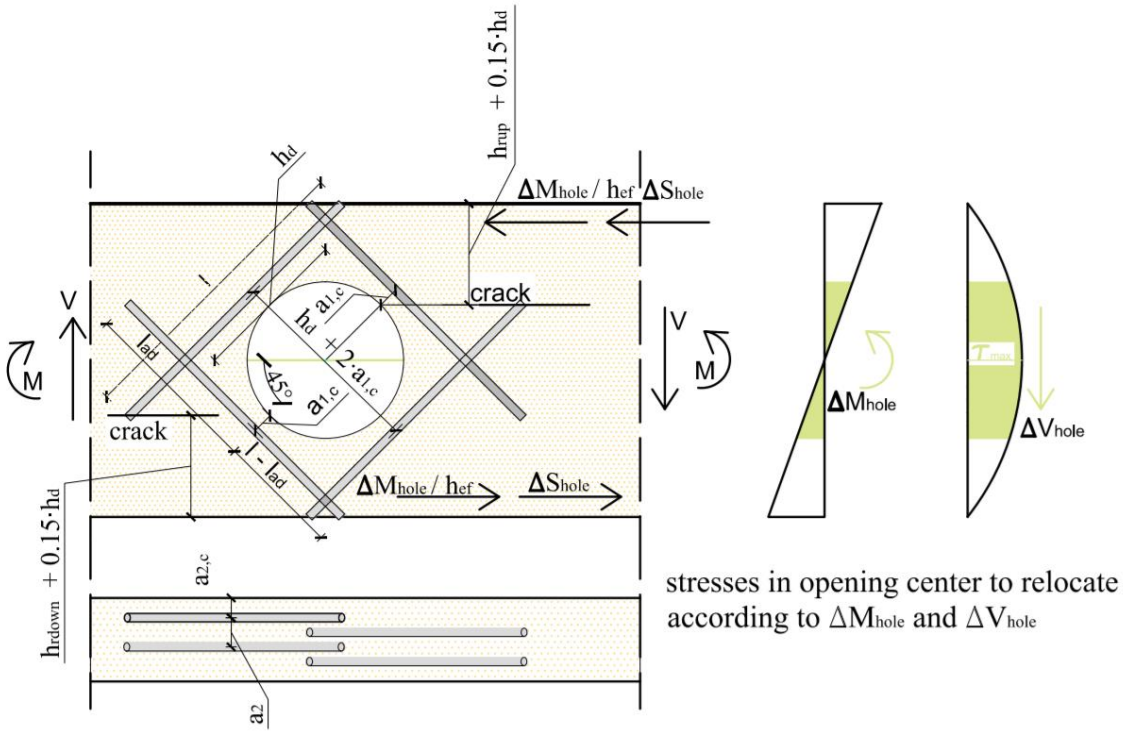

Figure 2.27: Geometry of the beam reinforced with inclined glued-in rods; stored stress according ΔM$_{hole}$ and ΔV$_{hole}$ [28] (adapted)

Glued-in threaded rods were in holes which were placed in the nearest distances to the edge of the opening under 45 degrees to reduce tensile stress perpendicular to the grain, and finally restore the load carrying capacity of a beam without an opening (see figure 2.27).

Due to the presence of the opening in the beam, part of the stress caused by inner forces ΔM_{hole} and ΔV_{hole} needs to be transferred by threaded rods.

The force within the threaded rod is presented in the equation 2.17 [28]:

$$F_{t,45,d} = \left(\frac{\Delta M_{hole}}{h_{ef}} + \Delta S_{hole} \right) \cdot \frac{1}{\sqrt{2}} \qquad 2.17$$

where the values for ΔM and ΔS are stated with the following equations [28]:

$$\Delta M_{hole} = M_{hole} \cdot \frac{h_d^3}{h^3} \qquad 2.18$$

$$\Delta S_{hole} = \tau_{max} \cdot l_{ef} \cdot b = \frac{3 \cdot V_{hole}}{2 \cdot b \cdot h} \cdot h_d \cdot \sqrt{2} \cdot b = \frac{3 \cdot V_{hole}}{2 \cdot h} \cdot h_d \cdot \sqrt{2} \qquad 2.19$$

It is assumed that the shear flow goes through the imaginary green line in the middle of the beam height (see figure 2.27), but it is interrupted by the presence of the opening, so that the remaining cross section has to take it over.

An overview of the distances between threaded rods is taken from DIN EN 1995-1-1/NA [22] according to the Z-9.1-778:2010 [43] and listed on the page 26 of this master thesis.

Experimental studies to GSA® reinforcements

This theoretical approach was evaluated by a series of 23 consecutive tests according to Strahm [44]. The height of the beams was 600-720 mm and beam width was kept at b = 140 mm (see figure 2.28). Load application and support areas were all reinforced in accordance with GSA® technology using threaded rods in combination with screws.

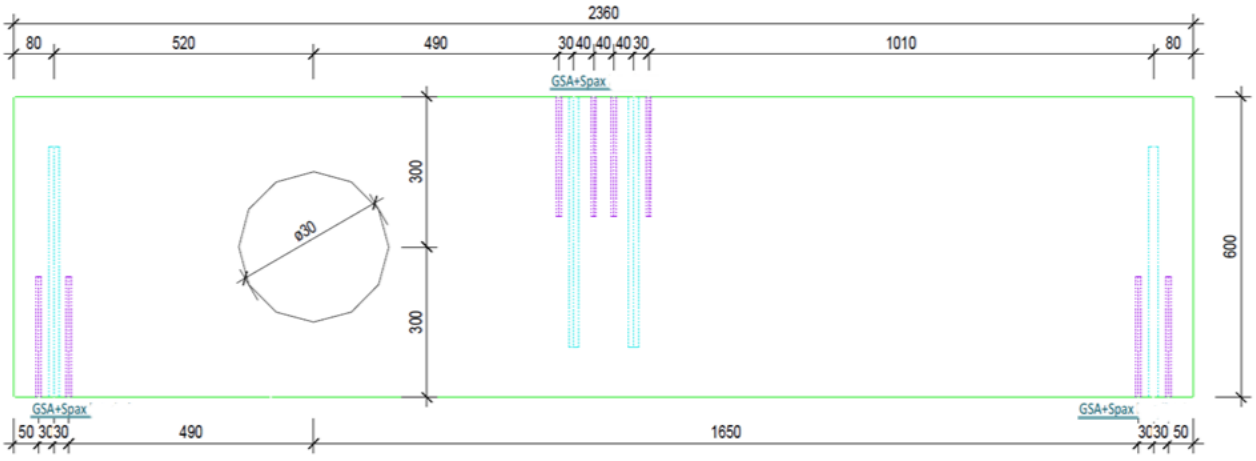

Figure 2.28: Elementary geometry of the tested beam [44]

In [47] different factors and effects on the shear problem in timber beams were inspected:

- cracks
- moisture content
- temperature
- size or volume effect.

Cracks in timber are unavoidable due to the drying process. Only for smaller timber parts such as boards, the appearance of the cracks through the drying procedure may be reduced or completely avoided. As the characteristic values, fixed in EN 1194 [45] (now replaced with EN 14080:2013 [46]), are too high and cannot be reproduced by tests a crack factor was introduced [47].

The shear strength was calculated for the gross cross section, not for the net cross section is required for the comparison of the different test setups. If the shear strength of a beam with a reinforced opening was equal or higher than the one of a beam without an opening, the reinforcement method could be seen as successful [44]. The shear area length *a* is the distance between the two inner screws for the reinforcement of the compression resistance perpendicular to the grain.

Overview of the tests according to Strahm [44] are given in table 2.4.

Table 2.4: Test parameters and failure modes [28] (adapted)

Year	Number of specimens	Type of timber	Cross section	Opening	Failure mode	Shear strength (gross cross section)
	n **[-]**	**-**	***A*** **[mm²]**	***d*** **[mm] or** $h_d \times a$ **[mm²]**	**-**	$\tau_{v,mean}$ **[N/mm²]**
2011	3	GL 28k spruce	140/600	Ø 260 (0.43 · *h*)	opening area	2.70
2012	1	GL 40k beech	120/600	Ø 240 (0.4 · *h*)	field	6.50
2013	2	GL 28k spruce	140/600	Ø 260 (0.43 · *h*)	field	3.52
2013	1	GL 28k spruce	140/600	Ø 300 (0.5 · *h*)	field	3.90
2013	1	GL 28k spruce	140/720	Ø 360 (0.5 · *h*)	field	3.38
2013	1	GL 28k spruce	140/720	260 (0.36 · *h*) × 410	opening area (ductile)	3.12
2013	1	GL 28k spruce	140/720	260 (0.36 ·*h*) × 320	opening area (ductile)	3.86
2013	2	GL 40k ash	140/600	Ø 300 (0.5 · *h*)	no failure, cancellation of the test	7.63

As seen in table 2.4, the results for the achieved shear strength were just above the comparable shear strength of the standard f_v = 2.7 N/mm^2, which was good enough according to Gehri [47]. Therefore, these tests showed that the beams reinforced with ALP GSA® method, were as good as beams without openings.

2. *Aicher and Tapia [15]*

Aicher and Tapia [15] did a case study based on FE modeling of GLT beams (GL32h) with internally reinforced round openings with inclined steel rods.

In this parametric case study, they investigated the influences of different angles of the inclined internal reinforcement (steel rods) of the openings in the glulam beams on the distribution of the tensile and compression stress perpendicular to the grain as well as the shear stress in the opening area [15].

The dimensions of the modeled beam with the round opening are shown in the figure 2.29 [15].

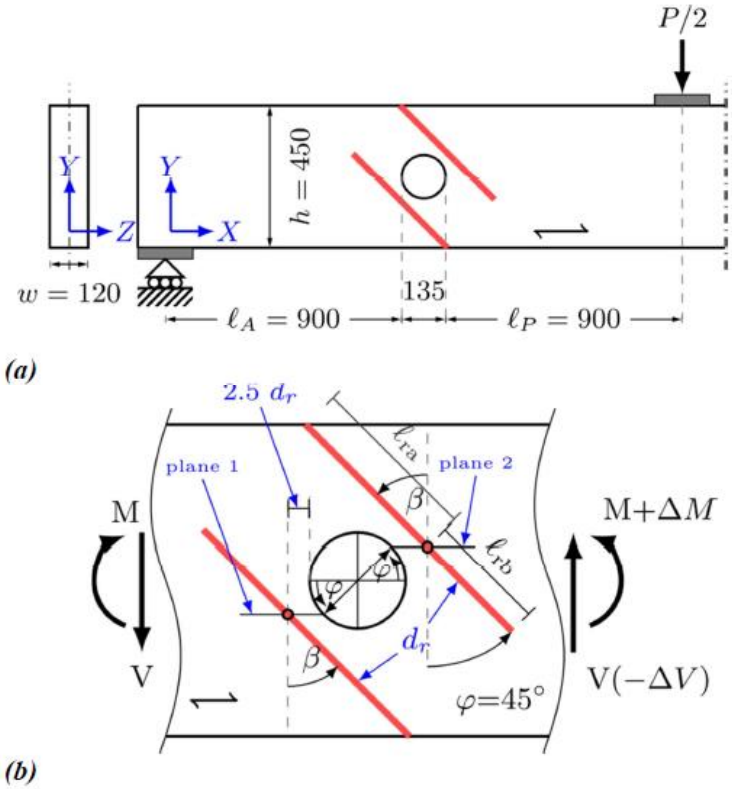

2.29: (a) Geometry of the glulam beam with round opening used for the FEM simulations; (b) positioning of internal reinforcements [15]

The beam length was 4110 mm, the height was 450 mm and the width was 120 mm. The round opening was placed in the middle, between the support and closest load application area with a diameter of 135 mm, where h_d / h-ratio was 0.3 and M / V-ratio was 1.03. Symmetry was applied on two planes. The first one at mid-span of the beam (ZY-plane) and the second one located at mid-width ($z = 0$), cutting the beam in the longitudinal direction (XY-plane) (see figure 2.29 (a)). The different inclinations of the steel rods β were measured from the vertical axis (see figure 2.29 (b)). The rod diameter d_r was set to 18 mm with the length of 200 mm. The choice of the specific rotation points was made because of the expected point of the maximum tensile and compression stress perpendicular to the grain (σ_y). The rotation points were planned on the plane of the estimated crack (plane 1, plane 2) in a distance of 2.5 d_r from the edge of the opening (see figure 2.29 (b)) [15].
In comparison with the vertical reinforced beams ($\beta = 0°$), which can bear 5 % to 14 % more stress than an unreinforced beam, the inclined reinforced areas ($\beta = 45°$) where able to increase till 28 % to 40 % (see figure 2.30 (a) to (d)) [15].

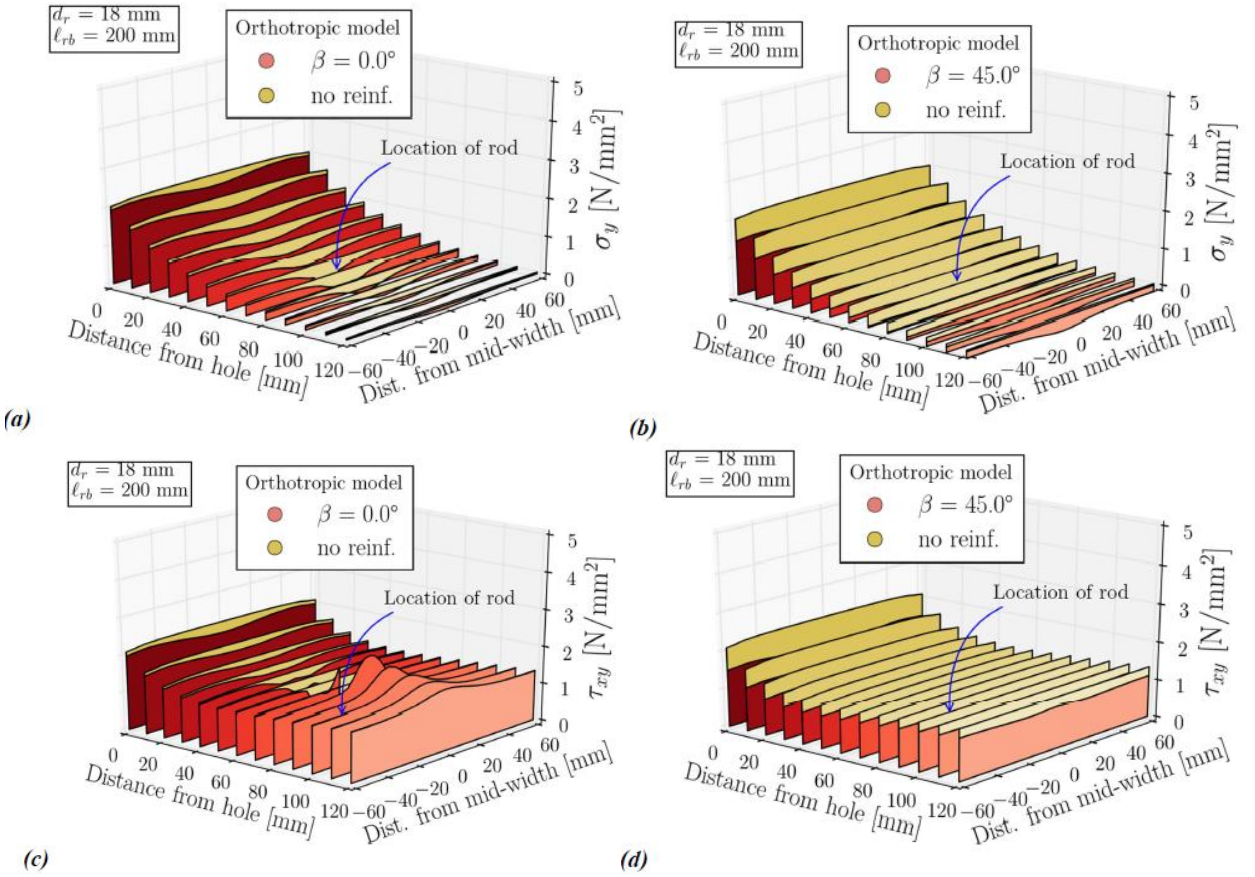

2.30: Stress distribution comparison between the internally reinforced and unreinforced opening on plane 2 (see figure 2.29) for the inclinations of β = 0° and β = 45° [15]

(a) and (b) stresses perpendicular to grain; (c) and (d) shear stresses

Considering the presented results the conclusion was that the internal reinforcement had effectively taken up about 34 % (plane 2) and 47 % (plane 1) (see figure 2.29) of the shear force responsible for the stresses on opening edges [15].
Over the damaged beams, the redistribution of the stresses σ_y and τ_{xy} was influenced by the horizontal crack in planes 1 and 2 (see figure 2.29) and representation is shown in figure 2.31. In figure 2.31 (a) a small reduction of the tensile stress perpendicular to the grain can be observed, which was caused by the vertical rods, but there was still a stress peak, while the inclined steel rods had noticeable reductions of the stresses. In figure 2.31 (b) the shear stress distribution is visible. The beams underwent no change in the region with the reinforcement in comparison to the undamaged ones. The second peculiarity was that, in the case of the inclined steel rods, the shear stress maintained a level only slightly higher than in the undamaged situation, which was an indication that the length of the crack had no effect on the shear stress [15].

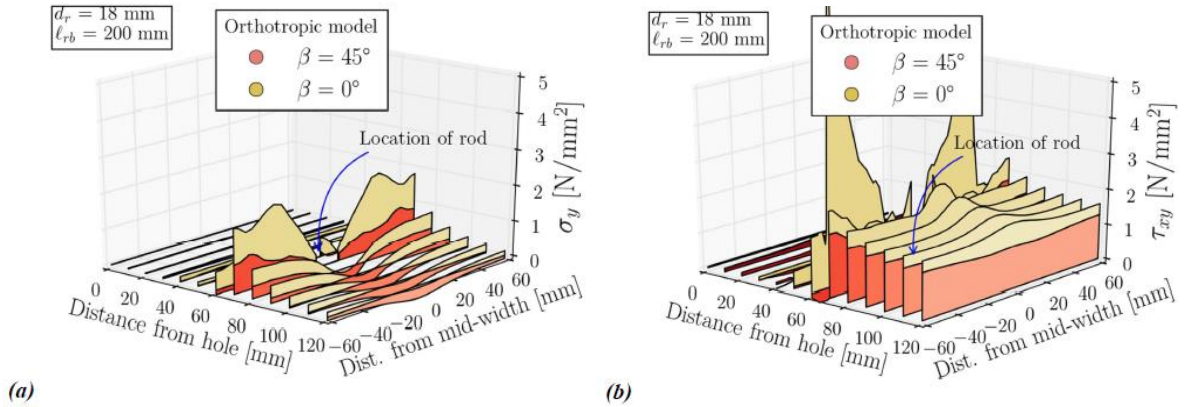

2.31: Stress distribution comparison of the plane 2 (see figure 2.32), with a crack propagation from the opening edge to the center of the threaded rod, with threaded rods inclined by the angles β = 0° and β = 45° [15]

a) stresses perpendicular to grain ***(b) shear stresses***

This parametric FE model showed that vertical internal reinforcement with glued-in steel rods or screws for beams with round openings as described in DIN EN 1995-1-1:2010 [22] had only a small impact on the stress perpendicular to the grain in the opening periphery. It was also shown that the vertical reinforcement has a negligible impact on the shear stress [15].
The numerically investigated inclined internal steel rod reinforcement showed that it is dependent on the rod inclination. Given the angle of the 45°, the peak stress at the periphery of the opening was reduced by 30 % and 40 % for tensile stress perpendicular to the grain as well as for shear stress in comparison to the unreinforced beams [15].

2-1.5 CROSS-LAMINATED TIMBER BEAMS (CLT)

2-1.5.1 Structure, development, production and standardization

In the Eurocode 5 [19], cross-laminated timber is defined as multilayered, glued, laminar wood product. The boards of the individual layers are arranged perpendicular to each other and the cross-sectional structure is symmetrical. Through the bonding, a rigid connection between the individual board layers can be assumed. Due to the surface bonding of differently oriented monolayers, a so-called "blocking effect" can be achieved, which should provide reduction of swelling and shrinkage across the grain.

Buildings with cross laminated timber could also be defined as so-called solid timber constructions. Originally, cross-laminated timber was designed to find an economic use for the remaining of by-product of side boards [48].

Although this new design is primarily a layer-like panel element, CLT is now used in many ways and can be combined as needed [48].

CLT can be loaded in two different ways:

• perpendicular to the plane and / or

• in plane.

Numerous scientific papers on the subject of cross-laminated timber and the research in this area lead to great advances, but there is yet no comprehensive standardization on European level. As each manufacturer has his own technical approval, rules and regulations for the production of the CLT elements, it is a uniform demand to uniform CLT on European level.

2-1.5.2 CLT beams with openings

Nowadays, CLT is used as flat elements for: ceiling, walls, and panels due to their excellent features when it comes to transferring loads within 2D systems. CLT beams have advantages in case of tensile stress perpendicular to the grain as well as for shear stresses. Compared to GLT beams, CLT beams are also less likely to break under the influence of these forces. Flaig [48] enlisted them as an alternative to reinforced GLT beams.

Present throughout the length of the CLT beams, cross layers make a positive contribution to transferring shear and tensile stress perpendicular to the grain. Unfortunately, the cross layers do not serve for transferring load in longitudinal layers.

CLT beams may be considered as an alternative to externally reinforced GLT beams with plywood panels. The cross layers in CLT beams not only transfer tensile stress perpendicular to the grain but also the shear stress due to the bending stress as the cross layers expand throughout the length of the beam. On the other hand, plywood panels are placed in the opening region only and serve exclusively for reinforcing the tensile stress perpendicular to the grain [48].

2-1.5.2.1 Types of shear failure mechanisms in the CLT beams

In his dissertation, Flaig [48] explained three failure mechanisms of CLT beams (see figure 2.32):

- shear failure of gross cross-section
- shear failure of net cross-section
- torsion

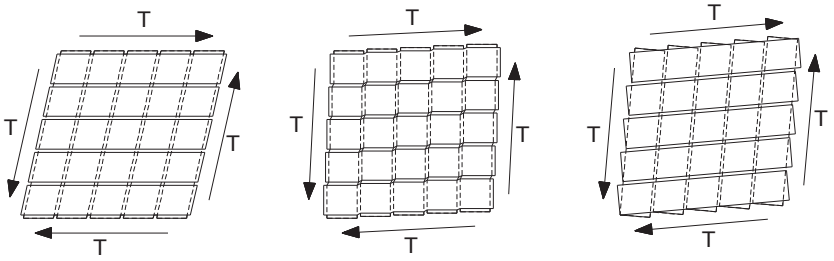

Figure 2.32: Failure mechanisms of cross-laminated timber for loads in panel area: gross shear (left) net shear (center) and torsion (right) from Flaig [48]

Shear failure in the gross cross section (see figure 2.32, left.) [28]:

The shear stress can be calculated according to equation 2.20 for the gross cross-section of the beam and should not exceed a shear strength of $f_{v,gross,k}$ = 3.5 N/mm² (acc. Blaß und Flaig [49]) [28]:

$$\tau_{xz,gross,d} = \frac{3 \cdot V_d}{2 \cdot h \cdot t_{gross}} \leq f_{v,gross,d} \qquad 2.20$$

$\tau_{xz,gross,d}$	...	design value of gross shear stress
V_d	...	design value of shear force
h	...	beam height
t_{gross}	...	beam width; $\Sigma t_l + \Sigma t_q$
Σt_l	...	sum of thicknesses of the longitudinal layers; also by Flaig [48] as $t_{net,long}$ marked
Σt_q	...	sum of thicknesses of the cross layers; designated by Flaig [48] as $t_{net,cross}$
$f_{v,gross,d}$	...	design value of gross shear strength

Shear failure in the net cross-section (see figure 2.32, center.) [28]:

It is assumed that CLT elements are produced without gluing the narrow sides of the board, whereby the shear forces have to be transferred by the corresponding net sections. In most cases, transverse board layers are the ones with the lower sum of the layer thicknesses than those in longitudinal direction. The net shear strength varies greatly with the thickness of the board layers (the smaller the thickness, the higher the resistance). The proof is obtained by:

$$\tau_{xz,net,d} = \frac{3 \cdot V_d}{2 \cdot h \cdot t_{net}} \leq f_{v,net,d} \qquad 2.21$$

$\tau_{xz,net,d}$	...	design value of the net shear stress
t_{net}	...	sum of the layer thicknesses of the transverse board layers; $t_{net} = \min \{\Sigma t_l; \Sigma t_q\}$
$f_{v,net,d}$	...	design value of the net shear strength

Torsion failure in the crossing areas (see figure 2.32, right.) [28]:

Due to the change in moment along the beam length, shear stresses in the x direction are also affected, and due to local load introduction or changes in the cross section stresses in z-direction have to be sonsidered too. These stresses have to be lower than the rolling shear strength $f_{r,k}$ = 1.25 N/mm². The transfere of the shear force from one lamella to the other also causes a torsional stress, which shloud not exceed the torsion strength of 1.98 ≤ $f_{tor,k}$ = 2.5 N/mm² [28], [48].

<u>Shear stress parallel to the beam axis [28]:</u>

$$\tau_{yx,d} = \frac{dM}{I_{net,long}} \cdot a_{i,max} \cdot \sum t_l \cdot b \cdot \frac{1}{n_{CA} \cdot b^2} =$$
$$= \frac{V \cdot b \cdot 12}{\sum t_l \cdot (m \cdot b)^3} \cdot \frac{m-1}{2} \cdot \frac{\sum t_l \cdot b}{n_{CA} \cdot b^2} = \frac{6 \cdot V_d}{b^2 \cdot n_{CA}} \cdot \left(\frac{1}{m^2} - \frac{1}{m^3} \right) \qquad 2.22$$

dM	...	moment change; $dM = V \cdot b$
$I_{net,long}$	...	moment of inertia considering the longitudinal layers; $I_{net,long} = (\Sigma t_l \cdot m^3 \cdot b^3) / 12$
$a_{i,max}$	...	distance from the board center to the top / bottom longitudinal boards to the median line of the total cross-section; $a_{i,max} = (m - 1) / 2$
n_{CA}	...	number of bonding surfaces between the transverse and longitudinal layers in the direction of the beam width
b	...	board width
m	...	number of boards of one longitudinal layers

Shear stress perpendicular to the beam axis [28]:

The loads acting in a perpendicular direction to the beam axis are to be taken first by the transversal layers of the CLT beam. Due to the stiffness of the layers parallel and transverse to the grain they need to be transferred through the glueline on the longitudinal layers of the beam (see figure 2.33).

$$\tau_{yz,d} = \frac{q_{z,d}}{n_{CA} \cdot m \cdot b} \qquad 2.23$$

$q_{z,d}$ ... loads acting perpendicular to beam axis

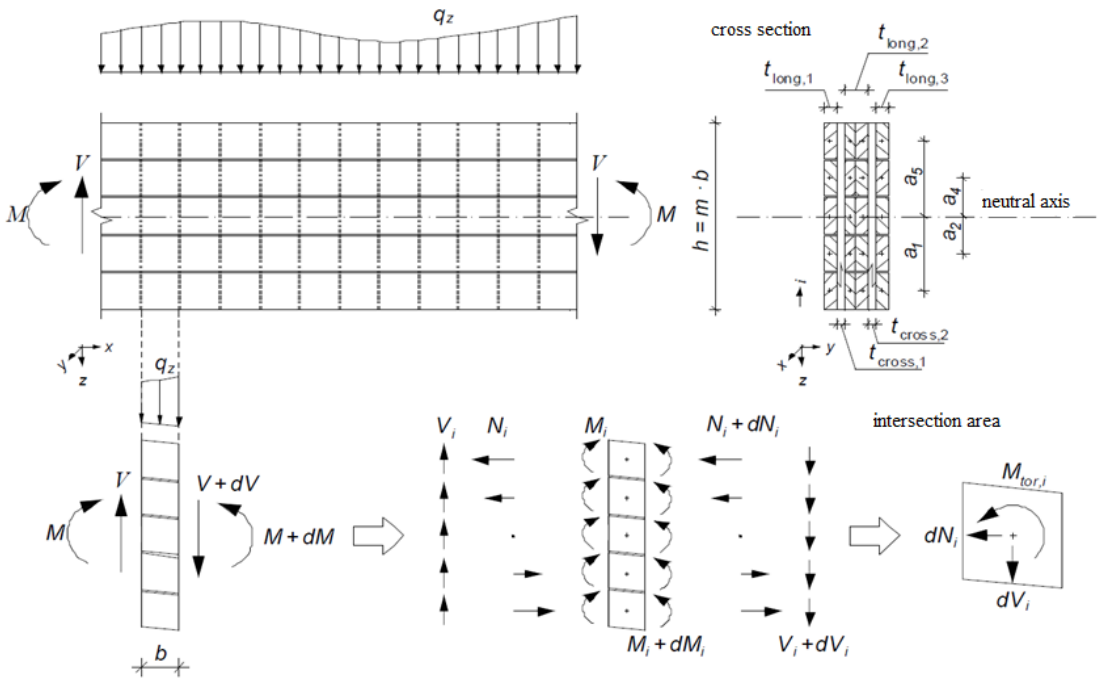

Figure 2.33: Stress components in the bonding surfaces of CLT beams from Flaig [48]

Torsional stress [28]:

$$\tau_{tor,d} = \frac{\sum_{i=1}^{m} M_{tor,i}}{n_{CA} \cdot \sum_{i=1}^{m} I_{p,CA}} \cdot \frac{b}{2} = \frac{3 \cdot V_d}{b^2 \cdot n_{CA}} \cdot \left(\frac{1}{m} - \frac{1}{m^3} \right) \qquad 2.24$$

$$\text{with } \sum_{i=1}^{m} M_{tor,i} = \frac{dM}{I_{net,long}} \cdot \sum t_{net,long} \cdot b \cdot \sum_{i=1}^{m} a_i^2 \text{ and } \sum_{i=1}^{m} I_{p,CA} = m \cdot \frac{b^4}{6}$$

$\Sigma M_{tor,i}$ ... torsion moment which acts on the m adhesive surfaces
$\Sigma I_{p,CA}$ ... polar moment of inertia of the m adhesive surfaces
a_i ... distance from the each board neutral axis to the neutral axis of the cross section

Coefficients k_1 to k_5 are introduced due to the lack of the cross section in the opening area for transferring the shear stresses, which then causes stress concentrations on the periphery of the opening (see equations 2.25 to 2.29). These equations are taken from Flaig`s [48] case study for a rectangular openings. Since there is no comparison of these coefficients to CLT beams with round openings, or any case study for CLT beams with round openings that introduces similar coefficients. It can be expected that those coefficients could lead to overestimations of the individual stress components for round openings.

$$k_1 = \frac{h}{h - h_d} \qquad 2.25$$

$$k_4 = 1 + \frac{h_d^2}{4 \cdot b^2 \cdot (m-1)} \qquad 2.26$$

$$k_2 = 0.381 \cdot \left(\frac{m \cdot l_d}{h_d} \right)^{0.555} \geq 1.0 \qquad 2.27$$

$$k_5 = 0.791 \cdot \left(\frac{m \cdot l_d}{h} \right)^{0.494} \qquad 2.28$$

$$k_3 = \frac{I_{tot,l}}{I_{net,l}} = \frac{h^3}{h^3 - h_d^3} \qquad 2.29$$

2-1.5.2.2 Experimental tests

As for the externally reinforced beams, the subject matter of this thesis are GLT beams reinforced internally with screws or threaded rods, therefore the experimental test will not be discussed into much detail here.

CHAPTER 3: MATERIALS AND METHODS

In this master thesis, internally reinforced GLT beams with screws and threaded rods will be discussed only. Therefore, all the following chapters will be related to them, with the exception of the description of the test series which were tested on Timber Engineering and Wood Technology, Graz, Austria.

3-1 TIMBER

The timber used for the investigation at the Institute of Timber Engineering and Wood Technology, Graz, Austria, was delivered on 09th June 2016 and on 27th July 2016 from the company HAAS Fertigbau Holzbauwerk Gesellschaft m.b.H. & Co. KG, Germany. By the first delivery, five series were delivered as already finished glue laminated beams with preordered drilled holes for the reinforcement of the supports, load introduction areas and openings reinforcements. Those five series had dimensions of length / height / width = 2700 / 600 / 160 mm. One series was delivered as wooden boards in dimensions of 4.04 m in length, 170 mm in width and 45 mm in height and were used to produce cross laminated timber beams. The second delivery contained fifteen GLT beams, in the same dimensions as the first one, but with pre drilled holes only in support and load introduction areas. The holes for the openings internal reinforcements as well as the gluing of the external reinforcement panels were done on the Institute.

The delivered beams and boards were produced from spruce, strength class GL32h.

3-2 STEEL

Steel screws and threaded rods were used for reinforcement of the beams and fixing the reinforcement panels on the beams.

There were three different types of steel reinforcement elements used:

- self-drilling screws 12 x 400 / 380 mm strength 8.8, from the company Schmidt Schrauben Hainfel GmbH, for reinforcement of supports and load application regions,
- self-drilling screws 12 x 500 / 480 mm strength 8.8, from the company Schmidt Schrauben Hainfel GmbH, for internal vertical reinforcement of openings
- threaded steel bars 16 x 3000 mm, from the company SFS INTEC, Germany, for inclined reinforcement of openings, each was cut and refinished on the length of 600 mm.

A total of 16 threaded rods were drilled with drills (diameter 4 mm) with the total depth of 320 mm. Furthermore, the displacement transducers were placed on the spot where the biggest levels of tensile and compression stress were expected, which was at 274.3 mm of the predrilled hole depth.

Metal spiral drills, were bought from the company Lackner & Urnitsch Ges.m.b.H, Austria. The durability of these drills was improved with the coating "Balint Latuma TOP", which was added by the company Oerlikon Balyers Coating Austria GmbH. With the help of this coating, it was possible to increase the precision of the holes in the threaded rods.

To further improve the precision of the holes, the drilling process was divided into several steps with different lengths of the drills like 75, 119, 160, 200, 250 and 315 mm. The threaded rods were drilled with the help of a turning machine. After drilling, the threaded rods were cleaned with acetone and tiny brushes and dried with pressurized air. At the end, each was equipped with one strain gauge.

3-3 ADHESIVES

For gluing the threaded rods in (series H) the LOCTITE® PUR CR 421 PURBOND two-component polyurethane adhesive with curing time of 10 hours was used. The holes were drilled with a diameter of 20 mm and 24 mm for the tension and compression zone respectively, which was 4 mm wider than the threaded rods nominal diameters. After inserting the threaded rods in the drilled holes the rest of the hole was filled with the adhesive. For the tension and compression zone the quantity of 67.858 cm^3 and 82.938 cm^3 of the adhesive were given for each hole respectively.

For the gluing the strain gauges into the threaded rods, the epoxy based adhesive A-2 was used. It is a product of the company Tokyo Sokki Kenkyujo Co., Ltd from Japan. The amount of 1 cm^3 was used for each threaded rod.

3-4 MACHINES AND TOOLS

3-4.1.1 Machines for screws

A power drill machine was used to screw the screws into the load application and support areas. It was also used for the vertical and inclined internal opening reinforcement (see figure 3.1 left) consisting of screws as well as threaded steel rods.

Socket wrench was utilized for tightening the screws flush with the load application area and the support area (see figure 3.1 right).

Figure 3.1: Power drill machine (left) and socket wrench (right)

3-4.1.2 Testing machine

The tests were carried out in the Laboratory of Structural Engineering (LKI). The machine used for this test was of the brand BETA 1000, and it has a servo-hydraulically controlled test cylinder with a maximum load of 1 MN. The static load was introduced with path-control.

The load transfer plate with sufficient stiffness for a uniform load distribution on the specimen (width 160 mm; 600 mm height) had a diameter of 300 mm and a thickness of 40 mm and is shown in the Figure 3.2. Intermediate plates were placed under the load transfer plate and on the support blocks in order to bridge gaps and to ensure full surface load introduction.

Figure 3.2: Testing machine BETA 1000

3-4.1.3 Displacement and deflection measurements

Displacements and deflections were measured in two ways for all the beams. A computer program called Mercury was used on one side of the beam. Mercury needs a contrast, consisting of a white background with very small spattered black spots on it. These spots can be captured with the help of two cameras, where Mercury is able to detect and calculate the movements of the surface along up to six axis (2D and 3D) (see figure 3.3 right up). The output data of Mercury contains the displacement of the required points as well as the measured force value of the testing machine, which allows an alignment to the additional measurement data.

On the other side of the beam, measurements were conducted with 2 DD1 (displacement transducer – shear cross) to measure the shear movements within the range of the opening. Another four displacement transducers are also measuring movements of the beam under the load on four points around the opening (see figure 3.3 left up).

For the measurements of series G, additional four strain gauges with the length of 50 mm were glued-on the beam. Positioning the strain gauge at the same height, distance from the opening and inclination as the strain gauge of the steel rods, enabled a direct compression of measurement results. They were connected as one fourth of a Wheatstone bridge (see figure 3.3 left down).

The strain gauges that were glued inside the threaded rods for the test series G were either the BTM-CTA6 or BTM-6C of the company Tokyo Sokki Kenkyujo Co., Ltd.

The test series H, which was reinforced with glued-in inclined steel rods under the angle of 40°, was equipped with glued-on strain gauges on the threaded rods, which measured the dilatations of the threaded rods (see figure 3.4). The strain gauges glued-on the threaded rods, for the test series H, had been LY43-6/120 from the company HBM. After gluing them on the threaded rod, they were covered with nitrile rubber NG150 and at the very end with aluminum foil coated knitting compound to protect the strain gauges against damages.

All of the strain gauge equipped steel rods for both series G and H were calibrated with three duty cycles whereat the last two cycles had a coefficient of determination higher than 0.9999.

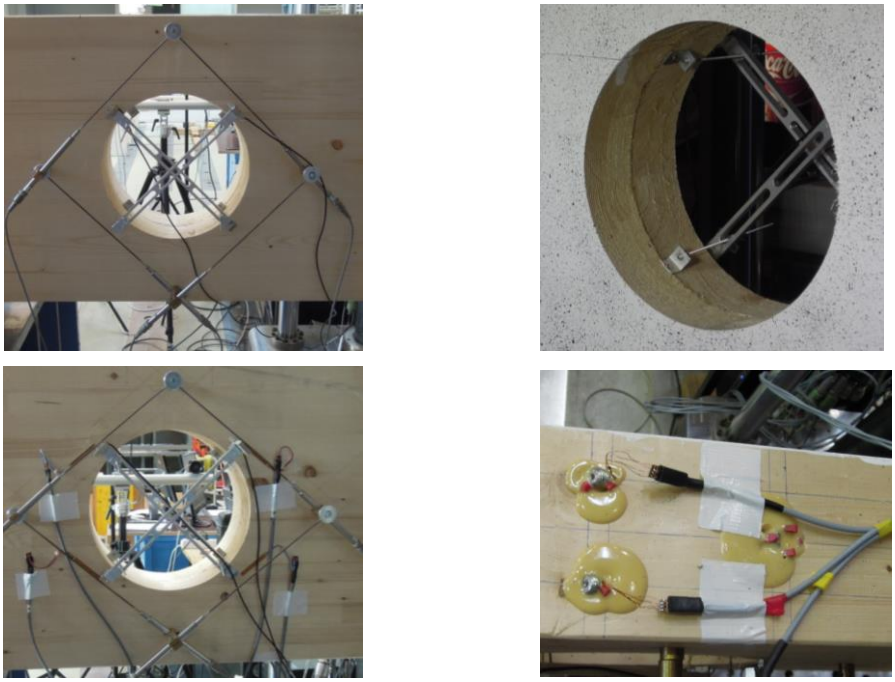

Figure 3.3: Displacement transducers and DD1 fixed on the test specimen beam (left up), prepared surface for the Mercury testing (right up); Displacement transducers and DD1 with additional strain gauges (left down); connection of the strain gauges for the measurement of the elongations of the threaded rods (right down)

Figure 3.4: Series H; the strain gauge glued on a threaded rod

Strain gauges [50]

The working principle of strain gauges is that the resistance of a conductor changes as the length of the conductor changes. The factor K and the influence of the change in length due to temperature differences are different, depending on the material of the conductor.

The basic requirements for strain gauges are as follows:

- B as bridge - factor should be as high as possible - even with a very small elongation ε the change in the ohmic resistance can be measured.
- The temperature changes should be as low as possible as they can distort the result.

In order to keep the temperature influence low, strain gauges are produced according to the thermal expansion coefficients of the measuring object (self-compensating strain gauges). Furthermore, it is possible, with the help of appropriate strain gauges settings, to measure with circuits which can compensate the influence of temperature.

The adhesive between the object, that should be measured, and the strain gauge, should be as thin as possible and the strain gauge should be protected from humidity.

The strain gauges are connected in a Wheatstone bridge. In figure 3.5, the bridge principle is schematically shown. The Whetstone bridge could be seen as the parallel connection of the resistors divided into two voltage dividers.

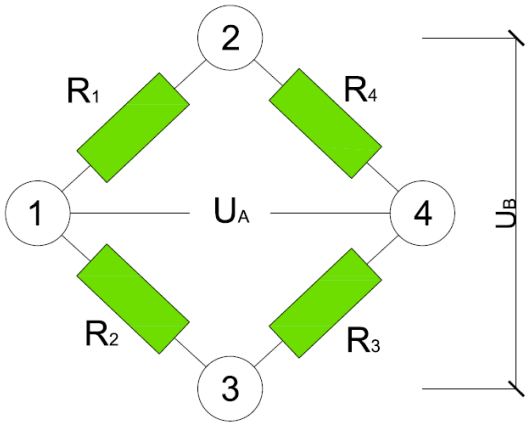

Figure 3.5: Schematic representation of Wheatstone bridge

The ratio between the output voltage and the input voltage is related to the resistance of the resistors as follows:

$$\frac{U_A}{U_B} = \frac{R_1}{R_1 + R_2} - \frac{R_4}{R_3 + R_4} \qquad 3.1$$

where:

U_A ... bridge output voltage, measuring signal [mV]
U_B ... bridge feeding voltage [V]

For the measurements of this work one quarter of the Wheatstone bridge was used, which means that the strain gauge as one resistor is a variable and the three others are fix resistors with a value of 120 Ω.

Equation 3.2 represents the calculation process for the one fourth of the Wheatstone bridge.

$$\frac{U_A}{U_B} = \frac{K}{4} \cdot B \cdot \varepsilon \qquad 3.2$$

where:

K	...	K-factor dependent on strain gauge type (for screwed-in threaded rods: 2.10; for glued-in threaded rods: 2.11)
B	...	bridge factor (for screwed-in threaded rods: 2.0; for glued-in threaded rods: 1.0); depended on the interconnection
ε	...	elongation ($\varepsilon = \Delta l / l$) *[m/m]*

In cases of displacement transducers without calibration data, force or the stress occurring can be calculated with the help of Hook`s law (see equation 3.3).

$$\sigma = E \cdot \varepsilon \qquad 3.3$$

where:

σ	...	normal stress in threaded rod ($\sigma = F / A$)
E	...	elastic modulus of threaded rods

As previously stated 16 of the threaded steel rods were drilled along the central axis. The drill diameter was 4 mm and the drilling was done to the depth of 320 mm at which the strain gauges were glued-in. Strain gauges were placed inside of the threaded rods in order to be able to measure strain reaction of the threaded rods.

Deflection of the beam was measured in two ways. First, with the deflection sensor, which was set in the beam mid-span and was taken off of the beam at the same time when the displacement transducers and shear cross were taken down. Second, the testing machine BETA 1000 has the ability to measure deflections. Thus, the results were gotten from these measurements and used for further calculations.

3-4.1.4 Drilling rig

The drilling rig was mandatory to get predrilled holes as precise as possible for the reinforcing screws and threaded rods. Due to the problems that occurred with the predrilled holes that were manufactured at company HAAS, the following holes for the second delivery were drilled on the Institute. This tool was used for precise drilling in timber and is able to provide a constant and precise drill axis until a depth of 600 mm, which was needed for inclined reinforcement of the opening (see figure 3.6).

Figure 3.6: Drilling support rig from side (left) and from above (right)

3-5 TEST CONFIGURATION

All test series underwent a three point bending test, therefore the moment distribution was triangular, where the maximum at mid-span of the beam (see figure 3.7). The three point bending test was chosen because of the simplicity of the calculation method and obtaining the greatest shear stress in the area of the opening, but the geometry for the calculation was taken from Gehri [47] calculation, where four point bending test was made. Apart from shear force and moment distribution, the main geometrical elements are presented in the figure 3.7 too which are important for the pre-calculation process. In the first draft, the shear length was assumed with $a = 1.75 \cdot h$ and is depicted in Figure 3.7 too. Further a length of 150 mm was outlined between the two shear field areas which is a relic of the four-point-bending test origin and describes the distance between the two imaginary load applications. Finally the shear area length is defined as the distance between the support and the load application at mid-height, in detail between the axes of the inner screws in case of compression reinforcements perpendicular to the grain.

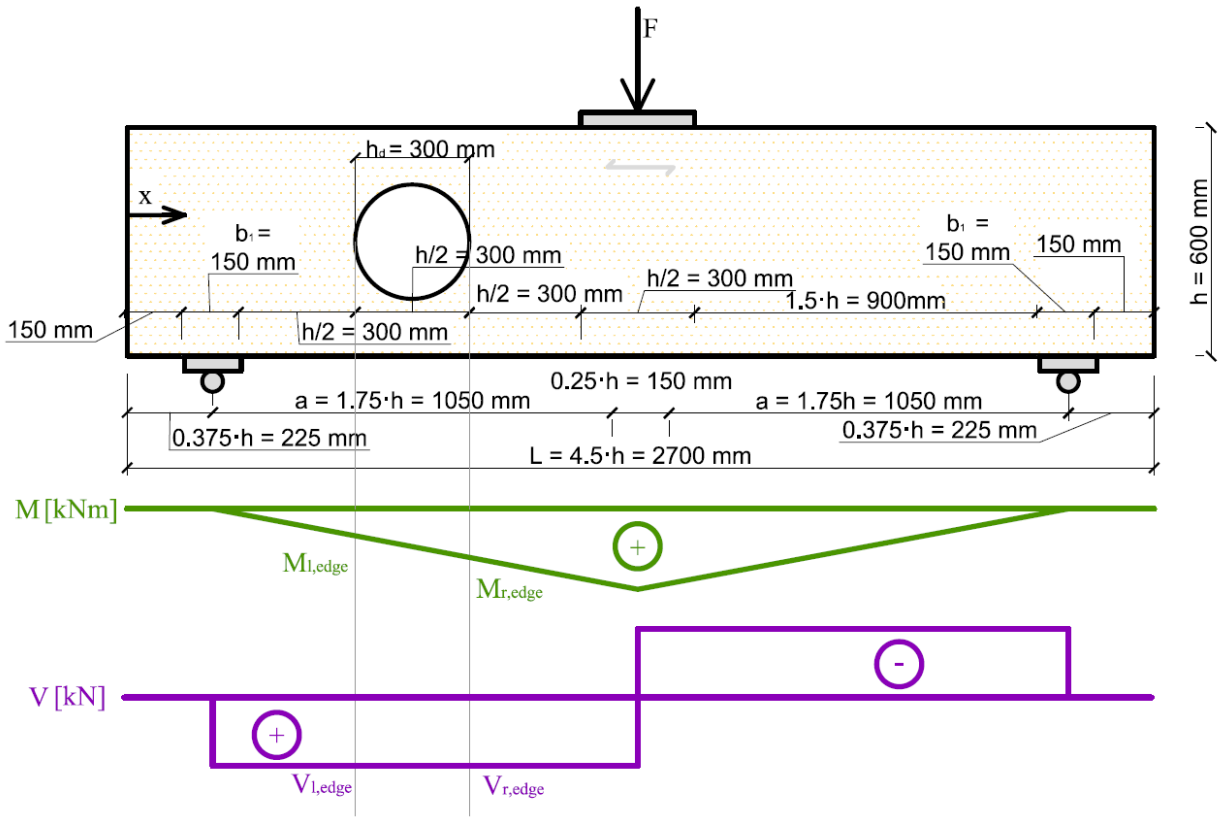

Figure 3.7: Schematic illustration of the three point bending test with geometry of tested beams

3-6 TEST SERIES

The first delivered beams were divided into 6 series (A, B, C, D, E and F), each consisting of five beams. The first five series were produced by the company HAAS Fertigbau Holzbauwerk Gesellschaft m.b.H. & Co. KG in strength class GL32h and were reinforced at the Institute. Series F was made from boards, which were used for the GLT of strength class GL32h which too were supplied by HAAS and processed in the laboratory.

The second delivery consisted of fifteen test specimens, which were divided into four test series of three test specimens (G, H, J and K) and three spare which were added to the test series C. The second delivery also was from HAAS with the same strength class GL32h.

Series A, B, C, D, E, G, H, J and K were produced with dimensions of length / width / height: 2700 / 160 / 600 mm. Only series F was a bit different as the width was made of four longitudinal layers with a thickness of 40 mm each, and two perpendicular layers with thickness of 20 mm each. All series from B to K have a round opening with a diameter of 300 mm.

Except for the series F every series was reinforced with screws at load application and support area. While the dimensions of the screws were the same (∅ 12 / 400 mm) for all reinforcements, the amount of screws was twelve at the load application area and six at each support area, except for the series B and some of C. These series only needed eight and four screws, as the maximum load was lower for them.

Application loads and bearing abilities were approximated according to series A and then reduced for the other series respectively.

Series A represented beams without an opening and should be used as reference series (see figure 3.8).

Series B consisted of beams with an unreinforced opening (see figure 3.8).

Series C had reinforced openings with vertical internal reinforcements in form of screws (∅ 12 x 500 mm) with the strength of 8.8 (see figure 3.8). Unfortunately, the beams were delivered with wrongly drilled holes for the vertical reinforcement. Instead of drilling the holes closer to the support side from down side of the beam and from the up side of the beam for those closer to the middle point, all of them were drilled from above. This was resolved by drilling the holes closer to the support through the existing holes. As the depth to diameter ratio was very high, the drill distorted on its way through the beam, which led to some faults. The load application and support areas were reinforced with 8 and 4 screws respectively for test specimens C01 through the C05 and with 12 and 6 screws respectively for the test specimens C06 through the C08.

Series D was made with reinforced openings, with 45° inclined screwed-in rods with diameter of 16 mm and 600 mm length (see figure 3.8). The holes for the steel rods were predrilled by the company HAAS and had the same lack of precision as the series C, so the two holes from the upper and lower side were crossing instead of passing by each other. Because of this fault, instead of inserting eight steel rods to each beam of series D, D02 and D03 were reinforced only with four steel rods in tension zone. The remaining specimens were first reinforced with steel rods in the tension area, screwed in to the complete length of 600 mm and second reinforcement in compression zone to the length of only 400 mm until the crossing reinforcement was hit.

Series E was built with external reinforcements made of the beech plywood panels in dimensions of approximately 700 x 600 x 30 mm on each side of the beam (see figure 3.8).

Series F consisted of CLT beams with an opening. In the load application area on each beam side, three reinforcement boards were glued-on. They were made of the same timber that was used for the production of the CLT beams (GL32h) and had the dimensions of 30 x 150 x 600 mm. At each support area two of the same boards were glued-on each beam side (see figure 3.8).

Series G had reinforced openings with inclined screwed-in threaded rods with dimensions of ∅ 16 x 600 mm (two on each tension side) and ∅ 20 x 600 mm (one on each compression side) under the angle of 40º. The holes for the threaded rods were drilled on the Institute with the help of the drilling rig in order to get the holes as precise as possible. Due to the adjustment of the steel rods diameter, as well as the number of the steel rods on each side of the beam, it was possible to get more precise holes across the beam width. The angle of 40º was chosen to shift the crossing point of the reinforcement axis away from the edge of the beam. This adjustment should benefit a higher bending strength of the net cross section.

Series H had a reinforced opening with glued-in threaded rods of ∅ 16 x 600 mm (two on each tension side) and ∅ 20 x 600 mm (one on each compression side) which are inclined under an angle of 40º.

Series J was built with external reinforcement of the beech plywood panels 700 x 600 x 20 mm, which were glued-on on both sides in the veneer press.

Series K was built with the same external reinforcement like series J, but was glued-on and pressed by screw pressing.

In figure 3.8 a schematic illustrations of all test series is depicted.

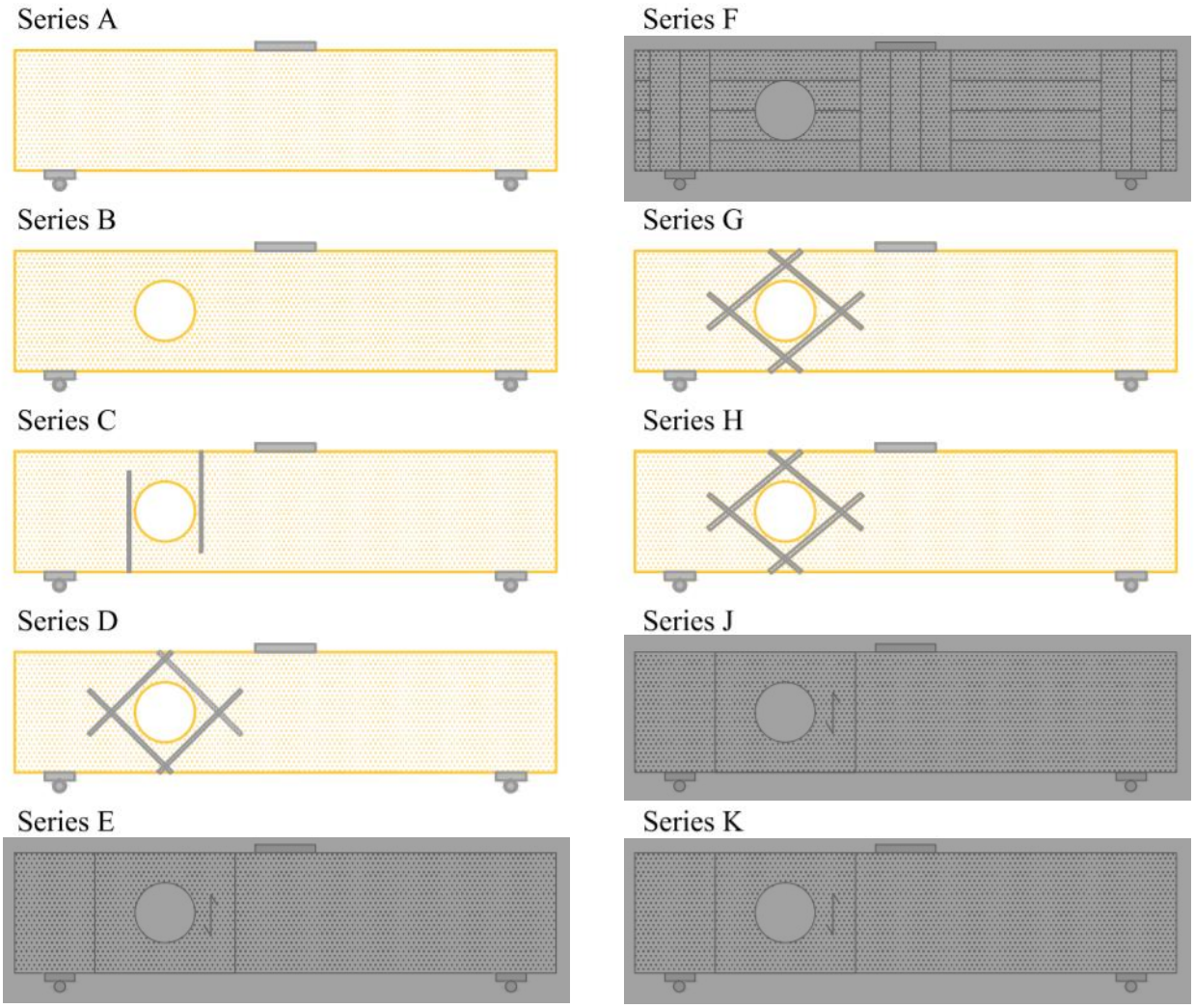

Figure 3.8: Schematic illustration of test series A, B, C, D, E, F, G, H, J and K

Table 3.1 gives an overview of the tested series.

Table 3.1: Overview of the test series

Series name (beams number)	**Descri-ption**	**Reinforcement of the load application /supports [mm]**	**Reinforcement of the opening**	**Production faults / adjust-ment**
A (5)	without opening	12 x ∅ 12 x 400 mm / 2 x 6 x ∅ 12 x 400	-	-
B (5)	with opening, not reinforced	8 x ∅ 12 x 400 mm / 2 x 6 x ∅ 12 x 400	none	-
C (8)	with opening, internally reinforced (90°)	8 or 12 x ∅ 12 x 400 mm / 2 x 4 or 2 x 6 x ∅ 12 x 400	internal: vertical screws ∅ 12 x 500 mm	wrongly pre drilled holes for vertical reinforcement
D (5)	with opening, internally reinforced (45°)	12 x ∅ 12 x 400 mm / 2 x 6 x ∅ 12 x 400	internal: inclined screwed-in threaded rods ∅ 16 x 600 mm	wrongly pre drilled holes for inclined reinforcement
E (5)	with opening, externally reinforced	12 x ∅ 12 x 400 mm / 2 x 6 x ∅ 12 x 400	external: beech plywood panels 700 x 600 x 30 mm	beech plywood instead of planed spruce plywood
F (5)	CLT beam	-	perpendicular layers of CLT	-
G (3)	with opening, internally reinforced (40°)	12 x ∅ 12 x 400 mm / 2 x 6 x ∅ 12 x 400	internal: inclined screwed-in threaded rods ∅ 16 x 600 mm and ∅ 20 x 600 mm	adjusted inclination of the opening reinforcement
H (3)	with opening, internally reinforced (40°)	12 x ∅ 12 x 400 mm / 2 x 6 x ∅ 12 x 400	internal: inclined glued-in threaded rods ∅ 16 x 600 mm and ∅ 20 x 600 mm	adjusted inclination of the opening reinforcement
J (3)	with opening, externally reinforced	12 x ∅ 12 x 400 mm / 2 x 6 x ∅ 12 x 400	external: beech plywood glued-on panels 700 x 600 x 20 mm	inclined screw holes closed with glue (except for J03); beech plywood panels as planned
K (3)	with opening, externally reinforced	12 x ∅ 12 x 400 mm / 2 x 6 x ∅ 12 x 400	external: beech plywood panels glued-on by screw pressing 700 x 600 x 20 mm	inclined screw holes closed with glue; beech plywood panels as planned

3-7 TESTING PREPARATIONS

3-7.1 PRELIMINARY DESIGN

For the preliminary design of the different reinforcements of the beams with an opening their load bearing capacities were calculated with the help of different standards, technical approvals and proposals in technical reports. The following listing gives an overview of used calculation methods for each test series (only reference and internally reinforced areas) [28]:

- Series A:
  - ON B 1995-1-1:2015 [19]
  - DIN EN 1995-1-1/NA:2010 [22]
- Series B:
  - ON B 1995-1-1: 2015 [19]
  - DIN EN 1995-1-1/NA:2010 [22]
- Series C:
  - ON B 1995-1-1:2015 [19]
  - DIN EN 1995-1-1/NA:2010 [22]
  - ETA-11/0190 [51]
- Series D, G and H:
  - ALP GSA® process from n'H neue Holzbau AG by Strahm [44]

According to ON B 1995-1-1:2015 [19], the maximum possible opening height varies depending on the design type of reinforcement. The tested openings height h_d, was $0.5 \cdot h$, which is beyond the allowed maximum opening size of the ON B 1995-1-1:2015 [19] but is in accordance to the tests conducted by Strahm [44] and Flaig [48].

The most important beam geometry and material specific parameters are listed in tables 3.2 and 3.3.

Table 3.2: Overview of beam geometry parameters

Description	Unit	Value
Beam width b	[mm]	160
Beam height h	[mm]	600
Beam length L	[mm]	2 700
Opening height h_d	[mm]	300
Girth height (up and down) h_r	[mm]	150
Distance from support to opening middle x_{hole}	[mm]	525
Distance from support to critical crack point $x_{45°}$(right side of opening)	[mm]	630
Distance from support to opening edge x_{edge} (right opening edge)	[mm]	675
Distance between supports	[mm]	2 250

For the calculation, characteristic strength values of GL32h according to EN 14080:2013 [46] and ON B 1995 -1- 1:2015 [19] were used.

The shear strength is crucial for the calculation. According to Gehri [47] (see equation 3.4) and Brandner [52] (see equation 3.5) two shear strengths were calculated and from those two the mean value for the calculation was established.

$$f_{v,mean} = 100 \cdot A_{shear}^{-0.28} = 100 \cdot (a \cdot b)^{-0.28} = 100 \cdot 168\,000^{-0.28} = 3.44\ N/mm^2 \quad 3.4$$

$$f_{v,mean} = 40.2 \cdot A_{shear}^{-0.2} = 40.2 \cdot 168\,000^{-0.2} = 3.62\ N/mm^2 \quad 3.5$$

where:

a	...	shear area length [mm]
b	...	beam width [mm]

A shear length of a = 1050 mm was used for the preliminary design, where the chosen mean value of shear strength for pre calculation was $f_{v,mean}$ = 3.5 N/mm^2. In case of the exact shear area length of 950 mm the shear strength would have been calculated to 3.54 N/mm^2 (equation 3.4) and 3.69 N/mm^2 (equation 3.5) respectively.

$$a = 1.75 \cdot h = 1.75 \cdot 600 = 1\,050\ mm \quad 3.6$$

$$A_{shear} = a \cdot b = 1\,050 \cdot 160 = 168\,000\ mm^2 \quad 3.7$$

where:

a	...	shear area length [mm]
A_{shear}	...	shear area [mm^2]

The mean value of all important calculating parameters had been calculated by assuming a normal distribution and COV-coefficient (see table 3.3):

$$f_{x,mean} = \frac{f_{x,k}}{1 - 1.645 \cdot COV} \quad 3.8$$

The 95 %-fractile value of all important calculating parameters had been calculated by assuming a normal distribution and COV-coefficient (see table 3.3)

$$f_{v,95} = f_{v,mean} \cdot (1 + 1.645 \cdot COV) \quad 3.9$$

Equations 3.8 and 3.9 were used to calculate all mean and 95 %-fractile values, which were needed for further calculation.

Table 3.3 provides an overview of most necessary parameters specific to materials parameters as well as their mean and 95 %-fractile values. These were used for further calculations for GL32h according to EN 14080 [46] and ON B 1995-1-1:2015 [19] are listed in table 3.3. The same table 3.3 lists specific parameters for needed screws and steel rods, as well as corresponding mean and 95 %-fractile values. These were used for further calculation according to ETA-11/0190 [51] and Z-9.1.-777 [53].

Table 3.3 also lists, aside from mentioned parameters, necessary glueline parameters, as well as their mean and 95 %-fractile values, used in further calculation according to Z-9.1-778 [43].

Table 3.3: Overview of most needed specific parameters for further calculation

Description	Unit	Characteristic value	Mean value	95 %-fractile value	COV-coefficient [%]
Bending strength f_m	[N/mm²]	32.0	42.48	52.96	15
Shear strength f_v	[N/mm²]	2.64	3.50	4.36	15
Rolling shear strength f_r	[N/mm²]	1.20	1.59	1.98	15
Compression strength perpendicular to the grain $f_{c,90}$	[N/mm²]	3.30	3.8	4.15	8
Tensile strength perpendicular to the grain $f_{t,90}$	[N/mm²]	0.5	0.745	0.990	20
Shear modulus $G_{0,mean}$	[N/mm²]	650	/	/	/
Density ρ_k	[kg/m³]	440	/	/	/
Pull out parameter for the screws f_{ax}	[N/mm²]	10	12.72	15.4	13
Characteristic tensile strength of screws f_{tens}	[kN]	45	53.86	62.7	10
Pull out strength parameter of the steel rods $f_{k,1}$	[N/mm²]	9.65	12.3	14.9	13
Characteristic glueline strength f_{k1}	[N/mm²]	6.18	7.86	9.45	13

According to EN 14080 [46] and ON B 1995-1-1:2015 [19] the value for compression strength perpendicular to the grain $f_{c,90,k}$ is 2.5 N/mm^2 but for the purpose of this master thesis a value of 3.3 N/mm^2 according to [54] was taken.

This work is focused on the discussion of Series C, D, G and H therefore series A and B will be covered too as they are the reference base. According to this definition, series E, F, J and K were not included in the subsequent parts of the preliminary design.

3-7.1.1 GLT beams without opening (series A)

For the preliminary calculation of the beams without an opening, the dimensions are shown in figure 3.9 and table 3.2. The values for the material specific parameters of GL32h are listed in table 3.3.

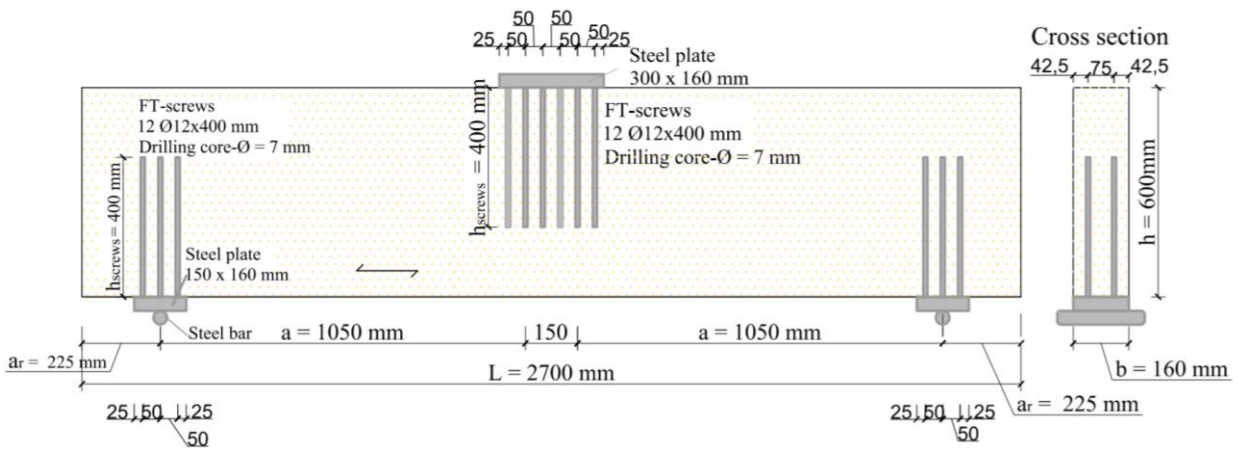

Figure 3.9: Outline and dimensions of the test specimens of series A [28] (adapted)

The calculation of the maximum load was done by reverse calculation of the shear strength as the shear failure was supposed to be authoritative:

$$\tau_v = \frac{3 \cdot V_{\max,mean}}{2 \cdot A} \leq f_{v,mean} \Rightarrow V_{\max,mean} = \frac{2 \cdot b \cdot h \cdot f_{v,mean}}{3} = \frac{2 \cdot 160 \cdot 600 \cdot 3.5}{3} = 224\ kN$$
$$\tau_v = \frac{3 \cdot V_{\max,95}}{2 \cdot A} \leq f_{v,95} \Rightarrow V_{\max,95} = \frac{2 \cdot b \cdot h \cdot f_{v,95}}{3} = \frac{2 \cdot 160 \cdot 600 \cdot 4.36}{3} = 279\ kN \quad (3.10)$$

$$F_{\max,mean} = 2 \cdot V_{\max,mean} = 2 \cdot 224 = 448\ kN$$
$$F_{\max,95} = 2 \cdot V_{\max,95} = 2 \cdot 279 = 558\ kN \quad (3.11)$$

The bending stress at the mid span of the beam was calculated with shear area length of 1 125 mm (see figure 3.7):

$$M_{Field} = a \cdot V_{\max,95} = 1.125 \cdot 279 = 314\ kNm \quad (3.12)$$

$$W_y = \frac{b \cdot h^2}{6} = \frac{0.16 \cdot 0.6^2}{6} = 9.60 \cdot 10^{-3}\ m^3 \quad (3.13)$$

$$\sigma_{\max} = \frac{M_{Field}}{W_y} = \frac{314}{9.60} = 32.7\ N/mm^2 \quad (3.14)$$

To proof no bending failure will occur, the bending shear stress must be at least larger than the characteristic bending strength $f_{m,k}$ (see table 3.3). This criteria was fulfilled as the utilization factor was 1.02 which was close enough to 1.0 (see equation 3.15).

$$\eta = \frac{\sigma_{\max}}{f_{m,k}} = \frac{32.7}{32.0} = 1.02 \leq 1.0 \quad \checkmark \quad (3.15)$$

Further the compressive strength perpendicular to the grain should also be higher than the compression stress at the load level of the shear failure.

While the support width was set at 160 mm, which was the same as the beam width, the support length was 150 mm. The overlap to the left side was 150 mm and was 1 050 mm to the right, which lead to a compressive coefficient perpendicular to the grain of $k_{c,90}$ = 1.80 according to the enBR [24] for GL32h. Similar to the bending stress, the characteristic compression strength $f_{c,90,k}$ was used which resulted in a utilization factor of η = 1.96 (see equation 3.17).

$$\sigma_{c,90,95} = \frac{V_{\max,95}}{b \cdot l_{support}} = \frac{279 \cdot 10^3}{160 \cdot 150} = 11.64\ N/mm^2 \quad (3.16)$$

$$\eta = \frac{\sigma_{c,90}}{k_{c,90} \cdot f_{c,90,k}} = \frac{11.64}{1.80 \cdot 3.30} = 1.96 \leq 1.0 \quad \times \quad (3.17)$$

where:

$k_{c,90}$ ... compression stress perpendicular to the grain coefficient

As the compression area of the load introduction was twice as much as one support area, the compressive stress was the same. Due to a compression stress higher than the material strength reinforcement of the supports and load application area had to be considered.

The reinforcement was performed with screws and calculated according to ETA-11-0190 - ASSY, Würth [51].

The nominal diameter *d* was 12 mm for both support and load application areas. At support areas, there were two rows of 3 screws in grain direction, which was 6 screws in total for each support. At the load application area two rows with 6 screws in grain direction were used, 12 screws in total.

The distances between the screws, both parallel and perpendicular to the grain, were chosen according to ETA-11-0190 - ASSY, Würth [51] and are shown in figure 3.9.

Characteristic load bearing capacity according to ETA-11-0190 - ASSY, Würth [51]:

$$R_{90,k} = \min \begin{Bmatrix} k_{c,90} \cdot B \cdot l_{ef,1} \cdot f_{c,90,k} + n \cdot \min \begin{Bmatrix} R_{ax,k} \\ \kappa_c \cdot N_{pl,k} \end{Bmatrix} \\ B \cdot l_{ef,2} \cdot f_{c,90,k} \end{Bmatrix} \quad 3.18$$

where:

B	…	support width [mm]
$l_{ef,1}$	...	effective contact length according to EN 1995-1-1:2004 + A1: 2008 [51] [mm], equal to $l_{support}$
$f_{c,90,k}$	...	characteristic compressive strength perpendicular to the grain [N/mm²]
n	...	number of reinforcing screws ; $n = n_0 \cdot n_{90}$
n_0	...	number of reinforcing screws in grain parallel direction
n_{90}	...	number of reinforcing screws in grain perpendicular direction
$f_{ax,k}$	...	characteristic thread pull out capacity of the screws [N/mm²]
d	...	screw nominal diameter [mm]

The missing parameters can be calculated as follows:

$$R_{ax,k} = f_{ax,k} \cdot d \cdot l_{ef} = 10 \cdot \left(\frac{440}{350} \right)^{0.8} \cdot 12 \cdot 300 = 43\ 232\ kN = 43.2\ kN \quad 3.19$$

$$\kappa_c = \frac{1}{k + \sqrt{k^2 - \overline{\lambda_k}^2}} = \frac{1}{0.966 + \sqrt{0.966^2 - 0.799^2}} = 0.663 \quad \text{for} \quad \overline{\lambda_k} > 0.2 \quad 3.20$$

$$k = 0.5 \cdot \left[1 + 0.49 \cdot (\overline{\lambda_k} - 0.2) + \overline{\lambda_k}^2 \right] = 0.5 \cdot \left[1 + 0.49 \cdot (0.799 - 0.2) + 0.799^2 \right] = 0.966 \quad 3.21$$

$$\overline{\lambda_k} = \sqrt{\frac{N_{pl,k}}{N_{ki,k}}} = \sqrt{\frac{39.59}{62.119}} = 0.799 \quad 3.22$$

$$N_{pl,k} = \pi \cdot \frac{d_1^2}{4} \cdot f_{y,k} = \pi \cdot \frac{7.1^2}{4} \cdot 1\ 000 = 39\ 592\ N \quad 3.23$$

$$N_{ki,k} = \sqrt{c_h \cdot E_s \cdot I_s} = \sqrt{147 \cdot 210\ 000 \cdot 125} = 62\ 119\ N = 62.1\ kN \quad 3.24$$

$$I_s = \frac{\pi \cdot d_1^4}{64} = \frac{\pi \cdot 7.1^4}{64} = 125\ mm^4 \qquad 3.25$$

$$l_{ef,2} = l_{ef} + (n_0 - 1) \cdot a_1 + \min\{l_{ef};\ a_{1,c}\} = \\ = 300 + (3-1) \cdot 50 + \min\{300;\ 175\} = 575\ mm \qquad 3.26$$

where:

$\overline{\lambda_k}$		related slenderness
$N_{pl,k}$	...	characteristic value of the standard plastic load carrying capacity of the net cross section [N]
l_{ef}	...	effective threaded screw length [mm]
a_1	...	distance of the screws center in the direction parallel to the grain [mm]
$a_{1,c}$	...	distance of the screw center to the end grain surface [mm]
d_1	...	core diameter of the screw [mm]
I_s		moment of inertia of the screws [mm^4]
ρ_k	…	density of GL32h
α	…	angle between screw axis and grain direction
E_s		modulus of elasticity of steel E_s = 210 000 N/mm^2

- $f_{y,k}$ = 1 000 N/mm² for Würth ASSY plus full threaded screws and ASSY, screws with full thread

-$f_{y,k}$ = 800 N/mm² for hot-dip galvanized Würth ASSY plus full threaded screws

Inserting the calculated parameters into equation 3.18 results in an load bearing capacity of 300 kN. The maximum applied load must be at least smaller than the load bearing capacity. This criteria was fulfilled as the utilization factor was 0.93 (see equation 3.28).

$$R_{90,k} = \min\left\{ \begin{matrix} k_{c,90} \cdot B \cdot l_{ef,1} \cdot f_{c,90,k} + n \cdot \min\left\{ \begin{matrix} R_{ax,k} \\ \kappa_c \cdot N_{pl,k} \end{matrix} \right\} \\ B \cdot l_{ef,2} \cdot f_{c,90,k} \end{matrix} \right\} = \\ = \min\left\{ \begin{matrix} 1.80 \cdot 160 \cdot 150 \cdot 3.3 + 6 \cdot \min\left\{ \begin{matrix} 43\ 000 \\ 0.663 \cdot 39\ 590 \end{matrix} \right\} \\ 160 \cdot 575 \cdot 3.3 \end{matrix} \right\} = \\ = \min\left\{ \begin{matrix} 300\ 049\ N \\ 303\ 600\ N \end{matrix} \right\} = 300.0\ \text{kN} \qquad 3.27$$

$$\eta = \frac{V_{max,95}}{R_{90,k}} = \frac{279}{300.0} = 0.93 \le 1.0 \quad \checkmark \qquad 3.28$$

3-7.1.2 GLT beams with unreinforced opening (series B)

As previously stated, the beams with unreinforced openings have different regulations in different standards. In figure 3.10 the areas with increased tensile stress perpendicular to the grain are at the opening edge on the top right and bottom left position, at α = 45° (±180°) to the longitudinal axis of the beam. According to the standard a simplified linear stress distribution $\sigma_{t,90d}$ is proposed with a triangular load spreading along $l_{t,90}$ (see equation 3.29).

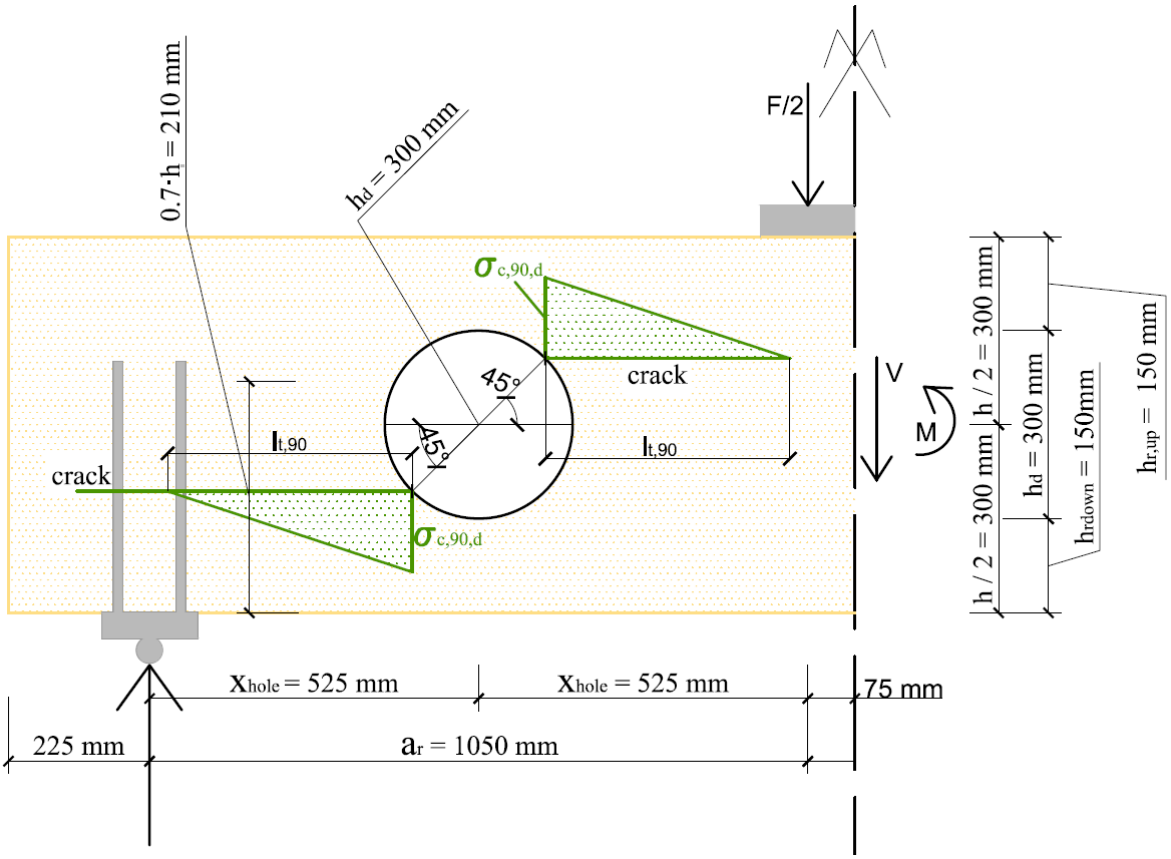

Figure 3.10: Outline and dimensions of the unreinforced GLT beams of series B [28] (adapted)

$$l_{t,90} = 0.35 \cdot h_d + 0.5 \cdot h = 0.35 \cdot 300 + 0.5 \cdot 600 = 405\,\text{mm} \qquad 3.29$$

Further the coefficient $k_{t,90}$ was needed to calculate the crucial tensile stress perpendicular to the grain (see chapter 2-1.2):

$$k_{t,90} = \min\left\{\left(\frac{450}{h}\right)^{0.5}\right\} = \min\left\{\left(\frac{450}{600}\right)^{0.5}\right\} = \min\left\{\begin{matrix}1\\0.87\end{matrix}\right\} = 0.87 \qquad 3.30$$

For estimating the authoritative failure mode the maximal load was calculated for the mean tensile strength perpendicular to the grain and for the 95 %-fractile value as stated in equations 3.8 and 3.9 and table 3.3.

The expected tensile force perpendicular to the grain was:

$$F_{t,90,mean} = f_{t,90,mean} \cdot 0.5 \cdot l_{t,90} \cdot b_{ef} \cdot k_{t,90} = 0.745 \cdot 0.5 \cdot 405 \cdot 160 \cdot 0.87 = 21.0\ kN$$
$$F_{t,90,95} = f_{t,90,95} \cdot 0.5 \cdot l_{t,90} \cdot b_{ef} \cdot k_{t,90} = 0.990 \cdot 0.5 \cdot 405 \cdot 160 \cdot 0.87 = 27.9\ kN \quad (3.31)$$

The shear force $V_{max,mean/95}$ and load $F_{max,m,mean/95}$ was calculated by transforming equation 2.8, where ($F_{max,mean/95} = 2 \cdot V_{max,mean/95}$, see equation 3.11):

$$F_{t,90,d} = F_{t,V,d} + F_{t,M,d} = \left[\frac{V_d \cdot h_d}{4 \cdot h} \cdot \left(3 - \frac{h_d^2}{h^2}\right)\right] + \left[0.008 \cdot \frac{M_d}{h_r}\right]$$

$$F_{t,90,mean,d} = \left[\frac{V_{max,mean} \cdot (0.7 \cdot h_d)}{4 \cdot h} \cdot \left(3 - \frac{(0.7 \cdot h_d)^2}{h^2}\right)\right] + \left[0.008 \cdot \frac{V_{max,mean} \cdot x_{45}}{h_r + 0.15 \cdot h_d}\right] =$$

$$= \left[\frac{21.0 \cdot (0.7 \cdot 300)}{4 \cdot 600} \cdot \left(3 - \frac{(0.7 \cdot 300)^2}{600^2}\right)\right] + \left[0.008 \cdot \frac{21.0 \cdot 630}{150 + 0.15 \cdot 300}\right] = 75.3\ kN \quad (3.32)$$

$$F_{t,90,d,95} = \left[\frac{V_{max,95} \cdot (0.7 \cdot h_d)}{4 \cdot h} \cdot \left(3 - \frac{(0.7 \cdot h_d)^2}{h^2}\right)\right] + \left[0.008 \cdot \frac{V_{max,95} \cdot x_{45}}{h_r + 0.15 \cdot h_d}\right] =$$

$$= \left[\frac{27.9 \cdot (0.7 \cdot 300)}{4 \cdot 600} \cdot \left(3 - \frac{(0.7 \cdot 300)^2}{600^2}\right)\right] + \left[0.008 \cdot \frac{27.9 \cdot 630}{150 + 0.15 \cdot 300}\right] = 100.1\ kN$$

$$F_{max,mean} = 150.6\ kN \qquad F_{max,95} = 200.2\ kN \quad (3.33)$$

According to the ON B 1995-1-1:2015 [19] (annex F), the bending stresses have to be calculated for the net cross-section. For the following calculations it was assumed, that the beam will fail on the tensile stress perpendicular to the grain for which reason the further failure models are verified by using the previously determined forces. Further only the worst case was checked except in cases of utilization factors higher than 1.0.

$$M_{hole,95} = V_{max,95} \cdot x_{hole} = 100.1 \cdot 0.525 = 52.5\ kNm \quad (3.34)$$

$$W_{net} = \frac{b \cdot \left[h^3 - h_d^3\right]}{12} \cdot \frac{2}{h} = \frac{160 \cdot \left[600^3 - 300^3\right]}{12} \cdot \frac{2}{600} = 8.40 \cdot 10^6\ mm^3 \quad (3.35)$$

According to [28] further bending verifications in two different sections are necessary for round openings. The first section pass through the position of the initial crack (α = 45°). The second one is loaded at the right edge (closer to load introduction) of the opening. For these section a secondary moment have to be considered.

The moment $M_{ri,45°,95}$ at the position of α = 45° was calculated according to equation 3.36:

$$M_{ri,45°,95} = V_{max,95} \cdot x_{45} = 100 \cdot 630 = 63.0\ kNm \quad (3.36)$$

Section modulus of the upper girth at α = 45° $W_{girth,up}$:

$$W_{girth,45°,up} = \frac{b \cdot \left(h_r + 0.15 \cdot h_d\right)^2}{6} = \frac{160 \cdot \left(150 + 0.15 \cdot 300\right)^2}{6} = 1.01 \cdot 10^6 \text{ mm}^3 \quad 3.37$$

The exact formulas for the bending stress are presented in chapter 3-6.2.6. By use of these equations the bending stress at α = 45° was calculated to:

$$\sigma_{m,45,95} = 13.24 \text{ N/mm²} \leq f_{m,k} = 32.0 \text{ N/mm²} \checkmark \quad \eta = 0.41 \leq 1.0 \checkmark \quad 3.38$$

Moment on the right edge of opening $M_{ri,edge,95}$:

$$M_{ri,edge,95} = V_{max,95} \cdot x_{edge} = 100 \cdot 0.675 = 67.5 \text{ kNm} \quad 3.39$$

Section modulus of the upper girth on the right edge of the opening $W_{girth,edge,up}$:

$$W_{girth,edge},up = \frac{b \cdot \left(\frac{h}{2}\right)^2}{6} = \frac{160 \cdot \left(\frac{600}{2}\right)^2}{6} = 2.40 \cdot 10^6 \text{ mm}^3 \quad 3.40$$

Bending stress on the right side of the opening is a combination of the $M_{ri,edge,95}$, $M_{hole,95}$ and $V_{max,95}$. The values of the bending stress and utilization factor are represented in equation 3.41:

$$\sigma_{m,edge,95} = 10.6 \text{ N/mm²} \leq f_{m,k} = 32.0 \text{ N/mm²} \checkmark \quad \eta = 0.33 \leq 1.0 \checkmark \quad 3.41$$

As the specimen will fail due to the shear stress at the 95 %-fractile load (see equation 3.45) a second verification with the mean load was conducted. For this calculation k_τ-coefficient was disregarded (see 2-1.2.2 [28]). An assumption for COV for $f_{v,k}$ was made with 15 %.

$$\tau_{net,mean} = 1.5 \cdot \frac{V_{max,mean}}{b \cdot \left(h - h_d\right)} = 1.5 \cdot \frac{75.3 \cdot 10^3}{160 \cdot \left(600 - 300\right)} = 2.35 \text{ N / mm}^2 \quad 3.42$$

$$\tau_{net,95} = 1.5 \cdot \frac{V_{max,95}}{b \cdot \left(h - h_d\right)} = 1.5 \cdot \frac{100.1 \cdot 10^3}{160 \cdot \left(600 - 300\right)} = 3.13 \text{ N / mm}^2 \quad 3.43$$

$$\eta = \frac{\tau_{net,mean}}{f_{v,mean}} = \frac{2.35}{3.5} = 0.67 \leq 1.0 \checkmark$$
$$\eta = \frac{\tau_{net,95}}{f_{v,k}} = \frac{3.13}{2.64} = 1.19 \leq 1.0 \times \quad 3.44$$

According to the equations 3.42 to 3.44 it is not sure whether the specimen will fail due to tensile or shear stress.

3-7.1.3 GLT beams with vertical screw reinforcement of the opening (series C)

According to ON B 1995-1-1:2015 [19], the beams with openings can be internally reinforced with steel rods, carried out either by self-drilling fully-threaded screws or glued-in rods. In this master thesis, for the vertical reinforcement of the opening self-drilling screws (∅ 12 x 500 mm) in strength of 8.8 were used.

The allowed opening height for vertically reinforced beams with openings is set to 30 % of the beam height (according to ON B 1995-1-1:2015 [19]). For purposes of this master thesis h_d was set to 50 % of the beam height. In the figure 3.11 and tables 3.2 and 3.3 some important geometry data for the calculation process as well as strength parameters are given.

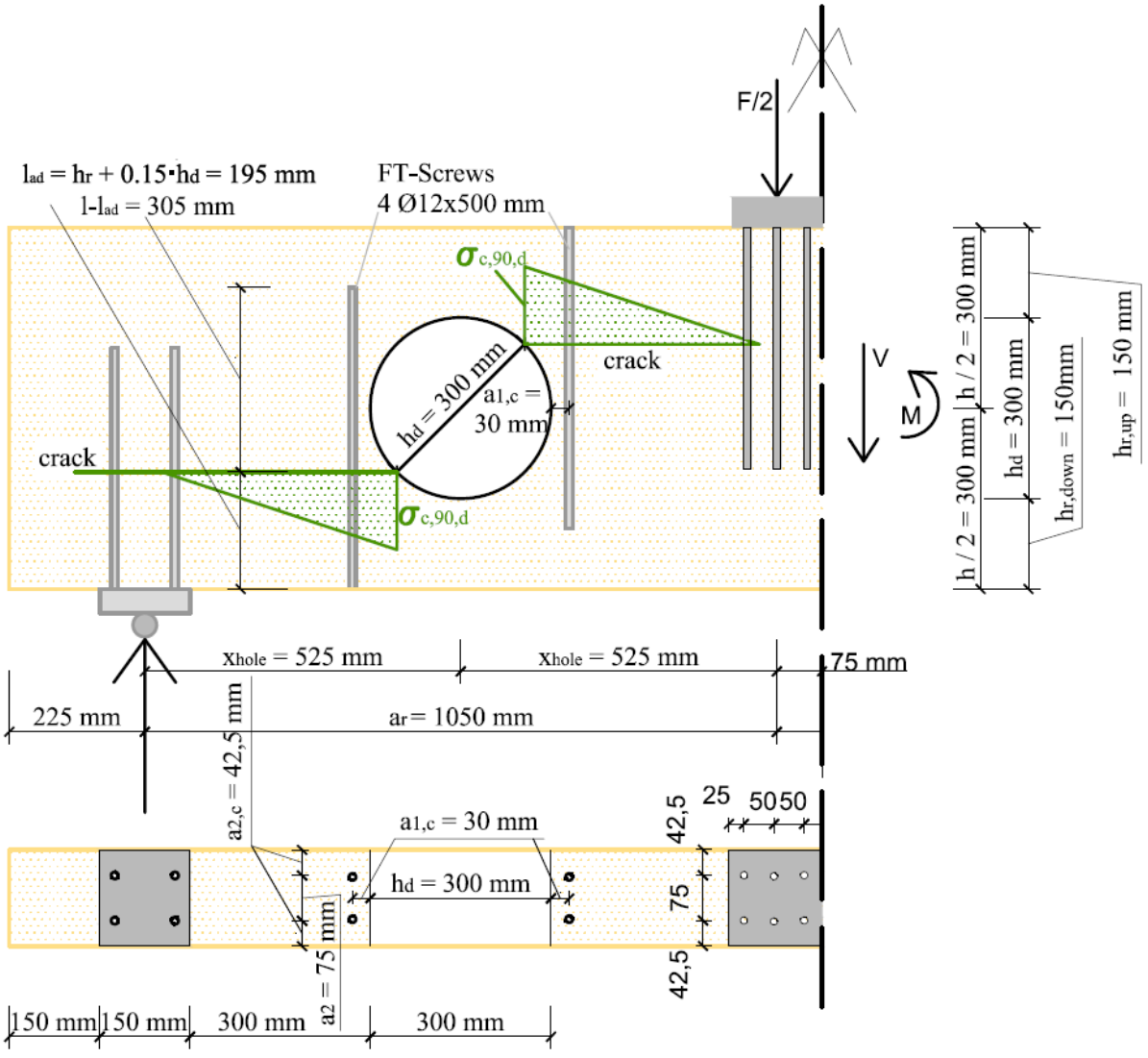

Figure 3.11: Outline and dimensions of the GLT beam with vertical screws as internal reinforcement of series C [28] (adapted)

The ON B 1995-1-1:2017 [19] sets the minimum distances from the screw to the opening edge along the grain direction to $a_{3,c} \geq 2.5 \cdot d = 30$ mm (equal to $a_{1,c}$). The distance $a_{3,c} \cong a_{1,c}$ was chosen with $a_{1,c} = 30$ mm.

The closest possible reinforcement of the opening, covers the most impacted places by stress perpendicular to the grain.

Further distances between the screws and edges are listed in the ETA-11/0190 [51] with $a_2 \geq 2.5 \cdot d$ and $a_{2,c} \geq 3.0 \cdot d$ which were met both.

The shear strength was, as previously stated, calculated as 3.5 N/mm^2 [47], [52]. The 95 %-fractile $f_{v,95}$ = 4.36 N/mm^2 was calculated with the help of the normal distribution as shown in equation 3.6.

The area of the net cross-section was calculated as shown in equation 3.45:

$$A_{net} = (h - h_d) \cdot b = (600 - 300) \cdot 160 = 48\ 000\ mm^2 \quad 3.45$$

The expected shear force at the 95 %-fractile of the shear strength was calculated by using the net cross section with the formula for shear stress in rectangular cross section but a reverse calculation was used:

$$V_{\max,95} = \frac{f_{v,95} \cdot A_{net}}{1.5} = \frac{4.36 \cdot 48\ 000}{1.5} = 139.5\ kN \quad 3.46$$

The maximum load force is double the value of $V_{\max,95}$:

$$F_{\max,95} = 2 \cdot V_{\max,95} = 2 \cdot 139.5 = 279.0\ kN \quad 3.47$$

Normal stresses of the opening region were calculated for the net cross-section.

The moment in the middle point of the opening was calculated with the help of the shear force $V_{\max,95}$ and x_{hole}, the distance between the support of the beam to the opening center:

$$M_{hole,95} = V_{\max,95} \cdot x_{hole} = 139.5 \cdot 0.525 = 73.2\ kNm \quad 3.48$$

The bending stress was calculated as follows:

$$\sigma_{m,hole,95} = \frac{M_{hole,95} \cdot h \cdot 6}{(h^3 - h_d^3) \cdot b} = \frac{73.2 \cdot 10^6 \cdot 600 \cdot 6}{(600^3 - 300^3) \cdot 160} = 8.71\ N/mm^2 \quad 3.49$$

The utilization factor was below 1.0, therefore, there was no problem overcoming the bending moment:

$$\eta = \frac{\sigma_{hole,95}}{f_{m,k}} = \frac{8.71}{32.0} = 0.27 \leq 1.0 \quad \checkmark \quad 3.50$$

The moment on the opening edge at the angle α = 45° was calculated with the help of $V_{\max,95}$ and x_{45}, the distance from the support of the beam to the right opening periphery (at α = 45°):

$$M_{ri,95} = V_{\max,95} \cdot x_{45} = 139.5 \cdot 0.630 = 87.89\ kNm \quad 3.51$$

The bending stress was calculated in the same way as previously stated in 3-6.1.2. The value is shown in equation 3.52:

$$\sigma_{m,45,95} = 18.5\ N/mm^2 \quad 3.52$$

The utilization factor was below 1.0 too, therefore, there was no problem for the beam to take the bending moment:

$$\eta = \frac{\sigma_{m,45,95}}{f_{m,k}} = \frac{18.5}{32.0} = 0.58 \leq 1.0 \quad \checkmark \qquad 3.53$$

The moment at right opening edge was calculated with the help of the $V_{max,95}$ and x_{edge}, the distance between the support of the beam to the right opening periphery:

$$M_{ri,edge,95} = V_{\max,95} \cdot x_{edge} = 139.5 \cdot 0.675 = 94.2\ kNm \qquad 3.54$$

The bending stress on the right opening edge was calculated in the same way as previously stated in 3-7.1.2. The value is shown in equation 3.55:

$$\sigma_{m,ri,95} = 14.7\ N/mm^2 \qquad 3.55$$

The utilization factor was below 1.0, therefore, there was no problem in overcoming the bending moment:

$$\eta = \frac{\sigma_{m,ri,45}}{f_{m,k}} = \frac{14.7}{32.0} = 0.46 \leq 1.0 \quad \checkmark \qquad 3.56$$

Tensile stress perpendicular to the grain:

The tensile force perpendicular to the grain $F_{t,90}$, at the critical points ($\alpha = 45° \pm 90^o$) were determined as shown in the following equations:

$$F_{t,90,95} = \left[\frac{V_{\max,95} \cdot (0.7 \cdot h_d)}{4 \cdot h} \cdot \left(3 - \frac{(0.7 \cdot h_d)^2}{h^2}\right)\right] + \left[0.008 \cdot \frac{V_{\max,95} \cdot x_{45}}{h_r + 0.15 \cdot h_d}\right] =$$
$$= \left[\frac{139.5 \cdot (0.7 \cdot 300)}{4 \cdot 600} \cdot \left(3 - \frac{(0.7 \cdot 300)^2}{600^2}\right)\right] + \left[0.008 \cdot \frac{139.5 \cdot 630}{150 + 0.15 \cdot 300}\right] = 38.7\ kN \qquad 3.57$$

The tensile stress perpendicular to the grain and utilization factor are shown in equation 3.58:

$$\sigma_{t,90,95} = \frac{F_{t,90,95}}{0.5 \cdot b \cdot l_{t,90} \cdot k_{t,90}} = \frac{38.7 \cdot 10^3}{0.5 \cdot 160 \cdot 405 \cdot 0.87} = 1.37\ N/mm^2$$
$$\eta = \frac{\sigma_{t,90,95}}{f_{t,90,k}} = \frac{1.37}{0.5} = 2.74 \leq 1.0 \quad \times \qquad 3.58$$

Because the tensile stress perpendicular to the grain was much higher than the tensile strength perpendicular to the grain there was a need for reinforcing the opening region.

Calculation of tensile stress in reinforcement:

On each opening side were screwed in two screws with the nominal diameter *d* of 12 mm.

The effective screws length:

$$l_{ad} = h_r + 0.15 \cdot h_d = 150 + 0.15 \cdot 300 = 195\ mm \qquad 3.59$$

The screws length has to be greater than $2 \cdot l_{ad}$, which was accomplished with their length of 500 mm.

The characteristic pull out parameter for the screws acc. ETA-11/0190 [51] is 10.0 N/mm^2.

The factor k_{ax} that takes the angle of 90° to the grain into consideration is 1.0. The technical approval ETA-11/0190 [51] defines the characteristic tensile strength of screws with $f_{tens,k}$ with 45 kN.

The load carrying capacity of a self-drilling screw was determined by the minimum of the pull out resistance and the steel fracture and in accordance with ETA-11/0190 [51] (see equation 3.60).

$$F_{ax,Rd,k} = \min \left\{ \begin{array}{c} k_{ax} \cdot d \cdot l_{ad} \cdot \left(\frac{\rho_k}{350} \right)^{0.8} \cdot f_{ax,95} = 1.0 \cdot 12 \cdot 195 \cdot \left(\frac{440}{350} \right)^{0.8} \cdot 10.0 = 28.1 \\ f_{tens,95} = 45.0 \end{array} \right\} = 28.1\ kN \qquad 3.60$$

Verification:

$$\begin{aligned} &F_{t,90,95} = 38.7\ \text{N} \ \leq\ n \cdot F_{ax,Rd} = 2 \cdot 28.1 = 56.2\ \text{kN} \quad \checkmark \\ &\eta = \frac{F_{t,90,95}}{n \cdot F_{ax,Rd}} = 0.69 \ \leq\ 1.0 \quad \checkmark \end{aligned} \qquad 3.61$$

3-7.1.4 GLT beams with screwed-in diagonal, internal threaded rods (series D)

As already described, the threaded rods were screwed in at an angle of 45° around the opening so that the optimum deflection of the shear forces can be expected. The layout was carried out according to a design by Strahm [44] and the ALP-GSA® system of the company n'H neue Holzbau AG in cooperation with professor Gehri. The arrangement of the steel rods and the relevant geometry for the design of the internal forces is illustrated in figure 3.12.

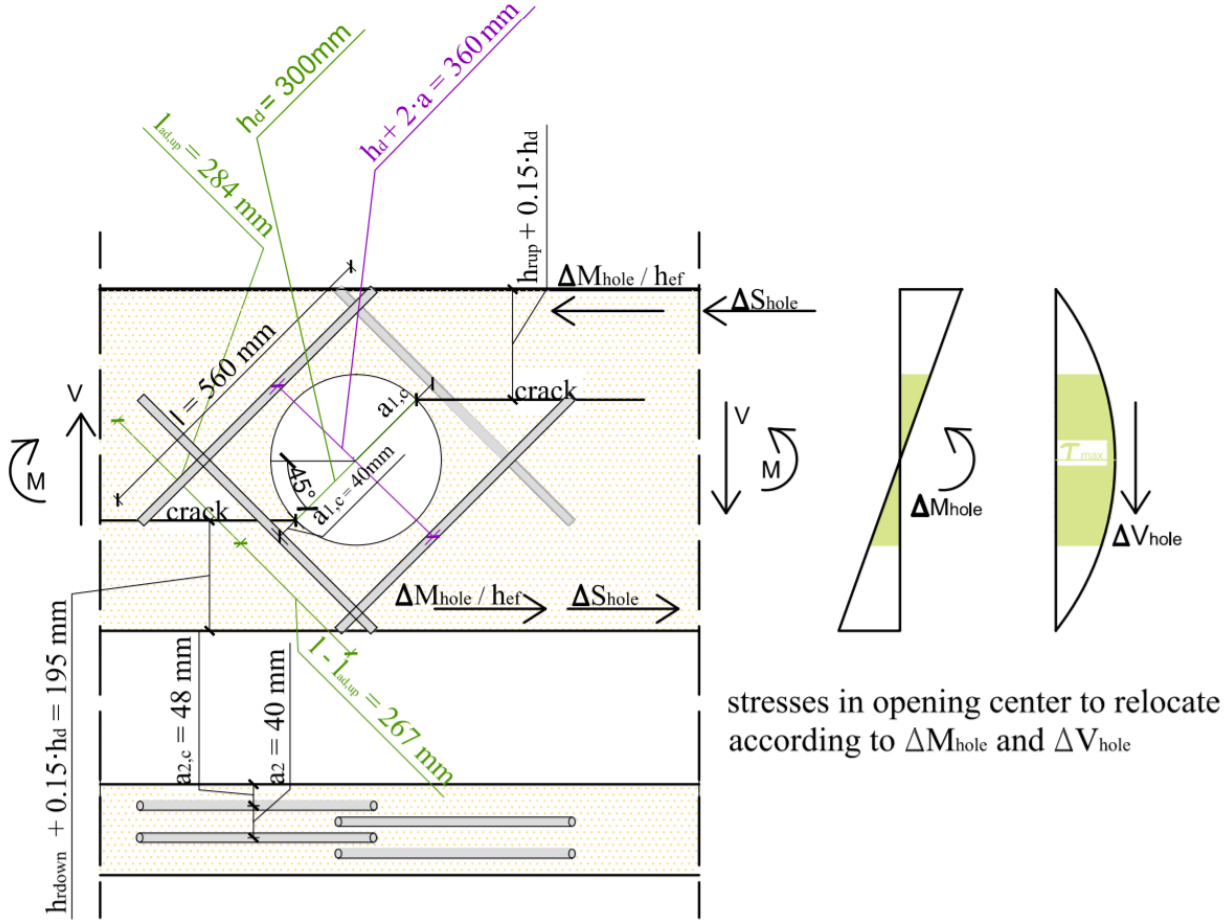

Figure 3.12: Outline and dimensions of the GLT beam internally reinforced with inclined threaded rods under an angle of 45°of series D [28] (adapted)

Moreover, two threaded rods in length of 560 mm were screwed under the angle of 45° on each side around the opening. The nominal diameter of the threaded rods was 16 mm, with the core diameter of 13.6 mm. The steel strength of the threaded rods was 8.8. The characteristic tensile strength of threaded rods therefore was 800 N/mm² and the yield strength $f_{y,k}$ was 640 N/mm², which is 80 % of the characteristic tensile strength $f_{u,k}$.

The minimum spacing of the threaded rods is defined (according to ETA-11/0190 [51]) as following:

-minimum distance to the opening edge parallel to the grain: $a_{1,c} = 5.0 \cdot d = 5.0 \cdot 16 = 80$ mm

-minimum spacing between the bars perpendicular to the grain: $a_2 = 2.5 \cdot d = 2.5 \cdot 16 = 40$ mm

-minimum distance from the lateral edge: $a_{2,c} = 3.0 \cdot d = 3.0 \cdot 16 = 48$ mm

Whereby for the $a_{1,c}$ 40 mm was taken, due to the closest possible reinforcement of the opening, covering the most impacted places by stress perpendicular to the grain.

Because of the inclination of the threaded rods the effective lever arm h_{ef} should be calculated as stated in equation 3.62:

$$h_{ef} = \left(h_d + 2 \cdot a_{1,c}\right) \cdot \sqrt{2} = \left(300 + 2 \cdot 40\right) \cdot \sqrt{2} = 537 \ mm \qquad 3.62$$

The effective length of the threaded rods in the down part is:

$$l_{ad,down} = (h_r + 0.15 \cdot h_d) \cdot \sqrt{2} = (150 + 0.15 \cdot 300) \cdot \sqrt{2} = 276 \ mm \qquad 3.63$$

The residual length of the threaded rod in the upper part is:

$$l_{ad,up} = l - l_{ad,down} = 560 - 276 = 284 > 276 \ mm \qquad 3.64$$

Design of the steel rods:

The characteristic pull out strength of the threaded rods was calculated according to the Z-9.1-777 [53] by using the characteristic pull out strength parameter and density of the used timber (GL32h):

$$f_{ax,k} = 0.52 \cdot d^{-0.5} \cdot l_{ef}^{-0.1} \cdot \rho_k^{0.8} = 0.52 \cdot 16^{-0.5} \cdot 276^{-0.1} \cdot 440^{0.8} = 9.65 \ N / mm^2 \qquad 3.65$$

The 95 %-fractile and mean value of the pull out strength parameter of the steel rods can be calculated with the help of normal distribution with the assumption of COV-coefficient of 13 % (see equations 3.8 and 3.9 and table 3.3):

Pull out force of a single threaded rod was calculated as in equation 3.66:

$$R_{k1,k} = f_{k1,k} \cdot l_{ad} \cdot d$$
$$R_{k1,k} = 16 \cdot 276 \cdot 9.65 = 42\ 614 \ N = 42.6 \ kN \quad R_{k1,mean} = 16 \cdot 276 \cdot 12.3 = 54\ 317 \ N = 54.3 \ kN \qquad 3.66$$
$$R_{k1,95} = 16 \cdot 276 \cdot 14.9 = 65\ 798 \ N = 65.8 \ kN$$

The tensile strength of the threaded rods f_u was calculated with help of the normal distribution, by assuming COV of 10 %. Based on a 5 %-fractile of 800 N/mm^2 the 95 %-fractile and mean values are 1 115 N/mm^2 and 958 N/mm^2 respectively (calculated the same way as in the equations 3.8 and 3.9).

Axial force for the single threaded rod was calculated also with the help of the normal distribution for the mean and 95 %-fractile values, and the 5 %-fractile is to be set at 91 500 N and their amounts are 109.5 kN and 127.5 kN respectively according to the [53] (by assuming COV of 10 %).

The axial forces in the threaded rods were calculated as shown in equation 3.67:

$$F_{ax} = n \cdot \min \begin{Bmatrix} R_{k,1} \\ R_{k,2} \end{Bmatrix} \qquad 3.67$$
$$F_{ax,k} = 119.6 \ kN \qquad F_{ax,mean} = 152.1 \ kN \qquad F_{ax,95} = 186.6 \ kN$$

In order to calculate the expected shear force, the axial force in steel rods has to be taken into consideration as well as the distance of the rods from the opening (see equation 3.68).

$$V_{max} = \frac{F_{ax}}{\frac{x_{hole} \cdot h_d^3}{h_{ef} \cdot h^3 \cdot \sqrt{2}} + \frac{3h_d}{2h}} \qquad 3.68$$

$$V_{max,k} = 143.0\ kN \qquad V_{max,mean} = 182.0\ kN \qquad V_{max,95} = 221.0\ kN$$

The maximum load force is double the value of the V_{max}:

$$F_{max} = 2 \cdot V_{max} \qquad 3.69$$

$$F_{max,k} = 286.0\ kN \qquad F_{max,mean} = 364.0\ kN \qquad F_{max,95} = 442.0\ kN$$

The net moment of inertia was calculated including the reduction by the steel rods holes:

$$I_{y,net} = \frac{b \cdot \left(h^3 - h_d^3\right)}{12} - 8 \cdot d \cdot d_{45} \cdot \left(\frac{h_{ef}}{2}\right)^2 = \frac{160 \cdot (600^3 - 300^3)}{12} - 8 \cdot 16 \cdot 22.6 \cdot 268.7^2 = 2.31 \cdot 10^9\ mm^4 \qquad 3.70$$

The net section modulus was calculated by the net moment of inertia:

$$W_{y,net} = \frac{I_{y,net}}{h/2} = \frac{2\ 311\ 140\ 737}{300} = 7.7 \cdot 10^6\ mm^3 \qquad 3.71$$

The bending moments were calculated by multiplying the shear force with the distance from the support to the point of interest. The value of the $M_{hole,95}$ was 115.9 kNm. As the diagonal rods transfer the shear force across the opening area, no secondary moments had to be considered for which reason $M_{right,edge}$ and M_{45} can be omitted.

The bending stress at the mid-opening is to be calculated as stated in equation 3.72:

$$\sigma_{m,hole,95} = \frac{M_{hole,95}}{W_{y,net}} = \frac{115.9 \cdot 10^6}{7.70 \cdot 10^6} = 15.05\ N/mm^2 \qquad 3.72$$

Verification of the bending stress is to be proven:

$$\eta = \frac{\sigma_{m,hole,95}}{f_{m,k}} = \frac{15.05}{32} = 0.47 \le 1.0 \quad \checkmark \qquad 3.73$$

According to the ALP-GSA®-System [44], the inclined rods should restore the full shear force capacity of a beam without an opening. Therefore the shear force can be calculated by applying the gross cross section (see equation 3.74).

$$\tau_v = \frac{3 \cdot V_{max,95}}{2 \cdot A} = \frac{3 \cdot 221 \cdot 10^3}{2 \cdot 160 \cdot 600} = 3.45\ N/mm^2 \qquad 3.74$$

$$\eta = \frac{\tau_{hole,95}}{f_{v,k}} = \frac{3.45}{2.64} = 1.31 \le 1.0 \quad \times \qquad 3.75$$

This series should be the replacement for the beams without openings. As the maximum bearing shear force by series A was 279 kN and that of series D 221 kN, it can be considered a sufficient replacement.

3-7.1.5 GLT beams with diagonal, internal screwed-in threaded rods (series G)

As already described, the threaded rods were screwed-in at an angle of 40° around the opening so that the optimum redirection of the shear forces can be expected. The design was carried out according to Strahm [44] and the ALP-GSA®-System of the company n'H neue Holzbau AG in cooperation with professor Gehri. The arrangement of the steel rods is illustrated in figure 3.13, as well as the relevant geometry for the design of the internal forces.

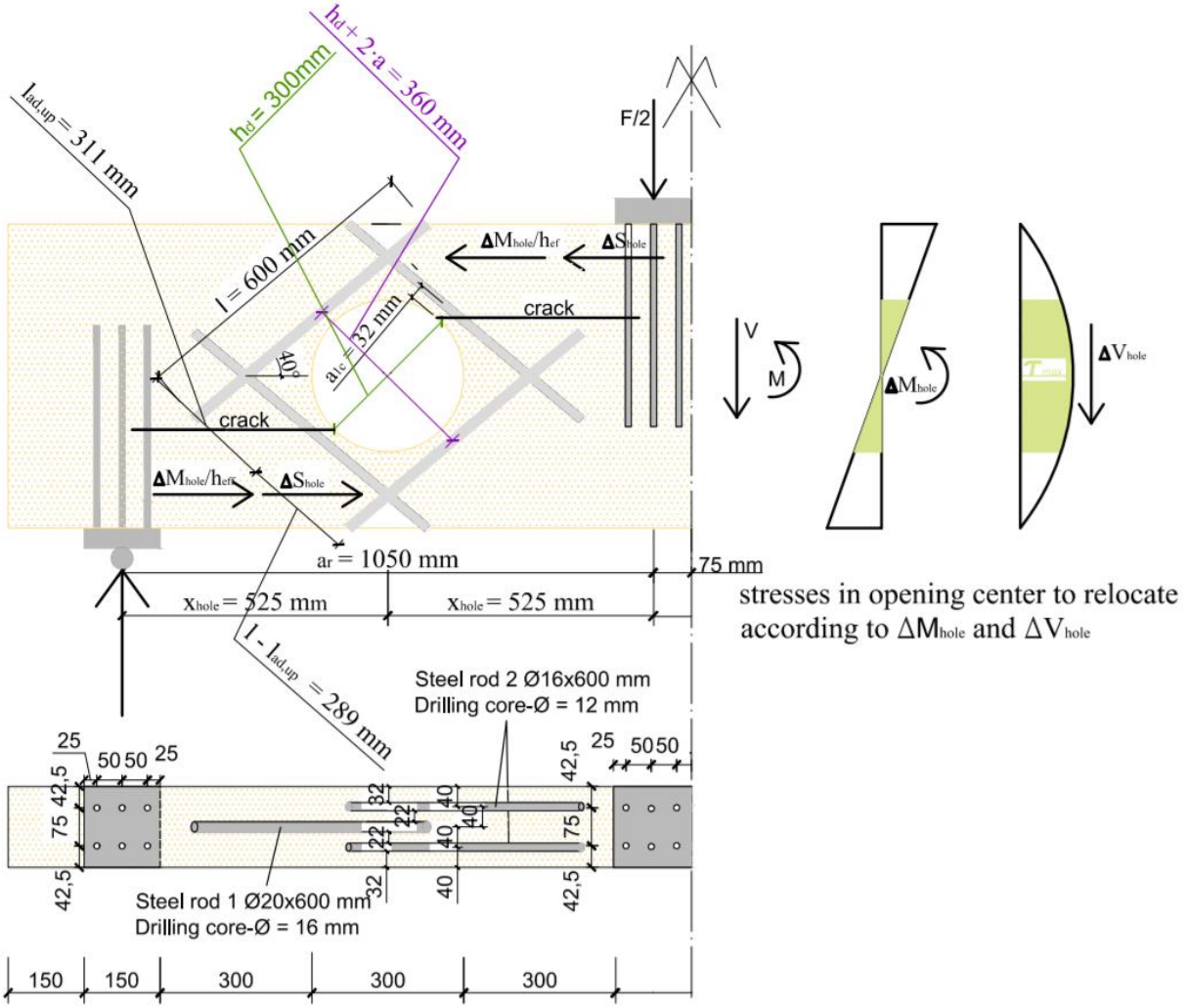

Figure 3.13: Outline and dimensions of the GLT beam with inclined screwed-in / glued-in threaded rods under an angle of 40°of series G and H [28] (adapted)

Two threaded rods in length of 600 mm were screwed-in under the angle of 40° to the grain into each of the two tension sides around the opening. On each compression side there was one screwed-in threaded rod with a nominal diameter of 20 mm under an angle of 40° too. The nominal diameter of the steel rods in the tension zone was 16 mm, with the core diameter of 13.6 mm. The characteristic tensile strength is 800 N/mm² and the yield strength $f_{y,k}$ is 640 N/mm² , which is 80 % of the characteristic tensile strength $f_{u,k}$.

The minimum spacing of the threaded rods is defined (according to ETA-11/0190 [51]) as following:

-minimum distance to the opening edge parallel to the grain: $a_{1,c} = 5.0 \cdot d = 5.0 \cdot 16 = 80$ mm

-minimum spacing between the bars perpendicular to the grain: $a_2 = 2.5 \cdot d = 2.5 \cdot 16 = 40$ mm

-minimum distance from the lateral edge: $a_{2,c} = 3.0 \cdot d = 3.0 \cdot 16 = 48$ mm

In order to cover the most of the stresses close to the opening edge that are caused by the stress perpendicular to the grain, the chosen value for $a_{1,c}$ was 32 mm.

Due of the inclination of the threaded rods, the effective lever arm should be calculated as stated in equation 3.76:

$$h_{ef} = \left(h_d + 2a_{1,c}\right) \cdot \frac{1}{\cos 40°} = \left(300 + 2 \cdot 32\right) \cdot \frac{1}{\cos 40°} = 475\ mm \qquad 3.76$$

The effective length of the threaded rod is:

$$l_{ad,up} = (h_r + 0.15 \cdot h_d) \cdot \frac{1}{\sin 40°} = (150 + 0.12 \cdot 300) \cdot \frac{1}{\sin 40°} = 289\ mm \qquad 3.77$$

The residual length of the threaded rod in the lower part is:

$$l_{ad,down} = l - l_{ad,up} = 600 - 289 = 311 \text{ mm} \qquad 3.78$$

Design of the steel rods:

The characteristic pull out strength of threaded rods was calculated with the characteristic pull out strength parameter and density of the used timber (GL32h) according to the enBR:2007 [24], which is the same as for the series D, and its amount is 9.65 N/mm^2:

The 95 %-fractile and mean value of the pull out strength of the steel rods can be found in table 3.3.

Pull out force of a single threaded rod was calculated as in the equation 3.79:

$$R_{ka} = d \cdot l_{ad} \cdot f_{k1,k}$$
$$R_{k1,k} = 44.6\ kN \quad R_{k1,mean} = 56.9\ kN \quad R_{k1,95} = 68.9\ kN \qquad 3.79$$

The tensile strength f_u was conducted by a normal distribution, with assumption of a COV of 10 % for both the 95 %-fractile and the mean value. The value of the 5 % fractile is 800 N/mm^2 and values of 95 %-fractile mean and are 1 115 N/mm^2 and 958 N/mm^2 respectively.

Axial force for the single threaded rod was calculated also with the help of the normal distribution for the mean and 95 %-fractile values, and the 5 %-fractile is to be set at 91 500 N and their amounts are 109.5 and 127.5 kN respectively [53].

The axial forces in threaded rods are to be calculated as shown in equation 3.80:

$$F_{ax} = n \cdot \min\left\{\begin{matrix} R_{1,k} \\ R_{2,k} \end{matrix}\right\}$$
$$F_{ax,k} = 89.2\ kN \quad F_{ax,mean} = 113.8\ kN \quad F_{ax,95} = 137.8\ kN \qquad 3.80$$

Verification of the bearing capacity of the drilled steel rods:

As some steel rods were pre drilled, in order to glue-in the strain gauges into them to get measurements of the elongation of the steel during the testing process, there was a need to prove bearing capacity of these threaded rods.

The force of the steel break is $F_{t,u,k}$ = 91 500 N according to [53].

As the drilling hole diameter was 4.0 mm the net cross section of the threaded rod was 132.7 mm^2 (threaded rod diameter was 16 mm).

The tensile strength of the steel rod is:

$$R_{t,u,k} = \frac{F_{t,u,k}}{A} \cdot A_{drilled} = \frac{91\,500}{113.1} \cdot 132.7 = 107\,357 N = 107.4\ kN \quad (3.81)$$

Considering the net cross section of the threaded rod, the axial force in n threaded rods $F_{ax,k}$ was calculated according to following equation:

$$F_{axial,k} = n \cdot \min\begin{Bmatrix} R_{ax,k} \\ R_{t,u,k} \end{Bmatrix} = 2 \cdot \min\begin{Bmatrix} 44.6\ kN \\ 107.4\ kN \end{Bmatrix} = 89.2\ kN \quad (3.82)$$

In order to calculate expected shear force, the axial force in threaded rods have to be taken into consideration as well as the distance between the rods and the opening.

$$V_{\max} = \frac{F_{ax}}{\frac{x_{hole} \cdot h_d^3}{h_{ef} \cdot h^3 \cdot 1/\cos 40°} + \frac{3h_d}{2h}} \quad (3.83)$$

$$V_{\max,k} = 140\ kN \qquad V_{\max,mean} = 178\ kN \qquad V_{\max,95} = 216\ kN$$

The maximum load force is double the value of the V_{max}:

$$F_{\max} = 2 \cdot V_{\max} \quad (3.84)$$

$$F_{\max,k} = 280\ kN \qquad F_{\max,mean} = 356\ kN \qquad F_{\max,95} = 432\ kN$$

The bending stress at the mid-opening was to be calculated in equation 3.85:

$$\sigma_{m,hole,95} = \frac{M_{hole,95}}{W_{y,net}} = \frac{216 \cdot 10^6}{7.70 \cdot 10^6} = 28.1\ N/mm^2 \quad (3.85)$$

Verification of the bending stress is to be proven:

$$\eta = \frac{\sigma_{m,hole,95}}{f_{m,k}} = \frac{28.1}{32.0} = 0.88 \le 1.0 \quad \checkmark \quad (3.86)$$

According to the ALP-GSA®-System [44], the inclined rods should restore the full shear force capacity of a beam without an opening. Therefore the shear force can be calculated by applying the gross cross section (see equation 3.87)

$$\tau_v = \frac{3 \cdot V_{\max,95}}{2 \cdot A} = \frac{3 \cdot 216 \cdot 10^3}{2 \cdot 160 \cdot 600} = 3.38\ N/mm^2 \qquad 3.87$$

$$\eta = \frac{\tau_{hole,95}}{f_{v,k}} = \frac{3.38}{2.64} = 1.28 \le 1.0 \quad \times \qquad 3.88$$

This series should be the replacement for the beams without openings. As the maximum bearing shear force by series A was 279 kN and that of series G 216 kN, it can be considered a sufficient replacement.

3-7.1.6 GLT beams with diagonal, internal glued-in threaded rods (series H)

As already described, the threaded rods were glued-in at an angle of 40° around the opening so that the optimum redirection of the shear forces can be expected. The design was carried out according to Strahm [44] and the ALP-GSA®-System of the company n'H neue Holzbau AG in cooperation with professor Gehri.

The arrangement of the steel rods is illustrated in figure 3.13, as well as the relevant geometry for the design of the internal forces was the same as for the test series G.

The minimum spacing of the glued-in rods was defined as following (according to Z-9.1-778 [43]):

- minimum distance to the opening edge parallel to the grain: $a_{1,c} = 2.5 \cdot d = 2.5 \cdot 16 = 40$ mm
- minimum spacing between the bars perpendicular to the grain: $a_2 = 3.75 \cdot d = 3.75 \cdot 16 = 60$ mm
- minimum distance from the lateral edge: $a_{2,c} = 1.875 \cdot d = 1.875 \cdot 16 = 30$ mm

In order to cover the most of the stresses close to the opening edge that are caused by the stress perpendicular to the grain, the chosen value for $a_{1,c}$ was 32 mm.

Design of the steel rods:

The rod slenderness must be less than 110 according to Z-9.1-778 [43]:

$$\lambda = \frac{l_{glued}}{d} = \frac{600}{16} = 37.5 < 110 \qquad 3.89$$

The characteristic glueline strength $f_{k1,k}$ for the effective gluing length of l_{ad} is (Z-9.1-778 [43]):

$$f_{k1,k} = 8.75 - 0.0106 \cdot l_{ad} = 8.75 - 0.0106 \cdot 242 = 6.18\ N/mm^2 \qquad 3.90$$

Pull out capacity was calculated as previously stated by test series G:

$$F_{ax} = \pi \cdot d \cdot l_{ad} \cdot f_{k1,x}$$
$$R_{k1,k} = 75.2\ kN \quad R_{k1,mean} = 95.6\ kN \qquad 3.91$$
$$R_{k1,95} = 116.1\ kN$$

The tensile strength of the steel f_u was the same as for the two previous series (the value of the 5 % fractile was 800 N/mm^2 and values of 95 %-fractile mean and were 1 115 N/mm^2 and 958 N/mm^2 respectively Z-9.1-778 [43]).

Tensile strength for a single threaded rod:

$$F_{tens} = \frac{d_{GK}^2}{4} \cdot \pi \cdot f_u \qquad 3.92$$

$$F_{tens,k} = 115.4\ kN \qquad F_{tens,mean} = 138.1\ kN \qquad F_{tens,95} = 160.8\ kN$$

The maximum axial force in the glued-in threaded rod under tensile load was:

$$F_{ax}(n=2) = n \cdot \min\left\{\begin{matrix} F_{tens} \\ F_{ax} \end{matrix}\right\} \qquad 3.93$$

$$F_{ax,k} = 150\ kN \qquad F_{ax,mean} = 191\ kN \qquad F_{ax,95} = 232\ kN$$

In order to calculate the expected shear force, the axial force in the threaded rods have to be taken into consideration as well as the distance between the rods and the opening.

$$V_{\max} = \frac{F_{ax}}{\frac{x_{hole} \cdot h_d^3}{h_{ef} \cdot h^3 \cdot 1/\cos 40°} + \frac{3h_d}{2h}} \qquad 3.94$$

$$V_{\max,k} = 176\ kN \qquad V_{\max,mean} = 223\ kN \qquad V_{\max,95} = 271\ kN$$

The maximum load force was double the value of the V_{max}:

$$F_{\max} = 2 \cdot V_{\max} \qquad 3.95$$

$$F_{\max,k} = 352\ kN \qquad F_{\max,mean} = 446\ kN \qquad F_{\max,95} = 542\ kN$$

The bending stress at the mid-opening was to be calculated as in equation 3.96:

$$\sigma_{m,hole,95} = \frac{M_{hole,95}}{W_{y,net}} = \frac{143.85 \cdot 10^6}{7.70 \cdot 10^6} = 18.68\ N/mm^2 \qquad 3.96$$

Verification of the bending stress is to be proven:

$$\eta = \frac{\sigma_{m,hole,95}}{f_{m,k}} = \frac{18.68}{32.0} = 0.58 \le 1.0 \quad \checkmark \qquad 3.97$$

According to the ALP-GSA®-System [44], the inclined glued-in rods should restore the full shear force capacity of a beam without an opening. Therefore the shear force can be calculated by applying the gross cross section (see equation 3.98)

$$\tau_v = \frac{3 \cdot V_{\max,95}}{2 \cdot A} = \frac{3 \cdot 271 \cdot 10^3}{2 \cdot 160 \cdot 600} = 4.23\ N/mm^2 \qquad 3.98$$

$$\eta = \frac{\tau_v}{f_{v,k}} = \frac{4.23}{2.64} = 1.60 \le 1.0 \quad \times \qquad 3.99$$

This series should be the replacement for the beams without openings. As the maximum bearing shear force by series A was 279 kN and that of series H 271 kN, it can be considered a sufficient replacement.

3-7.1.7 Preparation for the testing machine

The beam dimensions such as height, length and width, but also the mass, were measured before putting a beam into the testing machine. Also, before placing a beam into the machine frame, beams were painted partly in white color to get a contrast surface for Mercury program.

After setting the beam on supports and centering it, the beam was equipped with four displacement sensors, the shear-cross sensors and one deflection sensor, as well as with little black spots on the white surface.

After completing the set-up of the beam, computer was fed with information about 10 %, 40 % and 50 % of the maximum of the pre calculated maximum bearing load in order to set the hysteresis curve, as well as the speed of load application.

After the test a part of the beam was cut out and weighted and put in the oven for drying process moisture content was established according to the ON EN 13183-1 [55]).

Beams with internal reinforcement (vertical and inclined) were cut open to see if there were some changes in the timber grain flow and to get information about the screws or threaded rods pull out process.

Everything was documented, photographed and filmed to ensure that none of the information were missed.

Every beam, except A01, was filmed with two cameras. Series A was filmed once from the front with one camera and with the other camera from the backside of the beam. All the other series were filmed twice from front but one camera was directed to the upper left side of the opening, to film, assumed first crack- and the other one on the lower, right opening side to film the second crack and spreading of the crack to the support.

Summary

1. preliminary design
2. reinforcement of the beams (support and load application area, vertical and inclined reinforcement of the opening)
3. measurement of (to establish the density of the timber):
   - -mass
   - -length
   - -height
   - -width
4. white painting
5. setting the beam in testing machine
6. shear-cross, displacement transducers, deflection sensor, black spots on the white surface, strain gauges for the steel rods
7. putting information in the computer needed for the testing
8. testing the beam
9. cutting out test specimens to be weighted for the drying test
10. measuring the weight of the cut pieces
11. putting them in oven for the drying process
12. measuring the mass after drying process (establish the moisture content)

3-7.2 EVALUATION PROCEDURE

After finishing the tests in laboratory, the results were firstly processed in Excel 2003 and 2013.

Different calculations and processing of different data were undertaken and the process of this calculation is described in the following parts of this master thesis.

3-7.2.1 Density

The density was calculated for the each series differently, because each series had something different about itself. But the calculation was reduced to well-known calculation of the density out of the mass, which was measured with crane scale and the volume, which was calculated out of the measured dimensions (see equation 3.100).

$$\rho = \frac{m}{V} \qquad 3.100$$

The density depends on the early and late wood portion of the timber. For spruce the early wood, which is responsible for the water and nutrient transport, in essence, has a density of about 300 kg / m³, while the late wood, which takes over the task of consolidating predominantly, has a much higher density of about 1000 kg / m³ [1],[2].

Differences in the shear fracture behavior can be expected depending on the tree ring orientation and board geometry of the initial product used.

3-7.2.2 Determination of moisture

It is necessary to keep deviations from the reference moisture content of 12 % as low as possible, especially as the moisture content of the timber has a considerable influence on its mechanical properties. Therefore, the beams have been delivered in consultation with the manufacturer with the desired moisture content of about 12 % and then stored in an appropriate way at a temperature of 20°C and a relative humidity of 65 %. This climate corresponds to the EN 384:2010 [56] specified reference conditions. After the tests were finished, the mass of the cut of part of each test specimen was measured with the digital scale. The measured pieces were left for few days in the drying oven to dry out (EN 13183-1:2004 [55]). Determination of moisture was performed and carried out according to equation 3.101.

$$\mathrm{u} = \frac{m_1 - m_0}{\mathrm{m}_0} \cdot 100 \qquad 3.101$$

where:

u	...	moisture content [%]
m_1	...	mass of the specimen before drying [g]
m_0	...	mass of the specimen in the oven dry state [g].

The moisture correction factors according to the EN 384:2010 [56] were taken into the consideration and with those the further calculation was proceeded.

3-7.2.3 Correction factors

The timber moisture varied from about 10.30 % to 12.74 % for all test specimens, therefore, the moisture correction was done for the density, shear modulus, shear stresses and stiffness based on the obtained results of the testing in accordance to EN 384:2010 [56].

The correction factor for the shear modulus and stiffness was 2 %, which was taken from EN 384:2010 [56] and corrected with Neuhaus [57]. The density was corrected with 0.5 % according to EN 384:2010 [56].

The tests that estimate material strength are supposed to be conducted in normal climate (20°C and 65 % relative humidity) in which the moisture content should be 12 %. In fact for service class 2 the moisture

content can vary between 12 and 20 %. Due to the increased moisture content, the resisting forces acting against slipping between the layers internally along the grain decrease, which causes the decrease of shear strength and modulus by 2.5 % for 1 % increase of moisture content (see equation (3.102) [47].

$$f_{v,u\%} = f_{v,12\%} \cdot [1 - 0.025 \cdot (u - 12\%)] \quad 3.102$$

where:

$f_{v,u\%}$	...	material strength
$f_{v,12\%}$	...	material strength for the wood moisture content of 12%
u		wood moisture content

As shown in the equation 3.102 the shear stress was corrected by factor 2.5 % according to Gehri [47].

3-7.2.4 Determination of shear modulus and stiffness

The data of the Mercury program and the displacement transducers measurements were provided in excel sheet form from were combined in order to get the mean values of the two different measuring approaches on the two different sides of the beam.

The provided data out of the measurements were:

- force [kN]
- vertical displacement at midspan [mm]
- deflection measured by the testing machine [mm]
- 6 displacement transducers (4 around the opening; 2 DD1 in a shear-cross) [mm]
- time [s]
- for series G elongation of the additional strain gauges glued-in inside of the threaded rods
- for series G strain gauges glued-on the back side of the beam (opposite of white painting) under an angle of 40° (see figure 3.14)
- for series H elongation of the additional strain gauges glued-on the threaded rods (see figure 3.14)

The provided data out of the Mercury program:

- force [kN]
- 6 displacements corresponding to the 6 displacement transducers [mm]
- time [s]
- for series G the deformation under the angle of 40° was also measured aside the usual one under 45° [mm]
- for the series H only the deformation under the angle of 40° was taken into the consideration [mm]

The figure 3.14 is a schematic representation of the placement of the displacement transducers.

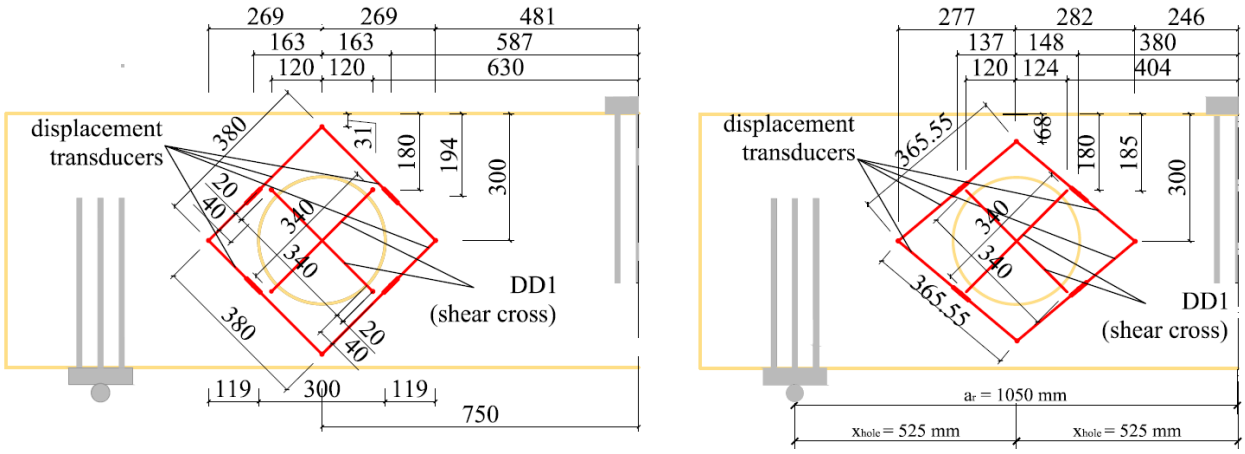

Figure 3.14: Schematic representation of the displacement transducers on the beam for the test series A, B, C, D (left) and test series G and H (right)

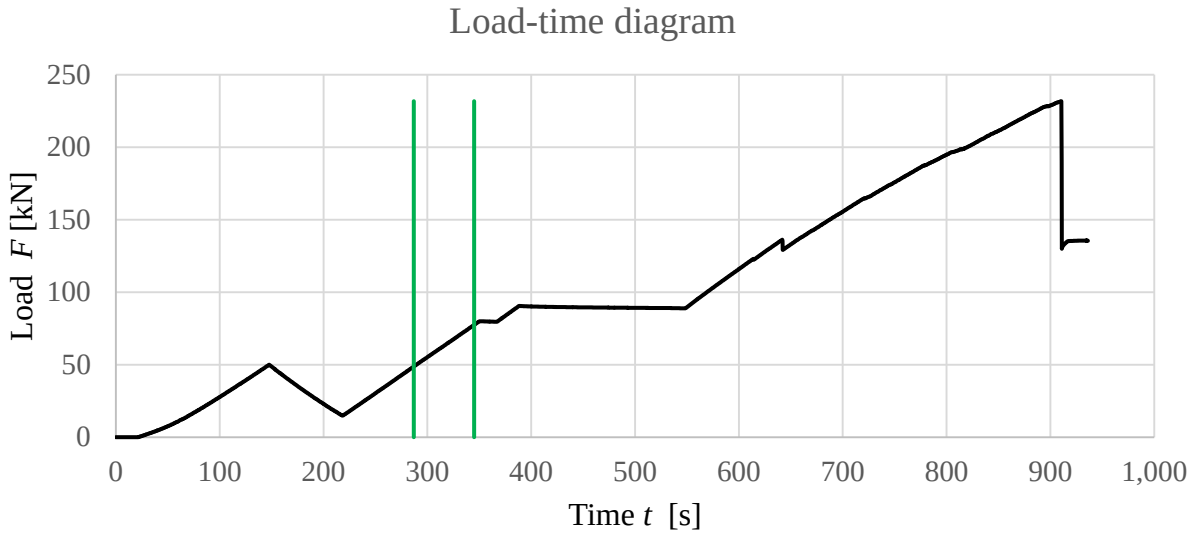

Figure 3.15: Load-time diagram of the test specimen B01

Figure 3.15 presents the load-displacement diagram for test specimen B01. On this graph, it is possible to see the load application process. Before the testing, hysteresis parameters were calculated and 10 % (maximal unload value), 40 % (maximal value of the first loading) and 50 % (the value at which the displacement transducers and shear cross were removed) of the maximal value of the precalculated load bearing capacity were obtained. As the tests on test series A were already conducted, the hysteresis was adjusted for the test series B. In this manner, test series B01 was loaded until the load level reached 33 % of the maximal precalculated load bearing value. Afterwards, the test specimen was unloaded to 10 % of the precalculated load value, then loaded to 60 % of the precalculated load. The horizontal straight line represents the break during which the displacement transducers, deflection gauge at beam mid-span and shear cross were removed. Followed by the application of the load onto the beam until the point of breakage which can be noticed in a sudden drop of the force. The green lines represent the area in which the data from Mercury program were approximated with the linear function. The size of this area, between the green lines, depended on the data acquired from Mercury program. In case there were larger jumps in the data acquired from Mercury program, it was necessary for them not to be included in the process of linearization. Therefore, these areas could be smaller or larger depending on the data.

In order to get the compatible deformations w_1 and w_2 for the measurements of the displacement transducers and Mercury and therefore the linear approximation of the data from the shear-cross (Δw_5 and Δw_6), the analysis was made at the same load level. Those values of deformations and loads were used for the calculation of the shear modulus.
The shear modulus was calculated for each test specimen according to the equation 3.103 (ON EN 408:2012 [58]).

$$G_{tor,s} = \alpha \cdot \frac{h_0}{b \cdot h} \cdot \frac{V_{s2} - V_{s1}}{w_2 - w_1} \qquad 3.103$$

with:

$$\alpha = \frac{3}{2} - \frac{h_0^2}{4 \cdot h^2} = \frac{3}{2} - \frac{340^2}{4 \cdot 600^2} = 1.420 \qquad 3.104$$

where:

$G_{tor,s}$	...	calculated shear modulus [N/mm²]
h_0		distance between two of the crossed displacement transducer (DD1)
α	...	factor depending on the length of the crossed displacement transducers and beam height
V_{s2}-V_{s1}	...	shear force difference [N]
b	...	beam width [mm]
h	...	beam height [mm]
w_2-w_1		mean value of the deformation from both crossed displacement transducers in the center of the opening (in this thesis they are numbered 5 and 6)

Also, for each series values of stiffness were calculated, obtained from displacement transducers and mercury data, as shown in following equation:

$$K_i = \frac{\Delta F}{\Delta w} = \frac{F_2 - F_1}{w_2 - w_1} \qquad 3.105$$

where:

K_i	...	calculated stiffness along the displacement transducers 1, 2, 3 and 4 (see figure 3.14) [N/mm]
ΔF		load difference in the linear-elastic region; $\Delta F = F_2 - F_1$ [N]
Δw	...	deformation difference in the linear-elastic region of the displacement transducers; 1, 2, 3 and 4; $\Delta w = w_2 - w_1$ [mm]

There is to be noted, that the displacement transducers were arranged under an angle of 45° for series A, B, C and D and under an angle of 40° for test series G and H.

3-7.2.5 Load-displacement diagram

The load displacement diagrams were established by using data out of the measurements of displacement transducers for the loads F in [kN] and displacement w in [mm] on the back beam side for each test specimen. These graphs visualize the load level F_{c0} of the first initial crack, the load level made this crack to spread over the opening width F_c, which load caused the shear failure of the beam F_f. For the test specimens that were loaded after first shear failure occurred, these graphs also serve to get information about whether the first shear failure was the maximum on bearing load, if some other shear failure F_{SF2} or bending failure F_{BF} happened as well as on which load level the force dropped after each failure ($F_{fall,1}$, $F_{fall,2}$, etc.) as well as maximum load bearing capacity. All of these changes are visible in the graphs and in

the excel sheet tables in leaps of the graph lines or values, respectively. To get better insight into what happened, the hysteresis and the pause during which the displacement transducers were taken off the beam had to be approximated into a single linear function. Figure 3.16 represents an exemplary test specimen with marked forces which are the most important for the description of the each test specimen. In this particular case F_{c0} and F_c forces take place at the same load, some specimens had a clear difference between those two.

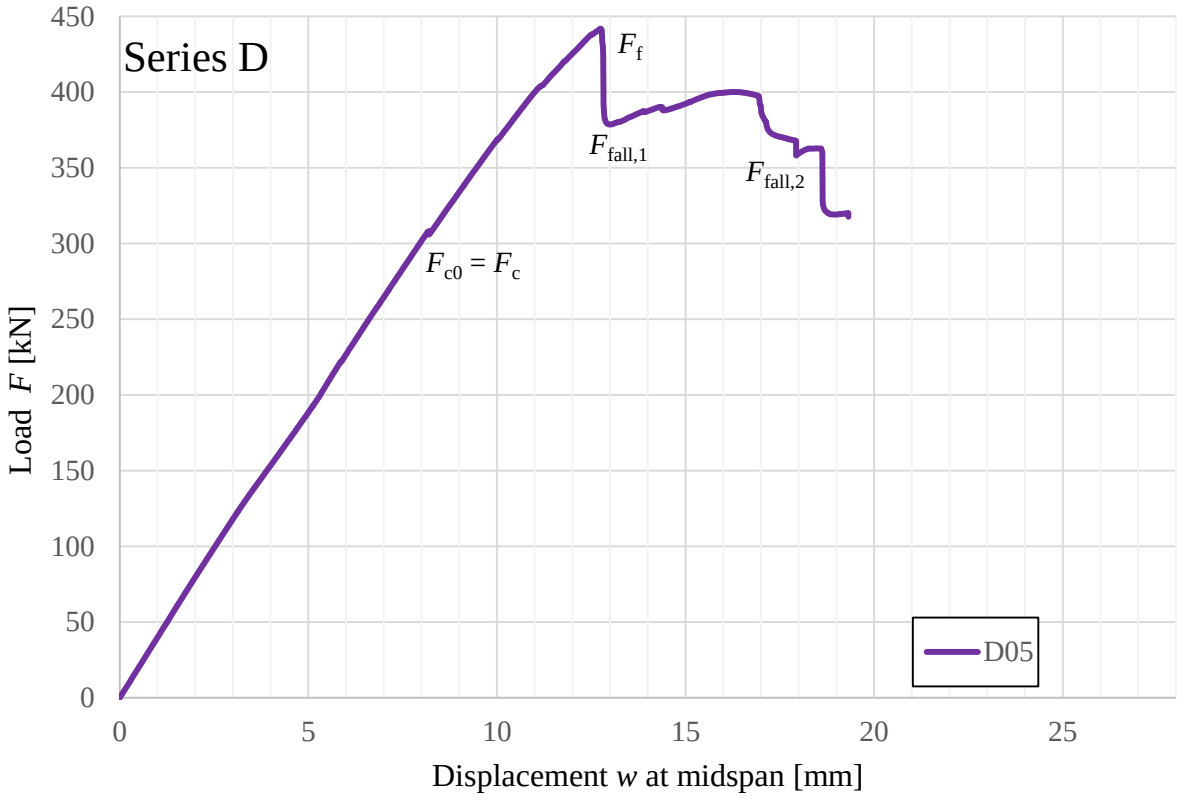

Figure 3.16: Load-displacement diagram of test specimen D05

3-7.2.6 Determination of normal and shear stresses for the tested values of the load

To be able to calculate the real shear and normal stresses that occurred during the testing, the maximum load bearing capacity was taken from the excel data as well as the measured geometry data. With the help of the formulas that were already introduced in the chapters 2 and 3 and some more precise ones for the accurate calculation of the stresses occurring in the tested beams the shear and normal stresses were calculated. The values for the beam height *h*, beam width *b* and all other necessary values for the calculation were taken from the geometry data, which were measured before the tests began. All test specimens of series A, B, D, G and H were calculated in the same way for the glue laminated timber beams according to the [19], Gehri [47] and the ALP GSA® method from n'H neue Holzbau AG by Strahm [44].
The following equations were used to calculate values that were determined from the measurements on the test specimens:

The shear stress on gross cross section is calculated with the help of the gross area and maximum shear force taken from the tests for each test specimen:

$$\tau_{gross} = 1.5 \cdot \frac{V_{\max}}{A_{gross}} \quad 3.106$$

where:

$$A_{gross} = h \cdot b \quad 3.107$$

The net shear stress was calculated with the help of the net area and maximum shear force gotten from the test specimen:

$$\tau_{net} = 1.5 \cdot \frac{V_{\max}}{A_{net}} \quad 3.108$$

where:

$$A_{net} = (h - h_d) \cdot b \quad 3.109$$

The position of the shear crack was determined as mean value of several measurements conducted on the front and back beam side, after testing of each test specimen was finished, and were used to calculate the shear stress τ_{crack} regarding the gross cross section. This shear failure height *z* was measured after tests on the front and back beam side on the opening edge and the mean value of those two measurements was established and used for the calculations.

$$\tau_{crack} = \frac{3 \cdot V}{2 \cdot b \cdot h} \cdot \left[1 - 4 \cdot \left(\frac{z}{h}\right)^2\right] \quad 3.110$$

where:

z ... distance from top / bottom edge of the beam to the crack

The maximum field moment and normal stress was calculated at mid-span of the beam:

$$M_{\max,\,field} = a \cdot V_{\max} = 1.125 \cdot V_{\max} \quad 3.111$$

$$\sigma_{m,\max,\,field} = \frac{M_{\max,\,field}}{\frac{b \cdot h^2}{6}} \quad 3.112$$

The maximum moment at the opening center was calculated as followed:

$$M_{\max,\,field} = x_{mid,hole} \cdot V_{\max} = 0.525 \cdot V_{\max} \quad 3.113$$

$$\sigma_{m,\max,\,field} = \frac{M_{\max,hole}}{I_{y,net}} \cdot h \qquad 3.114$$

where:

$$I_{y,net} = \frac{b \cdot \left(h^3 - h_d^3\right)}{12} \qquad 3.115$$

Due to the fact that the opening of the beam was set with $0.5 \cdot h$ which is not standardized in any known standard or norm for timber constructions, the secondary moments must be considered. In figure 3.17 the influences of the load on the different places of the opening are shown, which are resulting in secondary moments.

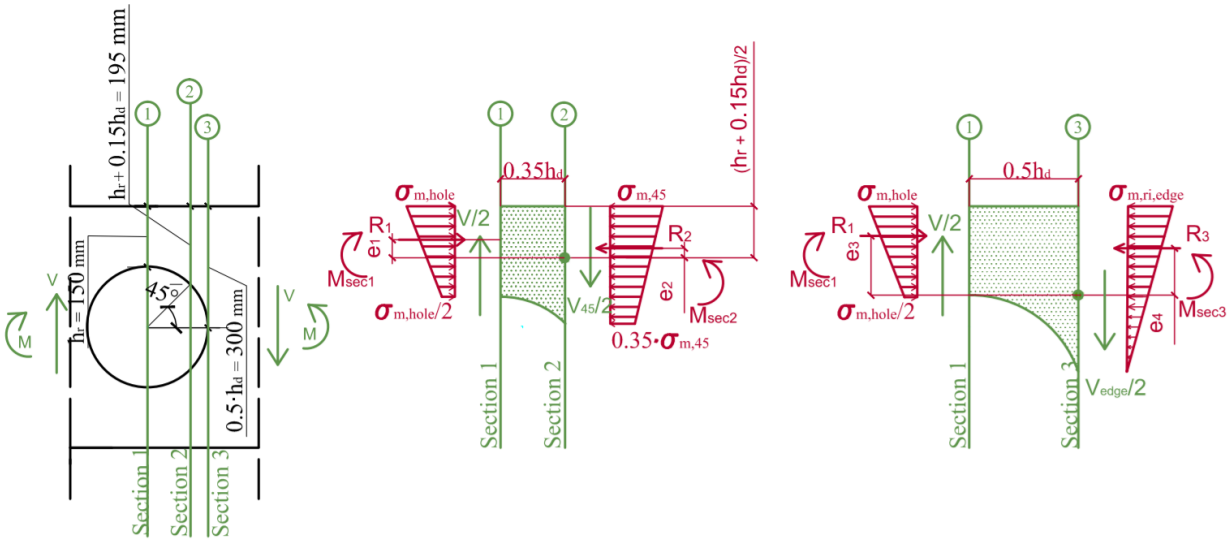

Figure 3.17: Schematic representation used for the secondary moment calculation [28] (adapted)

The section modulus of the net cross section in the section 2:

$$W_{net,2} = \frac{b \cdot (h^3 - (0.7 \cdot h_d)^3)}{12} \cdot \frac{2}{h} \qquad 3.116$$

The section modulus of the upper girder in section 2:

$$W_{girth,2} = \frac{b \cdot (h_r + 0.15 \cdot h_d)^2}{6} \qquad 3.117$$

The section modulus of the upper girder in section 3:

$$W_{girth3} = \frac{b \cdot \left(\frac{h}{2}\right)^2}{6} \qquad 3.118$$

The section modulus of the beam:

$$W_y = \frac{b \cdot h^2}{6} \tag{3.119}$$

The secondary moment in section 2:

$$M_{\sec 2} = \frac{V}{2} \cdot 0.35 \cdot h_d + R_1 \cdot e_1 - R_2 \cdot e_2 =$$
$$= \frac{V}{2} \cdot 0.35 \cdot h_d + \left(\frac{\sigma_{m,hole} + \frac{\sigma_{m,hole}}{2}}{2} \right) \cdot b \cdot h_r \cdot \left(\frac{h_r + 0.15 \cdot h_d}{2} - \frac{h_r}{3} \cdot \frac{\sigma_{m,hole} + 2 \cdot \frac{\sigma_{m,hole}}{2}}{\sigma_{m,hole} + \frac{\sigma_{m,hole}}{2}} \right) - \tag{3.120}$$
$$- \left(\frac{\sigma_{m,45} + 0.35 \cdot \sigma_{m,45}}{2} \right) \cdot b \cdot (h_r + 0.15 \cdot h_d) \cdot \left(\frac{h_r + 0.15 \cdot h_d}{2} - \frac{h_r + 0.15 \cdot h_d}{3} \cdot \frac{\sigma_{m,45} + 2 \cdot 0.35 \cdot \sigma_{m,45}}{\sigma_{m,45} + 0.35 \cdot \sigma_{m,45}} \right)$$

The secondary moment in section 3:

$$M_{\sec 3} = \frac{V}{2} \cdot 0.5 \cdot h_d + R_1 \cdot e_3 - R_3 \cdot e_4 =$$
$$= \frac{V}{2} \cdot 0.5 \cdot h_d + \left(\frac{\sigma_{m,hole} + \frac{\sigma_{m,hole}}{2}}{2} \right) \cdot b \cdot h_r \cdot \left(\frac{h}{2} - \frac{h_r}{3} \cdot \frac{\sigma_{m,hole} + 2 \cdot \frac{\sigma_{m,hole}}{2}}{\sigma_{m,hole} + \frac{\sigma_{m,hole}}{2}} \right) - \frac{\sigma_{m,ri,edge}}{2} \cdot b \cdot h_d \cdot \left(\frac{h}{2} - \frac{h_d}{3} \right) \tag{3.121}$$

The moment at the 45^o angle on the opening edge:

$$M_{\max,45} = V_{\max} \cdot x_{45} \tag{3.122}$$

The moment at the right edge on the opening:

$$M_{\max,ri,edge} = V_{\max} \cdot x_{edge} \tag{3.123}$$

The normal stress at the angle of 45^o:

$$\sigma_{m,45} = \frac{M_{\max,45}}{W_y} + \frac{M_{\sec 3}}{W_{girth3}} \tag{3.124}$$

The normal stress on right edge of the opening:

$$\sigma_{m,ri,edge} = \frac{M_{\max,ri,edge}}{W_{net2}} + \frac{M_{\sec 2}}{W_{girth2}} \tag{3.125}$$

Additionally, the tensile force perpendicular to the grain was calculated to be able to calculate the tensile stress perpendicular to the grain:

$$F_{t,90} = F_{t,V} + F_{t,M} = \left[\frac{V_d \cdot h_d}{4 \cdot h} \cdot \left(3 - \frac{h_d^2}{h^2}\right)\right] + \left[0.008 \cdot \frac{M_d}{h_r}\right] \quad 3.126$$

By means of $F_{t,90}$ the tensile stress perpendicular to the grain can be conducted:

$$\sigma_{t,90} = \frac{F_{t,90}}{0.5 \cdot l_{t,90} \cdot b_{ef} \cdot k_{t,90}} \quad 3.127$$

$$l_{t,90} = 0.35 \cdot h_d + 0.5 \cdot h \quad 3.128$$

$$k_{t,90} = \min\left\{\begin{array}{c} 1 \\ \left(\frac{450}{h}\right)^{0.5} \end{array}\right\} \quad 3.129$$

$$b_{ef} = k_{cr} \cdot b \quad 3.130$$

The k_{cr} is 1.0 so the effective width is the measured width of the beam.
In order to be able to calculate with the additional values obtained from the strain gauges that were glued-in the threaded rods for the series G and those glued-on the threaded rods for the test series H, as well as those glued-on outside on the non-painted side of the beam for the test series G, the additional calculations were made in Excel. The forces and elongations of the threaded rods were calculated for the series G and H. For the series G, the deformations of the timber on the surface of the non-painted side was also calculated.
The elongations of the steel rods for the test series G and series H were calculated with the following equation:

$$\varepsilon = \frac{4}{K \cdot B} \cdot \frac{Yi \cdot X_F \cdot 10^{-3}}{50\ kN} \quad 3.131$$

where:

ε	...	elongation of the steel rod [-]
k	...	coefficient depending on strain gauges (2.10-threaded rods screwed in; 2.11-threaded rods glued-in) [-]
B		bridge coefficient (1.0 -threaded rods screwed in; 2.0-threaded rods glued-in) [-]
Y_i	...	the voltage ratio out of the calibration [mV/V/50 kN]
X_F	...	force in the threaded rod [kN]

As the measurements for the displacement transducers on the timber surface was expected in [μm/m], there was no need for recalculation with this data it was possible to generate diagrams of the elongation the beam width for the test series G and H in order to get an overview of how the timber and the threaded rods behave during the load application process. As an example the elongation areas the beam width of specimen G03 is shown in figure 3.18, whereby at -80 mm the Mercury beam side i.e. front, white painted beam side and at +80 mm the back side of the beam i.e. the one with displacement transducers, non-painted side is presented. The local values represent the values obtained from the strain gauges glued-on the beam surface and the measurements obtained from the Mercury program for the same positions. The global ones represent the values obtained from the Mercury program and displacement transducers that measured elongations over the distance l_0 = 365.55 mm. The two values in the center were obtained from the strain gauges that were glued-in and glued-on the threaded rods for the test series G and H, respectively.

The similar diagrams are set for the test series H only without the local measurements, because those data were not obtained by this test series.

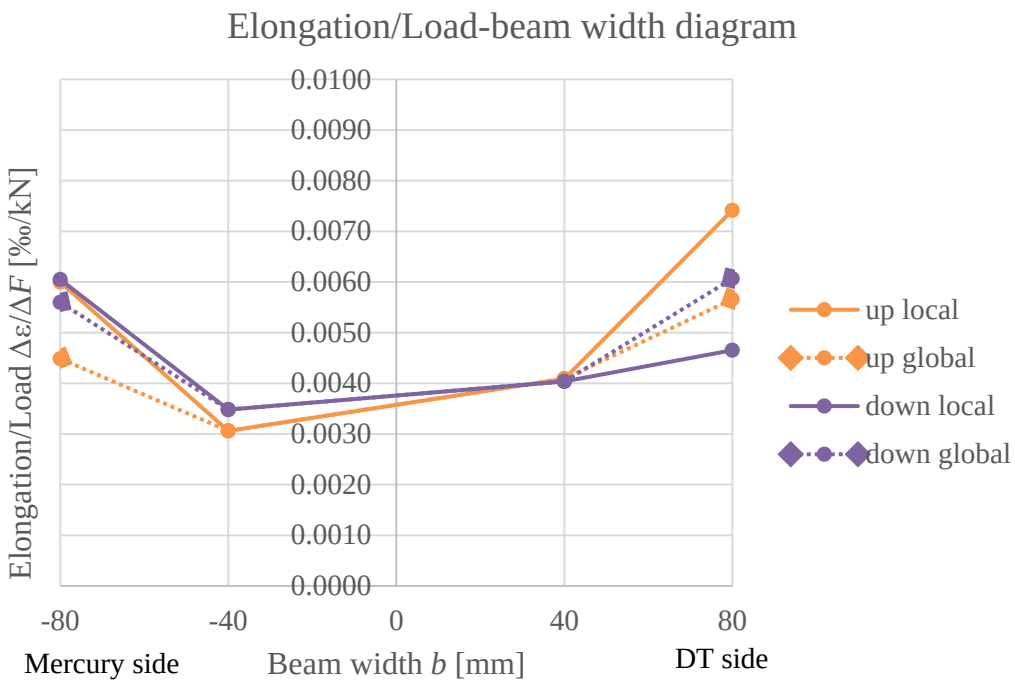

Figure 3.18: Elongation across the beam width for test specimen G03

CHAPTER 4: RESULTS

4-1 SERIES

The sketch of an exemplary beam with explanations of the beam sides and of the opening are shown in figure 4.1. They are the basis for further descriptions of the test series. α was the angle between the vertical beam axis and the crack appearance.

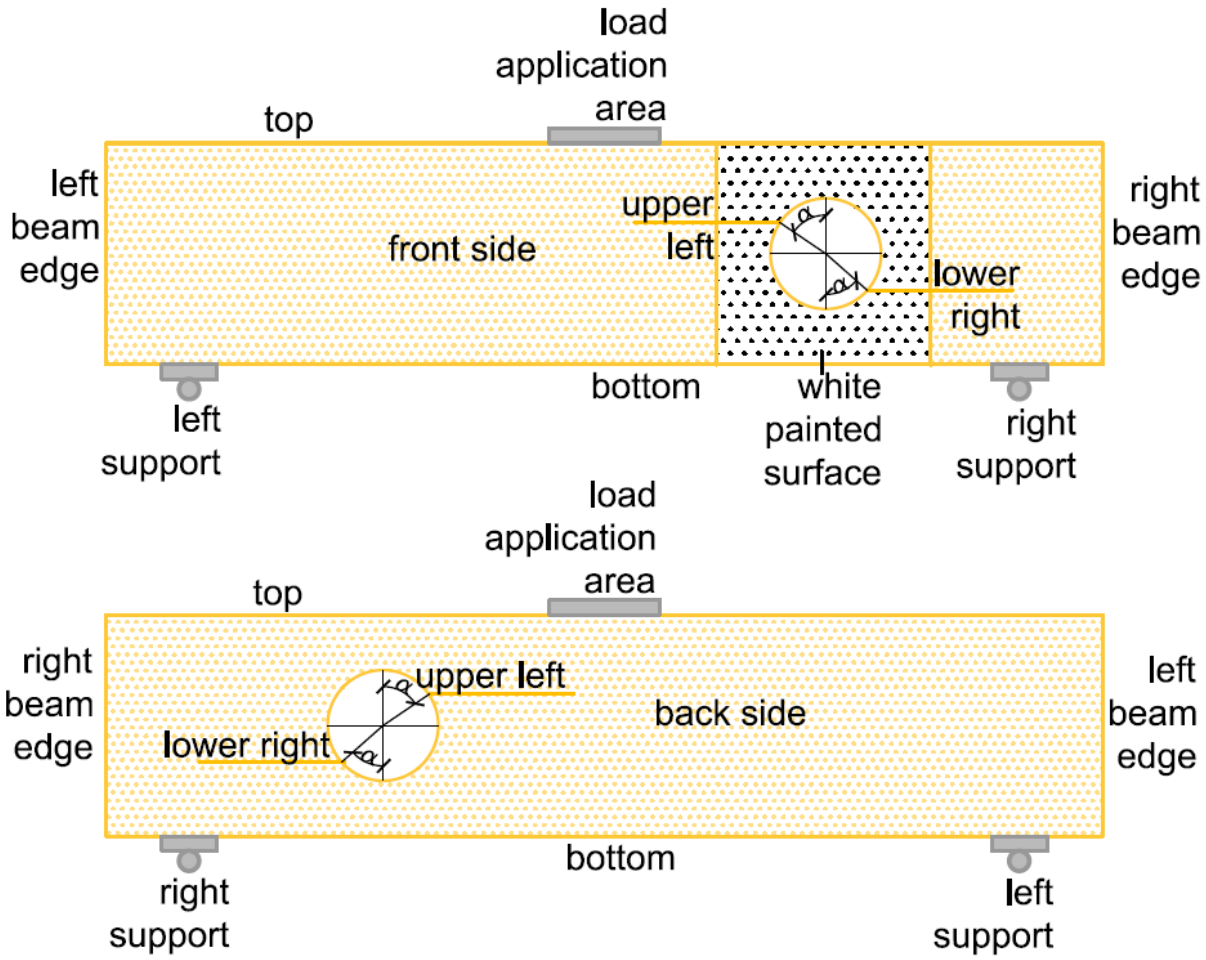

Figure 4.1: Schematic representation used for the beams description

Only test specimen A01 was filmed from the back side of the beam where displacement transducers were placed, on the right beam edge. All other test specimens of series A were filmed with two cameras, one on the same spot as by the test specimen A01 and the other one on the same side but at the left beam edge, where most of the shear failures happened for the series A. All of the specimens of other test series (B, C, D, G and H) were filmed with two cameras at front beam side. One was filming top left edge of the opening and the other camera the lower right edge of the circular opening. Therefore, this setup was supposed to capture the two most impacted places by tensile stress perpendicular to the grain, which was the case for all of the beams.

4-1.1 SERIES A

Series A consisted of five GLT beams without openings. The exemplary test specimen of this test series in the testing machine is shown in figure 4.2.

Figure 4.2: Test specimen A01 in the testing machine

The mean values of the maximum load bearing capacity estimated from the obtained test results as well as further load values of each test specimen are shown in table 4.1.

Table 4.1: Overview of the test results of the load and angles of crack appearance for test series A

	F_{c0}	α_{c0}	F_c	α_f	F_f	α_f	F_{fall}	F_{max}
	[kN]	**[kN]**	**[kN]**		**[kN]**	**[°]**	**[kN]**	**[kN]**
A01	/	/	/	/	654.92	/	325.8	654.92
A02	/	/	/	/	619.13	/	371.2	619.13
A03	/	/	/	/	625.04	/	265.6	625.04
A04	/	/	/	/	681.69	/	457.3	681.69
A05	/	/	/	/	645.86	/	402.4	645.86
mean	/	/	/	/	645.33	/	364.50	645.33

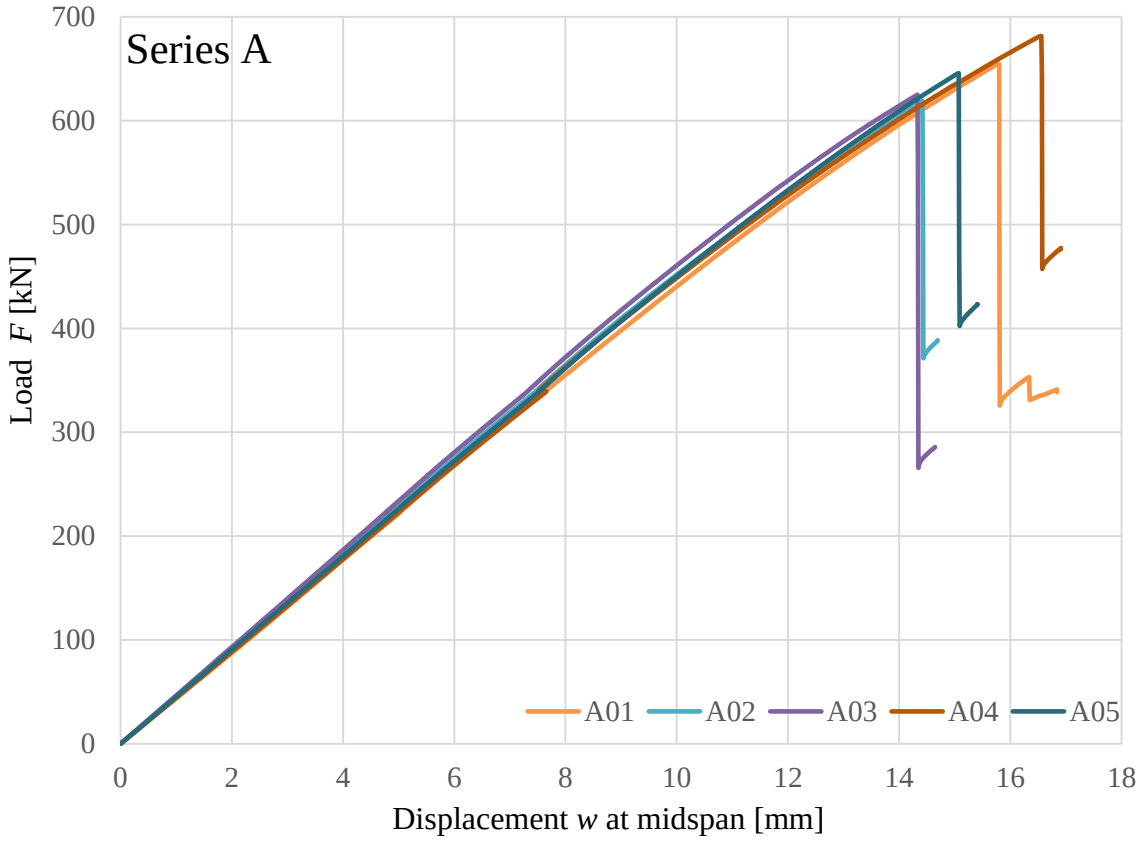

Figure 4.3: Load-displacement diagram of test series A

All tested beams of series A had a brittle shear failure spread to the left or right beam edge (see figure 4.3). The shear failure of all test specimens except for the test specimen A04 was on the lower side of the beam. The test specimen A03 had two shear failures closer to the bottom edge of the beam, but also about 20 cm from the top edge of the beam. The rest of the specimen showed only one shear failure.

The exact series description is depicted in appendix B1 and B4. Testing results of shear and normal stresses are shown in table 4.2.

Table 4.2: Overview of the test results of the shear and normal stress for test series A

Specimen	**Shear stress**		**Normal stress**
	τ_{gross}	τ_{crack}	$\sigma_{m,field}$
	[N/mm²]	**[N/mm²]**	**[N/mm²]**
A01	4.95	4.86	38.13
A02	4.73	4.72	36.05
A03	4.82	4.48	36.55
A04	5.23	4.39	39.79
A05	4.84	4.76	37.72
mean	4.91	4.64	37.65

4-1.2 SERIES B

Series B consists of five GLT beams with an unreinforced round opening. An exemplary specimen of this test series in the testing machine is shown in figure 4.4.

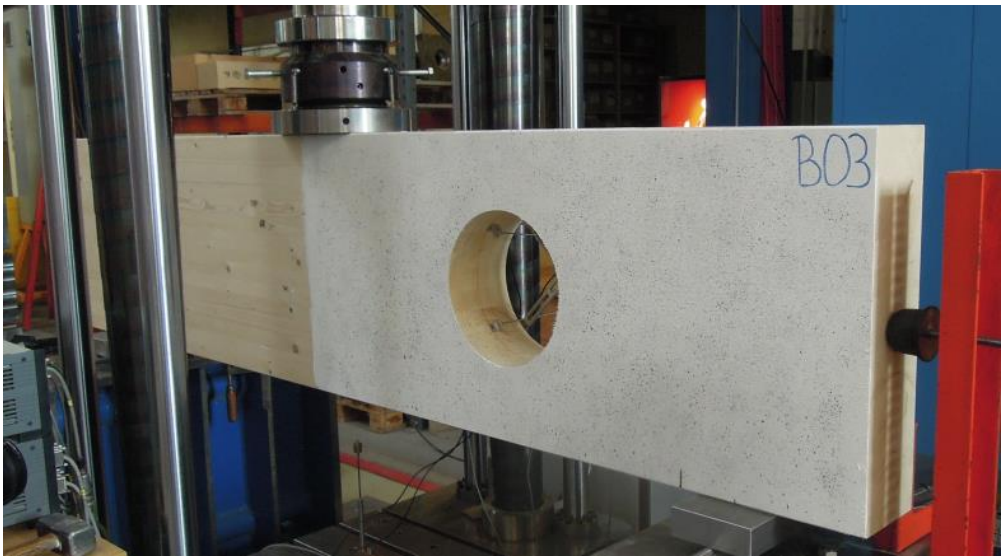

Figure 4.4: Test specimen B03 in the testing machine

The mean values of important proof loads as well as the angles of crack appearance for each test specimen are shown in table 4.3.

Table 4.3: Overview of the test results of the load and angles of crack appearance for test series B

	F_{c0}	α_{c0}	F_c	α_c	F_f	α_f	F_{fall}	F_{max}
	[kN]	**[°]**	**[kN]**	**[°]**	**[kN]**	**[°]**	**[kN]**	**[kN]**
B01	135.38	24	135.38	32	231.74	51	129.30	231.74
B02	115.00	39	122.89	45	278.91	52	187.44	278.91
B03	111.23	14	126.63	55	209.49	49	119.54	209.49
B04	97.33	48	124.03	41	226.22	13	161.15	226.22
B05	94.22	42	94.22	32	187.00	48	105.70	187.00
mean	110.63	33.40	120.63	41.00	226.67	42.60	140.63	226.67

The load-displacement diagram with all test specimens is shown in the figure 4.5.

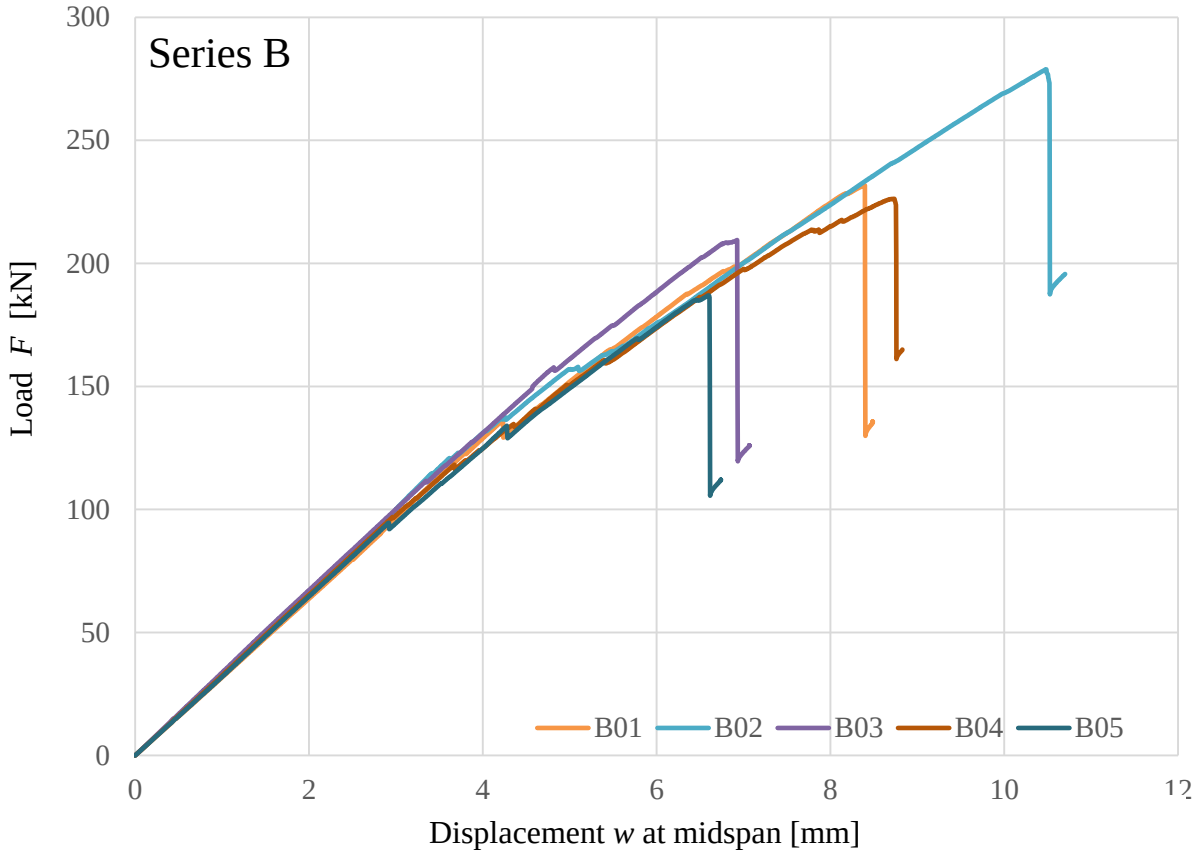

Figure 4.5: Load-displacement diagram of test series B

The mean load value of the shear failure of the test series B was 227 kN (the exact values of the forces for each test specimen are given in the table 4.3).

Firstly, all of the test specimens experienced tension stress perpendicular to the grain on the opening upper left or lower right edge, which was followed by the shear failure on the right support.

Only the test specimen B05 had lower load bearing capacity in comparison to the rest of the test specimens of the test series B (see figure 4.5).

The precise descriptions of all five test specimens are given in appendix B1 and testing results of shear and normal stresses are shown in table 4.4.

Table 4.4: Overview of the test results of the shear and normal stress of test series B

Specimen	Shear stress			Normal stress			
	τ_{net}	τ_{gross}	τ_{crack}	$\sigma_{m,field}$	$\sigma_{m,hole}$	$\sigma_{m,45}$	$\sigma_{m,edge}$
	[N/mm²]	[N/mm²]	[N/mm²]	[N/mm²]	[N/mm²]	[N/mm²]	[N/mm²]
B01	3.54	1.77	1.59	13.55	7.23	15.39	12.20
B02	4.22	2.12	1.90	16.24	8.65	18.52	14.72
B03	3.26	1.64	1.38	12.27	6.54	13.88	11.03
B04	3.44	1.75	1.45	13.21	7.04	14.96	11.89
B05	2.83	1.43	1.26	10.93	5.83	12.22	9.82
mean	3.46	1.74	1.52	13.24	7.06	14.99	11.93

4-1.3 SERIES C

Series C consisted of eight GLT beams with round openings, which were internally reinforced with two vertical full threaded screws on each side of the opening, in a length of 500 mm and a nominal diameter of 12 mm. An exemplary specimen of this test series in the testing machine is shown in figure 4.6. The first five test specimens were from the first delivery and test specimens C06 to C08 were from the second delivery. The first five were tested in July, and the 3 more were tested in August. Therefore, the test input parameters were adjusted from the first to the second testing.

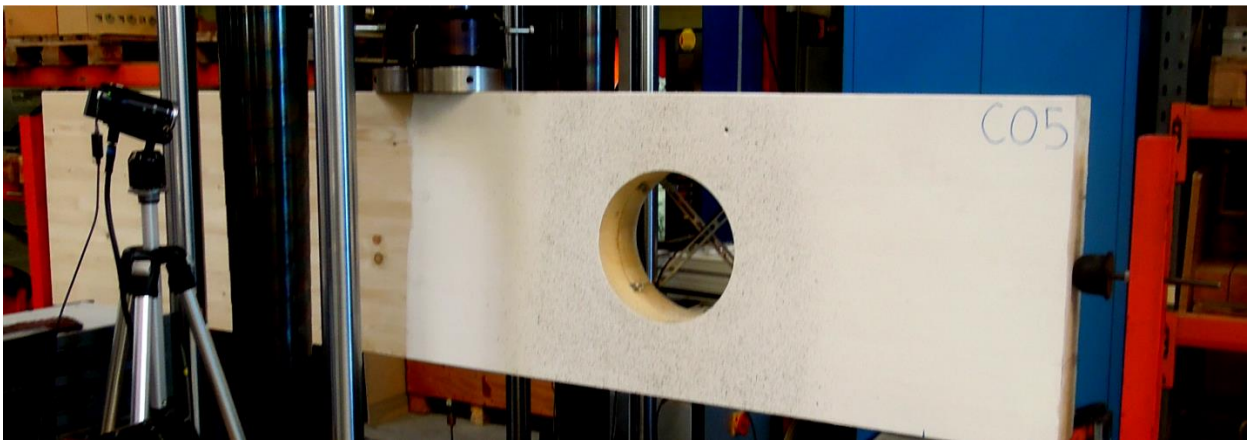

Figure 4.6: Test specimen C05 in the testing machine

The mean values of the force and angle for all eight specimens of this test series are represented in table 4.5, which is important for the further specimen description (see appendix B1 and B4).

Table 4.5: Overview of the test results of the forces and angles of crack appearance for test series C

	F_{c0}	α_{c0}	F_c	α_c	F_f	α_f	F_{fall}	F_{f2}	F_{fall2}	F_{max}
	[kN]	[°]	[kN]	[°]	[kN]	[°]	[kN]	[kN]	[kN]	[kN]
C01	139.56	13	152.06	13	330.81	38	190.92			330.81
C02	118.33	19	196.55	19	278.83	19	139.66			278.83
C03	154.99	21	160.91	26	275.26	28	156.61			275.26
C04	161.00	29	161.00	22	267.83	52	152.57			267.83
C05	191.50	48	227.68	53	242.65	48	147.49	275.73	190.92	242.65
C06	110.07	21	140.32	26	313.71	36	185.93	326.93	279.08	326.93
C07	179.72	58	179.2	69	308.98	32	163.04	301	220	308.98
C08	242.30	69	251.25	0	306.28	15	172.70	318.83	254	318.83
mean	162.18	34.75	183.62	28.50	289.44	33.50	163.70	305.62	236.00	286.55

The load-displacement diagram with all test specimens is shown in the figure 4.7.

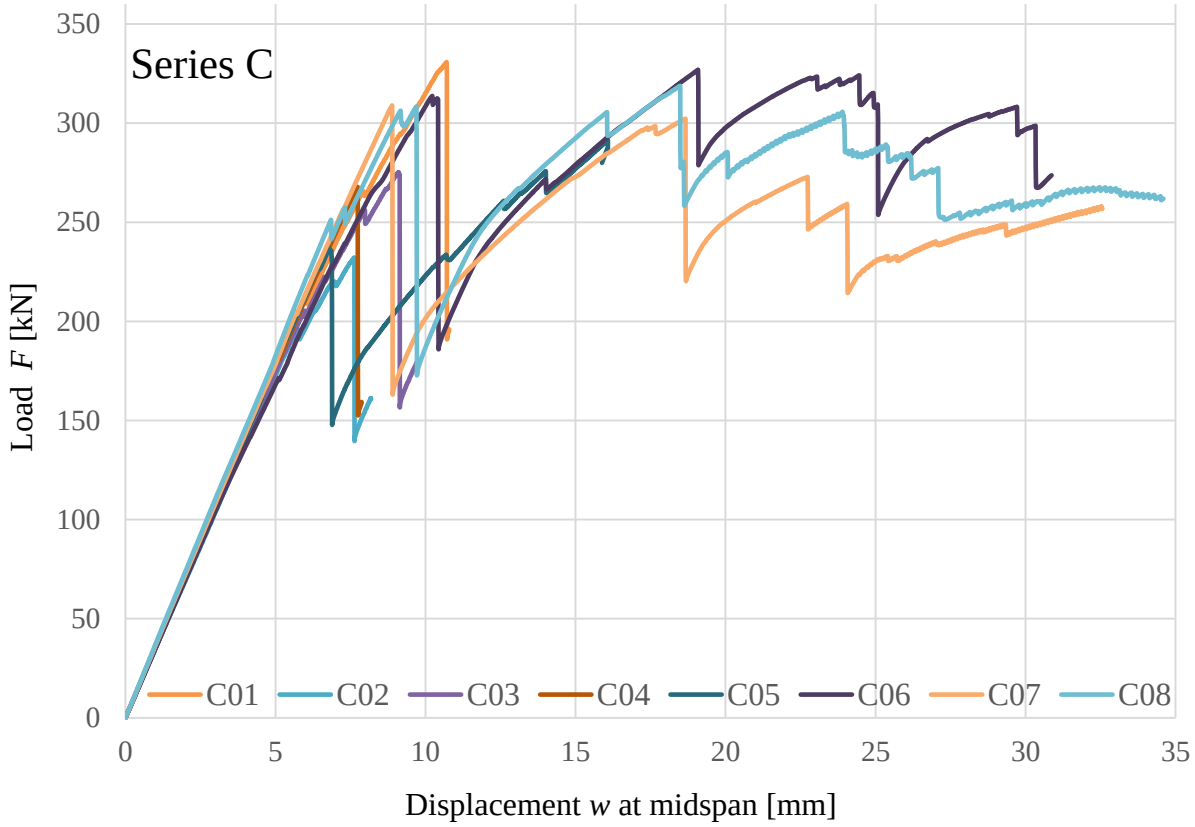

Figure 4.7: Load-displacement diagram of test series C

A crack caused by the tensile stress perpendicular to the grain occurred first at the upper left and lower right opening edge during the testing. After increasing the applied load a brittle shear failure followed (see figure 4.7).

A shear failure was the main failure within all the tested specimens of test series and occurred on the right edge. The specimens C06, C07 and C08 were continuously loaded until the force could not make any more growth, which was considered as the beam was completely broken and cannot carry over any more load. The bending failure was detected for test specimens C06 to C08.

After finishing the testing and cutting the beams through their width, the screw holes were inspected for damages, due to discrepancy in screw distances of the place where they, are planned to be and then actual position. As already explained in chapter 3, the test specimens C01 to C05 came with imprecise predrilled holes for the vertical reinforcements. As the holes for reinforcement closer to the right support were drilled from the beam top side through to the bottom side, discrepancies in the screw placement arose.

The vertical holes for the opening reinforcement for specimens C06 to C08 were drilled at the Institute of the Timber Engineering and Wood Technology in order to get more precise holes. As it was seen afterwards, these holes, due to their length of 450 mm, were not exact and had some declinations to the planned holes positions too.

Testing results of shear and normal stresses are shown in table 4.6.

Table 4.6: Overview of the test results of the shear and normal stress of test series C

Specimen	**Shear stress**			**Normal stress**			
	τ_{net}	τ_{gross}	τ_{crack}	$\sigma_{m,field}$	$\sigma_{m,hole}$	$\sigma_{m,45}$	$\sigma_{m,edge}$
	[N/mm²]	**[N/mm²]**	**[N/mm²]**	**[N/mm²]**	**[N/mm²]**	**[N/mm²]**	**[N/mm²]**
C01	5.03	2.51	2.01	19.31	10.31	21.98	17.37
C02	3.54	1.77	1.41	13.57	7.21	15.47	12.21
C03	4.23	2.10	1.68	16.12	8.60	18.40	14.50
C04	4.09	2.03	1.73	15.63	8.35	17.79	14.10
C05	3.74	1.84	1.62	13.81	7.34	15.69	12.42
C06	5.01	2.47	2.05	18.31	9.77	20.92	16.52
C07	4.82	2.42	2.10	18.04	9.67	20.60	16.28
C08	4.82	2.43	1.88	18.11	9.64	20.60	16.29
mean	4.41	2.20	1.81	16.61	8.86	18.93	14.96

4-1.4 SERIES D

Series D consisted of five GLT beams with a round opening, which was internally reinforced with screwed-in inclined threaded rods under an angle of 45°. The threaded rods had a length of 600 mm, with a nominal diameter of 16 mm. An exemplary test specimen of this test series in the testing machine is shown in figure 4.8

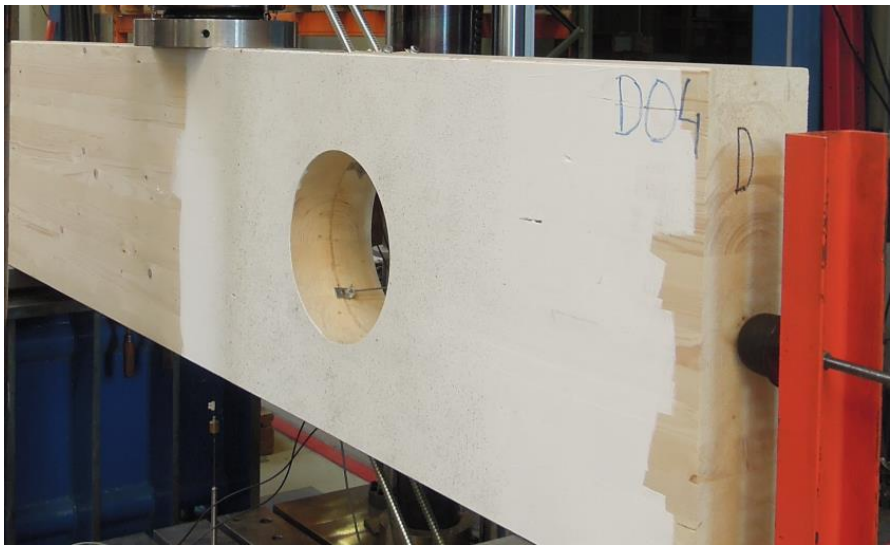

Figure 4.8: Test specimen D04 in the testing machine

The mean values of the forces as well as the angles under which the crack appeared on the opening edge are presented in table 4.7.

Table 4.7: Overview of the test results of the forces and angles of crack appearance for test series D

	F_{c0}	α_{c0}	F_c	α_c	F_f	α_f	F_{fall}	F_{f2}	F_{fall2}	F_{f3}	F_{fall3}	F_{max}
	[kN]	**[°]**	**[kN]**	**[°]**	**[kN]**	**[°]**	**[kN]**	**[kN]**	**[kN]**	**[kN]**	**[kN]**	**[kN]**
D01	165.92	26	249.9	26	399.4	48	317.8	357.7	321.9			399.8
D02	200.0	27	245.0	44	440.7	38	383.8	395.8	346.8			440.8
D03	142.50	55	170.7	64	369.8	31	363.4	377.5	298.3			377.5
D04	146.82	26	183.0	28	409.9	48	350.5	436.7	385.0	380.0	265.8	436.7
D05	222.32	26	280.0	37	441.9	37	378.6	400.1	359.2	362.9	319.2	441.9
mean	175.5	32	225.7	40	412.3	40	358.8	393.6	342.2	371.5	292.5	419.3

Series D was the series with the diagonally reinforced opening. The openings were reinforced with two screwed-in inclined threaded rods ($\emptyset = 16$ mm) under the angle of 45º from each side of the opening (8 steel rods overall). Test specimens D01, D04 and D05 had all 8 threaded rods screwed in, but the threaded rods were screwed to only 40 cm in compression zone, because the delivered beams were drilled with faults, so the two holes, of the tension and compression zones were crossing each other at the hole depth of the 40 cm. As the threaded rods in the tension zone were important for taking the load in case of cracks in the opening region, it was important that those rods are totally screwed in, so those in compression zone were

left in length of 20 cm out of the beams. Test specimens D02 and D03 had no inclined steel rods in the compression zone.

The load-displacement diagram with all test specimens is shown in the figure 4.9.

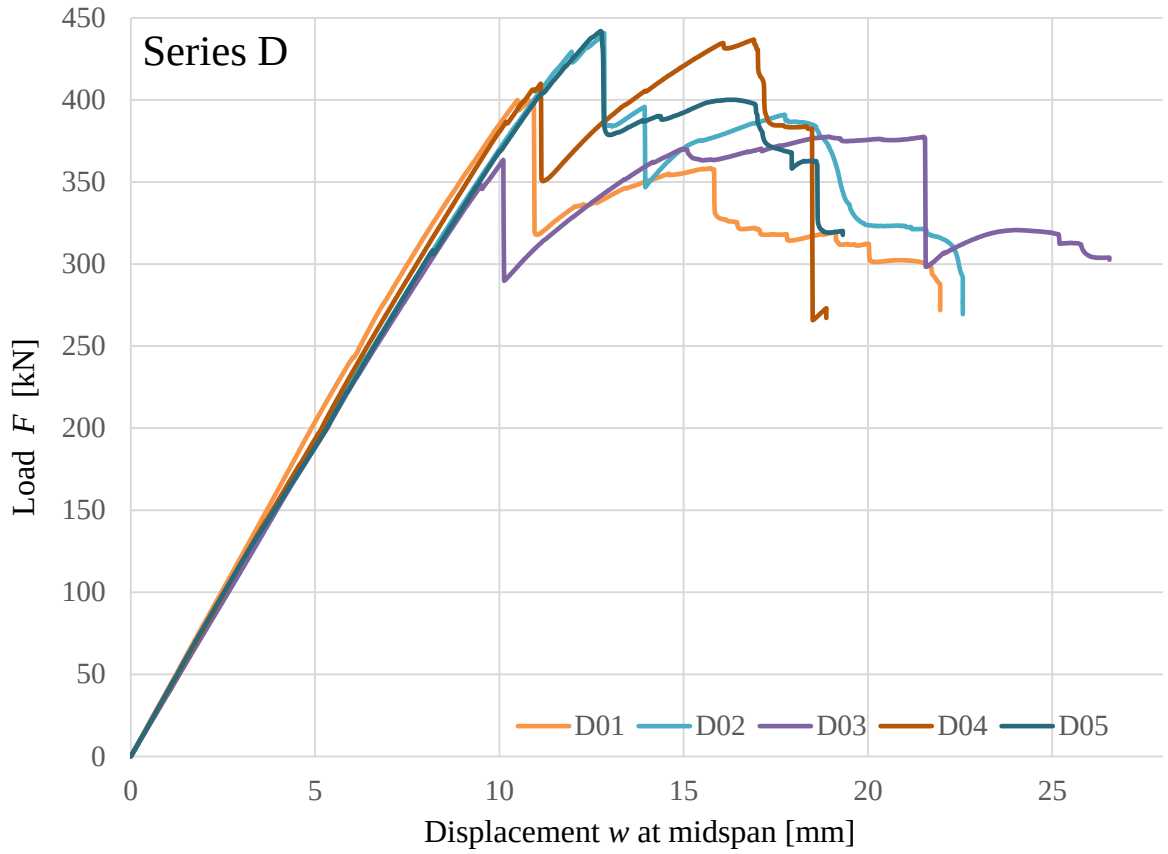

Figure 4.9: Load-displacement diagram of test series D

All beams of test series D first experienced tension stress perpendicular to the grain, which appeared as cracks on the upper left and lower right opening edge, followed by a shear failure closer to the right support of the beam. All the beams also failed on bending. The crack, caused by transverse tension stress, happened first on the upper left edge of the opening, except for test specimen D03 (exact places of the breakage are shown in table 4.7). All test specimens were continuously loaded until the force could not be increased any more, which was considered as though the beam was completely broken and cannot carry over any more load.

After finishing the testing and cutting through their width, the beams underwent an inspection of the threaded rod holes for damage and discrepancies between the planned and the actual position. As already explained in chapter 3, the test specimens D01 to D05 came with wrongly predrilled holes for the inclined opening reinforcement.

The threaded rods were recessed into the beam. The pull through effect could be seen at the holes of the threaded rods due to the fact that the cracking of the beam disabled the distribution of the shear force in timber, therefore, the rods took over the part of the bearing agent.

Exact description of each test specimen is to be found in appendix B1 and B4. Testing results of shear and normal stresses are shown in table 4.8.

Table 4.8: Overview of the test results of the shear and normal stress for test series D

Specimen	Shear stress			Normal stress			
	τ_{net}	τ_{gross}	τ_{crack}	$\sigma_{m,field}$	$\sigma_{m,hole}$	$\sigma_{m,45}$	$\sigma_{m,edge}$
	[N/mm²]	[N/mm²]	[N/mm²]	[N/mm²]	[N/mm²]	[N/mm²]	[N/mm²]
D01	6.07	3.01	2.53	23.41	12.45	26.60	21.04
D02	6.62	3.29	2.75	25.77	13.76	29.27	23.18
D03	5.48	2.73	2.27	21.27	11.34	24.18	19.08
D04	6.12	3.01	2.56	24.00	12.80	27.39	21.69
D05	6.60	3.33	2.68	25.79	13.74	29.31	23.19
mean	6.18	3.07	2.55	24.05	12.82	27.35	21.64

4-1.5 SERIES G

Series G consisted of three GLT beams with a round opening, which was internally reinforced with inclined screwed-in threaded rods under the angle of 40°. The fully threaded rods in the tension zone were extra equipped with the strain gauges inside of them. On the back side of the beam, four extra strain gauges were attached around the opening in the positions of the strain gauges of the steel rods, which was estimated as the places with maximum stress impact at an angle of the 40°.

The threaded rods had a length of 600 mm and a nominal diameter of 16 mm in the tension zone and 20 mm in the compression zone. In the tension zones, on each side, there were two threaded rods and on the compression sides there was one threaded rod on each side.

An exemplary test specimen of this test series in the testing machine is shown in figure 4.10.

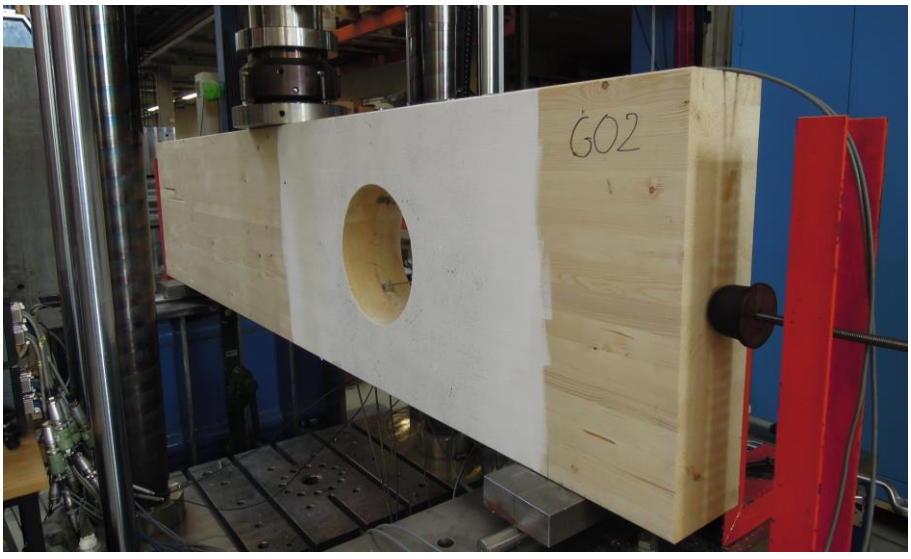

Figure 4.10: Tet specimen G02 in the testing machine

The mean values of the forces and angles of crack appearance on the opening edges for each test specimen are given in table 4.9.

Table 4.9: Overview of the test results of the forces and angles of crack appearance for test series G

	F_{c0}	α_{c0}	F_c	α_c	F_f	α_f	F_{fall}	F_{f2}	F_{fall2}	F_{f3}	F_{fall3}	F_{max}
	[kN]	[°]	[kN]	[°]	[kN]	[°]	[kN]	[kN]	[kN]	[kN]	[kN]	[kN]
G01	189.60	30	306.96	58	468.4	25	324.1	356.1	276.4	299.7	214.93	468.4
G02	172.86	15	360.0	22	431.6	28	210.8	445.3	425.3			445.3
G03	186.40	22	313.22	22	436.4	24	320.4	330.5	237.5	244.4	174.7	436.4
mean	183.0	22	326.7	34	445.5	26	285.1	377.3	313.1	272.1	194.8	450.0

The load-displacement diagram for all test specimens is shown in the figure 4.11, which is going to be explained in detail in appendix B1, B3 and B4. Testing results of shear and normal stresses calculated for maximum bearing load for each series are shown in table 4.11.

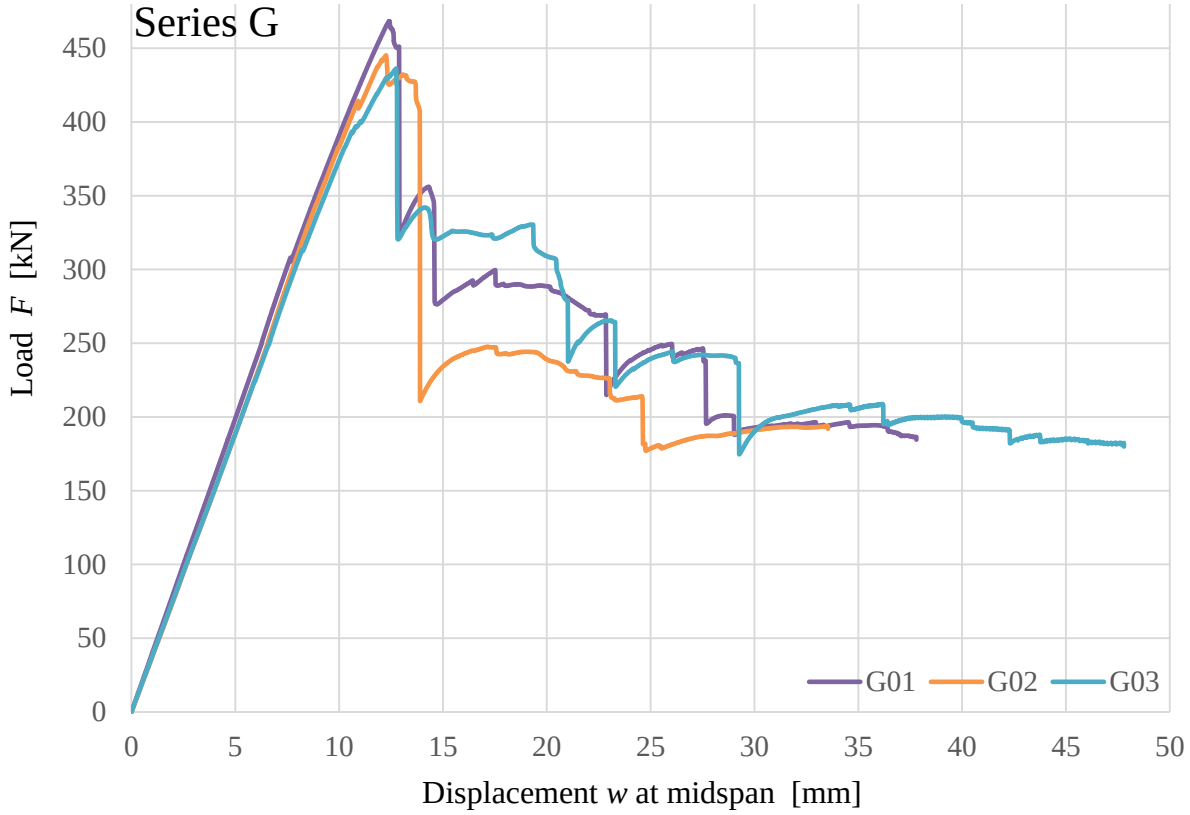

Figure 4.11: Load-displacement diagram of test series G

At all beams of test series G the tensile stress perpendicular to the grain caused cracks at the right support, which led to a shear failure. All the beams finally also failed on a bending failure in the net cross section. The initial cracks of test specimens G02 and G03 happened first on lower right opening edge and for G01 on the top left edge of the opening. All of the test specimens were continuously loaded until the force could not be applied any more, which was considered as though the beam was completely broken and cannot carry over any more load.

After finishing the testing and cutting through their width, the beams underwent an inspection of the threaded rod holes for damages and discrepancies between the planned and actual positions. As already explained in chapter 3, the test specimens G01 to G03 came without predrilled holes for the inclined opening reinforcement and they were drilled at the Institute with the help of the drilling rig to achieve a more precise placement of the threaded rods.

Each test specimen from test series G also had strain gauge equipped threaded rods, in the tension zone around the opening.

The placement of used threaded rods with description names for each test specimen of the test series G are shown in figure 4.12.

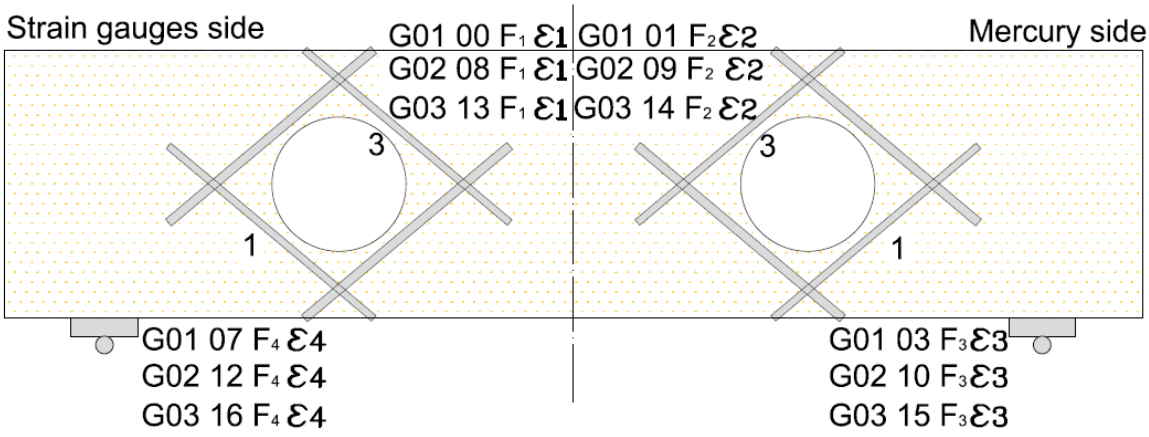

Figure 4.12: Placement of the threaded rods for the test series G

The values of the elongations and maximum forces for the first shear failure load in each threaded rod of each test specimen of the test series G are shown in the table 4.10.

Table 4.10: Overview of the test results of the forces and elongations in rods for test series G

Specimen	**Forces in threaded rods**				**Elongation in threaded rods**			
	F_1	F_2	F_3	F_4	ε_1	ε_2	ε_3	ε_4
	[kN]	**[kN]**	**[kN]**	**[kN]**	**[‰]**	**[‰]**	**[‰]**	**[‰]**
G01	55.23	45.85	57.83	50.33	0.0022	0.0019	0.0024	0.0022
G02	47.53	39.52	53.10	54.05	0.0020	0.0018	0.0020	0.0021
G03	53.04	51.21	50.32	44.52	0.0022	0.0021	0.0020	0.0019
mean	51.93	45.53	53.75	49.63	0.0021	0.0019	0.0021	0.0021

Table 4.11: Overview of the test results of the shear and normal stress for test series G

Specimen	Shear stress			Normal stress			
	τ_{net}	τ_{gross}	τ_{crack}	$\sigma_{m,field}$	$\sigma_{m,hole}$	$\sigma_{m,45}$	$\sigma_{m,edge}$
	[N/mm²]	[N/mm²]	[N/mm²]	[N/mm²]	[N/mm²]	[N/mm²]	[N/mm²]
G01	7.21	3.57	2.86	27.23	14.54	31.06	21.54
G02	7.00	3.50	3.08	26.04	13.89	29.65	23.45
G03	6.96	3.47	2.75	25.65	13.68	29.26	23.11
mean	7.06	3.51	2.90	26.31	14.04	29.99	22.70

4-1.6 SERIES H

Series H consisted of three GLT beams with a round opening, which was internally reinforced with inclined glued-in threaded rods under the angle of 40°. All threaded rods in the tension zone were extra equipped with glued-on strain gauges.

The threaded rods length was 600 mm with a nominal diameter of 16 mm in the tension zone and with a nominal diameter of 20 mm in the compression zone. The tension zone had two threaded rods on the each side, while the compression zone only had one threaded rod on each side.

The exemplary test specimen of this test series is shown in figure 4.13.

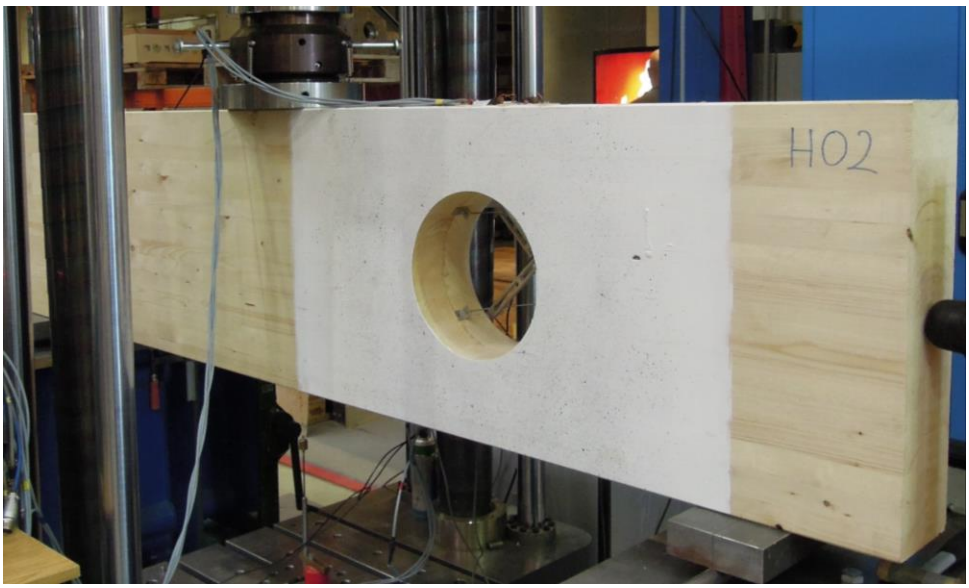

Figure 4.13: Test specimen H02 in the testing machine

The mean values of the forces and angles measured during and after testing are shown in table 4.12.

For test series H the angle α was measured from vertical beam axis, clockwise, to the upper right opening edge where first shear failure took place for all three test specimens. This was particular for this test series only due to the glued-in threaded rods were rearranged under angle of 40°.

Table 4.12: Overview of the test results of the forces and angles of crack appearance for test series H

	F_{c0}	α_{c0}	F_c	α_c	F_f	α_f	F_{fall}	F_{f2}	F_{fall2}	F_{max}
	[kN]	[°]	[kN]	[°]	[kN]	[°]	[kN]	[kN]	[kN]	[kN]
H01	195.30	26	413.90	32	533.44	67	262.61	293.00	217.33	533.4
H02	212.70	21	516.00	21	547.29	/	502.46	525.91	59.52	547.3
H03	267.50	42	498.23	32	572.55	73	192.43			572.6
mean	225.2	30	476.0	28	551.1	70	319.2	409.5	138.4	551.1

For test specimen H02 the shear failure was above the opening region, therefore, no angle could be measured, but the failure happened 142 mm measured from the top beam edge.

The load displacement diagram with all test specimens is shown in the figure 4.14, which is explained in detail in appendix B1, B3 and B4. Testing results of shear and normal stresses calculated with maximum bearing load for each series are shown in table 4.14.

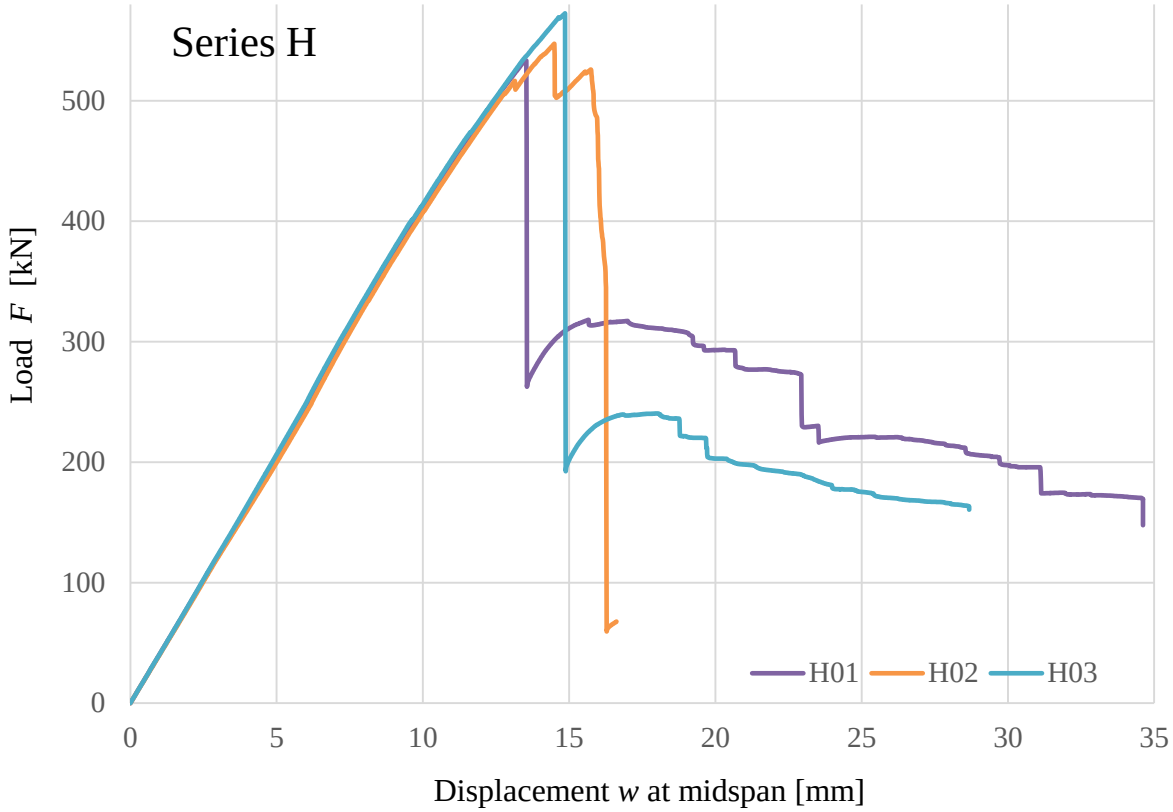

Figure 4.14: Load-displacement diagram of test series H

All of the beams had cracks on the upper left opening edge caused by the tensile stress perpendicular to the grain. Test series H had multiple shear failures on the right beam edge. All of the beams finally also failed due to a bending failure in the net cross section. At this test series the initial cracks happened in the top half of the beam height at the right support, which was characteristical only for this test series because of the placement of the glued-in threaded rods.

After the tests, the beams were cut widthwise in order to inspect the threaded rod holes for damages and discrepancies according to the hole positions As already explained in chapter 3 the test specimens H01 through H03 came without predrilled holes and were drilled with the help of the drilling rig to achieve a more precise placement of the threaded rods.

All of the test specimens in test series H were equipped with strain gauges glued on the threaded rods which were placed in the tension zone to get information about the elongation of the glued-in threaded rods close to the crack.

Furthermore, the glued-in threaded rods which were used here are listed in figure 4.15.

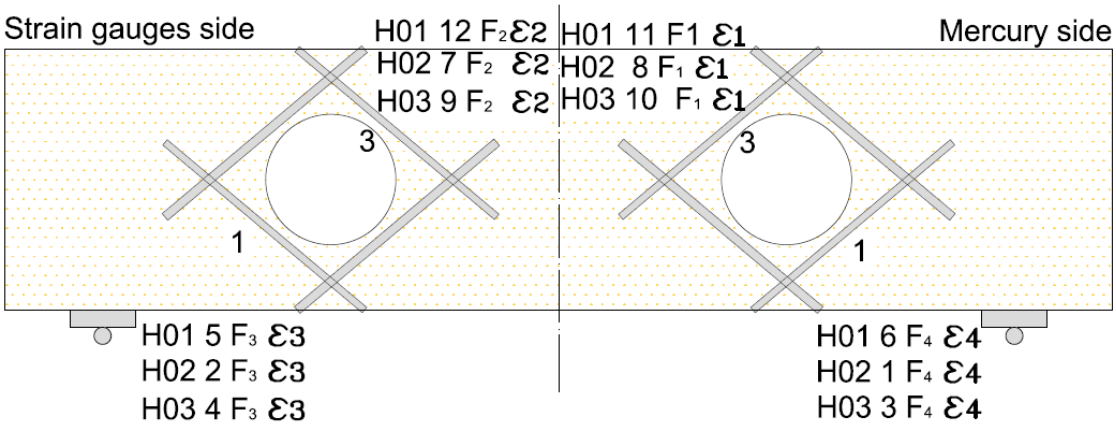

Figure 4.15: Arrangement of the threaded rods for the test series H

Table 4.13 shows obtained force values in the threaded rods as well as the measured elongations for the first shear failure load of each test specimen.

Table 4.13: Overview of the test results of the forces and elongations in the rods for test series H

Specimen	**Forces in threaded rods**				**Elongation in threaded rods**			
	F_1	F_2	F_3	F_4	ε_1	ε_2	ε_3	ε_4
	[kN]	**[kN]**	**[kN]**	**[kN]**	**[‰]**	**[‰]**	**[‰]**	**[‰]**
H01	33.05	35.45	38.45	36.84	0.0014	0.0013	0.0017	0.0016
H02	37.41	38.33	43.84	37.90	0.0017	0.0017	0.0018	0.0017
H03	33.14	39.13	49.32	41.44	0.0014	0.0018	0.0019	0.0018
mean	34.53	37.64	43.87	38.73	0.0015	0.0016	0.0018	0.0017

Table 4.14: Overview of the test results of the shear and normal stress for test series H

Specimen	Shear stress			Normal stress			
	τ_{net}	τ_{gross}	τ_{crack}	$\sigma_{m,field}$	$\sigma_{m,hole}$	$\sigma_{m,45}$	$\sigma_{m,edge}$
	[N/mm²]	[N/mm²]	[N/mm²]	[N/mm²]	[N/mm²]	[N/mm²]	[N/mm²]
H01	8.38	4.19	4.03	31.25	16.67	35.63	28.14
H02	8.61	4.31	3.31	32.25	17.20	36.70	29.02
H03	9.04	4.51	3.52	33.63	17.95	38.33	30.27
mean	8.68	4.34	3.62	32.38	17.27	36.88	29.14

4-2 MOISTURE CONTENT

Table 4.15 gives an overview off all statistical results, concerning timber moisture content for six test series. The mean value of the moisture content is 11.51 % (represented with orange line in figure 4.16).

Table 4.15: Statistical overview of the moisture content

Series	A	B	C	D	G	H	Sum
Number [/]	5	5	8	5	3	3	29
Minimum [%]	10.50	11.25	11.22	10.34	11.50	12.09	10.34
Mean value [%]	11.12	11.46	11.51	10.60	12.22	12.20	11.51
Median [%]	11.30	11.47	11.44	10.63	12.43	12.19	11.46
Maximum [%]	11.50	11.69	11.95	10.92	12.74	12.31	12.74

The mean values of each series out of table 4.15 as well as values for moisture content of each test specimen are represented in figure 4.16 as scatter and line diagram combined.

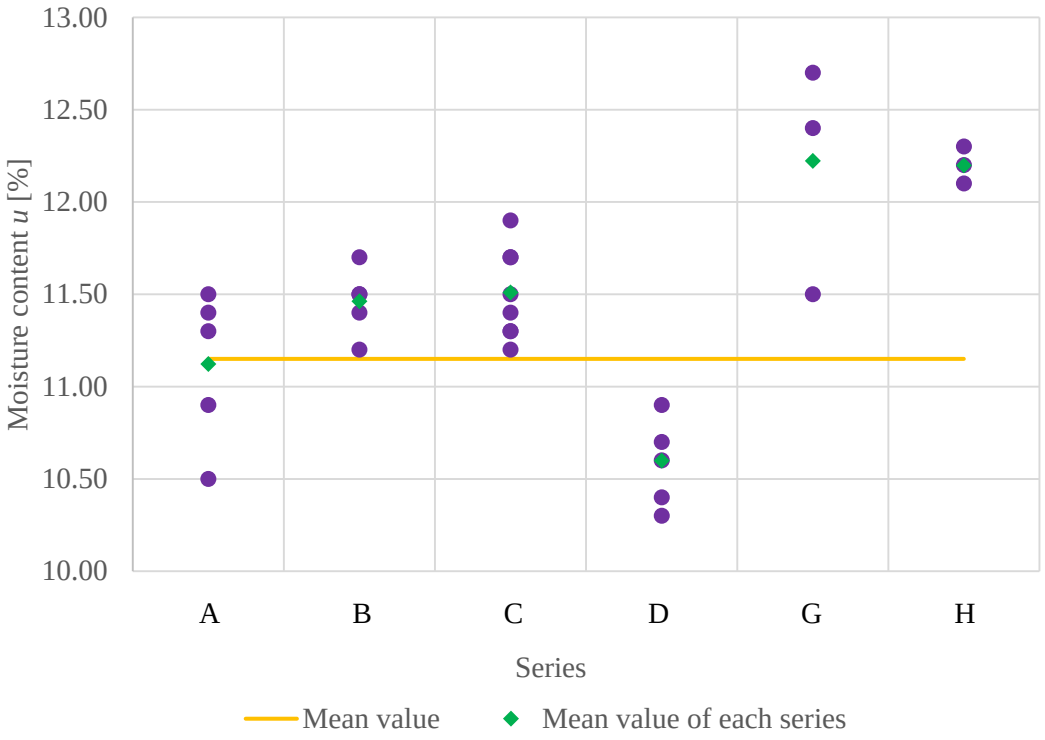

Figure 4.16: Scatter and line diagram of moisture content for tested series

The deviations from the reference moisture content of u = 12 % are negligibly low, since the test specimens were already delivered with the corresponding moisture content.

By comparing individual series, it is noticeable that the moisture values clearly differ in some cases. A possible reason for this could be that the series were delivered in two different deliveries and the manufacturer produced them from different timber, as well as the climate conditions were different for the

delivery periods. The beams were not inside of the climate chamber in the period between the delivery and the testing date, which also had some influence on the moisture content.

4-3 DENSITY

The representation of the density results of the considered series is in table 4.16. As presented, the mean value for the all GLT series was 510 kg/m^3 (represented with orange line in figure 4.17).

Table 4.16: Statistical overview of the density

Series	A	B	C	D	G	H	Sum
Number [/]	5	5	8	5	3	3	29
Minimum [kg/m^3]	497	500	498	486	505	513	486
Mean value [kg/m^3]	509	509	511	501	510	518	510
Median [kg/m^3]	511	510	512	503	510	518	511
Maximum [%]	515	520	529	514	516	523	529

The scatter and line diagram combined of the density for the test series A through the H is shown in figure 4.17 with presented mean values of each tested series and mean value for all six series.

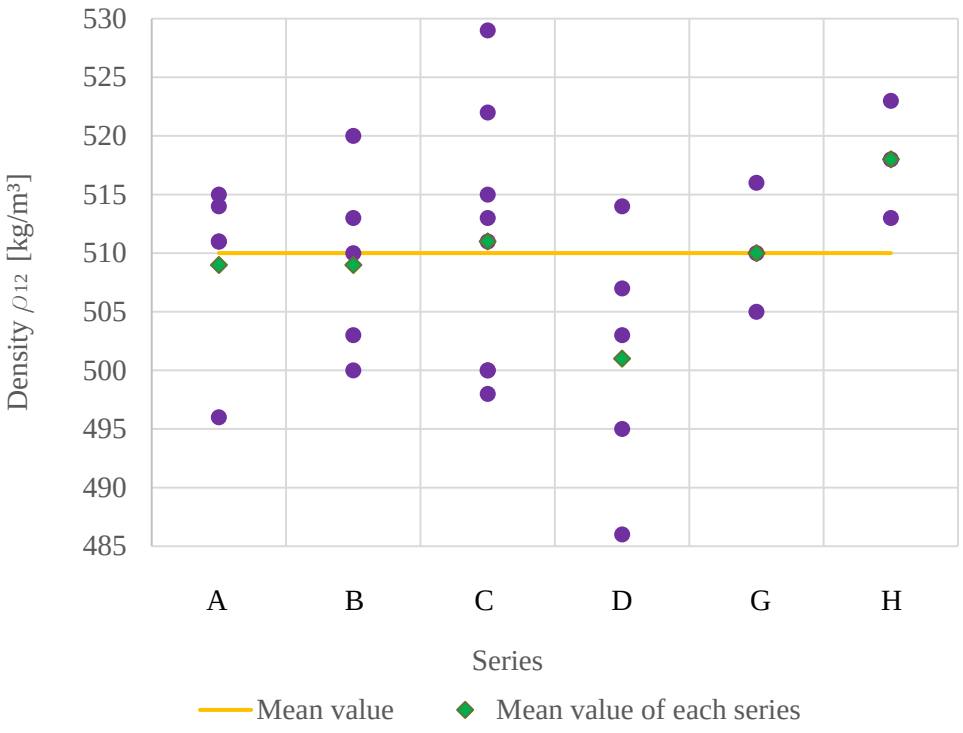

Figure 4.17: Scatter and line diagram of density results representation

By comparing individual series, it is noticeable that the density values differ in some cases. These deviations can be explained by the moisture content of two different timber deliveries for which different raw materials were used.

4-4 SHEAR MODULUS

The summary of the minimum, maximum, mean and median values of the shear modulus for all tested series is represented in table 4.17.

Table 4.17: Statistical overview of the shear modulus

Series	A	B	C	D	G	H	Sum
Number [/]	5	5	8	5	3	3	29
Minimum [N/mm²]	597	145	145	182	202	306	145
Mean value [N/mm²]	734	148	159	213	213	312	297
Median [N/mm²]	759	148	161	228	213	311	221
Maximum [N/mm²]	853	152	172	233	224	321	853

*For test series G and H the shear modulus was established for the displacement transducers under the angle of 40°. For all the other test series it was under a 45° angle.

The shear modulus calculated according to ON EN 408:2012 [58], is represented as scatter and line diagram in figure 4.18. While the shear modulus of series A can be seen as tested material data with high but reasonable value, the other shear moduli were obtained by including the weakening due to the opening. They can be compared in the following discussion by aiming at the stiffness behavior of the different reinforcements.

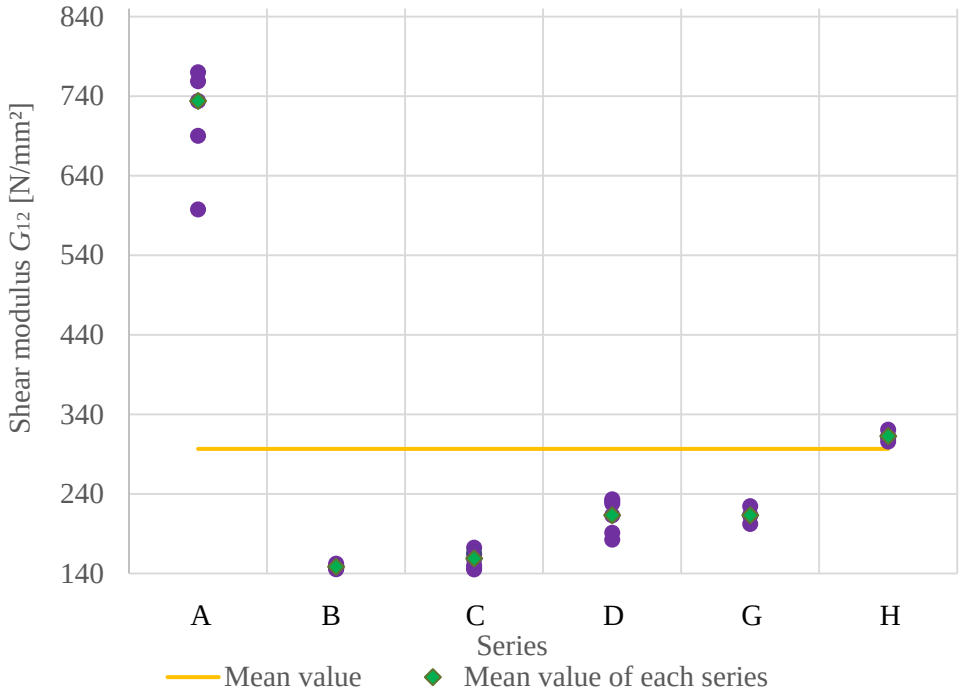

Figure 4.18: Scatter and line diagram of shear modulus results representation

4-5 STIFFNESS K

The stiffness of all 29 test specimens was measured in four directions around the beam opening, under the angle of 45° for the test series A, B, C, D and under the angle of 40° for the test series G and H. Summary of the obtained results is to be found in the table 4.18 and schematic representaion of them in figure 4.19.

Table 4.18: Statistical overview of the stiffness

	A	B	C	D	G	H
$K_{1mean,tensile}$ [N/mm]	828	263	248	422	477	848
$K_{2mean,compression}$ [N/mm]	-558	-217	-233	-271	-607	-439
$K_{3mean,tensile}$ [N/mm]	1153	224	264	474	483	1025
$K_{4mean,compression}$ [N/mm]	-636	-224	-248	-294	-344	-508

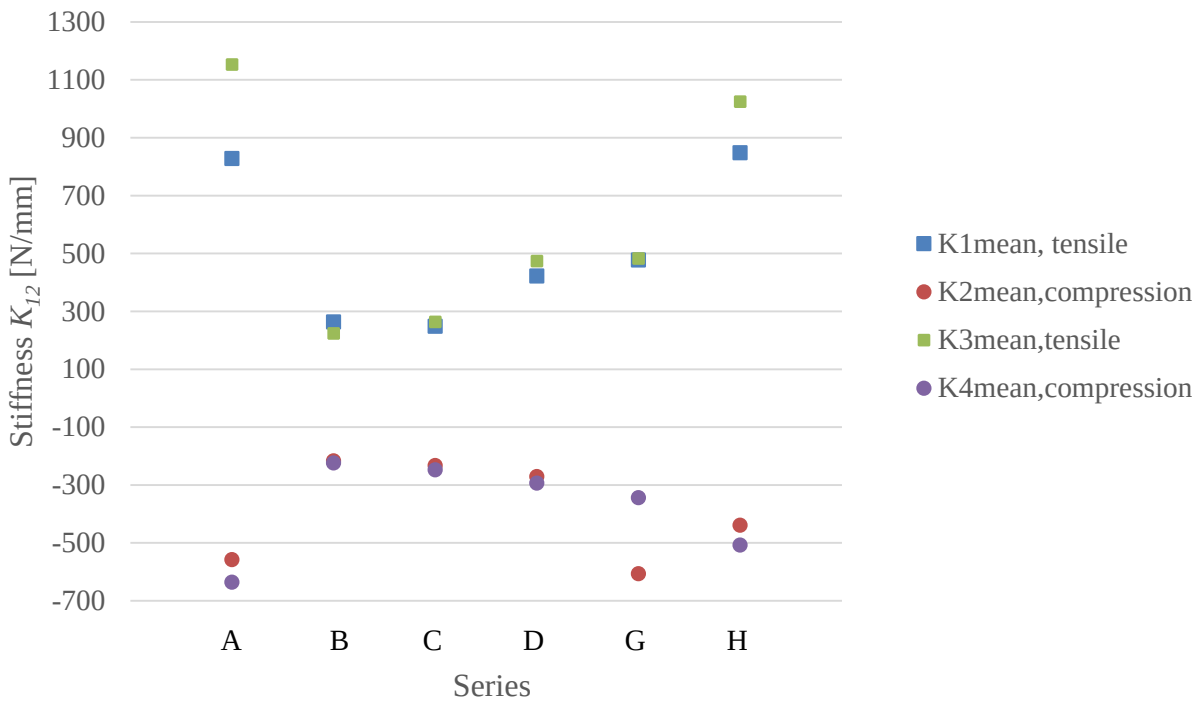

Figure 4.19: Scatter diagram of stiffness results representation

Some results could be considered to be excluded from the results investigation, because they deviate too much from the general mean values for each test series. These deviations can be explained due to the fact that the displacement transducers fell apart during the testing time.

The differences between series are explained due to the fact that the series A was a beam with no opening, series B was series with no reinforcement, series C, D, G and H had internal reinforcement, and different ones of those.

4-6 SHEAR STRESS

The values for the shear stress of each test specimen calculated from the obtained results are given in table 4.19. A graphical representation of all tested series and mean values of each series as well as the mean value for all tested specimens is shown in figure 4.20.

Table 4.19: Statistical overview of the shear stress

Series	A	B	C	D	G	H	Sum
Number [N/mm²]	5	5	8	5	3	3	29
Minimum [N/mm²]	4.73	1.43	1.77	2.73	3.47	4.19	1.43
Mean value [N/mm²]	4.91	1.74	2.20	3.07	3.51	4.34	3.30
Median [N/mm²]	4.84	1.75	2.26	3.01	3.50	4.31	3.26
Maximum [N/mm²]	5.23	2.12	2.51	3.33	3.57	4.51	5.23

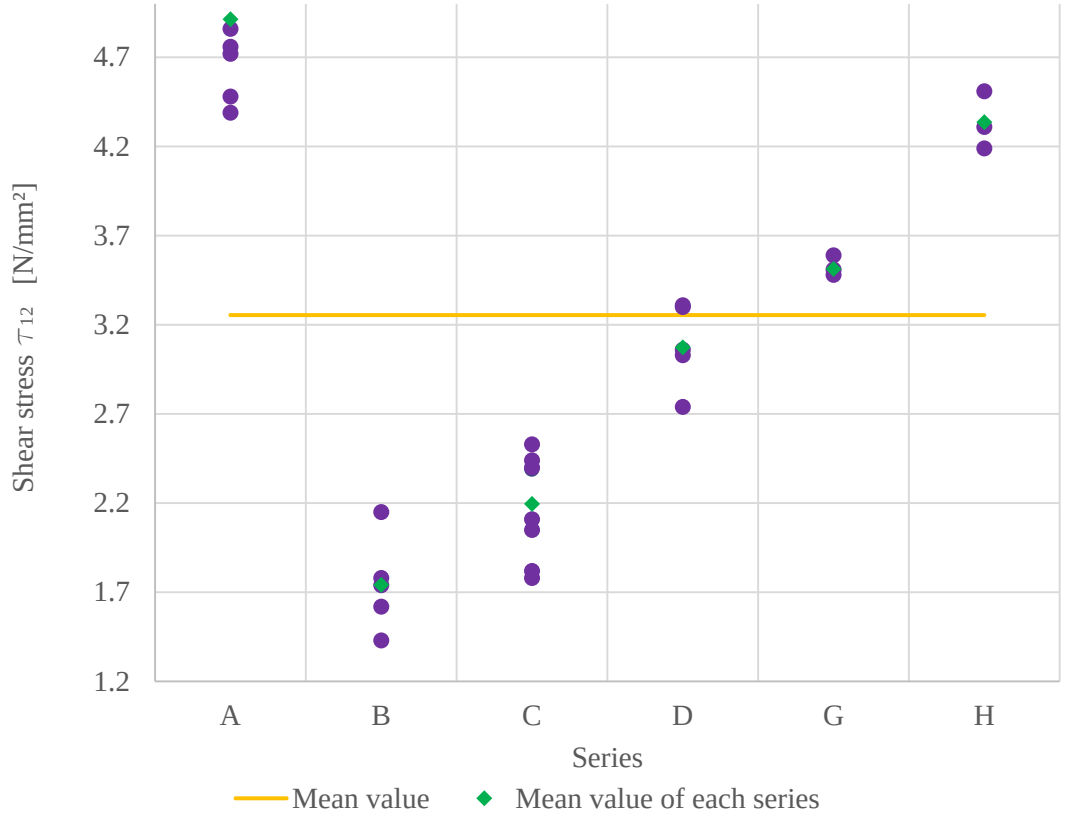

Figure 4.20: Scatter and line diagram of shear stress results representation

Test series A, without an opening, was the reference series, therefore, the obtained results from this series were significantly higher than for the other test series.

The test series B had significantly lower results in comparison to other series because this series had no reinforcement of the opening. Series H had the closest values to the series A.

CHAPTER 5:DISCUSSION

5-1 COMPARISSON OF THE TEST SERIES

5-1.1 MOISTURE CONTENT

The moisture content for all 29 test specimens was in the range of 10.3 % to 12.74 %. The results of moisture content should be close to 12 % because of the discrepancies in other test results, due to the different wood moisture content, which was held in range of 12 ± 2 %. The difference of the moisture content was due to the different climate influences, during delivery and storage of the two different deliveries that were made at different time (see appendix B4).

5-1.2 DENSITY

The density of the test series A, B, C, D, G and H was in the range of 486 to 529 kg/m^3. These differences were also due to the two deliveries and obviously different initial used material, even though it should have the same characteristics (see appendix B4). These values were a bit higher in comparison to the values obtained out of EN 14080:2013 [46].

5-1.3 SHEAR MODULUS

For the reference series A, a shear modulus of 734 N/mm^2 could be given, which was significantly lower for series B, at 148 N/mm^2, owing to the inserted opening.

The shear modulus mean value for series C was only insignificantly higher, at 159 N/mm^2. On the one hand this can be explained by the screw, bearing shear loads at a right angle in relation to its axis, which also represents the load bearing direction with a lower stiffness. On the other hand a minimal deformation of the surrounding timber is necessary to achieve the full load-bearing ability, as well as stiffness, which was not yet the case within the evaluated elastic range.

In the case of observing the results of series D, G, and H, the increase in the shear modulus to 213 N/mm^2 for series D and G, i.e. to 312 N/mm^2 for series H, can be explained with the same mechanism which was described for series C. Thus, by virtue of the reinforcement rods being inclined at 40° or 45° degrees to the grains main direction, they were also bearing a bigger load in the direction of their stiffer axis. On the other hand, the screw rods needs less deformations along the main axis. As glued-in threaded rods nearly necessitate no starting deformation, as opposed to screwed-in threaded rods, they come out stiffer, which can be seen in the shear modulus.

5-1.4 STIFFNESS

The stiffness was also calculated and used for comparisons between the test series, where the test series A had the biggest values for both compression and tensile stress perpendicular to the grain zones.

As the stiffness is based on similar measurements and calculations as the shear modulus, the observed values can be described with the same mechanisms as well. Therefore test series B, had the smallest mean value, as expected, because of the unreinforced opening.

Further the mean stiffness value for test series C was a bit higher than those of test series B too, but still very low in comparison to the other tested beams.

Series D had mean stiffness values higher than for series B and C, but still significantly smaller than for test series A. In comparison to the test series G and H, which also had inclined threaded rods around the opening, D showed smaller values than both of them. This differences were significantly smaller when comparing test series D and G than in comparing series D and H, whereby test series D had about 50% smaller stiffness than those of test series H.

5-1.5 SHEAR STRENGTH

The mean value of shear strength for test series B was 1.74 N/mm^2, which was significantly smaller than for test series A, but expected due to the presence of the unreinforced opening.

For test series C the mean shear strength value was higher than for test series B and was 2.20 N/mm^2, but this was still significantly smaller than for the test series A, due to the insufficient opening reinforcement.

Test series D, G and H were designed to take the same load as beams without openings (series A), which was the concept of experimental investigation of the ALP GSA® method from n'H neue Holzbau AG [44] in cooperation with Professor Gehri. In their tests of the 23 beams reinforced with ALP GSA® method [44], the proven shear strength of the beams was 2.7 N/mm^2 for the gross cross section which proved that this method can reinforce the opening in the GLT beams as they were beams without openings.

The mean value of shear stress of test series A was 4.91 N/mm^2. For test series H it was 4.34 N/mm^2, 3.51 N/mm^2 for series G and 3.07 N/mm^2 for test series D. All of these shear stress values showed that the obtained values were in the range of the calculated ones, even a bit higher and therefore the assumptions of 3.5 N/mm^2 were fulfilled.

Test series H had the highest shear stress and the closest areas to the test series A, which was planned in order to get the best possible solution for beams with openings which are going to reach the load carrying capacity of a beam without an opening.

By looking at series A it appears that it had such strong parameters for stiffness and strength due to excellent wood sorting and good ratio of small and big wood knots, so the mean values of the shear stress were in the range of 4.91 N/mm^2. The values of other series could seem to be too low, but realistically were not and those inclined screwed-in and glued-in reinforcements should be considered as very good.

5-1.6 ANGLES, LOAD LEVELS AND TYPES OF FAILURE AND ORDER OF APPEREANCE

Angles

Aicher and Höfflin [8], [11], [12] proved that the tensile stress perpendicular to the grain caused the most stress and cracks in the corners of the rectangular openings and at the angle of about 45° ± 90° measured from the beam length axis of the circular openings.

Aicher and Tapia [15] did some FEM investigations and identified the angle of 45° to the grain as the optimal angle for reinforcing circular openings in GLT beams.

In this case study the tensile stress perpendicular to the grain was as expected the first damage for all beams. These damages appeared on the upper left or lower right opening edge at the angles of 13 to 73°, instead the expected 45°.

Test series B was not reinforced, but the deflections of the expected 45° still were visible.

Series G and H also had angles that were mostly lower than 40° which was due to the internal inclined reinforcement.

It was noticeable that the angles of test series G were the smallest, which could be explained by the inclined screwed-in threaded rods under the angle of 40°.

Different angles for the initial crack appearance, as well as the spreading of the crack and shear failure position could be explained by different angles of the internal reinforcement as well as by the different grain prolongation, moisture content, density and faults in the beam production that were not visible.

Load levels

The representation of the load levels of initial crack appearance, crack propagation and load bearing capacity are presented and explained in the next section. Beside the representation of the obtained results, some of the most important, experimental results of the literature are compared with this case study.

Series A had no initial crack appearance or crack propagation load levels, therefore series A was excluded from those diagrams.

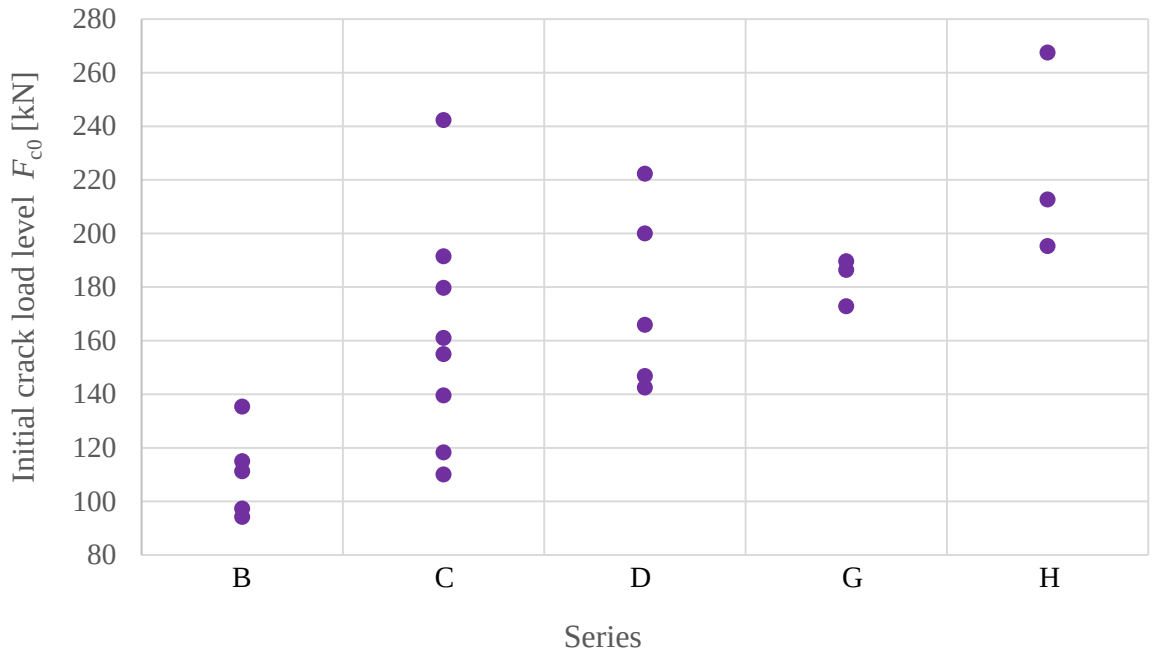

Figure 5.1: Scatter diagram of initial crack load level

Aicher and Höfflin [13] discussed and investigated internally reinforced beams, with vertical either self-tapped screws or threaded rods that were glued-in. The small, but still noticeable increase of crack initiation load level was about 27-41 % in comparison to unreinforced beams, which happened in this case study too.

The mean initial crack force of test series B, in comparison to the load bearing capacity of series A, was in range of 17 %, whereby for series C this percentage was a bit higher (25 %) for all test specimens (see figure 5.1).

The mean value of load level for test series D, that caused the first crack on the opening edge F_{c0}, was 175.51 kN. In comparison to the beams with unreinforced openings i.e. for test series B, this force was greater by 59 %. Test series D had a slight increase of the initial crack force with 27 % in comparison to

mean value of load bearing capacity of test series A, which was not much higher than series C, but showed some significant improvement in comparison to series B (see figure 5.1).

The mean value of load for test series G which caused the first crack on the opening edge F_{c0} was 162.18 kN. In comparison to initial crack load level of test series B, this force was greater by 47 %. Similar to test series D, test series G had an initial crack force percentage of about 28% in comparison to the load bearing capacity of series A. Therefore, the more precise implementation of the screws as well as the rearrangement of the inclination angle was not of too much help for this force level (see figure 5.1).

The mean load level for test series H, that caused the first crack on the opening edge F_{c0} was 337 kN. In comparison to the beams with unreinforced openings i.e. test series B this force was greater by 205 %. The initial crack force of series H was in range of 35 % of the mean load bearing capacity of test series A (see figure 5.1).

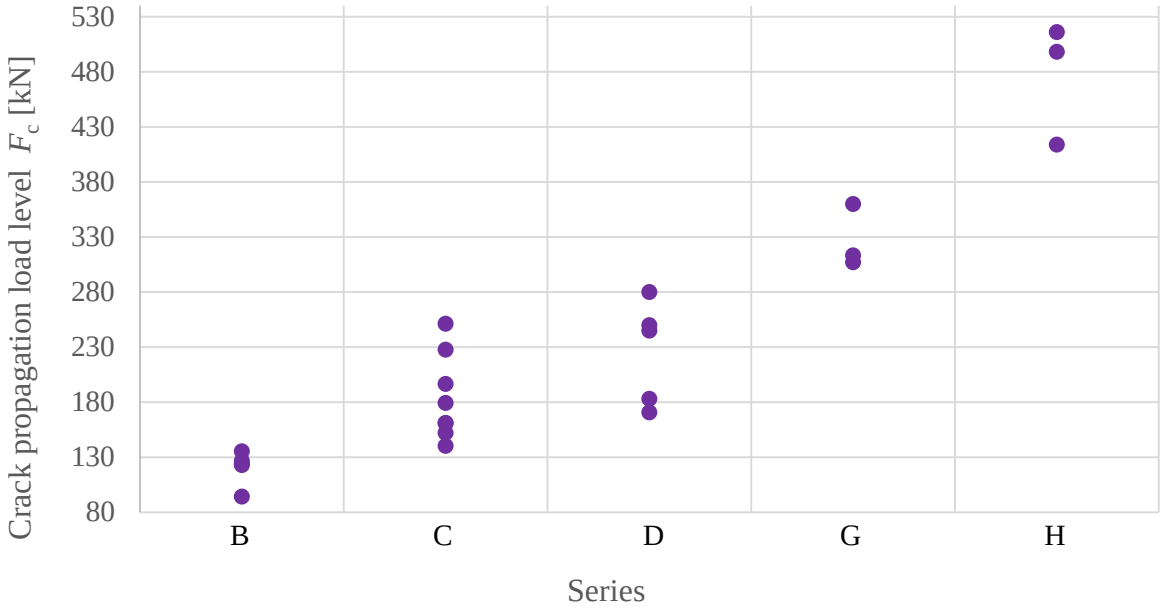

Figure 5.2: Scatter diagram of crack propagation load level

The propagation of the initial crack through the opening width for series B was almost at the same load level as for the initial crack load level which was about 18.6 % in comparison to load bearing capacity of test series A. For test series C this percentage was at about 28 %.

In the investigation of Aicher and Höfflin [13] a small but still significant increase of 38-49 % in comparison to the unreinforced beam showed the load level that lead to an initial crack through the opening width, which was the similar case in this case study, whereby an increase of the crack propagation force of series C compared to the unreinforced series B was greater by 52 % (see figure 5.2).

The mean value of load level responsible for the crack propagation through the opening width F_c for the test series D was 225.70 kN, which was greater by 95 % in comparison to the same load level of test series B. The initial crack propagation through the opening width force by the series D was 35 % of the load bearing capacity of test series A, which was also higher than for series B and C (see figure 5.2).

The mean value of load level responsible for the crack propagation through the opening width F_c for test series G was 326.70 kN, which was greater by 171 % in comparison to the same load of test series B (see figure 5.2).

The mean value of crack propagation load F_c of test series H was 476 kN, which was greater by 295 % in comparison to the same force at test series B. The force for the initial crack propagation through the beam opening width was at 74 % of the ultimate load bearing capacity of test series A (see figure 5.2).

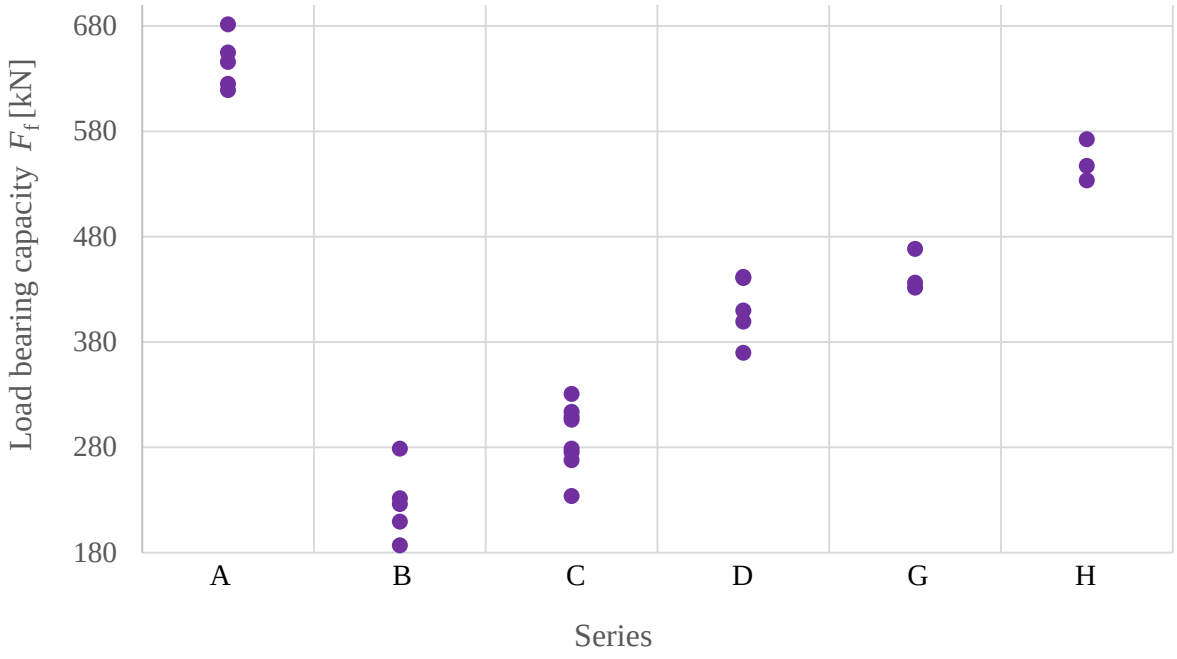

Figure 5.3: Scatter diagram of load bearing capacity

Aicher and Höfflin [13] had an increase of 55-64 % in comparison to the load bearing capacity of unreinforced beams, which was also noted by this case study in an increase of 53-60 %.

As expected for test series B, with an unreinforced opening, the smallest percentage of about 35 % of the mean load bearing capacity compared to the test series A was achieved, followed by test series C with the a percentage of 45.5 % (see figure 5.3).

Test series D, was the test series with inclined threaded rods under an angle of 45°, whereby not all of the threaded rods could be screwed in. The percentage of the load bearing capacity in comparison to test series A was about 65 % (see figure 5.3).

Test series G was the test series with screwed in threaded rods under the angle of 40°. This test series could be compared not only to the test series A where the bearing load was about 70 % of test series A, but also with test series D and H. In comparison to test series D the test series G could take over a bit more load. But in comparison to the test series H which could take over about 85 % of the load bearing capacity of test series A, test series D and G were to be considered as ones to be improved or to be used for smaller expected loads (see figure 5.3).

For the beams with unreinforced openings in [8], [11], [12], the load bearing was the smallest of all the tested specimens, as well as for test series B of this case study.

The differences in initial crack force, propagation of the crack force and load bearing capacity between series B and C were very small. Therefore, it should be reconsidered if the vertical internal reinforcement of the beams with opening should be included as a good reinforcement agent in new drafts of norms and standards.

The concept of experimental investigation of the ALP GSA® method from n'H neue Holzbau AG [44], in cooperation with Professor Gehri, was in accordance to test series H, whereby the shear strength was about 80-85 % of the shear strength for beams without opening. Series H was the series with loads closest to test series A which was due to the threaded rods glued-in the beams and their placement rearranged from 45° to 40°. After several tests it was assumed that the most impacted area was going to be covered better with a new arrangement of the threaded rods screwed-in or glued-in at an angle of 40°.

To sum up, it can be stated that the glued-in threaded rods under angle of 40° have the best abilities in comparison with a beam without opening, followed by screwed-in threaded rods under an angle of 40°, then screwed-in threaded rods under an angle of 45°. Unreinforced large openings as well as large openings with vertical internal reinforcements should be considered as not suitable ones.

In the test investigations by Aicher and Tapia in 2016 [15] several FEM tests showed that the opening should be further apart from the support area, because that area is the weakest one. The opening position was also influenced by the opening dimensions, as the opening gets bigger, it should be placed as far as possible away from the support. The opening diameter was enlarged to $0.5 \cdot h$, but all of the standards and regulations allowed the biggest opening diameter of $0.3 \cdot h$ for internally reinforced openings, therefore, the used calculations are for the $0.3 \cdot h$ and might not be directly applied to openings with a diameter of $0.5 \cdot h$.

Failure type and order of appearance

Kolb and Frech [34] did a research on beams with unreinforced rectangular and circular openings at midspan. These test series by [34] all failed on a bending failure beside experiencing cracks on tensile stress perpendicular to the grain around the opening. The other tested beams had one opening on each side of the beam, close to the supports. All these beams failed on the tension stress perpendicular to the grain and experienced the shear failure.

Aicher and Höfflin [8], [11], [12] proved that beams with unreinforced and reinforced opening were first experiencing cracks due to the tensile stress perpendicular to the grain on the opening edges, followed by the shear failure and in some cases also the bending failure of the beam, which was the exact development of the failures by all the tested beams in this case study.

All of the tested series experienced tension stress perpendicular to the grain, which eventually caused a shear failure of the beam, on the beam edge, closer to the opening.

The shear failure was the next expected failure of the beam, which happened, as already stated, in all of the cases.

All test specimen of test series D, G and H and test specimens C06, C07, C08 experienced a bending failure among other already listed failures. The bending failure happened only due to further loading after the first shear failure.

CHAPTER 6: CONCLUSION

The lab tests provided the carrying and deformation capacity in form of 6 series which in sum gives 29 test specimens.

The test series were divided into:

- A – GLT beams without openings (5 beams)
- B – GLT beams with round unreinforced openings (5 beams)
- C – internally reinforced GLT beams with vertical screws 2 x 12 x 500 mm on each opening side (8 beams)
- D – internally reinforced GLT beams with inclined screwed-in threaded rods with nominal diameter of 16 mm under the angle of 45°, 2 on each tension and compression side of the opening (5 beams)
- G – GLT beams with internally reinforced opening with inclined screwed-in threaded rods with the nominal diameter of 16 mm under the angle of 40°, 2 on each tensile side and with one threaded rod out of the nominal diameter of 20 mm on each compression side (3 beams)
- H – GLT beams with internally reinforced opening with inclined glued-in threaded rods of the nominal diameter of 16 mm under the angle of 40°, 2 on each tensile side and with one threaded rod out of the nominal diameter of 20 mm on each compression side (3 beams)

Out of the test records that were made during the testing process, with filmed videos and calculated values it was possible to get the precise sequence of events.

The calculations were done after testing sessions were finished with the help of the results obtained from the testing machine. Some important results obtained are listed as follows:

- Moisture content: u = 11.51 % (mean value of all 6 test series)
- Density: ρ_{12} = 510.0 kg/m^3 (mean value of all 6 test series)
- Shear modulus: G_{12} = 734.0 N/mm^2 of test series A
- Shear strength: $f_{v,12}$ = 4.91 N/mm^2 of the test series A
- Shear strength: $f_{v,12}$ = 2.97 N/mm^2 mean value of other five test series

Test series B, an unreinforced reference, reached 35 % of the mean load bearing capacity of series A. Test series C could be loaded more than test series B, but the difference was small. The placement of the self-tapped screws or threaded rods as vertical reinforcement should be done as precise as possible in order to get the most out of this type of reinforcement.

Due to very small load bearing capacities of beams with unreinforced opening and a brittle failure there is a question if they should be even considered as allowed in norms and standards anymore.
Due to the low bearing capacity of the vertically reinforced beams, it should be rethought whether these reinforcing methods should be taken into consideration when it comes to solving a problem with glulam beams with large round openings.

Test series D and G should have reached a load bearing capacity close to the ultimate shear load of test series A, which in mean was 646 kN, but they did not. Test series D and G had 63% and 71 % of load bearing capacity of series A, respectively.

The test results showed that the precision of the introduction of the inclined threaded rods is very important. As the threaded rods were placed more precisely around the opening, the ultimate shear force was higher.

Test series H had the closest load bearing capacity to the series A, which was about 85 %.

Alternative ways of reinforcing the opening of GLT beams were shown with test series D, G and H which had inclined threaded rods screwed-in or glued-in under an angle of 45° or 40°. They should be considered as a new possible solution for the reinforcement of GLT beams with opening due to their high effectiveness.

New alternative ways of reinforcement are still not listed in any norm or standard known.

The completion of the holes for the threaded rods or glued-in rods might be challenging due to the angle of 40° and 45°, timber strength and faults in timber structure which premise a drilling rig with high precision to guarantee a good insertion with small spacing between the threaded rods and also opening edge.

As it was noted, the angle of 40° was more suitable for the inclined threaded rods and glued-in rods as internal reinforcement of the opening in the GLT beams due to the better coverage of the shear forces appearing in the opening region.

The glued-in rods have even better load bearing capacity in comparison to the screwed-in threaded rods, due to the glueline strength between threaded rod and timber as well as the higher stiffness of the reinforcement.

Unfortunately, none of the tested specimens had achieved the ultimate shear load of the reference test series A. Precalculations were made according to the norms and standards that regulate GLT beam opening diameter with $h_d \leq 0.4 \cdot h$, which in this master thesis, and for this case study was not present.

Even though the opening diameter were enlarged to $h_d = 0.5 \cdot h$ the beams still had good load bearing capacities, therefore permission to enlarge openings diameter should be taken into consideration in new drafts of standards and norms.

APPENDIX A INDEX

A-1 Literature

[1] Stojić, D.: Drvene konstrukcije i skele (in Serbian), Univerzitet u Nišu, Građevinski fakultet Niš, Srbija, 1996

[2] Gojković, M; Stojić, D.: Drvene konstrukcije (in Serbian), Građevinski fakultet u Beogradu, Srbija, 1999

[3] Muravljov, M; Stevanović, B.: Zidane i drvene konstrukcije zgrada (in Serbian), Građevinski fakultet u Beogradu, Srbija, 1999

[4] Aicher, S., Höfflin, L.: Glulam beams with round holes - A comparison of different design approaches VS. test data, CIB-W18/35-12-1, Otto-Graf-Institute, Stuttgart, Germany, 2002

[5] Aicher, S., Höfflin, L.: Fracture behavior and design of glulam beams with round holes, MPA University of Stuttgart, Germany, 2008

[6] Aicher, S., Höfflin, L.: Runde Durchbrüche in Biegeträgern aus Brettschichtholz Teil 2: Tragfähigkeit und Bemessung, Bautechnik 84 (2007), Heft 12 (in German), Berlin, Germany, 2007

[7] Aicher, S., Höfflin, L.: New Design Model for Round Holes in Glulam Beams. WCTE 2004, Lahti, Finland, 2004

[8] Aicher, S.; Höfflin, L.: A contribution to the analysis of glulam beam with round holes, Otto-Graf-Journal Vol. 11, Stuttgart, Germany, 2000

[9] Aicher, S., Tapia, C.: Glulam beams with internally and externally reinforced holes – tests, detailing and design, CIB-W18/44-12-4, MPA University Stuttgart, Germany, 2011

[10] Aicher, S., Tapia, C.: Glulam with laterally reinforced rectangular holes. WCTE 2012, Auckland, New Zeeland, 2012

[11] Aicher, S., Höfflin, L.: Runde Durchbrüche in Biegeträgern aus Brettschichtholz, Teil 1: Berechnung, Bautechnik 78 (2001), Heft 10 (in German), Stuttagrt Germany, 2001

[12] Aicher, S., Höfflin, L.: Weibull based design approach of round holes in glulam, Otto-Graf-Institute, Stuttgart, Germany, 2003

[13] Aicher, S., Höfflin, L.: Glulam Beams with Holes Reinforced by Steel Bars, CIB-W18/ 42-12-1, Dübendorf, Switzerland, 2009

[14] Aicher, S., Tapia, C.: Rechnerische Untersuchungen zu Mindestabstände von Durchbrüchen in Brettschichtholz (in German), ResearchGate, Stuttgart Germany, March 2016

[15] Aicher, S., Tapia, C.: Holes in glulam – Orientation and design of internal reinforcement, WCTE 2016, Vienna, Austria, 2016

[16] ON EN 1995-1-1: Design of timber structures – Part 1- 1: General - Common rules and rules for buildings, European Committee for Standardization (CEN), Brussels, 2008-06

[17] DIN 1052: Entwurf, Berechnung und Bemessung von Holzbauwerken – Allgemeine Bemessungsregeln und Bemessungsregeln für den Hochbau (in German), Deutsches Institut für Normung, 2004-08

[18] SIA265: Holzbau. Schweizer Norm SN 505 265, Schweizerischer Ingenieur- und Architektenverein (in German), Zurich, 2012-01-01

[19] ON B 1995-1-1: Bemessung und Konstruktion von Holzbauten – Teil 1-1: Allgemeines – Allgemeine Regeln und Regeln für den Hochbau (in German), Österreichisches Normungsinstitut, 2015-06-15

[20] ON B 1995-1-1: Bemessung und Konstruktion von Holzbauten – Teil 1-1: Allgemeines – Allgemeine Regeln und Regeln für den Hochbau (in German), Österreichisches Normungsinstitut, 2014-11-15

[21] ON B 1995-1-1: Bemessung und Konstruktion von Holzbauten – Teil 1-1: Allgemeines – Allgemeine Regeln und Regeln für den Hochbau (in German), Österreichisches Normungsinstitut, 2010-08-15

[22] DIN EN 1995-1-1/NA: Nationaler Anhang – National festgelegte Parameter –Bemessung und Konstruktion von Holzbauten – Teil 1-1: Allgemeines – Allgemeine Regeln und Regeln für den Hochbau (in German), Deutsches Institut für Normung, 2010-12

[23] DIN 1052: Entwurf, Berechnung und Bemessung von Holzbauwerken – Allgemeine Bemessungsregeln und Bemessungsregeln für den Hochbau (in German), Deutsches Institut für Normung, 2008-12

[24] enBR: Holzbauwerke – Entwurf, Berechnung und Bemessung. Bearbeitung durch: Krenn, H., Meinhardt, G., Schickhofer, G., holz.bau forschungs gmbh (in German), Graz, Austria, 2007-04

[25] Limträhandbok Glulam Handbook, origin: www.svensktlimtra.se, date of access: 09. May 2016, Olle Carling Ingenjörsbyrå AB, Svenskt Limträ AB, 2003

[26] prEN 1995-1-1: Design of timber structures – General rules and rules for buildings. Final Draft, European Committee for Standardization (CEN), 2002-10-09

[27] Larsen, H.J.: Essay 3.1 – Stresses around holes in beams. CIB_W18 Timber Structures – A review of meeting 1-43 – Part 3: Structures and structural member, Alghero, Italy, 2011

[28] Dröscher, J., Schickhofer, G., Augustin, M.: Durchbrüche in Tragstrukturen aus BSH und BSP (in German), Technische Universität Graz, Austria, 2016

[29] Harzer Statik Softwer, origin: http://www.harzerstatik.de/index.php/programmeadmin/allgemein/durchbruch-holz, date of access: 2016-07-31

[30] Danielsson, H.: The strength of glulam beams with holes; A Probabilistic Fracture Mechanics Method and Experimental Tests, Lund University, Sweden, 2009

[31] Kolb, H., Epple, A.: Verstärkung von durchbrochenen Brettschichtholzbindern. Report, Research Project I.4 – 34810, Research and Materials Testing Institute Baden-Württemberg (in German) Otto-Graf-Institute, Stuttgart, 1985

[32] Dietsch, P.: Einsatz und Berechnung von Schubverstärkungen für Brettschichtholzbauteile (in German), Technishe Universität München, München, Germany, 2005

[33] prEN 1995-1-1: Design of timber structures - Part 1-1: General - Common rules and rules for buildings, European Committee for Standardization (CEN), Brussels, 2003-12

[34] Kolb, H., Frech, P.: Untersuchungen an durchbrochenen Binder aus Brettschichtholz, Report (in German) Otto-Graf-Institute, Stuttgart, 1977

[35] DIN 1052: Design of timber structures. General rules and rules for building. draft 2000-05, Beuth Verlag Berlin, 2000-05

[36] Danielsson, H., Gustafsson P.J.: The strength of glulam beams with holes test of quadratic holes and literature test results compilation, CIB-W18/41-12-4, Lund University, Sweden, 2008

[37] Jeleč, M., Varevac, D., Zovkić, J.: Gulam beams with holes, University of Osijek, Osijek, Hrvatska, 2014

[38] ON EN 13986: Holzwerkstoffe zur Verwendung im Bauwesen -Eigenschaften, Bewertung der Konformität und Kennzeichnung (in German), Österreichisches Normungsinstitut, 2005-04-01

[39] ON EN 636: Sperrholz - Anforderungen (in German), Österreichisches Normungsinstitut, 2012-11-01

[40] ON EN 14374: Holzbauwerke – Furnierschichtholz für tragnede Zwecke – Anforderungen (in German), Österreichisches Normungsinstitut, 2005-02-01

[41] Steiger, R.: In Brettschichtholz eingeklebte Gewindestangen – Stand des Wissens zu einer leistungsfähigen Verbindungstechnik, 18. Internationales Holzbau-Forum IHF (in German), Garmisch-Partenkirchen, Germany 2012

[42] DIN 1052: Bemessung und Konstruktion von Holzbauten – Teil 1-1: Allgemeines – Allgemeine Regeln und Regeln für den Hochbau, (in German), Deutsches Institut für Normung, 2013-08

[43] Z-9.1-778 2K-EP-Klebstoff GSA-Harz und GSA-Härter für das Einkleben von Stahlstäben in Holzbaustoffe. Allgemeine Bauaufsichtliche Zulassung, Antragsteller: neue Holzbau AG, Geltungsdauer: 31.10.2012 – 31.10.2017 (in German), Deutsches Institut für Bautechnik DIBt, 2012-10-31

[44] Strahm, T.: Lastpfad-Anordnung eingeklebter Stahl-Stangen bei Durchbrüchen im Holzbau. 19. Internationales Holzbau-Forum IHF (in German), Garmisch-Partenkirchen, Germany, 2013

[45] EN 1194 Holzbauwerke – Brettschichtholz – Festigkeitsklassen und Bestimmung charakteristischer Werte (in German), Österreichisches Normungsinstitut, 1999-09-01

[46] EN 14080: Holzbauwerke – Brettschichtholz und Balkneschichtholz – Anforderungen (in German), Österreichisches Normungsinstitut, 2013-08-01

[47] Gehri, E.: Shear Problems in Timber Engineering – Analysis and Solutions. WCTE 2010, Riva del Garda, Italy, 2010

[48] Flaig, M.: Biegeträger aus Brettsperrholz bei Beanspruchung in Plattenebene; Band 26 der Reihe Karlsruher Berichte zum Ingenieurholzbau; Dissertation (in German), Fakultät für Bauingenieur-, Geo- und Umweltwissenschaften, Karlsruher Institut für Technologie, Germany, 2013

[49] Blaß, H.J., Flaig, M.: Stabförmige Bauteile aus Brettsperrholz, Karlsruher Berichte zum Ingenieurholzbau, Lehrstuhl für Ingenieurholzbau und Baukonstruktionen (in German), Karlsruher Institut für Technologie (KIT), Germany, 2012

[50] Hoffmann, K.: Applying the Wheatstone Bridge Circuit, HBM, W1569-1.0en, Darmstadt, Germany, 2012

[51] ETA-11/0190 Würth Schrauben. Inhaber: Adolf Würth GmbH & Co. KG, Geltungsdauer: 27.06.2013 – 27.06.2018 (in German), Deutsches Institut für Bautechnik (DIBt), 2013-06-27

[52] Brandner, R., Gettering, W., Schickhofer, G.: Determination of shear strength of structural and glued laminated timber. Präsentation, CIB-W18, Vaxjö, Sweden, 2012

[53] Z-9.1-777 SFS intec GmbH Gewindestangen mit Holzgewinde als Holzverbindungsmittel. Allgemeine Bauaufsichtliche Zulassung, Antragsteller: neue Holzbau AG, Geltungsdauer: 01.12.2015 – 01.12.2020 (in German), Deutsches Institut für Bautechnik DIBt, 2015-11-30

[54] Krapfenbauer T.: Bautabellen, 18. Ausgabe (in German), Wien, Austria, May 2011

[55] EN 13183-1: Feuchtegehalt eines Stückes Schnittholz; Teil 1: Bestimmung durch Darrverfahren (EN13183-1:2002 + AC:2003) (in German), Österreichisches Normungsinstitut, 2004-02-01

[56] EN 384: Bauholz für tragende Zwecke – Bestimmung chrakteristischer Werte für mechanische Eigenschaften und Rohdichte (in German), 2015-11-30

[57] Neuhaus, F.-H.: Elastizitätszahlen von Fichtenholz in Abhängigkeit von der Holzfeuchtigkeit. Dissertation, Institut für Konstruktiven Ingenieurbau (in German), Ruhr-Universität Bochum, Germany, 1981

[58] ÖNORM EN 408: Holzbauwerke- Bauholz für tragende Zwecke und Brettschichtholz – Bestimmung einiger physikalischer und mechanischer Eigenschaften (in German), Österreichisches Normungsinstitut, 2012-09-01

A-2 List of figures

A-3 List of tables

APPENDIX B OTHER APPENDICES

B-1 Series descriptions

1 Series A

Series A01

Taking off the displacement transducers was set at 50 % of the pre calculated load capacity for series A, which was 224 kN. Until that point beam was not damaged.

At a load of 654.56 kN, the test specimen experienced a serrated shear failure at a bit more than the half height of the beam and spread to about half length of the beam. This was measured from the top edge of the beam on the left side. After the shear failure had occurred, the force dropped at about half of the maximum shear force value. After the first shear failure, the beam was not loaded any further.

There is a visible damage caused by tensile force in the area under the load application on the front side of the beam (see figure B.1).

Figure B.1: Influence of the tensile force on the beam front side

Specimen A02

After testing the first specimen, it was obvious that the pre calculated maximal bearing load was too low. It was undervalued for about 1 / 3, so the hysteresis was adjusted to fit the real load bearing abilities of the beams. The 50 % of the bearing load now was set at 280 kN when the displacement transducers were removed. At this load level, no damages have taken place on the beam. The beam was damaged by shear failure at the left support by the load of 619.13 kN and the load dropped to the 40 % of the maximum value. The shear failure extends to the half of the length of the beam. After a few seconds, the load application was stopped and no further load was applied to the test specimen A02. The shear failure happened closer to the left support, in a serrated form, at half of the beam height.

Specimen A03

The beam was loaded the same way as the specimen A02 and has not experienced any damages until the point of removing the displacement transducers.

Two shear failures occurred simultaneously. The first one at about 200 mm from top edge of the beam. The second one at about 500 mm from the top beam edge. Both of them happened on the left part of the beam at the load of 625.04 kN, which dropped to about 58 % of the maximum bearing load after shear failure and was not increased anymore. The shear failures extended up to about half the length of the specimen and both of them followed the line of the tree rings.

An influence of the tension force was visible on the left from the load application on the front side.

Specimen A04

Up to the load of 681.69 kN, which was the highest load achieved for all of the test specimens, nothing occurred. At that point beam failed on shear failure on the left part of it, at height of 1 / 3 of the beam height measured from the top edge of the test specimen A04 and cracked along the line of the tree rings (see figure B.2). The beam was not loaded any further after the force dropped to about 67 % of the shear failure force.

Figure B.2: Shear failure at the left end of specimen A04

Specimen A05

As for all previous specimens of series A, no damages on the beam occurred until the shear failure. In case of specimen A05, it occurred at a load of 645.86 kN, which was the mean value for test series A, closer to the right support of the beam. The force dropped to 62 % of the maximum force after shear failure which followed the tree ring lines a bit below the half of the beam height.

There was visible influence of the tensile force at about 300 mm from the right support on the beam front side, similar as shown in figure B.1.

2 Series B

Specimen B01

The act of taking off the displacement transducers was set at the 50 % of the calculated load capacity for series B, which was 90 kN. Until that point the beam was not damaged.

At the load of 136.23 kN, the specimen experienced a tensile stress perpendicular to the grain damage simultaneously on the upper left opening edge at 163 mm (the initial angle α 24°) from top edge of the beam and on the lower right side by the height of the 393 mm (the initial angle α 52°). This crack was the same for the shear failure and measured from the top edge of the beam. By increasing the load one more crack appeared above from the initial upper left crack. By the force of 231.74 kN the beam experiences serrated shear failure on the right support by which the force dropped on the level of 56 % of the maximum bearing load. The beam was not loaded any further after the first shear failure occurred.

The lower right crack went straight through the beam width, but on the top left side went aslant but not through the tree rings line.

Specimen B02

After testing the first specimen, it was obvious that the calculated maximal bearing load was underestimated so the hysteresis was adjusted to fit the real load bearing abilities of the beams. The 50 % of the bearing load now was set at 100 kN when the displacement transducers were taken off. At this load, still, no damages had taken place on the beam. At 113 kN there was some visible dust on the upper left side of the opening, but there were no visible cracks. The beam was damaged by tensile stress perpendicular to the grain on the front beam side which instantly spread through the opening width at the angle of 32° and the force dropped for a few kilonewtons. After that, by increasing the load, the lower right edge of the opening experienced a crack caused by tensile stress perpendicular to the grain while the upper one spread towards the beam mid-span. The upper left crack spread almost straight through the opening width and the lower right break on the tree rings line (see figure B.3). The shear failure was in serrated form on the right edge and was followed by a bending failure of the net cross section closer to the load application area which happened at the load of 278.83 kN and led to a load drop of about 33 %. After these failures no further load was applied.

Figure B.3: Tensile stress perpendicular to the grain on the upper left and lower right opening edge of the specimen B02

Specimen B03

Test specimen B03 experienced cracking which spread through the whole opening width instantly on the upper left opening edge before taking off the displacement transducers. The crack opened on the back side of the beam. For this test specimen, 50 % of the load application was, again, adjusted according to the previous two test specimens and set at the value of 150 kN. While removing the displacement transducers, the lower right opening edge also cracked due to tensile stress perpendicular to the grain and spread immediately through the width of the opening. Until the test had been conducted the upper left and lower right cracks spread lengthwise and became wider.

The shear failure occurred at a load of 209.49 kN by an extending of the lower right crack to the right support. After shear failure, the force dropped to 57 % and was not increased anymore. The place of the tensile crack for the lower right edge of the opening, which cracked through the tree rings line, was at about 2 / 3 of the beam height measured from the top edge of the beam. The upper left crack spread in a serrated manner through the opening width.

Specimen B04

As for specimen B03, B04 was showing signs of damage at the force of 150 kN, which was set as 50 % of the load bearing capacity, and the load point for taking the displacement transducers off of the beam. A first crack happened on the lower right edge at the mid width of the opening. This crack spread to the front and back side of the beam simultaneously by 124.03 kN of load at the angle of 48° and 41° for front and back side respectively, which falls by 1 kN after the crack appeared. After that opening cracked, on the upper left edge, one more crack appeared. After those two cracks appeared, the displacement transducers were taken off. By further load application, the upper left crack spread

lengthwise in direction of the load application area. Afterwards, by loading the beam further, both cracks were spreading lengthwise and were getting wider until the shear failure occurred, caused by the lower right crack spreading through the right support and to the end of the beam by 223.78 kN force. This force falls to 71 % of the maximum shear force value after the shear failure. The shear failure was at the height at about 2 / 3 of the beam height measured from the top edge of the beam and followed the tree rings line. The lower right crack had a cogged pattern and followed the tree ring lines, but the top cracks spread almost straight through the opening width at the height of about 1 / 3 of the beam height from the top edge of the beam.

Specimen B05

This test specimen was special, because the first crack already appeared on the upper left front part of the opening edge at 94.22 kN at an angle of 42°, at the height of 190 mm measured from the top edge of the beam, and almost immediately spread almost straight through the opening width to the angle of 32°. The force dropped to 91.97 kN. After that, the displacement transducers were taken off, in order to do not damage them. This was followed by cracking on tensile stress perpendicular to the grain, on the lower right edge of the opening. The crack spread almost straight through the width of the opening at the load of 134.01 kN, which then dropped to 128.95 kN. The shear failure also occurred at an early stage of only 187.34 kN, at an angle of 42° by which the force dropped to the 105.57 kN (56 % of the maximum shear force). The shear failure happened at 380 mm from the top edge of the beam, and extended to the right support along the tree ring lines (see figure B.4).

Figure B.4: Shear failure on the right edge of the beam of specimen B05

3 Series C

Specimen C01

Before the displacement transducers were removed, the first crack propagation appeared on the upper left opening edge at 26 % of the beam height, which spread instantly through the opening width to the same height. Then, following the act of removing the displacement transducers at 160 kN, the lower right opening edge cracked next, followed by the shear failure on the right lower edge, which occurred at the force of 330.81 kN. This shear failure followed the flow of the tree rings. The force dropped to 58 % of the maximum shear load. The beam was not loaded any further after this shear failure occurred. Near the shear failure an additional crack occurred above the first initial upper left crack. The shear failure had a leap from one to another layer of the glulam beam (see figure B.5 left).

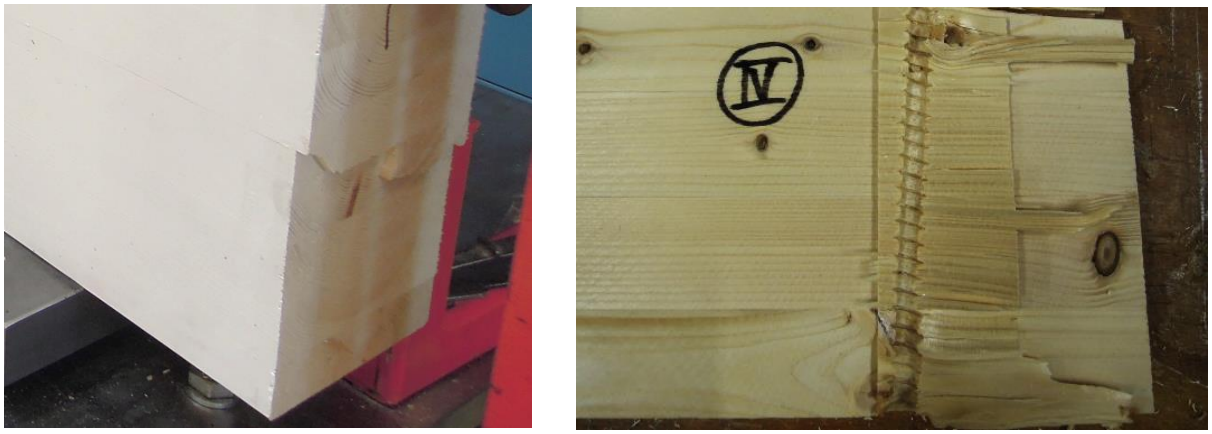

Figure B.5: Shear failure on the right edge (left); screw hole (right) of specimen C01

The screw holes did not show any disturbance on the force application as no pull through effects of the screws were seen. A misalignment of the screw holes was identified (see picture B.5 right).

Specimen C02

Before the displacement transducers were removed no crack occurred. The first crack happened on the lower right opening edge and spread immediately from the front side to the back. Shortly after the first crack, the second crack on the upper left edge of the opening happened.

The shear failure happened on the right edge of the beam at the 2 / 3 of the beam height, and followed the tree ring lines. The load at the shear failure was 232.22 kN dropped to 60 % after the failure and was not raised any further.

The crack on the upper left edge of the opening first developed straight through the beam width from the front to one fourth of the width, then dropped to the midpoint and from there to the back side along the rings line flow (see figure B.6 left). The lower right crack from the front to the midpoint was almost straight in the first two thirds of the width and long the tree ring line for the last third (see figure B.6 right).

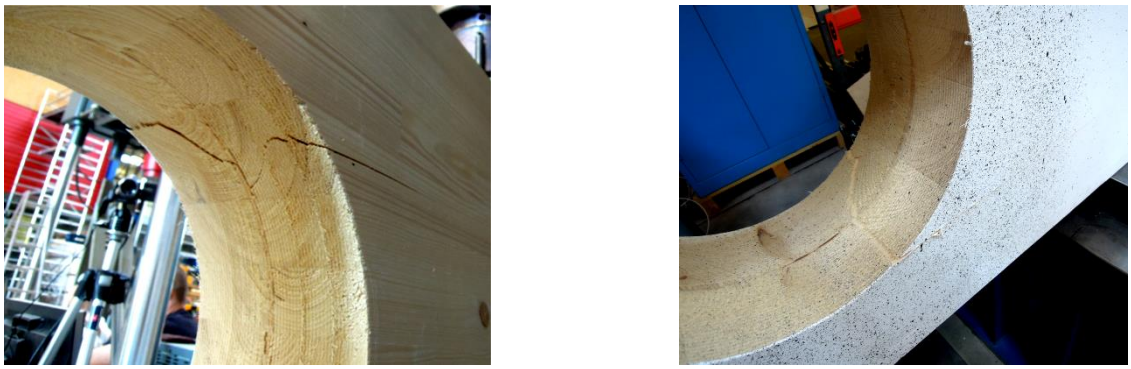

Figure B.6: Cracks due to tensile stress perpendicular to the grain on the upper left opening edge (left) and on the lower right opening edge (right) for specimen C02

No visible changes provoked by the applied axial load could be seen in the screw holes of the vertical reinforcement of the opening.

Specimen C03

At the point of removing the displacement transducers, a first crack, which followed the ring lines, appeared on the upper left opening edge and spread through the opening width. After that, a second crack happened and spread from the front to the back side on the lower right opening edge. At the force of 205.41 kN the cracks were spreading even further along the grain. Furthermore, one more crack above the initial upper left crack appeared also and spread through the opening width following the tree rings. At the same time, one more crack opened under the lower right initial crack. The shear failure occurred on the right beam edge, at the force of 275.26 kN and at 72 % of the beam height. This shear failure did not follow the tree rings and was slightly toothed. After the shear failure, the beam was not loaded any further and the force dropped to the value of 57 % of the maximum applied load.

Screw holes were intact for all of the screws for the vertical reinforcement.

Specimen C04

The first crack appeared on the upper left edge of the opening. After the displacement transducers were removed, at a load level of 212.14 kN, the crack spread almost straight from the front to back side. The second crack appeared on the lower right opening edge and spread to the front side, following the tree rings line as the force was increased. The shear failure occurred at 267.83 kN and the force dropped to 57 % of the maximum load, whereby no further load was applied onto the beam. The shear failure followed the rings partially.

There were no changes or damages in all of the screw holes.

Specimen C05

Specimen C05 had no cracks whatsoever until the displacement transducers were removed. A first crack appeared on the upper left opening edge and spread immediately from the front side to the back side, at the force of 227.68 kN. A second crack happened on the lower right opening edge shortly after the first one. By increasing the load, one more crack opened above the initial upper left crack.

The upper left initial crack did not follow the tree ring lines. It had one fall and one jump through the opening width (see figure B.7 left). The lower right one was straight (see figure B.7 right) and the shear failure followed the tree ring lines.

Figure B.7: Crack due to tensile stress perpendicular to the grain on the upper left opening edge (left) and on the lower right opening edge (right) of specimen C05

As for the previous four specimens there were no changes in any of the screw holes used for the vertical reinforcement.

Specimen C06

The displacement transducers were still not removed, as the first crack on the lower right opening edge appeared, spreading from the front side and through the opening width unevenly to the back side. A second crack appeared on the upper left edge of the opening. The shear failure appeared at the force of 313.71 kN, whereby the force dropped at the level of 59 % of the shear failure force. The shear failure appeared at the height of the first initial crack on the lower right edge of the opening. Furthermore, at the force of 326.93 kN, the next shear failure happened, whereby the force dropped to 85 %. At the same force, an additional crack appeared under the initial lower right crack. Moreover, a bending failure also occurred in the net cross section. The influence of the tensile force was visible on the front beam side.

In total, the beam experienced four shear failures, where 2 upper ones were following the tree ring lines flow and two lower ones were serrated (see figure B.8 left). Bending failure spread from the beam back and front side to the bottom side of the beam (see figure B.8 right). Also, there was a visible bending failure at the bottom side of the beam in the load application area.

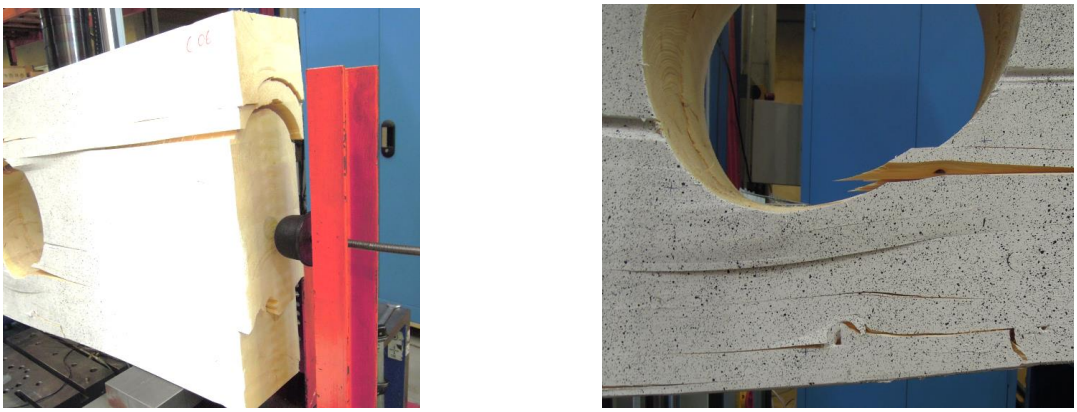

Figure B.8: Tensile stress perpendicular to the grain and four shear failures (left); bending failure in the net cross section under the opening (right) of specimen C06

After the first shear failure appeared, the screws were pulled in the beam, which could be seen in the screw holes (see figure B.9 left). The screws were also bent in areas where the beam was cracked (see figure B.9 right).

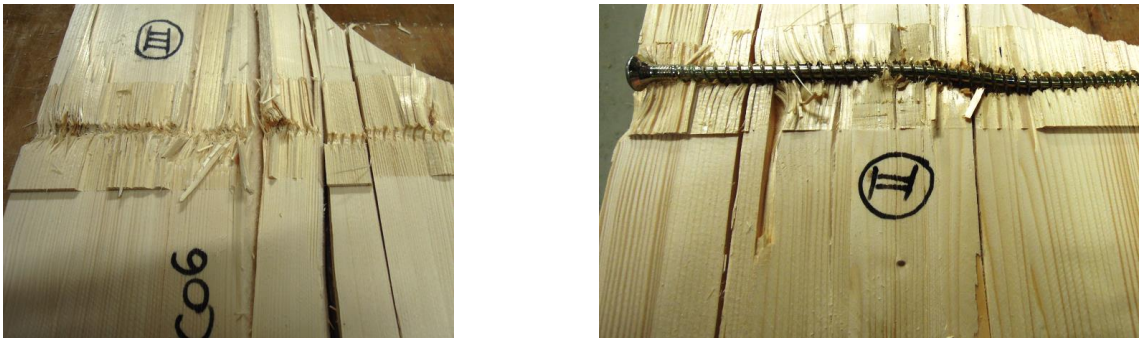

Figure B.9: Damaged screw hole by pull through effect of the screws (left) and bended screw (right) of specimen C06

Specimen C07

After removing the displacement transducers, a first crack appeared at the lower right edge of the opening and spread through the tree ring lines immediately across the opening width, at the load level of 179.72 kN. A second crack occurred on the upper left edge of the opening, at the load level of 247.95 kN and spread through the tree ring lines widthwise.

The first shear failure appeared at a load level of 308.98 kN on the beam right edge. The drop in force was 53 % of the overall bearing load. The beam was further loaded after this failure.

A bending failure at net cross section of the beam happened at 270 kN, while a crack appeared simultaneously above the first upper left crack. After that, below the initial lower right crack, the beam got one more crack followed by the bending failure in gross cross section close to the load application (see figure B.10).

Figure B.10: Bending failure on the bottom side of the beam under the load application area of specimen C07

As a result of further load application, the screws were pulled into the beam, which was the same for the previous specimen. The screw holes appeared similar to the one of test specimen C06 and showed signs of the pull through effects similar to smudging the edges of the threads into the timber.

Specimen C08

The first crack appeared on the lower right opening edge at the load of 251.25 kN. This crack first appeared on the front side of the beam and spread straight to the mid width of the opening and followed the tree ring lines from the midpoint to the back side.

The second crack spread instantly through the width opening, at the load of 257.49 kN.

The first shear failure appeared on the right beam edge at the force of 306.28 kN and followed the tree ring line. The force dropped for 7 kN and load was further applied, which caused the initial upper left crack to spread in stepped manner in the up left direction at the force of 305.56 kN (see figure B.11 left).

Figure B.11: Stepped propagation of the upper left crack on the opening on the beam front side (left); finger joints failure mixed with the bending failure in the gross cross section (right) of specimen C08

A bending failure at the net cross section followed and the force dropped to the 254 kN. Force was further raised to 319 kN.

The finger joints failed on the bottom side of the beam below the load application (see figure B.11 right).

As a result of the further load application, the screws for the opening reinforcement on the booth opening sides were pulled into the beam as it was the case for the previous two specimens (see figure B.12 left). The screw holes appeared similar to the ones of the test specimens C06 and C07 by smudging the edges of the threads of the screws into timber (see figure B.12 right).

Figure B.12: The screws which were pulled into the beam after finished testing (left); part of the damaged screw hole by pull through effect of the screws (right)

4 Series D

Specimen D01

The test specimen D01 was reinforced with internal reinforcement in the shape of four threaded rods inclined under the angle of 45° around the opening in the tension zone. On both tension sides, all four were screwed in their maximum length of 600 mm. On both compression sides, in total of 4 threaded rods, were only screwed-in in length of 400 mm because of the fault in crossing of the predrilled holes.

During the pause in the load application, while the displacement transducers were taken off of the beam, the first crack appeared by the force of 250 kN, due to the tensile stress perpendicular to the grain. Shear force induced stress perpendicular to the grain on the upper left edge of the opening and on the lower down edge of the opening, on the front side of the beam and instantly spread through the opening width on the lower right edge of the opening to the back side, whereby the force dropped to the value of 243 kN (see figure B.13).

Figure B.13: Tensile stress perpendicular to the grain cracks on the upper left and lower right opening edge of specimen D01

On the upper left side, the crack spread in wave form through the opening width and additionally cracked through the opening in vertical direction (see figure B.14 left) while on the lower right side the crack developed along the tree rings (see figure B.14 right).

Figure B.14: Spreading of the crack through the opening vicinity on the upper left side (left) and lower right side (right) of specimen D01

By applying further load, the first shear failure occurred on the right edge, at the force of 399.42 kN. This shear failure spread in a serrated manner through the beam side (see figure B.15 left). After the shear failure occurred, the force dropped to 80 % of the shear force failure force.

Figure B.15: Serrated shear failure on the right beam edge (left); the initial cracks on the lower right and upper left edge of the opening with additional crack and bending failure in the net cross section (right) of specimen D01

Load was further applied until load level of 357.69 kN whereby the beam cracked below the lower right crack which caused the force to drop on the value of 321.90 kN (see figure B.15 right).

The bending failure occurred in net cross section below the opening on the beam front side at the force of 353 kN (see figure B.15 left) This was also to be seen on the beam bottom side around the threaded rods (see figure B.16 left).

Figure B.16: Bending failure on the bottom side of the beam (left); threaded rod in the hole and pull through effect on the timber inside of the hole (right) of test specimen D01

The threaded rods were recessed into the beam. The pull through effect could be seen around the holes of the threaded rods in tension zones due to the fact that the cracking of the beam disabled the distribution of the shear force in timber, therefore, the rods took over the part of the bearing agent (see figure B.16 right).

The threaded rods holes had slight deviations and visible pull through effect in tension zone on both beam sides. On the tension side, closer to the load application area, in the upper part and in the tension zone, closer to the support in the lower part of threaded rods.

Specimen D02

The test specimen D02 was reinforced with two inclined threaded rods under the angle of 45° on the each tensile sides of the opening. In the compression zones, there were no reinforcements even though the holes were predrilled by the manufacturer.

At the force of 200 kN, on the upper left side of the opening from the back side of the beam, the first crack appeared at the force of 245 kN and spread through the opening width to the front side in almost straight line.

On the back side of the opening edge on the lower right side, by the force of 250 kN, the second crack appeared and spread in a serrated manner through the beam width to the front side of the beam after reaching the force of 290 kN.

The first shear failure at 423 mm from the top edge (angle of 35°). followed the tree rings line and was caused at the load level of 395.79 kN, which then dropped to 346.79 kN.

Further load was applied onto the beam and at the force of 440.77 kN the bending failure in the net cross section took place and made the force to drop to the value of 383.82 kN. Bending failure was also visible on the bottom beam side around the threaded rod holes.

By further load application, the initial cracks spread further length and widthwise.

As for the test specimen D01, the influences of the tension force on the beam sides were also visible (see figure B.17).

The first two initial cracks, the bending failure and the influence of the tensile force of the test specimen D02 are shown in figure B.17.

Figure B.17: Tensile stress perpendicular to the grain cracks on the upper left and lower right opening edge and bending crack of specimen D01

As for the previous specimen, test specimen D02 showed the pull through effect of the steel rods, too.

The holes for threaded rods in tension zone, in the front and back beam region experienced the pull through effect, as by the test series D01.

The threaded rods hole was slightly deviated in tension zone, on the back side, in the support area.

Specimen D03

Specimen D03 was reinforced as the specimen D02 which is: two inclined threaded rods screwed in under the angle of 45^{o} on each tensile side of the opening and no threaded rods in the compression zones.

At the time when the first crack occurred on the lower right opening edge at the force of 160.06 kN and spread in a serrated manner, from the back to the front side of the beam, the displacement transducers were still attached to the beam.

The displacement transducers were left on the beam as planed until the force of 250 kN and further load was applied afterwards.

At the force of 369.75 kN and the angle of 31°, the first shear failure occurred on the right beam edge and simultaneously on the upper left opening edge the crack spread from front to the back beam side. All this caused force to drop for 6 kN (see figures B.18 and B.19).

In figure B.18 the moment of the upper left crack opening was captured, with appearance of the timber dust by this process.

Figure B.18: Initial cracks on the upper left and lower right opening edge at 250 kN of test specimen D03

Figure B.19: Fully spread cracks on the upper left (left) and lower right (right) opening edge of specimen D03

Further load was applied and at the force of 377.5 kN the second shear failure took place.

The bending failure happened on the back side of the beam in the net cross section and showed up on the bottom beam side around the predrilled holes of the threaded rods (see figure B.20).

Figure B.20: Bending failure on the back and bottom side of the beam of test specimen D03

The pull through effect was also visible on this test specimen, which was caused by pulling the threaded rods by the applied load because timber was cracked and could not bear the load application any further (see figure B.21).

By laying open the rods holes, it could be observed that the hole for the threaded rod on the front beam side closer to the support area, was noticeably deviated. The hole of the threaded rod closer to the load application area, on the front side was on the planned place.

The threaded rod holes on the back side on the (load application and support area) were deviated.

The pull through effect was visible on the same places as by the previous two specimens.

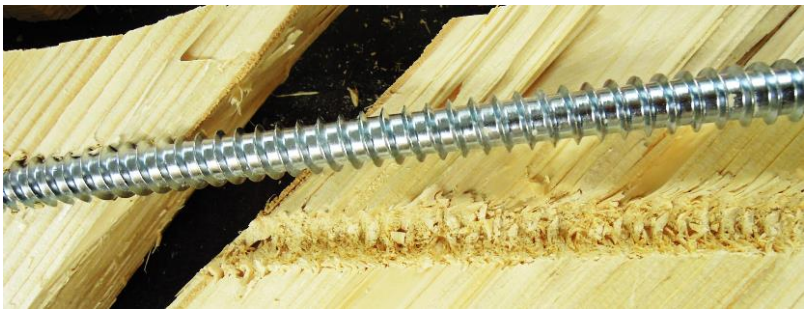

Figure B.21: Pull through effect by the threaded rod hole of test specimen D03

Specimen D04

The test specimen D04 was reinforced the same way as the test specimen D01 i.e. with two threaded rods on each tensioned opening side screwed in with a full length of 600 mm and two on the each compression side until a length of 400 mm. The remaining 200 mm of the compressed rod was left to stick out from the beam (see figure B.22).

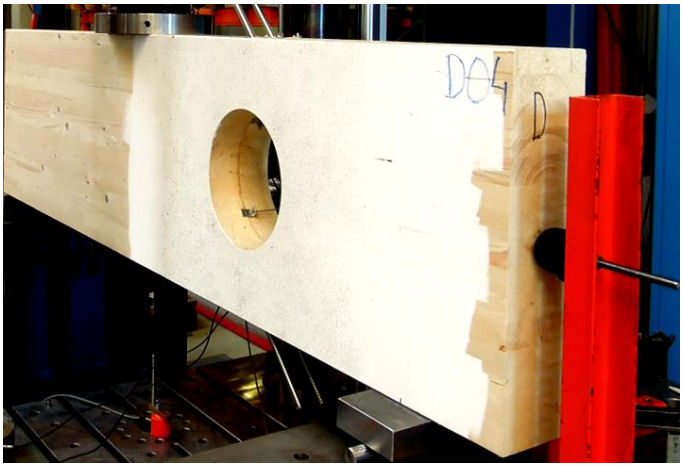

Figure B.22: Test specimen D04 inside the testing machine

The displacement transducers were still attached to the beam when the first crack occurred on the upper left opening edge at the force of 183 kN and spread by the ring line through the opening width from the front (at the angle of 26°) to the back side (at the angle of 28°).

At the force of 197 kN on the lower right opening edge, a crack spread from the front beam side to the mid width of the opening. The full spreading of the lower right crack occurred along with the first shear failure appearance at the force of 409.93 kN. The shear failure happened on the right beam edge and spread in a serrated manner. The force dropped to the value of 350.49 kN.

The force was further increased and the maximum was established at the value of 436.67 kN, whereby a first smaller fall caused existent cracks to spread even further at the force of 384.99 kN a bending failure in the net cross section and a second shear failure appeared whereby the force dropped to the level of 265.81 kN.

Finger joints also failed during the testing on the bottom beam side in region due to the bending failure in the net cross section (see figure B.23).

Figure B.23: Finger joints failure of test specimen D04

The threaded rod holes showed damage by pull through effect, as well as with all the previous test specimens.

The predrilled holes of the manufacturer were not the same as where the threaded rod was drilled in for both threaded rods on the front beam side in the tension zone.

Specimen D05

The test specimen D05 was reinforced like the test specimens D01 and D04. On both tension sides, the total of four threaded rods were screwed in their maximum length of 600 mm. On both compression sides, a total of 4 threaded rods were only screwed-in until a length of 400 mm because of the fault in crossing of the predrilled holes.

After the displacement transducers were taken off, the first timber dust and therefore cracks appeared on the upper left opening edge at the force of 240 kN. At a force of 280 kN, the upper left crack spread through the opening width and on the lower right side first crack occurred on the back side of the beam and spread straight to the mid opening width and further along the tree ring lines to the front side.

The first shear failure occurred at a load level of 441.91 kN and at the same force an additional crack, above the first upper left crack arose. These failures caused a force drop to 86 % of the initial shear force.

Further load was applied until a bending failure in the net cross section occurred at 400.05 kN. This failure showed up on the bottom of the beam side around the threaded rods.

Further load application caused further spreading of the cracks causing the multiple shear failures on the right edge of the beam.

Test specimen D05 too showed pull through effects in the threaded rods holes.

In the region of the support, the threaded rods were heading away from the predrilled holes while staying in correct position at the load application area.

5 Series G

Specimen G01

The first crack appeared on the upper left opening edge, at the angle of 30° and spread to the back side at an angle of 27°, at the time the displacement transducers were being taken off of the beam at the force of 250 kN (see figure B.24 right).

The second crack happened on the lower right opening edge at the force of 300 kN and spread in a serrated manner through the opening width instantly (see figure B.24 left).

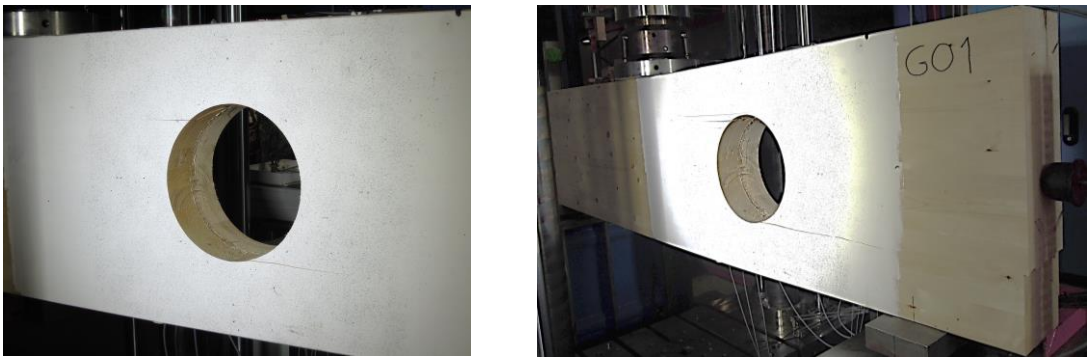

Figure B.24: Initial and second crack in the opening area (left); shear failure with multiple cracks around the opening (right) of test specimen G01

The first shear failure occurred at the force of 468.4 kN along the lower right crack which spread to the right edge which caused a force drop to 129.9 kN. The shear failure happened at the angle of 25°. By the same force, one more crack occurred above the initial crack on the upper left opening edge (see figure B.24 right).

The force was again raised to the point of 356.11 kN and dropped to 78 % of its previous value where the existing cracks spread even further in width and length.

The next increase of the force was up to the force of 299.69 kN, whereby, bending failure occurred in the net cross section and dropped the force on the value of 72 % of this value (see figure B.25).

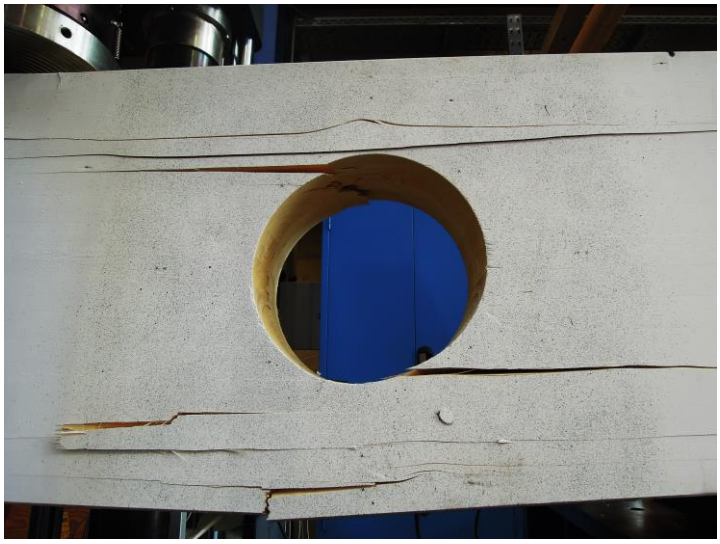

Figure B.25: Bending failure in the net cross section and cracks around the opening of test specimen G01

The upper left crack spread in a serrated manner from the front side to the middle width of the opening and along the tree ring lines from mid-point to the back side (see figure B.27).

The top shear failure on the right end of the beam followed partly the tree rings line and the bottom one was serrated (see figure B.26).

Figure B.26: Shear failures of test specimen G01

The bending failure, within the net cross section spread around the holes of the threaded rods (see figure B.27).

Figure B.27: Bending failure and cracks on the upper left opening edge of test specimen G01

The pull-through effect of the threaded rods was visible as a consequence of the threaded rods taking part in bearing the applied load after the beam was damaged (see figure B.28).

Some deviations of the planned distances of the rods to the vertical axes were also to be determined due to the imprecise introduction of the threaded rods inside of the beams.

Figure B.28: Threaded rod hole of test specimen G01

The measured force inside the threaded rods was in a calculated range of about 60 kN. All of the forces of the test specimen are shown in table 4.10. In appendix B2, $\Delta\varepsilon/\Delta F$ - beam width diagrams and B3 force-time diagrams are given for each test specimen of the series G.

Specimen G02

The first crack appeared on the lower right edge of the opening, at the angle of 15°, during the displacement transducers were removed, at 250 kN of force. Afterwards, at the force of 360 kN, the crack spread almost straight through the opening width from the front to the midpoint and from the mid-point to the back side almost straight, too (at the angle of 22°).

The second crack happened on the top left opening edge at the force of 390 kN, when there was some timber dust to see and spread in a serrated way through the opening width.

At a force level of 445.25 kN, there were further widening of the cracks which caused the load to drop for 20 kN.

The force raised to the value of 431.63 kN and caused the occurrence of the first shear failure at the angle of 28° and simultaneously bending failure in net cross section, which caused the force to drop to the level of 49 % of 431.63 kN (see figure B.29).

Figure B.29: Multiple cracking of the beam opening and bending failure in net cross section of the beam of test specimen G02

The tension force influence was visible on the beam side in the mid beam span in the first third of the beam height measured form the top beam edge under the load application on the beam back side (see figure B.30).

Figure B.30: Tension force influence on the beam back side of test specimen G02

For test specimen G02, damages of the finger joints were found too on the bottom side closer to the back side closer to the right support of the beam (see figure B.31).

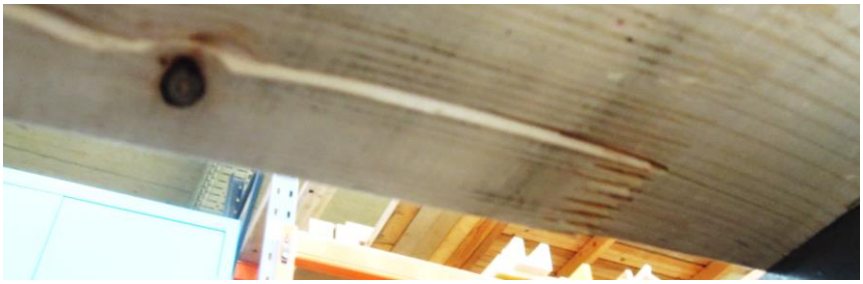

Figure B.31: Finger joints damage of test specimen G02

This test specimen experienced the pull through effect of the threaded rods as the previous one (see figure B.32).

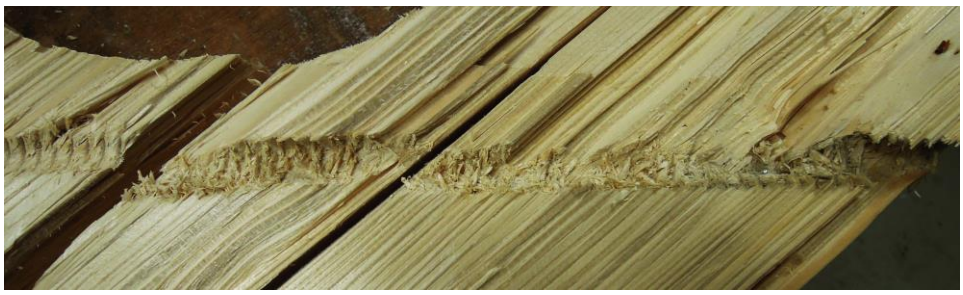

Figure B.32: Pull through effect of the threaded rods of test specimen G02

As for the test specimen G01, the measured force inside of the threaded rods were in the calculated range of about 60 kN (exact values are in table 4.10).

Specimen G03

The first crack occurred on the upper left edge of the opening at the force of 200 kN on the front side and spread in a serrated way through the opening width (see figure B.33).

The second crack happened on the lower right opening edge on the back side of the beam and spread to the mid-point of the opening width, following the tree rings and from that point to the front beam side in a serrated manner, at the force of 250 kN (see figure B.33).

At the force of 400 kN, above the upper left initial crack, one more crack appeared and the lower right crack spread even further (see figure B.33).

The first shear failure occurred at the load level of 436.35 kN (at the angle of 24°) and caused the force to fall to the value of 320.41 kN (see figure B.33).

By further load application, a bending failure in the net cross section happened at the force of 330.49 kN and made the shear force drop to 237.49 kN (see figure B.33).

The second shear failure occurred, after further load application, at the shear force of 244.36 kN and caused the force to drop on the value of 174.67 kN (see figure B.33).

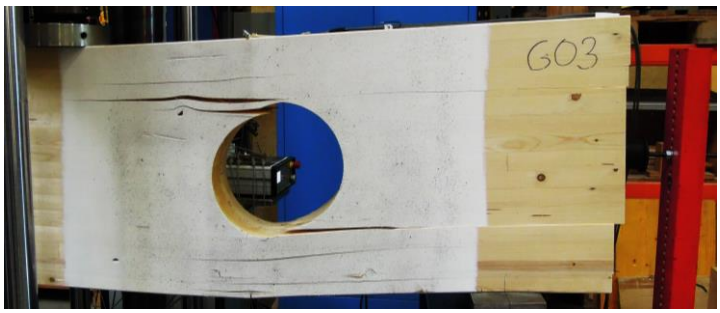

Figure B.33: Multiple cracks around the opening, due to multiple shear failures, bending failure in net cross section of test specimen G03

The pull through effect of the inclined threaded rods was also visible on this test specimen of the test series G as on the previous ones. The pull through effect of the threaded rod can be seen in the hole of the threaded rod (see figure B.34).

Figure B.34: Threaded rod hole with the threaded rod in the hole of test specimen G03

As for the previous two test specimens, the measured forces inside the threaded rods were about the value of 60 kN, and that was the pre calculation value for the pull through effect of the threaded rods (see table 4.10 and appendix B for the diagrams).

6 Series H

Specimen H01

The first crack appeared on the upper left edge of the opening, at the force of 345 kN and at an angle of 26°. The complete brakeage through the opening width was caused by the force of 400 kN and spread in a serrated manner through the width at an angle of 20° (see figure B.35).

Figure B.35: Serrated initial crack on the upper left opening edge of test specimen H01

The second crack, on the test specimen H01, appeared at the lower right opening edge and spread immediately in an almost straight manner through the opening width.

By reaching the shear force value of 533.40 kN, the first shear failure occurred, as well as the bending failure under the opening in the net cross section (see figure B.36). These failures caused the force to drop to the value of 49 % of the initial force. The shear failure at the right edge of the beam followed the tree rings at the height of 247 mm (the angle of 67°) from the top edge.

The force raised again and a crack at about 30 mm from top beam edge appeared, followed by upper shear failure at 293 kN, which brought the force to drop to 217.33 kN.

The test specimen H01 is shown in the figure B.36 representing the finished specimen, with all of the shear, tensile and bending failures and cracks.

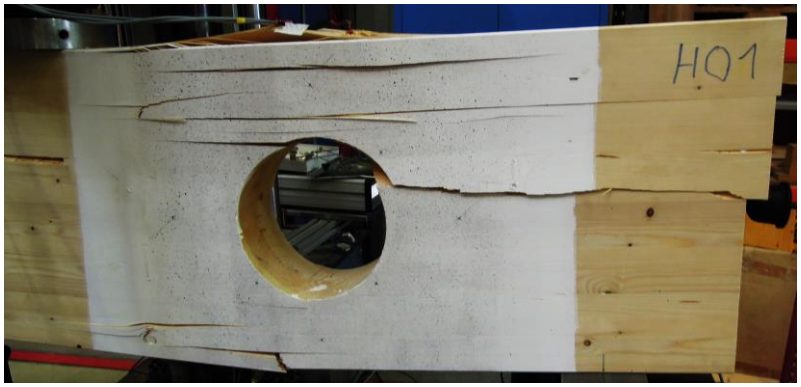

Figure B.36: Test specimen H01 front view after testing with all failures

On the beam back side, there was one outbreak, which did not cause a shear failure in the whole beam width, but spread from the opening to the right beam edge (see figure B.37).

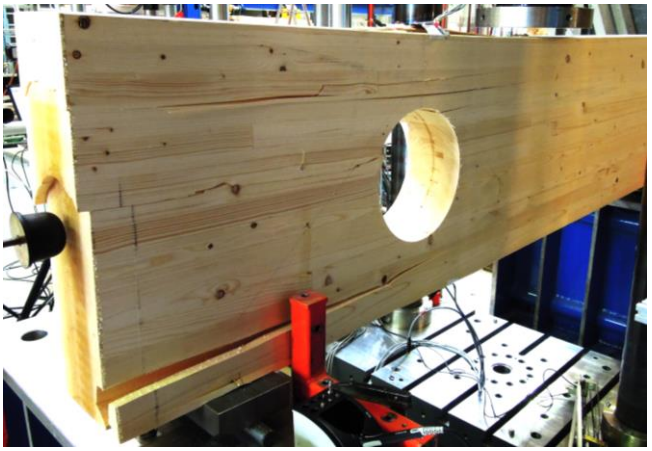

Figure B.37: Test specimen H01 back view with outbreak of timber part

On the top side of the beam, the timber was damaged too by the influence of the threaded rods, which were pulled into the beam and caused the beam to crack (see figure B.38).

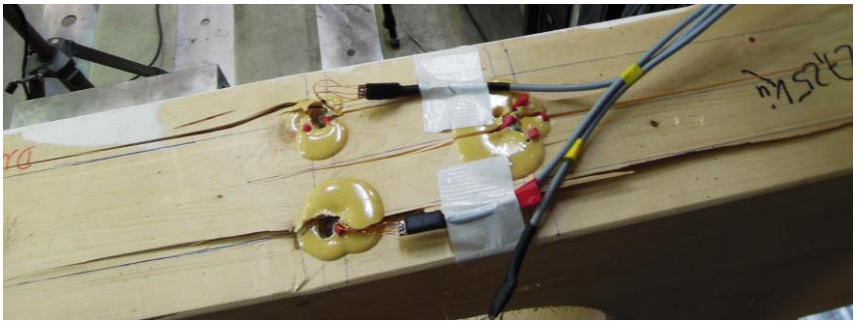

Figure B.38: Top side of test specimen H01 after testing with drown in glued-in threaded rods

This was the first of all the tested beams that experienced shear failure in the first half of the beam height on the right beam edge, measured from the top beam edge, which was caused by the position of the glued-in threaded rods inside of the beam (see figure B.38).

The glue around the threaded rods had not failed, but the timber around it had. The threaded rods took over a part of the bearing the load, after the beam was damaged and failed by reaching its load bearing capacity (see figure B.39).

Figure B.39: Threaded rod inside of the hole with the glue on it of test specimen H01

The values of the measured forces on the threaded rods in the tension zone are represented in appendix B3.

All of the forces of test specimen are shown in table 4.13. In appendix B2, $\Delta\varepsilon/\Delta F$ - beam width diagrams and B3 force-time diagrams are given for each test specimen of the series H.

Specimen H02

For test specimen H02, the first crack appearance happened at 213 kN of shear force, on the lower right opening edge in the middle of the opening width and spread following the tree rings to the back beam side, then to the front side at the force of 405 kN by following the tree rings too (at the angle of 21°).

As the load was raised further, at the force of 370 kN, on the upper left edge of the opening, the crack appeared on the front side. Spreading of the crack occurred through the opening width as the force fall from 547.29 kN to 502.46 kN. At the same force, the first shear failure at an angle of 16° appeared.

The force raised again to the point of 525.91 kN, whereby the force dropped to 59.52 kN (11 %) which was caused by the bending failure at the beam mid-span (bending failure in gross cross section) and bending failure under the opening (bending failure in net cross section), which dropped in the form of steps in downward direction to the right support. At the same force, one more crack opened above from the upper left initial one.

The specimen H02 is shown in the figure B.40, after completed testing with all failures: bending failure in the net and gross cross section, shear failure and multiple cracks on the beam sides.

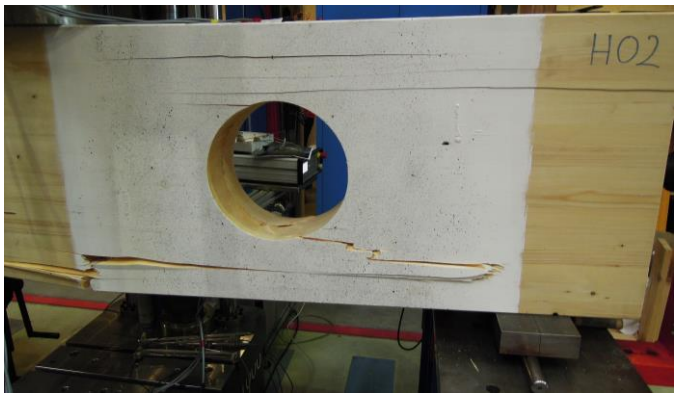

Figure B.40: Test specimen H02 after completed testing

The glue around the threaded rods was not damaged as the timber in the contact area experienced damages only (see figure B.41).

Figure B.41: Glued-in threaded rod inside of the damaged timber of test specimen H02

As for test specimen H01, the shear failure only occurred in the first half of the beam height from the top edge.

The forces in the threaded rods, as already mentioned, were measured with the help of the strain gauges that were glued onto the threaded rods in the tension zone (see appendix B3 for the graphics and table 4.13 for the values).

Test specimen H03

For test specimen H03, the first crack appearance happened at 316 kN of applied load, on the upper left opening edge and spread in a serrated manner to the front, at an angle of 32° at the force of 500 kN.

The second crack appeared at the load value of 420 kN on the back side of the beam, on the lower right opening edge and spread in a serrated way to the front at the force of 550 kN.

As the load was further increased, at the force of 572.55 kN the first shear failure and the bending failure in the net cross section occurred simultaneously, which was followed by one more crack above the initial one as well as the second shear failure. These damages caused the shear force fall to 33.6 % of the highest value. No further rise of the load was possible.

The glue for the glued-in threaded rods had not failed. The failure was in the timber around the glued-in threaded rods as for the previous two test specimens.

The shear failure crack was in the first half of the beam height from the top edge which aligned with the end of the tensioned reinforcement.

As for the first two described test specimen from the test series H, the values of elongations and forces on the glued-on threaded rods, in the tension zone around the opening, for the test specimen H03, were in the represented in table 4.13 (see appendices B2 and B3 for the graphs).

B-2 Δε/ΔF - beam width diagrams

G01

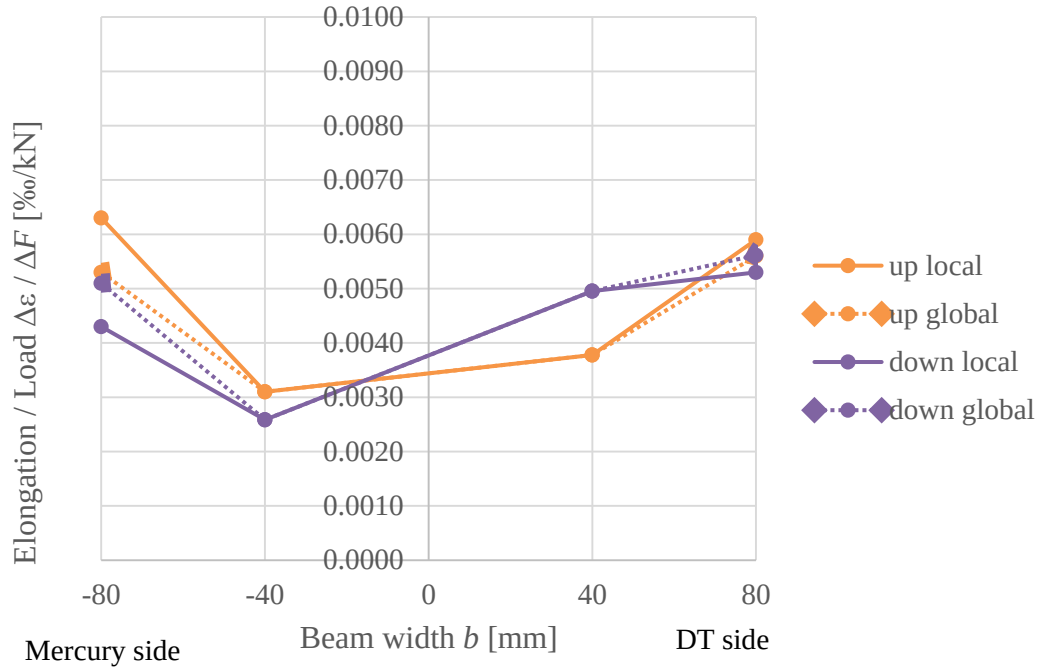

G02

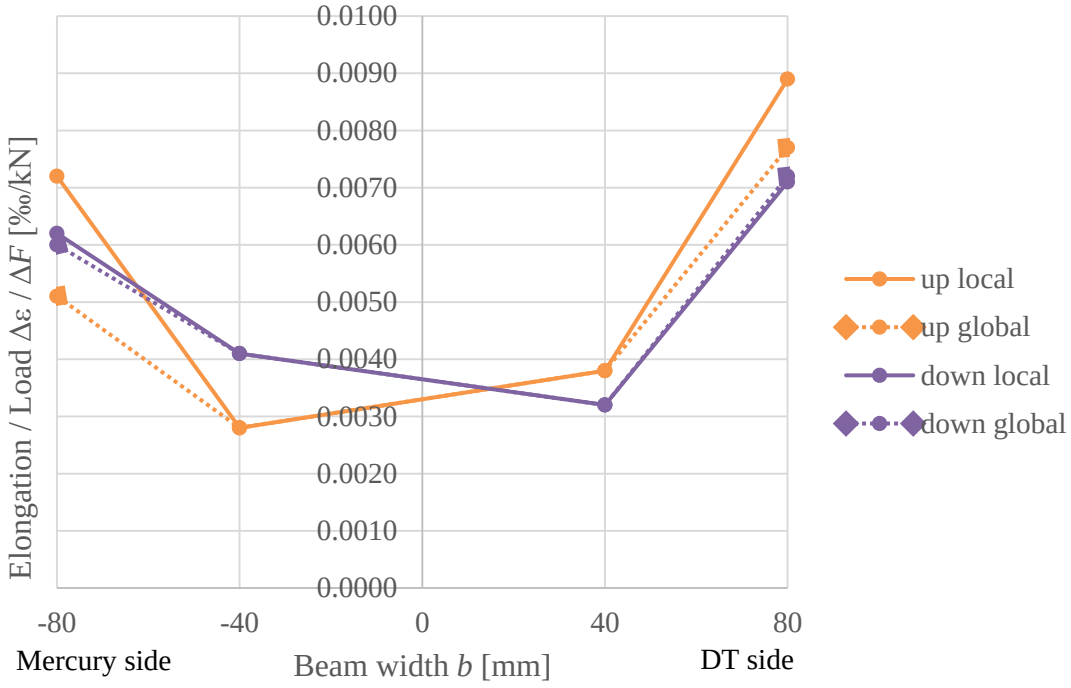

G03

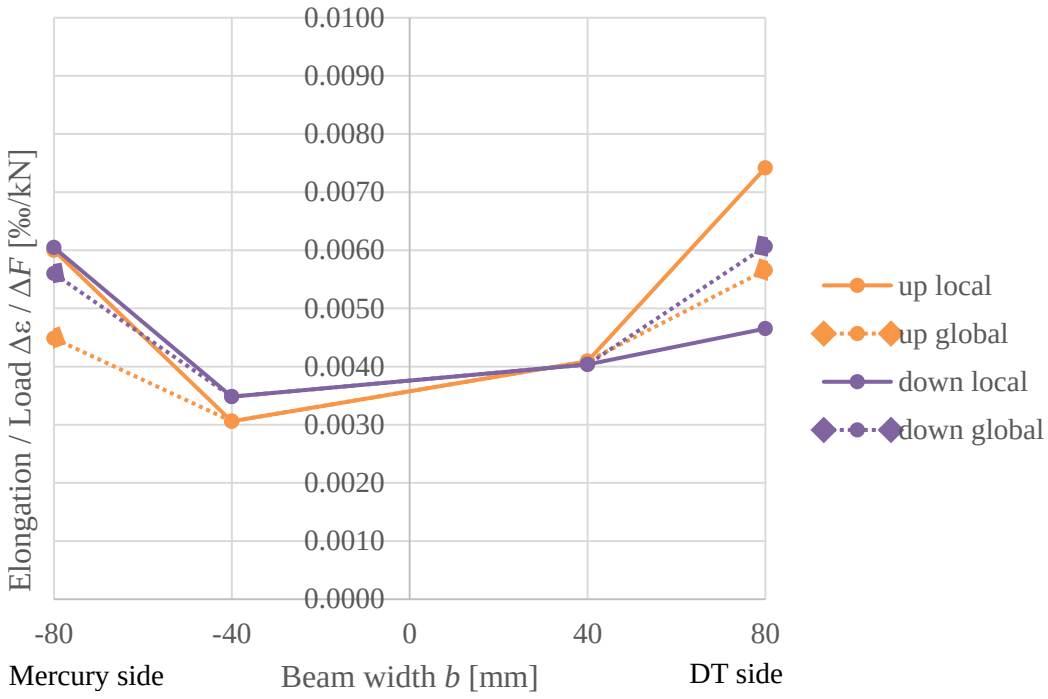
0.0100
0.0090
0.0080
0.0070
0.0060
0.0050
0.0040
0.0030
0.0020
0.0010
0.0000
Elongation / Load Δε / ΔF [‰/kN]
-80
-40
0
40
80
Mercury side
Beam width b [mm]
DT side
up local
up global
down local
down global

H01

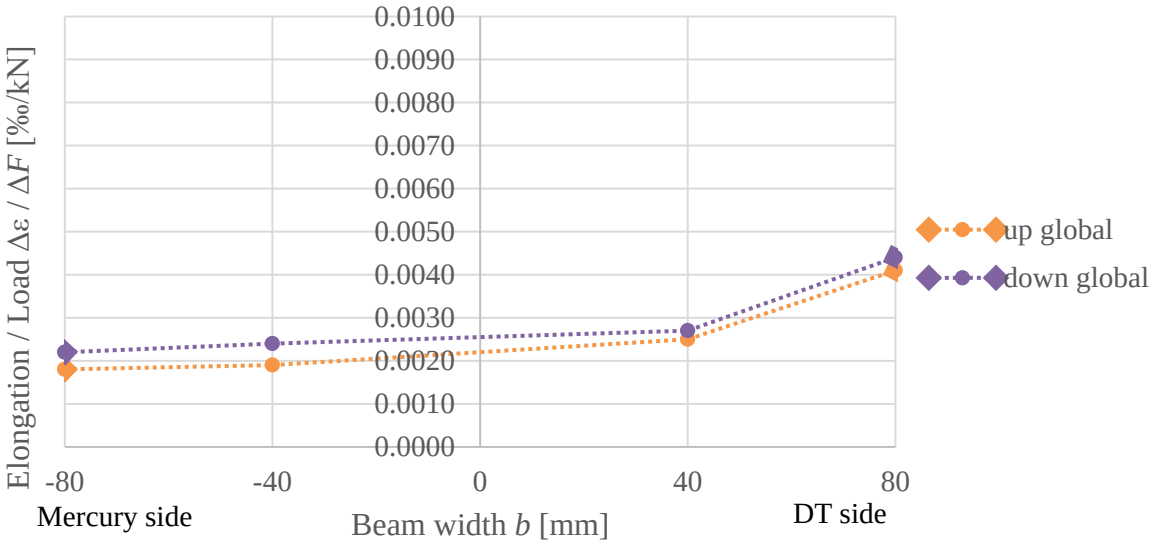
0.0100
0.0090
0.0080
0.0070
0.0060
0.0050
0.0040
0.0030
0.0020
0.0010
0.0000
Elongation / Load Δε / ΔF [‰/kN]
-80
-40
0
40
80
Mercury side
Beam width b [mm]
DT side
up global
down global

H02

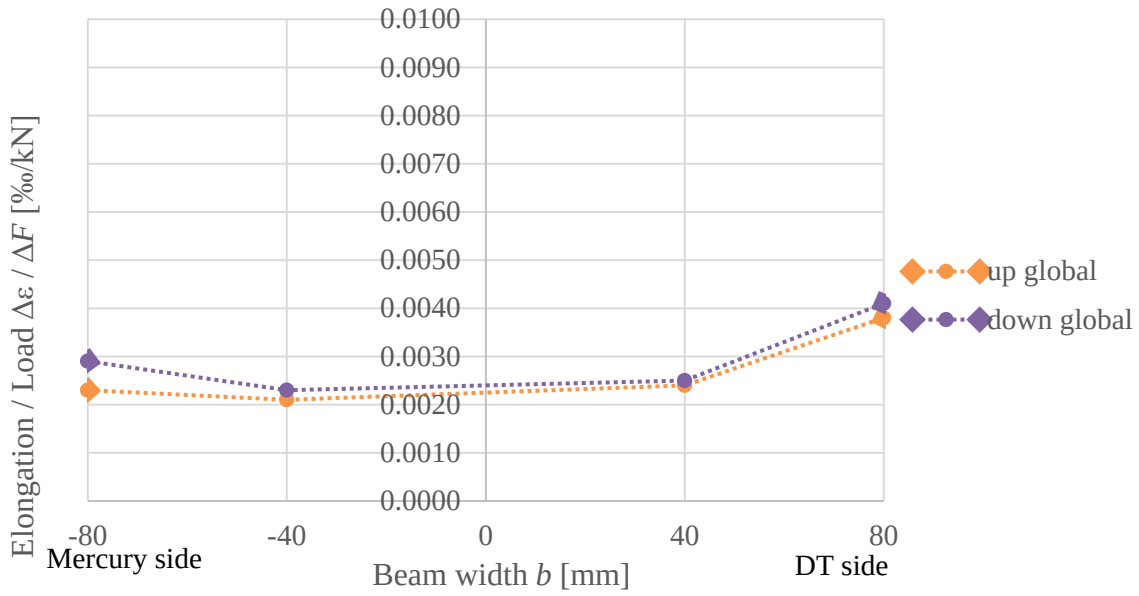
0.0100
0.0090
0.0080
0.0070
0.0060
0.0050
0.0040
0.0030
0.0020
0.0010
0.0000
Elongation / Load Δε / ΔF [‰/kN]
-80
-40
0
40
80
Mercury side
Beam width b [mm]
DT side
up global
down global

H03

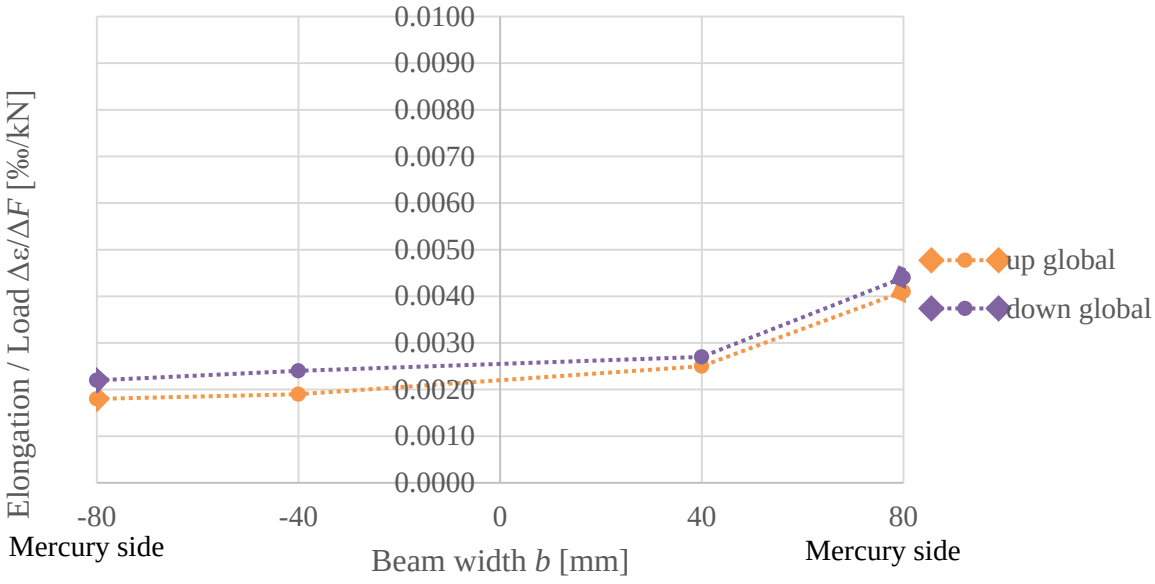
0.0100
0.0090
0.0080
0.0070
0.0060
0.0050
0.0040
0.0030
0.0020
0.0010
0.0000
Elongation / Load Δε/ΔF [‰/kN]
-80
-40
0
40
80
Mercury side
Beam width b [mm]
Mercury side
up global
down global

B-3 Force-time diagrams of threaded rods

G01

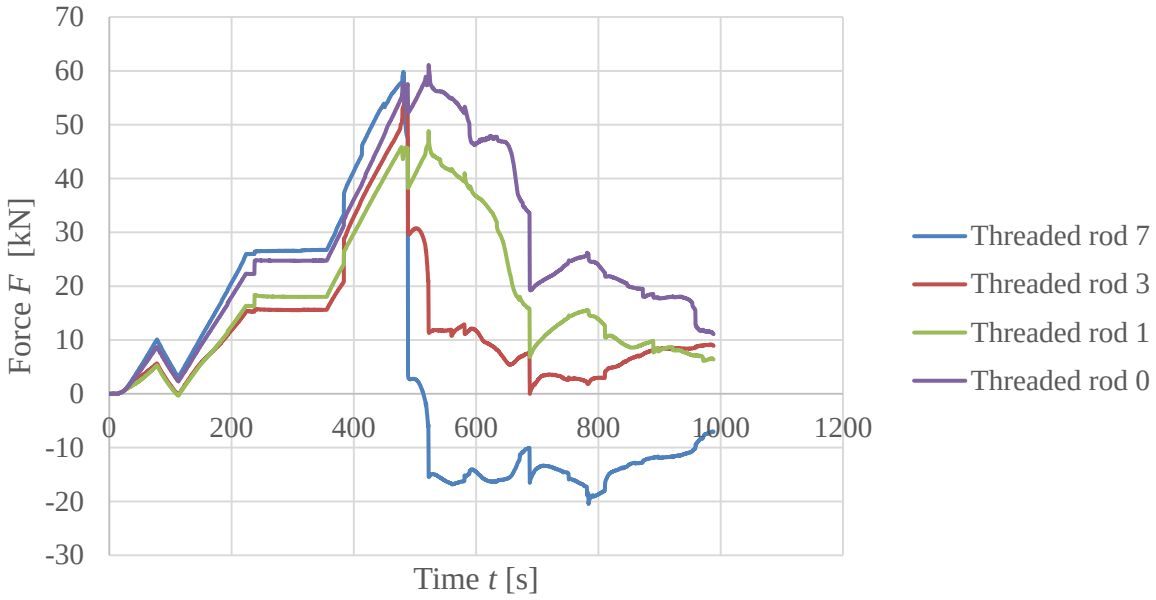

G02

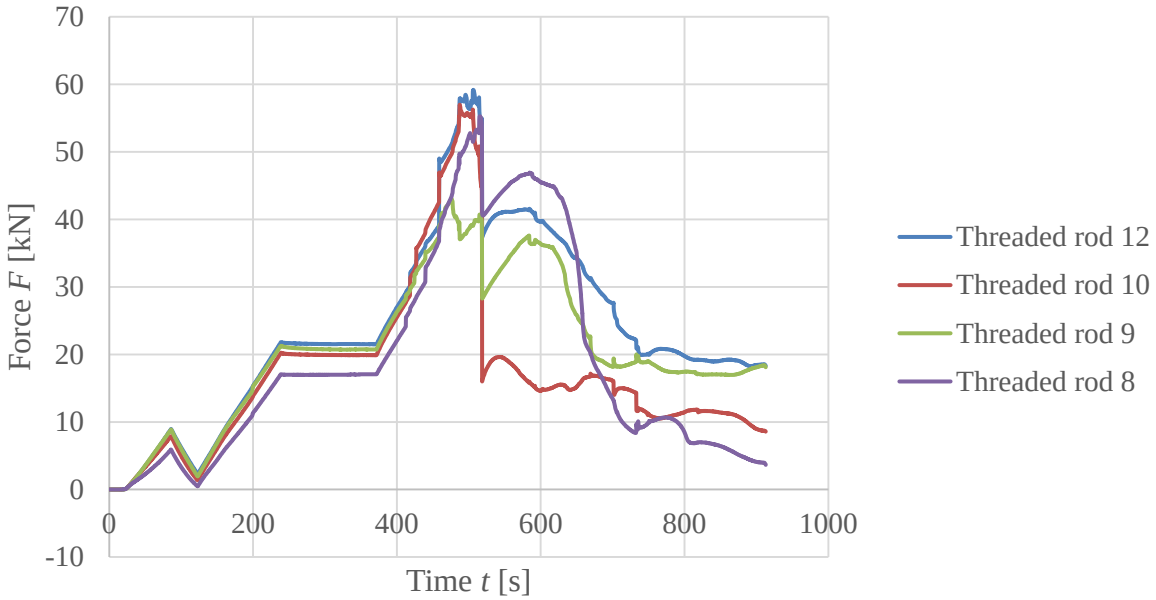

G03

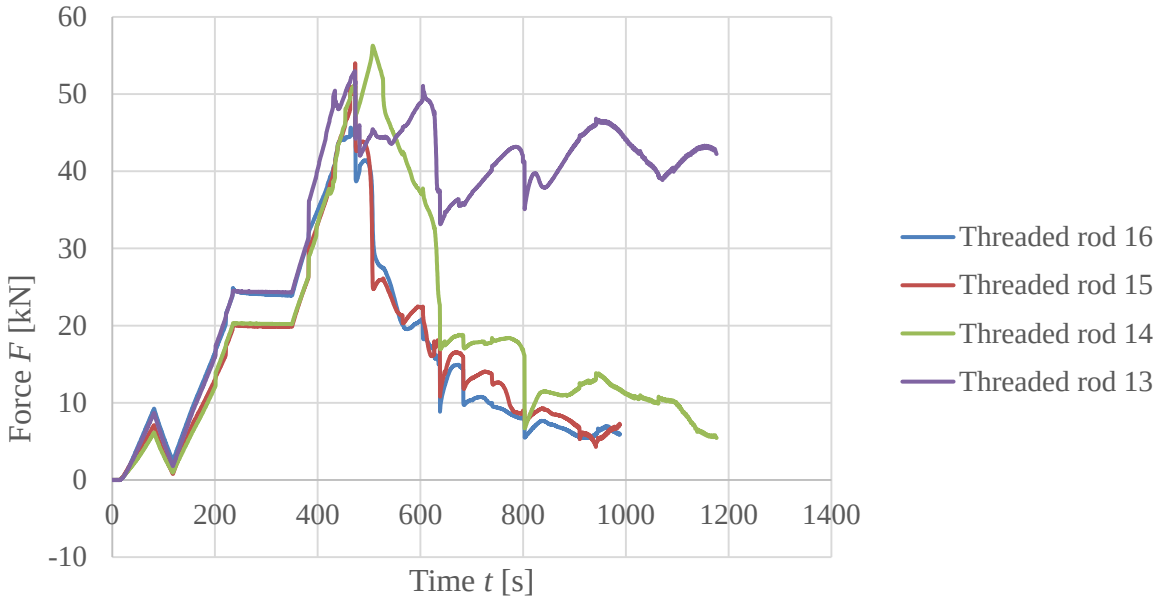
60
50
40
30
20
10
0
-10
0
200
400
600
800
1000
1200
1400
Force F [kN]
Time t [s]
Threaded rod 16
Threaded rod 15
Threaded rod 14
Threaded rod 13

H01

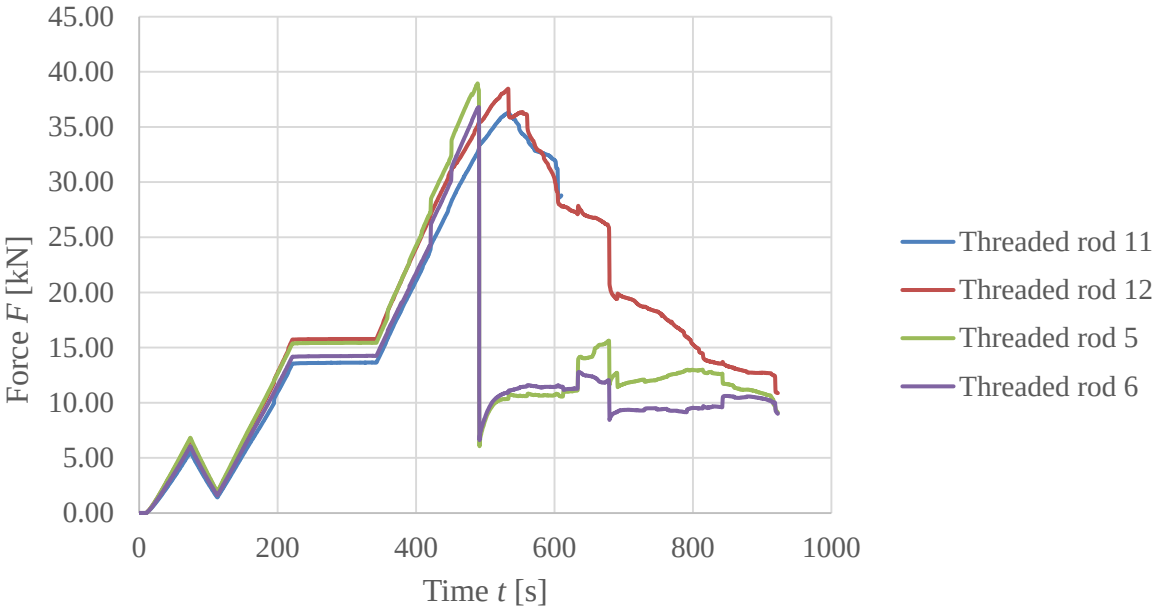
45.00
40.00
35.00
30.00
25.00
20.00
15.00
10.00
5.00
0.00
0
200
400
600
800
1000
Force F [kN]
Time t [s]
Threaded rod 11
Threaded rod 12
Threaded rod 5
Threaded rod 6

H02

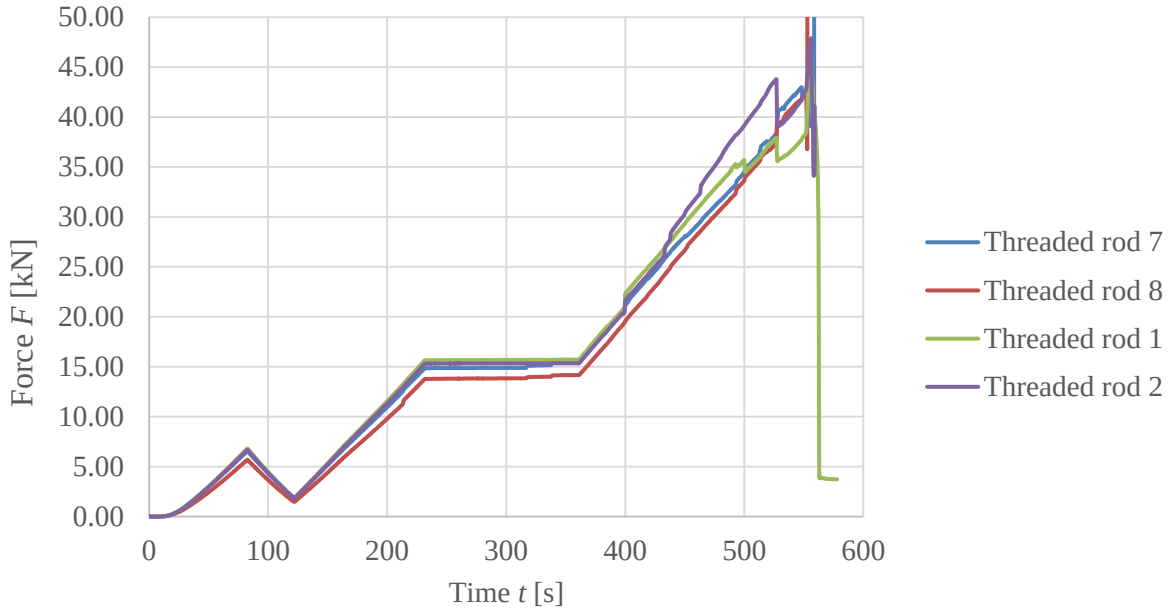
50.00
45.00
40.00
35.00
30.00
25.00
20.00
15.00
10.00
5.00
0.00
Force F [kN]
0
100
200
300
400
500
600
Time t [s]
Threaded rod 7
Threaded rod 8
Threaded rod 1
Threaded rod 2

H03

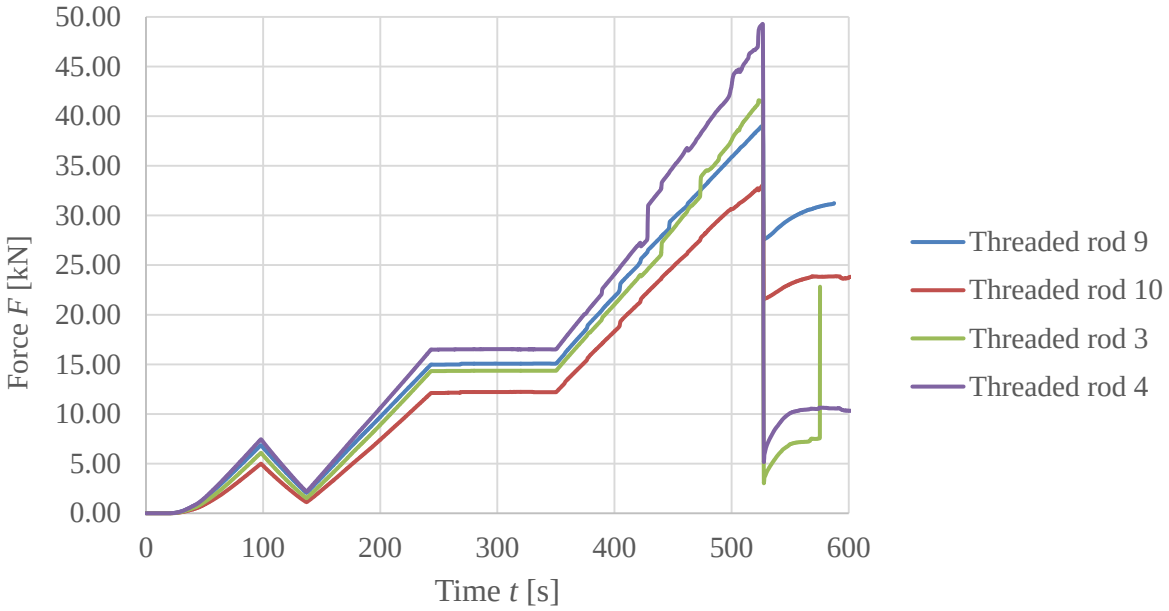
50.00
45.00
40.00
35.00
30.00
25.00
20.00
15.00
10.00
5.00
0.00
Force F [kN]
0
100
200
300
400
500
600
Time t [s]
Threaded rod 9
Threaded rod 10
Threaded rod 3
Threaded rod 4

B-4 Summary of the EXCEL (2013) results

Series A

Specimen	Shear modulus	Moisture content	Density	Stiffness			
	G_{12}	u	ρ_{12}	$K_{1,12}$	$K_{2,12}$	$K_{3,12}$	$K_{4,12}$
	[N/mm²]	[%]	[kg/m³]	[N/mm]	[N/mm]	[N/mm]	[N/mm]
A01	769.87	10.91	497	817.59	588.99	1413.03	658.11
A02	758.67	11.30	515	957.61	525.55	1413.84	563.76
A03	852.60	11.50	511	983.18	611.09	1351.01	779.38
A04	690.06	11.40	514	648.29	552.19	805.85	578.14
A05	597.37	10.50	511	733.79	511.53	784.58	600.79
mean	733.71	11.12	509	828.09	557.87	1153.66	636.04

Series B

Specimen	Shear modulus	Moisture content	Density	Stiffness			
	G_{12}	u	ρ_{12}	$K_{1,12}$	$K_{2,12}$	$K_{3,12}$	$K_{4,12}$
	[N/mm²]	[%]	[kg/m³]	[N/mm]	[N/mm]	[N/mm]	[N/mm]
B01	146.58	11.47	503	247.39	220.67	259.41	254.83
B02	147.98	11.48	510	274.32	209.54	224.66	224.66
B03	152.25	11.69	520	296.29	209.02	202.85	202.85
B04	149.64	11.42	513	248.62	248.79	232.71	232.71
B05	145.09	11.25	500	249.19	195.45	202.41	202.41
mean	148.31	11.46	509	263.16	216.70	224.41	223.49

Series C

Specimen	Shear modulus	Moisture content	Density	Stiffness			
	G_{12}	u	ρ_{12}	$K_{1,12}$	$K_{2,12}$	$K_{3,12}$	$K_{4,12}$
	[N/mm²]	[%]	[kg/m³]	[N/mm]	[N/mm]	[N/mm]	[N/mm]
C01	164.13	11.22	500	234.05	246.45	265.64	255.70
C02	144.98	11.30	511	204.82	208.31	237.71	230.77
C03	172.25	11.34	500	243.16	228.10	263.10	245.45
C04	149.90	11.37	515	233.45	210.11	243.67	217.34
C05	157.87	11.49	498	250.51	243.22	262.17	242.39
C06	146.93	11.87	513	244.99	238.51	275.82	274.02
C07	166.30	11.65	522	297.21	232.73	267.55	256.99
C08	167.63	11.74	529	276.64	257.56	298.47	263.33
mean	158.75	11.50	511	248.10	233.12	264.27	248.25

Series D

Specimen	Shear modulus	Moisture content	Density	Stiffness			
	G_{12}	u	ρ_{12}	$K_{1,12}$	$K_{2,12}$	$K_{3,12}$	$K_{4,12}$
	[N/mm²]	[%]	[kg/m³]	[N/mm]	[N/mm]	[N/mm]	[N/mm]
D01	233.15	10.92	507	414.80	313.30	514.49	334.20
D02	190.94	10.63	514	455.12	249.20	432.10	249.43
D03	182.28	10.73	503	348.23	223.67	380.01	215.41
D04	227.88	10.34	495	460.29	295.48	498.77	317.88
D05	230.66	10.37	486	432.73	275.04	543.84	352.55
mean	212.98	10.60	501	422.23	271.34	473.84	293.89

Series G

Specimen	Shear modulus	Moisture content	Density	Stiffness			
	G_{12}	u	ρ_{12}	$K_{1,12}$	$K_{2,12}$	$K_{3,12}$	$K_{4,12}$
	[N/mm²]	[%]	[kg/m³]	[N/mm]	[N/mm]	[N/mm]	[N/mm]
G01	202.02	11.50	516	528.81	315.81	490.92	320.01
G02	224.46	12.43	510	472.22	310.11	474.29	392.03
G03	212.89	12.74	505	428.46	319.04	483.56	320.23
mean	213.12	12.22	510	476.50	314.99	482.93	344.09

Series H

Specimen	Shear modulus	Moisture content	Density	Stiffness			
	G_{12}	u	ρ_{12}	$K_{1,12}$	$K_{2,12}$	$K_{3,12}$	$K_{4,12}$
	[N/mm²]	[%]	[kg/m³]	[N/mm]	[N/mm]	[N/mm]	[N/mm]
H01	310.90	12.19	513	955.92	438.95	1072.44	491.03
H02	305.64	12.09	518	774.61	441.23	894.19	469.99
H03	320.60	12.31	523	814.20	436.22	1110.08	563.08
mean	312.38	12.20	518	848.24	438.80	1025.57	508.03

Dies ist eine Veröffentlichung des

FACHBEREICHS INGENIEURBAUKUNST (IBK) AN DER TU GRAZ

Der Fachbereich Ingenieurbaukunst umfasst die dem konstruktiven Ingenieurbau nahe stehenden Institute für Baustatik, Betonbau, Stahlbau & Flächentragwerke, Holzbau & Holztechnologie, Materialprüfung & Baustofftechnologie, Baubetrieb & Bauwirtschaft, Hochbau & Industriebau, Bauinformatik und Allgemeine Mechanik der Fakultät für Bauingenieurwissenschaften an der Technischen Universität Graz.

Dem Fachbereich Ingenieurbaukunst ist das Bautechnikzentrum (BTZ) zugeordnet, welches als gemeinsame hochmoderne Laboreinrichtung zur Durchführung der experimentellen Forschung aller beteiligten Institute dient. Es umfasst die drei Laboreinheiten für konstruktiven Ingenieurbau, für Bauphysik und für Baustofftechnologie.

Der Fachbereich Ingenieurbaukunst kooperiert im gemeinsamen Forschungsschwerpunkt „Advanced Construction Technology".
Dieser Forschungsschwerpunkt umfasst sowohl Grundlagen- als auch praxisorientierte Forschungs- und Entwicklungsprogramme.

Weitere Forschungs- und Entwicklungskooperationen bestehen mit anderen Instituten der Fakultät, insbesondere mit der Gruppe Geotechnik, sowie nationalen und internationalen Partnern aus Wissenschaft und Wirtschaft.

Die Lehrinhalte des Fachbereichs Ingenieurbaukunst sind aufeinander abgestimmt. Aus gemeinsam betreuten Projektarbeiten und gemeinsamen Prüfungen innerhalb der Fachmodule können alle Beteiligten einen optimalen Nutzen ziehen.

Durch den gemeinsamen, einheitlichen Auftritt in der Öffentlichkeit präsentiert sich der Fachbereich Ingenieurbaukunst als moderne Lehr- und Forschungsgemeinschaft, welche die Ziele und Visionen der TU Graz umsetzt.

Nummerierungssystematik der Schriftenreihe

S – Skripten, Vorlesungsunterlagen | F – Forschungsberichte
V – Vorträge, Tagungen | M – Masterarbeiten

Institutskennzahl:
1 – Allgemeine Mechanik | 2 – Baustatik | 3 – Betonbau
4 – Holzbau & Holztechnologie | 5 – Stahlbau & Flächentragwerke
6 – Materialprüfung & Baustofftechnologie | 7 – Baubetrieb & Bauwirtschaft
8 – Hochbau & Industriebau | 9 – Bauinformatik

Fortlaufende Nummer pro Reihe und Institut / Jahreszahl